GEOCHRONOLOGY OF METAMORPHIC TERRAINS BY THE $^{40}AR/^{39}AR$ AGE SPECTRUM METHOD

by

JAN ROELOF WIJBRANS

A thesis submitted for the degree of

DOCTOR OF PHILOSOPHY

at the

RESEARCH SCHOOL OF EARTH SCIENCES,

THE AUSTRALIAN NATIONAL UNIVERSITY

April 1985

STATEMENT

This thesis is based on experimental work carried out at the Research School of Earth Sciences, the Australian National University between July 1981 and April 1985. Unless otherwise acknowledged, the work and the conclusions presented in this thesis are those of the author.

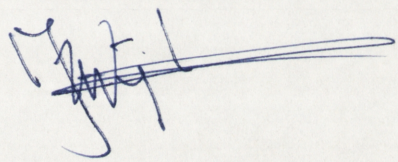

Jan Roelof Wijbrans

ACKNOWLEDGEMENTS

At the end of my PhD course at RSES I would like to express my gratitude to the many persons that have contributed to the progress of my course. I would like to thank the Director and academic staff of RSES for creating and maintaining an environment committed fully to scientific research.

My supervisor, Dr Ian McDougall, has supported this work through all its stages; I have benefitted strongly from discussions and practical advise concerning every aspect of my course. It has been a pleasure to work under his guidance.

Discussion with academic staff, students, and visitors of RSES have contributed enormously to my understanding of the earth sciences. From this group, I would especially like to thank Drs Peter Zeitler, Greg Housman, Malcolm McCulloch, Bill Compston, Mark Harrison and Ken Collerson for their interest in my work, and for helpful suggestions. Drs. Chris Klootwijk, Phil McFadden, and Gordon Lister from the Bureau of Mineral Resources have contributed with ideas, and comments on various aspects of my research. I would like to thank my fellow students, especially those who shared the evening and weekend shifts, for friendship and lively discussions.

The always cheerful technical assistance of Terry Davis and Robyn Maier are highly appreciated. Robyn's help with chemistry, and advise on drafting figures have contributed to the work presented here. Thin sections were prepared by Keith Massey. M. Cowan and R. Rudowski gave their assistance during the mineral separation. Nick Ware assisted with the electron microprobe analyses. The computing facilities were kept up to standard by Les Allinson and Gloria Robbins.

Professor R.D. Schuiling, and Drs P.A.M. Andriessen, K.D. Collerson and N. McNaughton contributed samples. Dr N. McNaughton is thanked for making available unpublished work from the University of W. Australia on the Shaw Batholith area.

During his course at RSES the author was in receipt of an ANU postgraduate scholarship.

Abstract

The $^{40}Ar/^{39}Ar$ age spectrum method of dating has the potential for resolving ^{40}Ar concentration gradients in common metamorphic minerals such as white mica and hornblende. Concentration gradients in minerals may be the result of either diffusion of ^{40}Ar from, or into minerals. These effects may cause significant scatter in conventional K-Ar and $^{40}Ar/^{39}Ar$ total fusion ages, whereas by applying the age spectrum technique, information may be obtained on the cause of this scatter.

In this thesis the $^{40}Ar/^{39}Ar$ age spectrum method has been applied to metamorphic rocks from the Attic Cycladic Metamorphic Belt on the island of Naxos, Greece, and to metamorphic rocks from the Archaean Pilbara and Yilgarn Blocks in Western Australia. Previous studies of the geology and geochronology of these areas indicated that both terrains have experienced complex metamorphic histories. Therefore, a study of these terrains with the $^{40}Ar/^{39}Ar$ age spectrum method may potentially demonstrate the usefulness of the method for deciphering the thermal evolutions of metamorphic terrains.

$^{40}Ar/^{39}Ar$ age spectra of phengitic white micas formed during the early, M_1, high pressure, low to medium temperature metamorphism on Naxos show $^{40}Ar^*$ loss patterns indicating that these minerals cooled below the closure temperature of phengite for argon about 50 Ma ago. The scatter in conventional K-Ar ages in the area least affected by subsequent overprinting was shown to be caused by diffusion of $^{40}Ar^*$ from these minerals. Along the metamorphic temperature gradient caused by overprinting during the M_2 thermal dome metamorphism (a medium pressure, greenschist to upper amphibolite grade event), resetting of the argon isotopic ages of white micas takes place by two separate mechanisms: (1) argon loss from the original phengites by volume diffusion, and (2) crystallization of muscovite at the expense of the M_1-formed phengites. These two processes caused complex, upward-convex age spectra in the white micas from the area where the two generations of white mica occur side by side. Upward-convex age spectra of white micas can be understood in terms of $^{40}Ar^*$ release from a mixture of two generations of white micas with slightly different physical properties. Thus the observation of such age spectra, in combination with the identification of

M_1-formed phengites in the area where overprinting during M_2 reached amphibolite facies grade, were used to constrain the M_2 metamorphism as a short thermal pulse. Much of the scatter in K-Ar ages of M_2 metamorphic hornblendes was shown to be the result of incorporation of varying amounts of excess ^{40}Ar into these minerals. Consequently, we argue that most of the metamorphic hornblendes from Naxos were formed, or started to accumulate argon about 15 to 16 Ma ago. Slightly younger ages were measured on hornblendes from the north of Naxos (11.8 $\pm$ 0.1 Ma), and from the granodiorite intrusive along the west coast of the island (about 12.7 Ma). Muscovite and biotite from the high grade rocks of central Naxos yielded excellent flat age spectra, indicating, in combination with the hornblende $^{40}Ar/^{39}Ar$ data and additional biotite and muscovive K-Ar data, that the M_2 metamorphism was followed by a period of rapid cooling.

Numerical thermal models of the Attic Cycladic Metamorphic Belt were developed in support of the interpretation that the M_1 metamorphism was caused by thickening of the continental crust along the southern margin of the Apulian-Anatolian Microplate during the Cretaceous. These events were followed by rapid restoration of an average crustal thickness about 50 Ma ago. The M_2 metamorphism is interpreted as the result of a transient heat source which acted upon the system about 15 to 16 Ma ago, and was followed by the intrusion of a granodiorite immediately to the west of the high grade terrain somewhat before about 12.7 Ma ago. The close temporal relation between thermal dome metamorphism and granitoid intrusion suggests a genetic link between the two events, which probably occurred when part of the Attic Cycladic Metamorphic Belt, including Naxos, was in an island arc tectonic setting.

$^{40}Ar/^{39}Ar$ age spectrum analyses of metamorphic hornblendes from within an Archaean greenstone belt in the eastern part of the Pilbara Archaean Block, Western Australia, indicate that metamorphism of these rocks occurred at some time before 3200 Ma ago, during an event which was probably caused by tectonic thickening of the crust. This event was followed by tectonism about 2950 Ma ago, during which the present configuration of granitoid-gneiss domes and synclinal greenstone belts was formed. The rocks of the granitoid-gneiss terrains and the greenstone rocks along their margins experienced amphibolite to upper

amphibolite facies grade metamorphism, but the more central parts of the greenstone belts were left virtually unaffected. Posttectonic granitoids intruded the granitoid-gneiss terrains and the greenstone rocks at their margins, causing overprinting at upper amphibolite facies grade. One of these intrusives was dated at 2866 $\pm$ 5 Ma by measuring a $^{40}Ar/^{39}Ar$ age spectrum of a high grade hornblende from greenstone rock into which this granitoid was intruded. A younger pegmatite was dated by K-Ar at 2671 $\pm$ 25 Ma. The data presented in this thesis confirm high grade metamorphism in the eastern Pilbara about 2950 Ma ago, but indicate that this event was confined to the granitoid-gneiss terrains and their margins.

These results suggest that the Archaean history of the east Pilbara was characterized by a number of discrete tectonic and thermal events, rather than being the result of slow, continuous tectonic activity over long periods of time.

Hornblendes from rocks of the Narryer metamorphic belt in the northwestern part of the Archaean Yilgarn Block record cooling below the closure temperature of hornblende for argon after high grade metamorphism 2720 to 2780 Ma ago. Within the metasedimentary rocks of Mount Narryer occur detrital zircons with igneous morphologies and near concordant U-Pb ages of 3250 to 3100 Ma. Thus we argue that the sedimentation age of these rocks must lie between 3100 and 2800 Ma, and postdates the metamorphic event dated by a Rb-Sr whole rock isochron at about 3350 Ma on adjacent orthogneisses. A high grade metamorphism at about 2800 Ma had not previously been documented in this region. Subsequent retrogression of these rocks at greenschist facies grade occurred during the Mid Proterozoic; K-Ar ages on biotites of 1780 to 2020 Ma and a $^{40}Ar/^{39}Ar$ age of 1620 Ma in a plagioclase age spectrum were associated with this event.

Table of Contents

Chapter 1

Introduction

1.1 Introduction

The study reported in this thesis consists of investigations into the geochronology and thermal evolution of rocks from metamorphic terrains by the $^{40}Ar/^{39}Ar$ age spectrum method of dating. The $^{40}Ar/^{39}Ar$ and the K-Ar methods of dating are based on the accumulation of radiogenic ^{40}Ar in geological materials, resulting from radioactive decay of ^{40}K. When a number of assumptions are fulfilled, a geologically meaningful age can be calculated from the ^{40}Ar to ^{40}K ratio in a sample. By presenting two case histories it is demonstrated that the $^{40}Ar/^{39}Ar$ method can be applied to metamorphic minerals and may contribute significantly to the understanding of metamorphic terrains by precisely dating metamorphism and subsequent cooling. The method is a variation of the K-Ar method of dating, and was described first in a publication by Merrihue and Turner (1966) as an analogue of the I-Xe technique for dating meteorites. A brief description of the method is given in Appendix I.

The intrinsic advantages of the $^{40}Ar/^{39}Ar$ age spectrum method over the conventional K-Ar method include the possibility of resolving radiogenic argon ($^{40}Ar^*$) gradients by stepwise heating and the potential for more precise measurements; these advantages were first utilized in studies of meteorite and lunar samples. In many cases the results of studies of extraterrestrial samples were very encouraging, because by applying the stepwise heating technique it could be demonstrated that disturbed samples did not contain a uniform distribution of $^{40}Ar^*$, and that variations in apparent ages in $^{40}Ar/^{39}Ar$ age spectra could be understood in terms of models based on the assumption that $^{40}Ar^*$ was lost from crystals by volume diffusion (Turner et al. 1966, Turner 1968, 1970a, b). In contrast, studies of terrestrial samples often revealed much more complex age spectra, from some of which only little age information could be extracted (Lanphere and Dalrymple 1971, Brereton 1972, Pankhurst et al. 1973). These early results were disappointing, and it was concluded by Lanphere and Dalrymple (1971) that disturbed age spectra did not reflect the age of crystallization of the sample in any obvious way, and, more disturbingly, biotites analyzed by Pankhurst et al. (1973) which had incorporated substantial amounts of excess ^{40}Ar yielded flat, undisturbed looking age spectra. Perhaps these early

studies aimed for an unrealistic goal, because the samples came from terrains which had experienced complex geological histories, and it was known from conventional K-Ar analyses that the samples were disturbed. Subsequent studies by Lanphere and Dalrymple (1976) on minerals containing excess argon, and by Hanson et al. (1975) and Berger (1975) on the overprinting relations in the contact aureoles originally studied by Hanson and Gast (1967) and by Hart (1964), demonstrated the value of the $^{40}Ar/^{39}Ar$ method for application to terrestrial problems more clearly.

Previous studies carried out in the ANU argon laboratory indicated that the $^{40}Ar/^{39}Ar$ stepheating technique applied to minerals from rapidly cooled high level intrusions, and from volcanic rocks from areas with simple thermal histories yielded excellent undisturbed age spectra (Tetley 1978, McDougall 1980), and that hornblendes from a thermal contact aureole had lost argon and contained $^{40}Ar^{*}$ gradients that could be understood in terms of argon loss by a process involving volume diffusion (Harrison and McDougall 1980a, b). A study of minerals from a high grade metamorphic terrain demonstrated the influence of high partial pressures of ^{40}Ar in the ambient metamorphic fluid on age spectra of hornblendes and plagioclases (Harrison and McDougall 1981).

The present study is an attempt to further evaluate the usefulness of the technique for dating purposes in regional metamorphic terrains. Geochronological and thermal studies in regional metamorphic terrains have, in comparison with similar studies of contact aureoles and high level intrusions, two additional uncertainties. Firstly, an obvious heat source with a well constrained geometry is absent in many regional metamorphic terrains. Secondly, it is often substantially more difficult to obtain suitable samples in regional metamorphic terrains, because of partial recrystallization of the minerals. Such problems are considerably less important in studies of rapidly cooled high level intrusions, or of contact aureoles. By definition, metamorphic rocks are the products of (re-)crystallization caused by exposure to changed physical conditions, excluding those experienced during weathering and diagenesis (Winkler 1974). Crystallization and recrystallization may occur over extended periods of time, and during tectonic events which are not

necessarily accompanied by clearly defined thermal effects. Partial recrystallization will affect the stability of the argon isotopic system, and will complicate the interpretation age spectra, because in such cases variations in apparent ages cannot be readily understood in terms of volume diffusion of argon from the original minerals. Thus the meaning of results from an argon isotopic study depends strongly on proper characterization of the materials used for dating. In this thesis, some effort will be made to interpret the results in terms of the petrological and microstructural relations observed in mineral assemblages. Generally, when minerals belonging to a stable mineral assemblage could be dated, either flat undisturbed age spectra, or patterns which could be interpreted as caused by diffusion of argon out of, or into the minerals were obtained. The more intricate patterns were obtained from samples containing more than one generation of a mineral, with different isotopic signatures contributing to the age spectra.

1.2 Areas studied for this thesis

The first project reported in this thesis (Chapters 2, 3 and 4) is a study of the metamorphic history of the island Naxos, which is part of the Attic Cycladic Metamorphic Belt (ACMB) in the Aegean Sea. As part of the Alpine orogenic belt in southern Europe, the ACMB is located in a still very active tectonic environment. The metamorphic history of the region is mainly confined to the Tertiary, with ages of 45 $\pm$ 5 Ma associated with the earliest event, and evidence for a younger metamorphism with which isotopic ages as young as 10 to 15 Ma are found (Andriessen et al. 1979).

The second project reported in this thesis is a study of metamorphic rocks from the Archaean crustal blocks of Western Australia. The major part of this study is on the Western Shaw Greenstone Belt and its adjacent granitoid-gneiss terrains in the eastern part of the Pilbara region of tropical Western Australia (Chapter 5). A smaller project was a study of the Mount Narryer metamorphic belt in the northwestern section of the Yilgarn Block (Chapter 6). In these areas, continental crust was formed during the Early Archaean. In the Pilbara the earliest recognized crustal formation occurred between 3.6 and 3.45 Ga ago (Pidgeon 1978a, Hamilton et al. 1981, Bickle et al. 1983), whereas in the northern Yilgarn Block early crustal formation occurred between 3.6 and 3.75 Ga ago (De Laeter et al. 1981b, 1985, Kinny et al. 1985), and possibly as long ago as 4.2 Ga (Froude et al. 1983). Most of the metamorphic and tectonic history of these areas is confined to the Archaean, which resulted in the excellent preservation of the Archaean signatures in these rocks.

1.2.1 The study of Alpine metamorphism on Naxos

On Naxos, the largest and central island of the Cycladic Archipelago in the Aegean Sea, many of the features of the ACMB are well represented: the early high pressure, medium temperature metamorphism, designated M_1, is recognized; a subsequent medium pressure, high temperature metamorphism, M_2, associated with the formation of a thermal dome in central Naxos; and a late I-type granodiorite intrusive is located on the west coast of the island. Its varied geology have made Naxos target for a series of

petrological, geochemical, and geochronological studies (summarized in Chapter 2), providing a background to the present study.

Only a few studies have as yet applied the $^{40}Ar/^{39}Ar$ age spectrum technique to minerals from metamorphic rocks from the Alpine orogenic belt in southern Europe. Chopin and Maluski (1980) have studied overprinting and resetting of white micas from the Gran Paradiso area in northern Italy, Roddick et al. (1980) have studied biotites containing excess argon from Austria, and Spray and Roddick (1980) and Roddick et al. (1979) report work on ophiolites in southeastern Europe. The study of Chopin and Maluski (1980) is concerned with some of the problems related to the interpretation of white mica ages during low grade overprinting. The white micas studied by them come from a geological environment, which is very similar to that found in southeast Naxos. The problems related to resetting of isotopic ages of white micas in such environments will be discussed in Chapter 3 and in Appendix III, which contains the manuscript of an article dealing with the resetting of isotopic ages of white micas. Also, little $^{40}Ar/^{39}Ar$ data exist on young metamorphic hornblendes. In this study, age spectra are presented on hornblendes from metamorphic rocks of Naxos with ages in the range of 11 to 16 Ma; these results indicate that useful information can be obtained from stepheating experiments on minerals with low potassium contents in this age range. In Chapter 4, an investigation into the thermal evolution of the ACMB is given, on the basis of constraints obtained from the isotopic study.

1.2.2 $^{40}Ar/^{39}Ar$ geochronology of W. Australian Archaean Terrains

Studies of Archaean rocks by the $^{40}Ar/^{39}Ar$ age spectrum method are still relatively few. Earlier studies by Pankhurst et al. (1973) and by Dallmeyer (1982) concentrated on the geochronology of Archaean high grade gneiss terrains, whereas Martinez et al. (1984) studied very low grade metavolcanic rocks using wholerock samples. Thus our attempt to date the metamorphic evolution of a greenstone belt in the Pilbara region of Western Australia by stepheating experiments on metamorphic minerals is the first of its kind. The study had two objectives, firstly to

test the suitability of the method for dating metamorphic minerals of Archaean age, and secondly, upon a positive outcome of the first objective, to apply the method to metamorphic minerals from a greenstone environment. The area where the major part of this study was carried out is the Western Shaw Greenstone Belt in the southeast of the Pilbara region of Western Australia, and has been previously the focus of detailed study of the stratigraphy (Hickman and Lipple 1978, Hickman 1980, 1983), the geological structure (Bickle et al. 1980, Bettenay et al. 1981, Bickle et al. 1984), and the geochronology (De Laeter et al. 1975, Oversby 1976, Pidgeon 1978a, b, Cooper et al. 1982, Blake and McNaughton 1984). These studies provide a fairly detailed background of the geology of this region, which justifies the initiation of a study concentrating specifically on dating of metamorphic minerals.

The eastern Pilbara region is a typical example of a granitoid-greenstone terrain. Following an early period of crustal formation between about 3.6 and 3.45 Ga, two discrete periods of tectonism were documented in the Western Shaw area during its subsequent geological history. The youngest event caused the formation of greenstone belts and granitoid-gneiss domes in their present configuration. This event was probably accompanied by regional high grade metamorphism which was argued to have occurred about 2950 Ma ago (Oversby 1976, Hickman 1981). Within the greenstone belts, there is evidence for earlier metamorphism and deformation. This event is not very well dated, but from structural inferences it was argued to have preceded the late regional high grade metamorphism, and possibly was not related to processes related to dome forming in the granitoid-gneiss terrains (Bickle et al. 1980, Bettenay et al. 1981). The present study concentrates on mineral samples from metavolcanic rocks from within the greenstone belts and from rocks located near, or within the granitoid-gneiss terrains, aiming to identify different ages in both groups, either to find confirmation of regional high grade metamorphism, or more excitingly, to find older ages which can be attributed to earlier metamorphism within the greenstone belts.

A separate study into the geochronology of the Mount Narryer metamorphic belt is reported in Chapter 6. Located in the northern part of the Western Gneiss Terrain of the Yilgarn Archaean Block in Western Australia, the Mount Narryer metamorphic belt has become a focus of detailed geochronological study in recent years, because of the identification of several 4100 to 4200 Ma old detrital zircons in metasedimentary quartzites (Froude et al. 1983). In this thesis, a joint study by D.O. Froude and myself into the age of deposition and subsequent metamorphic history of the metasedimentary belt is reported. This work has implications for the interpretation of the regional geology of this area, including possibly deriving constraints on the time when the very old source rocks of the above mentioned detrital zircons were still present at the Earth's surface, and on the age of high grade metamorphism in the metasediments.

1.3 Argon dating

1.3.1 Basic assumptions

Both the conventional K-Ar and the $^{40}Ar/^{39}Ar$ methods rely on the accumulation of $^{40}Ar^*$ in a material, which was formed by radioactive decay of naturally occurring ^{40}K. An age can be calculated from the ratio of $^{40}Ar^*$ to ^{40}K in a sample. $^{40}Ar^*$ is measured mass spectrometrically after the argon is extracted from the sample in a high vacuum extraction line. For the conventional K-Ar method, the absolute amount of $^{40}Ar^*$ is measured, using a known quantity of a high purity ^{38}Ar spike, whereas in the $^{40}Ar/^{39}Ar$ method an age is calculated from the $^{40}Ar^*/^{39}Ar_K$ ratio of an extracted gas fraction (for details see Appendix I). In practice, the amount of ^{40}K of the sample is measured indirectly, by chemical determination of the potassium concentration using a flame photometer in the conventional K-Ar method, or from the ^{39}Ar content of a gas fraction (which is a measure for the ^{39}K content of a sample) in the $^{40}Ar/^{39}Ar$ method. Both methods for determining the ^{40}K content of a sample are based on the assumption that the isotopic composition of naturally occurring potassium is constant, and independent of the geological environment of the sample. In the present study, the recommended values for the abundance and for the decay constants of ^{40}K were used (Steiger and Jäger 1977).

For a calculated K-Ar age to have a geological meaning, some basic assumptions need to be fulfilled. Firstly, decay of ^{40}K should occur at a constant rate, and should be independent of factors which influence the geological environment of the sample. Secondly, all ^{40}Ar in the sample is either produced by in situ decay of ^{40}K, or a contaminant with the isotopic composition of present day atmospheric argon. Thus, during crystallization no extraneous, or inherited ^{40}Ar may have been incorporated in the crystal structure. Thirdly, the minerals should have remained a closed system to both K and Ar during the time interval between the start of argon accumulation and analysis. Lastly, for a calculated age to have geological significance, cooling after an event during which a mineral was formed should have been rapid.

The $^{40}Ar/^{39}Ar$ age spectrum method is potentially more powerful, because gradients in the ^{40}Ar concentration of a sample can be detected, thus making the requirement of closed system behaviour for argon less stringent. Further, recent analyses of slowly cooled K-feldspars from an area with a well known thermal history yielded $^{40}Ar^{*}$ concentration gradients which could be understood in terms of a model based on the assumption that argon was lost from the minerals by volume diffusion (Harrison and McDougall 1982).

1.3.2 Interpretation of results

In contrast with the conventional K-Ar method, for which an age is calculated from measurement of the absolute amounts of ^{40}K and ^{40}Ar on different splits of a sample, in the $^{40}Ar/^{39}Ar$ method an age is obtained from measuring isotopic ratios of argon in a single split of a sample (see Appendix I). This approach is made possible by irradiation of the samples with fast neutrons in a nuclear reactor to cause the reaction ^{39}K (n,p) ^{39}Ar. The ^{39}Ar content of the sample thus becomes a measure of the potassium concentration in the sample, and when the conditions of irradiation are known (usually from simultaneous irradiation of a standard with a known K-Ar age), an apparent age can be calculated from the $^{40}Ar^{*}/^{39}Ar_{K}$ ratio of the sample. The technique has the potential of more precisely dating small samples, because sample splitting is avoided and measurement of absolute concentrations is not necessary. A second important advantage of the $^{40}Ar/^{39}Ar$ method is that because age information is obtained from the ratio of isotopes of the noble gas argon, multiple extraction using a step wise heating technique becomes possible. The results of a stepheating experiment, a series of $^{40}Ar^{*}/^{39}Ar_{K}$ (i.e radiogenic ^{40}Ar, potassium derived ^{39}Ar) ratios, are usually presented as a series of apparent ages plotted against the fraction of ^{39}Ar released per temperature step. Another possible form of presenting results is in a $^{39}Ar/^{40}Ar$, $^{36}Ar/^{40}Ar$ isotope correlation diagram.

In its simplest form a $^{40}Ar/^{39}Ar$ age spectrum consists of a number of identical apparent ages obtained from gas fractions extracted at progressively higher temperature steps, from typically about 400 ^{o}C until fusion of the sample. This kind of age spectrum is expected for samples that cooled rapidly after crystallization, and have remained undisturbed until analysis. If radiogenic ^{40}Ar was partially lost from the minerals by volume diffusion during a thermal disturbance subsequent to crystallization, the remaining $^{40}Ar^{*}$ in the minerals will display a concentration gradient, increasing from low concentrations at the rims of the crystals to higher concentrations in the cores. In ideal cases, such ^{40}Ar concentration gradients can be resolved by stepheating experiments. When the resolution in the age spectrum is sufficient, the interpretation under Turner's diffusion model suggests that high ages in the high temperature steps of the experiment approximate the age of original initiation of argon accumulation within the crystals, and low ages obtained in the low temperature steps approximate the time of thermal overprinting (Turner et al. 1966, Turner 1968, see also Fig. 1.1 and its caption).

Harrison (1983) has discussed the effect of multiple episodic loss on this model, and concluded that in many cases it is impossible to distinguish between single and multiple episodic loss, because differences are beyond the resolution of an age spectrum. Also, because of the finite resolution in an age spectrum, the exact time of overprinting is generally not well constrained in age spectra that have experienced only limited subsequent argon loss. Both complications suggest that additional information is desirable to constrain the age of overprinting more precisely. Meaningful information as to gradients in the distribution of radiogenic or excess ^{40}Ar can only be obtained when the resolution of the age spectrum is good enough to recognize trends of apparent ages (Harrison 1983). In this thesis a balance was sought between the resolution required, the minimum stepsize that can be accurately measured, and a time efficient experimental technique. For Alpine hornblendes, which are relatively low in $^{40}Ar^{*}$, experiments typically consisted of 12 to 15 steps, whereas the other minerals, Alpine muscovites and biotites, and Archaean hornblendes, muscovite and plagioclase

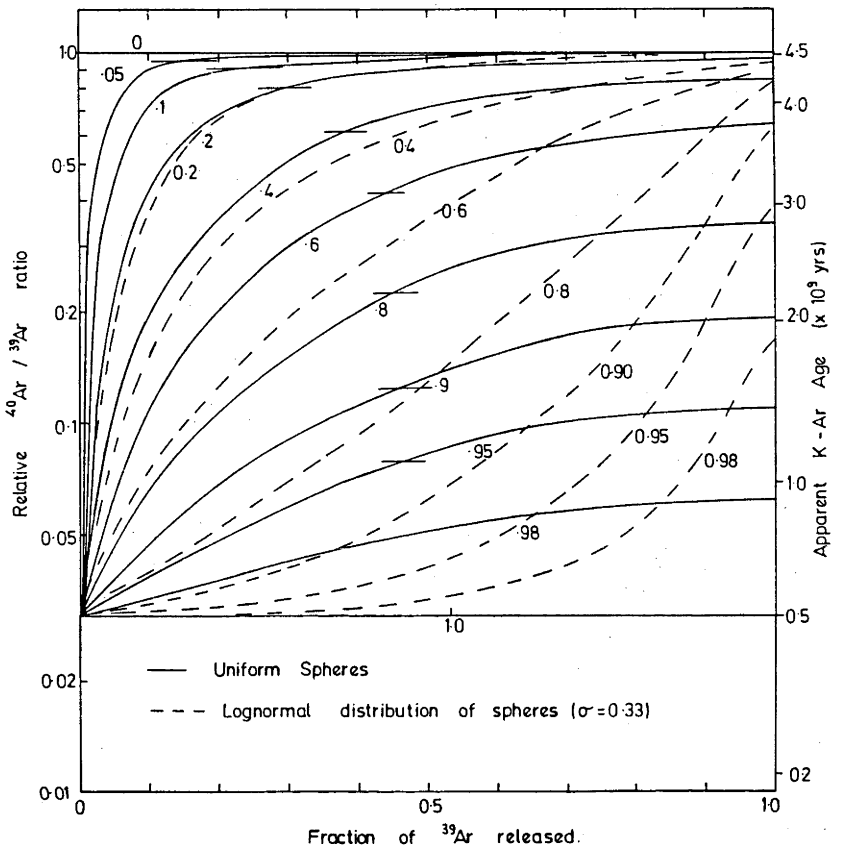

Figure 1.1. Theoretical age spectra calculated with the model of Turner (1968) for a sample with an original age of 4.55 Ga and loss of radiogenic argon during a thermal pulse 0.5 Ga ago. For the calculation Turner assumed diffusion from spherical grains. The solid curves represent the model age spectra for a sample with one uniform grain size, and the dashed curves represent model age spectra assuming a lognormal grain size distribution. The implications of this model for the interpretation of age spectra are discussed in the text.

contained sufficient $^{40}Ar^{*}$ to allow at least 15 to 20 steps to be measured.

Diffusion of excess ^{40}Ar into the crystals subsequent to the beginning of argon accumulation in the crystals may cause high apparent ages in the low temperature steps of an experiment decreasing to apparent ages which approximate the 'true' age in the higher temperature steps. Another group of age spectra commonly associated with excess argon are the U- or saddle shaped age spectra, which consist of high apparent ages in the low temperature steps decreasing to a minimum, and increasing again in the highest temperature steps. This sort of age spectrum, which is common in feldspars, for example, cannot be explained by diffusion of argon from, or into a simple crystalline material. Interpretations of such age spectra in terms of diffusion from chemically distinct regions in the minerals at contrasting diffusion rates, or from different classes of crystallographic sites within the minerals have been discussed (Harrison and McDougall 1981, Claesson and Roddick 1983). Saddle shaped age spectra from areas with well known geological histories indicate that the minimum ages of these age spectra must be interpreted as maximum estimates for the age of initiation of argon accumulation in the minerals (Lanphere and Dalrymple 1976, Harrison and McDougall 1981). Recently, attempts have been made to understand more complex age spectra of mixtures of minerals in terms of summation of diffusion losses expected for the individual phases (Gillespie et al. 1982).

The reaction ^{39}K (n,p) ^{39}Ar, on which the $^{40}Ar/^{39}Ar$ method is based, occurs under the influence of fast neutrons in a nuclear reactor. Some of the energy involved in this nuclear reaction is released as kinetic energy of the newly formed argon isotope. The recoil effect is a potential source of uncertainty for $^{40}Ar/^{39}Ar$ dating, because it may alter the distribution of ^{39}Ar with respect to potassium and $^{40}Ar^{*}$ in the material used for dating. Experiments designed to assess the importance of recoil on age spectra were discussed by Turner and Cadogan (1974), and by Huneke and Smith (1976). These experiments suggest that the combination of small particle sizes and a mixture of phases with contrasting potassium contents in the sample may cause recoil artifacts in an age spectrum. In terrestrial studies, including

this thesis, the method is applied to coarse grained monomineralic samples. Under these conditions recoil effects are in general unimportant. This view is supported by perfectly flat age spectra obtained from samples in areas with well known simple cooling histories (e.g Tetley 1978, McDougall 1981).

Another approach to the interpretation of data from $^{40}Ar/^{39}Ar$ stepheating experiments is by isotope correlation diagrams. For the presentation of results from stepheating experiments, the $^{39}Ar/^{40}Ar$, $^{36}Ar/^{40}Ar$ diagram is the most appropriate type (Roddick 1978). This diagram is based on the assumption the measured gas fractions are a mixture of a radiogenic and a non-radiogenic component. By fitting a straight line (York 1969) through a set of points of approximately similar age, the one intercept ($^{39}Ar=0$) will provide a measure of the isotopic composition of the non-radiogenic component of the gas, and the other intercept ($^{36}Ar=0$) the isotopic composition and apparent age of the radiogenic component. For the present study, most (sub-)horizontal segments in age spectra were examined by this technique, and in many cases good agreement with calculated integrated ages was obtained. However, in some cases variation in the non-radiogenic component was minor so that no good mixing line was defined.

1.3.3 $^{40}Ar/^{39}Ar$ age spectra as diffusion experiments

As discussed above, the $^{40}Ar/^{39}Ar$ age spectrum method is most powerful when the results can be understood in terms of models based on diffusion theory, which implies that a stepheating experiment is essentially a diffusion experiment. For the interpretation of results from diffusion experiments one of the ground rules is that the original mineral must remain stable during the experiment (Mussett 1969, Giletti 1974). This rule is normally violated in stepheating experiments on hydrous minerals, because in a high vacuum line dehydration reactions will occur at moderate temperatures. However, although this may cause problems in obtaining reproducible diffusion parameters from $^{40}Ar/^{39}Ar$ stepheating experiments, the observation is that from white micas and hornblendes ^{40}Ar concentration gradients can be resolved, thus providing empirical support for interpreting stepheating experiments in terms of diffusion models. The experience with

biotites is that in many cases no ^{40}Ar gradients can be resolved, as indicated by seemingly undisturbed age spectra, which, on the basis of independent evidence, must be interpreted as affected by excess argon (Pankhurst et al. 1973, Roddick et al. 1980, Foland 1983).

In the interpretation of age spectra, in many cases special significance is given to observed (sub-)horizontal segments, or plateaus, as 'improved' K-Ar ages. Commonly used criteria defining an acceptable plateau were discussed by Fleck et al. (1977) for the interpretation of their wholerock data on Antarctic volcanic rocks. It follows from the discussion presented above that for the interpretation of $^{40}Ar/^{39}Ar$ age spectra of disturbed metamorphic minerals the plateau concept is of less value, because under diffusion models, as described by Turner et al. (1966) and by Harrison (1983), sub-horizontal segments in disturbed age spectra will only approximate the original age of the sample. A good approximation of the original age is obtained only when gas losses are less than about 20 percent (Fig. 1.1 and caption). Greater gas losses will result in substantial deviations from the original age when the sample has a uniform grain size distribution, and when the sample has a lognormal grain size distribution no (sub-)horizontal segment will be recorded at all. Thus when an age spectrum contains a (sub-)horizontal segment, but the individual apparent ages rise slowly to a maximum in the final step, the apparent age of that final step will more closely approximate the original age of the mineral than the averaged age over the sub-horizontal segment. In this thesis, in cases where an average age is calculated over a sub-horizontal or plateau segment of an age spectrum, it will be designated as an integrated age, to indicate that it is interpreted as an average age over that segment of the age spectrum only.

1.4 Thermal histories

The interpretation of results of geochronological work in terms of thermal histories of a region is based on the empirical observation that some minerals resist resetting during thermal overprinting better than others. This observation was documented in contact zones (Hart 1964, Hanson and Gast 1967), as well as in regional metamorphic terrains (Armstrong et al. 1966, Jäger et al. 1967, Wagner et al. 1977, Purdy and Jäger 1976). From these observations a generalized trend of decreasing retentivity was established, where hornblende K-Ar ages were found to be the most retentive, followed by muscovite Rb-Sr ages, muscovite K-Ar ages, biotite K-Ar and Rb-Sr ages, and apatite fission track ages. In the Swiss Alps, a temperature calibration for resetting of these minerals was obtained from the petrology of overprinting mineral assemblages: hornblende K-Ar, about 540 ^{o}C (Steiger 1964), muscovite Rb-Sr 500 $\pm$ 50 ^{o}C (Jäger 1973, 1979), muscovite K-Ar 350 $\pm$ 50 ^{o}C (Jäger 1979), and biotite K-Ar and Rb-Sr 300 $\pm$ 50 ^{o}C (Jäger 1979).

When reliable diffusion data are available, closure temperatures can be calculated for cooling through the temperature interval where the change occurs from fully open system to closed system behaviour for diffusion loss of radiogenic argon (Dodson 1973, 1979). For this case the closure temperature of a mineral was defined as the temperature of the mineral at its apparent age. The closure temperature can be calculated from the equation:

$$T_c = Q \,/\, (R.\ln((A.T_c^2.D_o.R) \,/\, (a^2.\mp.Q))$$

In this equation T_c is the closure temperature, A a geometrical factor (55 for a sphere, 27 for a cylinder), D_o the diffusion constant, R the gas constant, a the diffusion radius, Q the activation energy for diffusion, and $\mp$ the cooling rate. Using available data on diffusion in hornblende, muscovite and biotite obtained from hydrothermally controlled experiments (see Table 1.I and caption), closure temperatures can be calculated assuming an average diffusion radius of 0.0085 cm, and a cooling rate of 30 ^{o}C/Ma. For the diffusion radius, the average sample grain radius was used. Because it is demonstrated subsequently (see Chapter 3, 5 and 6) that ^{40}Ar gradients can be resolved, the

average grain radius provides a maximum estimate for the effective diffusion radius of the samples. The closure temperatures for hornblende, muscovite and biotite are 519 °C, 409 °C, and 309 °C respectively. Apart from the T_c for muscovite which is slightly higher than the estimate from petrological calibration, agreement with the previously mentioned values for blocking temperatures is good. In areas where the cooling rate was 3 °C/Ma, instead of 30 °C/Ma, calculated closure temperatures would be about 10 percent lower. For both areas studied in this thesis, there are arguments that justify an assumption that cooling after high grade metamorphism was rapid (i.e. in the order of 10 to 50 °C). Thus estimates for closure temperatures of 500 to 550 °C for hornblendes, 360 to 420 °C for muscovites and 280 to 320 °C for biotite K-Ar ages will be used.

Combination of geochronological data with closure temperature information allows the derivation of thermal histories for an area (Harrison et al. 1979). Such an approach can be valuable when precise geochronological information is available, and when it can be established that the area was not affected by mild subsequent thermal events which caused partial resetting of some less retentive isotopic systems, leaving the more retentive systems unaffected. Thus, such an approach is likely to be most promising in younger metamorphic terrains, as the Attic Cycladic Metamorphic Belt on Naxos. For the very old metamorphic history of the eastern Pilbara region of Western Australia, where there is some evidence for younger mild overprinting, such an approach will be more difficult.

Table 1.I. Argon retention in minerals

mineral	Q(kcal/mol) $D_0(cm^2/s)$	T_c 1)	T_c 2)	T_b 3)
biotite	49.7 4) 0.13	283	309	300 5)
muscovite	40.0 6) $6.03*10^{-7}$	366	409	350 5)
hornblende	64.1 7) 0.024	483	520	540 8)

Comparison of blocking temperatures as estimated for the Swiss Alps, with closure temperatures calculated for cooling systems using the equation of Dodson (1973, 1979). The equation and parameters used to obtain the numbers as listed under 1) and 2) are discussed in the text.

1) closure temperature, cooling rate 3 °C/Ma
2) closure temperature, cooling rate 30 °C/Ma
3) blocking temperature, estimated for Swiss Alps
4) diffusion parameters of biotite (Harrison et al. 1985)
5) blocking temperature (Jäger 1979)
6) diffusion parameters of muscovite (Robbins 1972)
7) diffusion parameters of hornblende (Harrison 1981)
8) blocking temperature (Steiger 1964)

Chapter 2

The geology of Naxos, and its place in the Alpine Orogeny

2.1 Introduction

2.1.1. Aims of present work

The next chapters report a study into the geochronology and thermal history of the Attic Cycladic Metamorphic Belt (ACMB) as exposed on Naxos, an island in the Aegean Sea. The Aegean Sea is located between mainland Greece and Turkey. Its southern margin is formed by the island of Crete (Fig. 2.1a, b). Current interpretations identify the Aegean as a back arc basin, formed by crustal extension in the last 4 to 13 Ma (McKenzie 1978, Le Pichon and Angelier 1979, Horvath and Berckhemer 1982). It was suggested that oceanic lithosphere belonging to the most eastern of the Mediterranean basins, the Levantine Basin, subducts below continental lithosphere of the Apulian-Anatolian Microplate from a trench system consisting of the Hellenic Trench, the Plini Trench and the Strabo Trench, positioned in a semicircle from the west of the Peloponesos, via the south of Crete to just south of the island of Rhodos (Fig. 2.1a, b). Evidence for island arc volcanism is found at Aegina, Mylos, Thira, Antiparos and Kos in the southern part of the Aegean Sea and is considered to be related to subduction from this trench system (Nicholls 1971, Dewey et al. 1973). South of the volcanic arc is the Sea of Crete which is interpreted as a young extensional basin, locally more than 1000 m deep, and underlain by thinned continental crust (Makris 1978).

Just north of the volcanic arc, the Attic Cycladic Metamorphic Belt is exposed (Fig. 2.1a, b). Rocks from this belt, on the Greek mainland, can be traced to the north as far as Mt Olympos. To the east the Attic Cycladic Metamorphic Belt can be followed into Turkey in the Menderes Massif. Rocks from this belt are mainly of Mesozoic sedimentary origin and have experienced high pressure metamorphism between the Late Cretaceous and the Eocene (Dürr et al. 1978, Altherr et al. 1979, Andriessen et al. 1979, Bonneau et al. 1980, Maluski et al. 1982). Subsequently, during the Miocene local high temperature metamorphism occurred, accompanied by the intrusion of granitoids. The metamorphic history of the Attic Cycladic Metamorphic Belt is determined by processes that take place in the vicinity of an active Benioff zone (Ernst 1973) and subsequently further away from the Benioff

zone within the continental crust. The metamorphic history suggests that in the beginning of the Tertiary, the continental crust in the Aegean may have been in excess of 60 km thick. Presently, the thickness of the continental crust under the ACMB is estimated at 30 to 32 km (Makris 1978). A study of the metamorphic history rocks from the Attic Cycladic Metamorphic Belt may provide important constraints on the geodynamic evolution of the Aegean Basin.

It is important for understanding the tectonic evolution of the region that the metamorphic phases are dated accurately. The present work attempts to provide a detailed thermal history, by dating minerals formed during various stages of the thermal history using the $^{40}Ar/^{39}Ar$ stepheating method. Naxos was chosen for this study, because of its central location in the Attic Cycladic Metamorphic Belt and because most thermal and tectonic phases experienced by rocks of the belt are well represented on Naxos.

In the second part of this study attempts are made to place the metamorphic history of Naxos in a geodynamic context. The pressure-temperature-time path (P-T-t path) for Naxos will be evaluated with computed thermal histories based on numerical thermal models (Harrison and Clarke 1979, Parrish 1982). From this kind of work it may be possible to assess the importance of some of the parameters, as for example radioactive heat production, or uplift rate, which constrain in the evolution of the thermal structure of continental crust.

In relation to Naxos one of the outstanding problems is the formation of the thermal dome in the centre of the island. The origin of thermal domes is a matter of discussion. They are generally too small to be formed by blanketing with a thick sedimentary pile as proposed for the Tessin metamorphism in the Swiss Alps (Trümpy 1973). Other interpretations involve deepseated hydrothermal heat transfer (Schuiling and Kreulen 1979), intrusion of magma at depth (Tetley 1978, Vernon 1982) and the thermal effects of differential uplift and erosion (England and Richardson 1977). Thermal modelling may provide constraints as to the various possibilities.

Figure 2.1. a Tectonic sketch map of the Aegean and surrounding areas. N = Naxos, R = Rhodes, P = Peloponesos, E = Evvia, o = Olympos belt, ac = Attic Cycladic belt, m = Menderes belt, va = volcanic arc, h = Hellenic Trench, p = Pliny Trench, s = Strabo Trench. Open arrow indicates movement of the Levantine Basin seafloor with respect to the Eurasian Plate. Thin arrow indicates the movement of Crete with respect to the Attic Cycladic belt. Circle with arrow indicates the rotation of the Peloponesos in the last 5 Ma. (after Angelier et al. 1982. Le Pichon et al. 1982, Laj et al. 1982). The Hellenic

Trench system is located at the southern margin of the Apulian Microplate. Presently arc related volcanism occurs only in the Aegean Sea. Major transform faults separate the African Plate from the Arabian Microplate in the east, the Turkish subplate, part of the Apulian Microplate moves west along transform faults with the African plate in the south, the Arabian Microplate in the east and the Eurasian Plate in the north. In the Greek subplate the mainly sedimentary outer arc is located on the continental side of the trenches, in the Aegean Sea it is followed by a major extensional basin (the movement of Crete toward the trench is indicated), the south Aegean volcanic arc is located in a semicircle parallel to the Attic Cycladic Metamorphic Belt. Granitoid intrusives in the ACMB were dated between 8 Ma and 15 Ma (Dürr et al. 1978, Altherr et al. 1982). Box I indicates an area where 25 to 30 Ma old granitoids occur (Dürr et al. 1978). Box II indicates an area where an about 28 Ma old granitoid and about 25 to 16 Ma old calc-alcaline volcanism occurs (Innocenti et al. 1982). Box III indicates an area where about 25 to 16 Ma and 12 Ma old calc-alcaline volcanism occurs (Innocenti et al. 1982). These ages which are related to arc magmatism suggest migration of the arc toward the south since the Miocene.

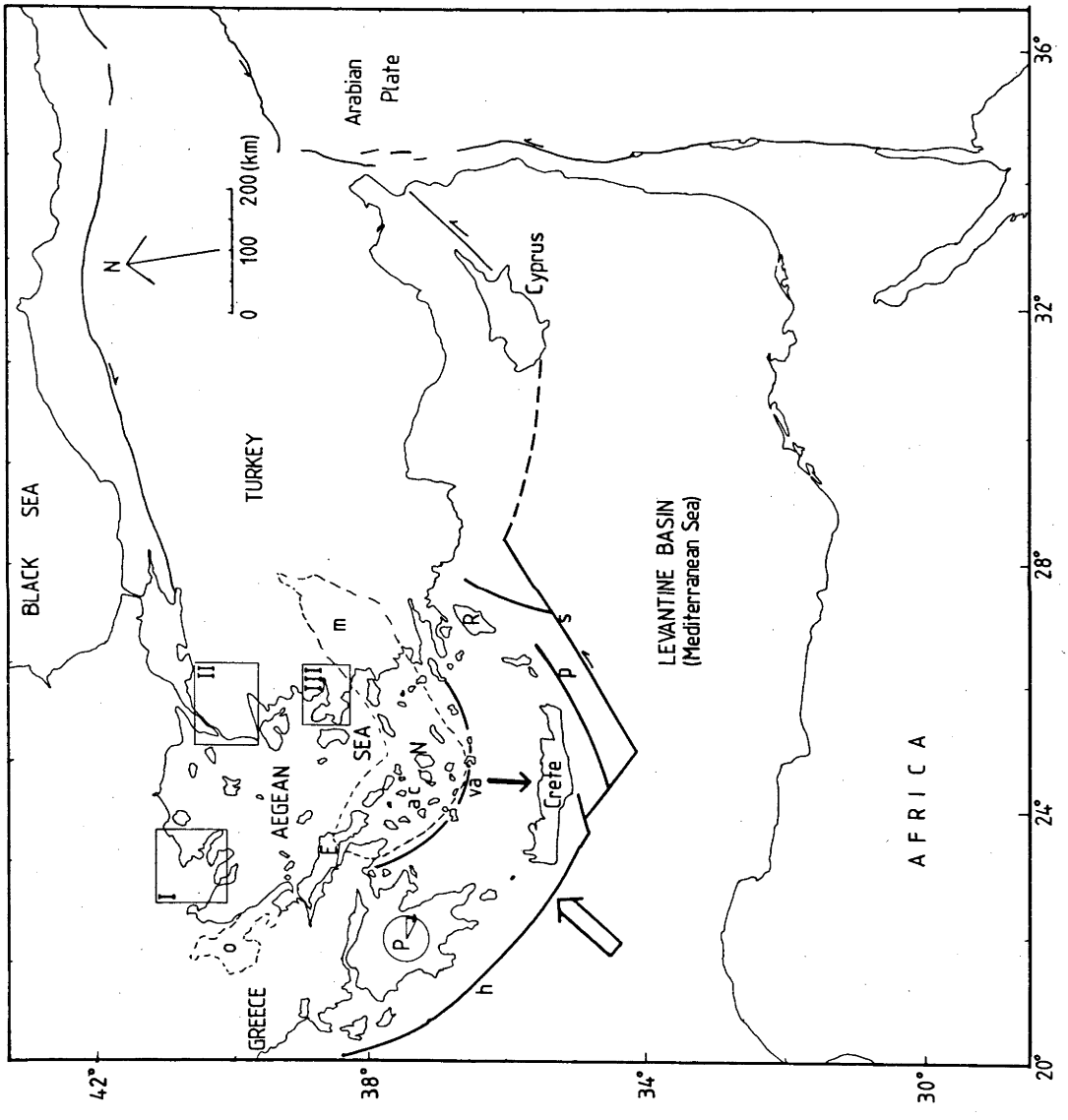
BLACK SEA
TURKEY
Arabian Plate
N
0 100 200 (km)
Cyprus
LEVANTINE BASIN
(Mediterranean Sea)
AEGEAN SEA
GREECE
Crete
AFRICA
I
II
III
m
R
s
p
h
P
42°
38°
34°
30°
20°
24°
28°
32°
36°

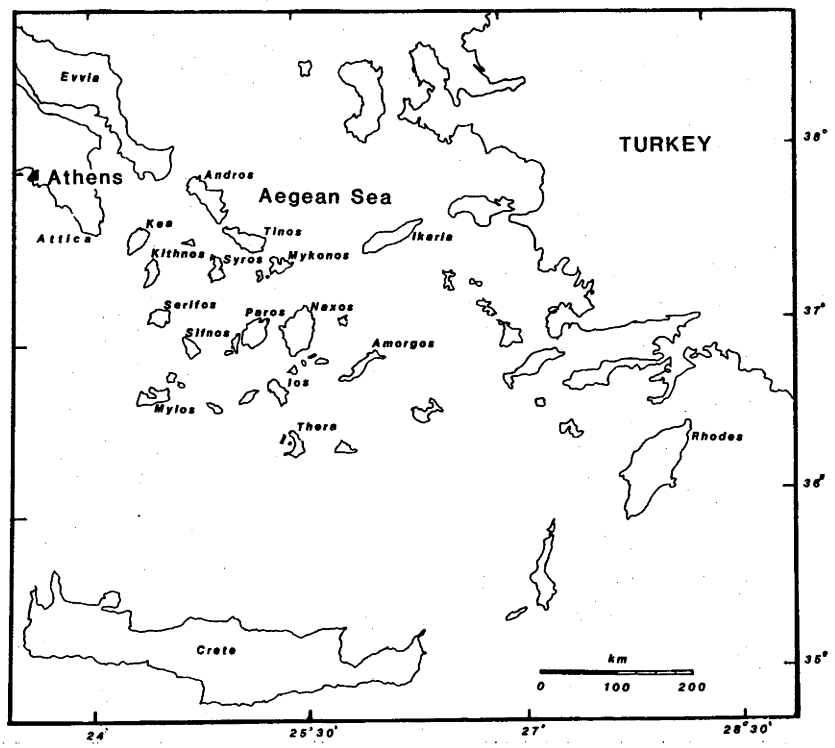

b Geography of the Aegean Sea and surroundings.

2.1.2 An Alpine perspective

The Alpine Orogeny can be defined as resulting from interaction between the African Plate and the Eurasian Plate since the beginning of the opening of the Atlantic Ocean, which led to the closure of the Tethys Ocean in the Mesozoic. Large areas in Southern Europe and the Middle East have been affected by it. The present study concentrates on a small part of that area. It may, therefore, be useful to place this study in an Alpine perspective.

The idea that the Alpine mountain chain might result from interaction between Africa and Europe was already suggested in the beginning of this century by Argand (1916), Heim (1922) and Staub (1924). It is, therefore, interesting to note that after the plate tectonic model was established in the mid to late 1960's, application to Alpine Europe had a rather slow start. This may have been the result of, on the one hand, an apparent lack of obvious plate tectonic features like island arcs, trench systems and subduction zones. On the other hand, there were theories readily available which explained many tectonic features of the Alps, without invoking large scale plate movements (e.g. Van Bemmelen 1972).

From palaeomagnetic study of southern Europe, since the middle 1960's (Zijderveld 1967), and from seismic observations (McKenzie 1970), and subsequently from the cruises of the Deep Sea Drilling Project in the Mediterranean Sea, it became apparent that the Mediterranean could provide important keys to the understanding of the geodynamic history of southern Europe. Important results of this early interest in the Mediterranean were:

1. The recognition that in the past, parts of what is presently southern Europe, have moved independently as microplates, or have moved as a part of the African Plate (Dewey et al. 1973, Hsü et al. 1978, De Jong et al. 1969, Zijderveld et al. 1970, Lowrie and Alvarez 1975, Channel and Tarling 1975, Klootwijk and Van den Berg 1975).
2. From the seismicity, especially in the eastern part of the Mediterranean, the location of presently active plate boundaries could be determined (McKenzie 1970, Dewey et al. 1973).

3. The recognition of trench systems, arc related volcanism and subduction zones (e.g. Nicholls 1971, Hsü 1971, Dewey et al. 1973).

These observations suggested that the geodynamic evolution of southern Europe could be interpreted in terms of a plate tectonic model.

2.1.2.1 The tectonic evolution of S.E. Europe

The tectonic evolution of the Mediterranean and surrounding areas from the Mesozoic until the present is mainly characterized by compression. The relative movement between the Eurasian Plate in the north and the African Plate in the south has caused a gradual decrease of the width of the space separating the two plates (Fig. 2.2). This movement has led to the closure of the oceanic basin, the Tethys, which originally separated the two plates. The tectonic history is considerably complicated by processes which occurred at a smaller scale while closure of the Tethys Ocean progressed. During the Mesozoic parts of the northern margin of the African Plate broke away, which resulted in the formation of a series of small oceanic basins along the northern margin of the African Plate. The Levantine Basin of the Mediterranean is commonly interpreted as an example of the basins, which were formed during this period (Smith and Woodcock 1982, Dewey and Sengör 1979, Bonneau 1982, Altherr et al. 1982b). The blocks of continental crust which separated from the African Plate in the Mesozoic have accelerated the closure of the Tethys Ocean and are presently locked against the southern margin of the Eurasian Plate (Fig 2.2). Taken together, they are referred to as the Apulian-Anatolian microplate (Smith and Woodcock 1982), which comprises parts of Turkey, Greece, Jugoslavia and Italy. Within the Apulian-Anatolian microplate, there is evidence for a complex tectonic history. It is suggested that parts of the Apulian-Anatolian microplate have moved independently in the past and are still to some degree moving independently today (Dewey et al. 1973, Dewey and Sengör 1979, Jacobshagen et al. 1978, Bonneau 1982, Altherr et al. 1982b, Sengör and Yilmaz 1982). A different interpretation was proposed by Nur and Ben-Avraham (1982), who contend that the southern margin of Eurasia consists of a great number of displaced terrains, and the main convergent margin is

Figure 2.2. Main plate movements in the Eastern Mediterranean. The movements of the individual plates are given with respect to a fixed window ($20^{o}W$ - $60^{o}E$, 0^{o} - $50^{o}N$). Each frame contains two positions, the position at the beginning of the time interval is given in a light line, the position at the end of the time interval is given in a heavy line. The relative movement of Eurasia and Africa with respect to the window is indicated by the arrows. The position of the Apulian-Anatolian microplate at the beginning of a time interval is given by the heavily shaded outline and its position at the end of the time interval is indicated by the light horizontially lined outline. The closure of the Tethys Ocean through time is indicated by the crossed double arrows on the right of each frame.

A = Present to 20 Ma BP.

B = 20 Ma to 60 Ma BP.

C = 60 Ma to 100 Ma BP.

D = 100 Ma to 180 Ma BP.

(after Smith and Woodcock 1982).

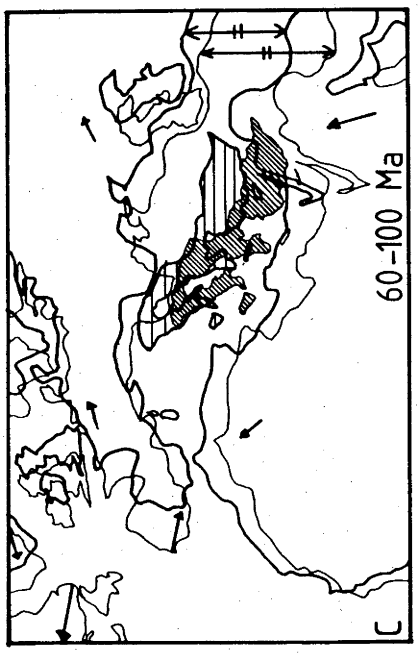
C
60-100 Ma

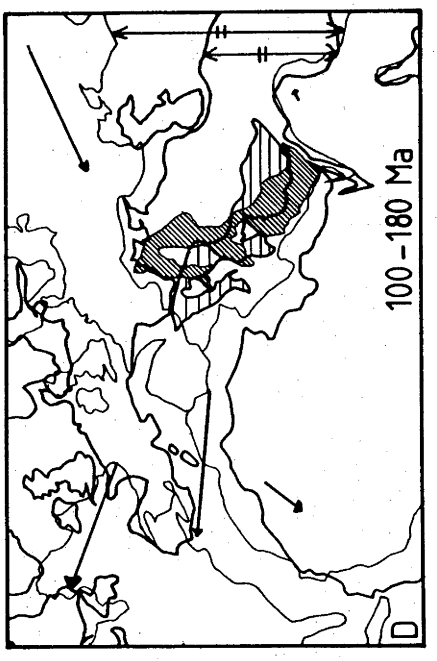
D
100-180 Ma

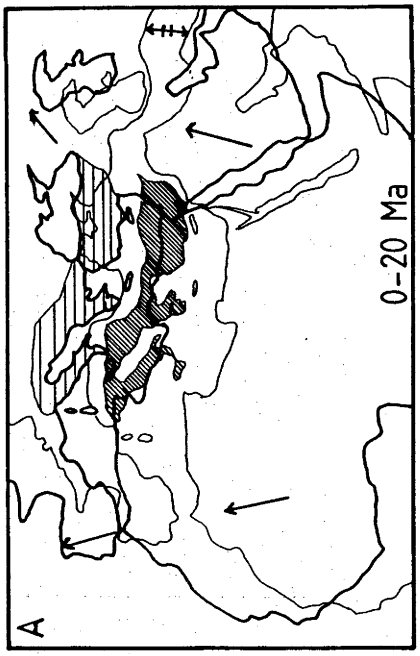
A
0-20 Ma

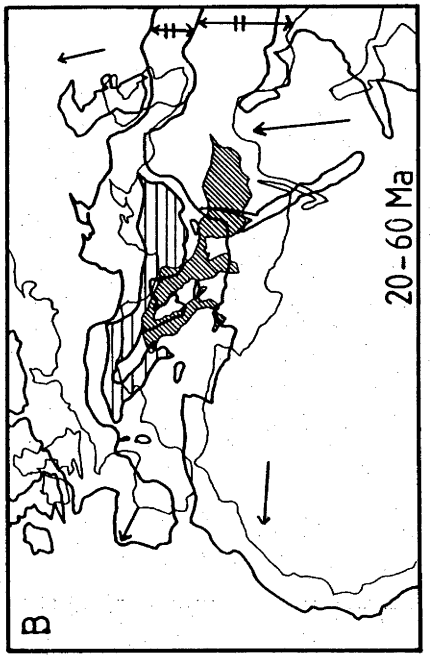
B
20-60 Ma

between oceanic crust of the Tethys Ocean and the southern margin of the Eurasian Plate. This interpretation emphasizes the main convergent margin between the Eurasian Plate and the Tethys, and may thus be more appealing than a model for the tectonic history based on a number of small oceanic basins.

Because movement to the north and east is blocked by the Eurasian Plate and the Arabian Microplate, respectively (Fig. 2.1, 2.2), stress relief is sought by motion along east-west transform faults (e.g. the northern Anatolian fault system). The southern margin of the Apulian-Anatolian microplate is convergent. South of the Aegean and south of the Turkish mainland, oceanic lithosphere belonging to the Levantine Basin which is part of the African Plate, is subducted under the continental lithosphere of the Apulian-Anatolian microplate (McKenzie 1978, Le Pichon and Angelier 1979). Cloetingh et al. (1981) argued from a seismic study that most of the crust under the Levantine Basin should be interpreted as thin continental crust. This interpretation implies that subduction along the Hellenic Trench System is in its last stages. The presence of a convergent margin to the south of the Apulian-Anatolian microplate in the Aegean has placed the continental crust of the Aegean in an extensional regime.

It has been argued by several authors that prior to the start of subduction at the present location about 13 Ma ago (Le Pichon and Angelier 1979), convergent margins between small oceanic basins and continental crust may have existed to the north of the present position of the Hellenic Trenches (Dewey and Sengör 1979, Bonneau 1982, Altherr et al. 1982b, Sengör and Yilmaz 1982).

2.1.2.2 The Aegean Sea and surroundings

At present, much attention is focussed on the Aegean Sea because it is one of the few region affected by the Alpine Orogeny, where trench-arc relations can be studied in detail. The tectonic history of the Aegean and its surroundings is complex. On the Greek mainland to the northwest of the ACMB and on the Turkish mainland to the east of the ACMB, the major lithological units are separated by tectonic contacts (Jacobshagen et al. 1978). The close association of continental shelf sediments and

ophiolites is commonly interpreted as evidence for the interaction of small oceanic basins and small continental crustal blocks during the Mesozoic and Tertiary evolution of the area (Dewey et al. 1973, McKenzie 1978, Jacobshagen et al. 1978, Dewey and Sengör 1979, Sengör and Yilmaz 1981, Bonneau 1982). In this environment one may expect that the rate at which interactions proceed is high enough to cause the abnormally low thermal gradients which are required for the formation of blueschist belts.

Most paleogeographic reconstructions based on plate motions since the end of the Jurassic, position the Aegean on the the Apulian-Anatolian microplate (Smith and Briden 1977, Smith and Woodcock 1982, Biju Duval et al. 1978). An important point is that since the Late Cretaceous the tectonic setting of the Aegean need not have changed dramatically in order to interpret the presently exposed rocks. After opening of the Levantine Basin, compression in the area caused by movement of the African plate with respect to the Eurasian plate would have caused tectonism along the southern margin of the Apulian-Anatolian plate.

South of the ACMB, Miocene high pressure, low temperature metamorphic rocks are exposed near the trench at Crete (Seidel et al. 1982). Older high pressure, low temperature rocks of Eocene age can be found within the ACMB, further north of the present location of the trench. The occurrence of young, Miocene, high temperature, medium pressure metamorphic rocks in the ACMB suggests the interpretation of the Aegean basin as a paired metamorphic belt of the western Pacific type (Lister et al. 1984, Miyashiro 1973). Thus, the area has experienced a complex metamorphic history, and this history can be traced from the mineral assemblages of the rocks of the Attic Cycladic Metamorphic Belt. Study of these mineral assemblages may help to provide a tectonic and thermal history for the region which extends back to the beginning of the Tertiary.

The present study of the thermal history of the Attic Cycladic Metamorphic Belt on Naxos may have wider significance than just for the geodynamic history of the Aegean Basin. It is noted that the metamorphic histories of the ACMB in Greece and other areas affected by the Alpine Orogeny (e.g. the internal

zones of the Swiss and French Alps) are very similar from the Late Mesozoic until the present. The ACMB, as well as the Swiss and French Alps, contain supracrustal rocks which have experienced high pressure, low temperature metamorphism (Ernst 1973), and were exposed to this type of metamorphism during the Paleocene to Eocene (Frey et al. 1974, Altherr et al. 1979, Andriessen et al. 1979). Subsequently, these terrains experienced widespread greenschist facies metamorphism and locally further high temperature, medium pressure metamorphism, in the Attic Cycladic Metamorphic Belt on Naxos, Paros and Tinos, and in the Alps in Ticino in the south of Switzerland. Cooling after high temperature metamorphism occurred in both areas in the Miocene (Frey et al. 1974, Altherr et al. 1982a, Andriessen et al. 1979). This similarity of metamorphic histories suggests that these terrains were exposed to similar conditions of metamorphism over approximately the same time interval. Thus models describing the history of the one area may be of relevance to the other. It further indicates that similar conditions may have existed over very long distances along what was at that time the southern margin of the Eurasian Plate.

2.2 Geology of Naxos

Naxos is the largest island of the Cycladic Archipelago (Fig. 2.3, 2.4), with a surface area is about 400 km^2. It is located about 200 km southeast of Athens, in the central part of the Aegean Sea. Naxos is mountainous with a fertile coastal plain along its west coast (granodiorite) and a more elevated plain which dips gently from the centre of the island towards the south coast (mainly mica schists). Its highest mountains have an altitude of about 1000 m. Approaching the island from the northwest on a clear day offers a particularly impressive view of the mountain land.

The geology of the ACMB, and its relation to other geologic units in the Aegean Sea was described by Dürr et al. (1978), Jacobshagen et al. (1978), and Altherr et al. (1982a). The main unit found in the ACMB is a metamorphosed sequence of platform sediments. This unit was argued by Dürr et al. (1978) to be of Mesozoic sedimentary age. In tectonic windows, the unit below these meta-sediments is exposed. Detailed work on the geology and geochronology of these basement rocks on Ios has revealed that they consist of pre-Alpine continental crustal material (Van der Maar 1981, Henjes-Kunst and Kreuzer 1982, Van der Maar and Jansen 1983). The ACMB was intruded by I-type granitoids during the Miocene (Altherr et al. 1982a, 1982b). Non-metamorphic sediments of Permian to Tertiary age can be found in thrust contact with the metamorphic rocks of the ACMB. These rocks have been thrust over the ACMB from the north, and on the Greek mainland they may cover the metamorphic rocks of the ACMB completely (Jacobshagen et al. 1978).

The geology of Naxos was originally described by Papavasiliou (1909). More recently, a description of the geology of Naxos was given by Jansen (1973, 1977b). The rocks of Naxos can be divided into three main groups:

(1) The major part of the island consists of regional metamorphic rocks which are part of the Attic Cycladic Metamorphic Belt (Fig. 2.3). These rocks comprise a schist-marble sequence of possibly Mesozoic sedimentation age (Dürr et al. 1978). It was argued that this sedimentary sequence was deposited on a continental basement in which evidence can be found for igneous and metamorphic

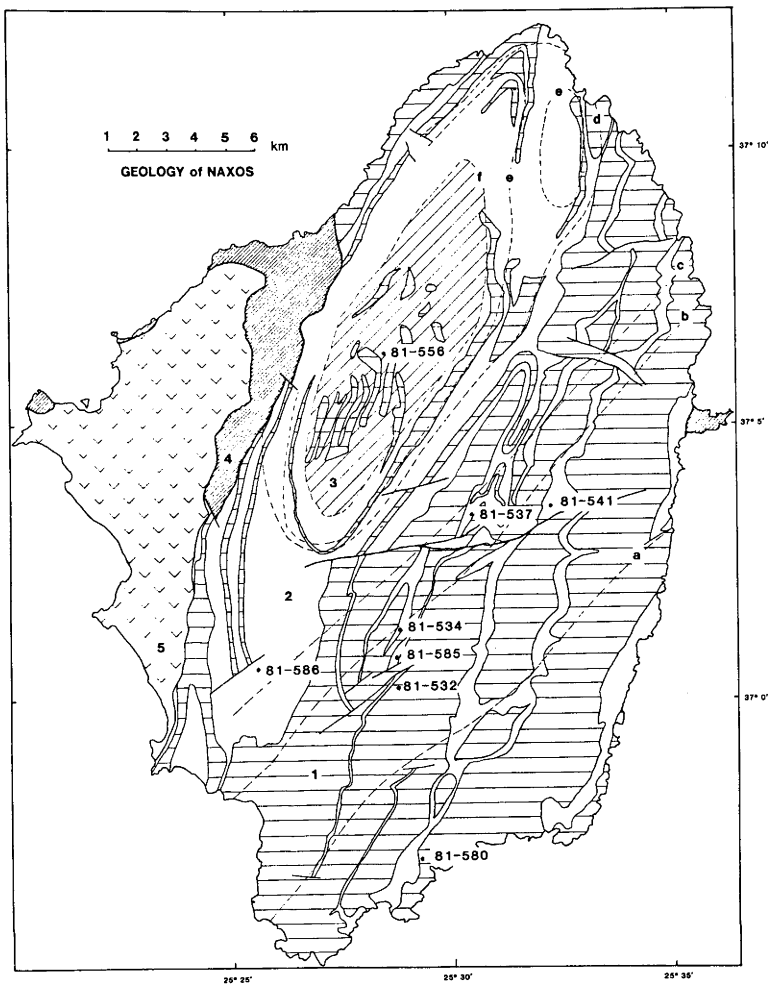

Figure 2.3. Geology of Naxos. (after Jansen 1973). (1) predominantly marble, (2) predominantly micaschist, (3) migmatite, (4) non metamorphic sediments, (5) granodiorite. (a) + corundum isograd, (b) + biotite isograd, (c) - chloritoid isograd, (d) + sillimanite isograd, (e) - kyanite isograd, (f) + meltphase line.
The sample locations are those of white micas discussed in section 3.4.2.5.

activity during the Paleozoic (Henjes-Kunst and Kreuzer 1982). The sedimentary sequence was metamorphosed during the Tertiary (Andriessen et al. 1979, Altherr et al. 1979, Bonneau et al. 1980, Altherr et al. 1982a). Two major metamorphisms were recognized. The M_1 metamorphism caused the formation of high pressure, low to medium temperature mineral assemblages throughout the ACMB. Its age was argued to be 45 $\pm$ 5 Ma (Andriessen et al. 1979). This event was followed by the M_2 metamorphism which caused the formation of a thermal dome in the centre of Naxos. This event was dated at 25 $\pm$ 5 Ma (Andriessen et al. 1979). The petrology of Naxos will be discussed in section 2.3.

(2) A granodiorite intruded the metamorphic complex (Fig. 2.3). The mineralogy of this pluton includes green hornblende and some minor pyroxene (Jansen 1977b). Therefore, it can be classified as an I-type pluton (Chappell and White 1974, Altherr et al. 1982a).

(3) Non-metamorphic rocks cover a minor part of the surface of Naxos (Fig. 2.3). They can be divided into two different groups. The first group is of allochthonous origin, it includes Permian to Early Tertiary sediments, some gabbroic rocks and serpentinites. The second group comprises autochthonous sediments of Pliocene and younger age (Jansen 1977b, Roesler 1978).

The following sections summarize the geology of Naxos, with some reference to the geology of the adjacent islands. The information presented here is based mainly on a series of recently published articles reviewing the area (Dürr et al. 1978, Jacobshagen et al. 1978, Roesler 1978, Altherr et al. 1982a, Jansen and Schuiling 1976, Jansen 1977b, Van der Maar and Jansen 1983), as well as on the the author's own observations.

2.2.1 Metamorphic rocks

2.2.1.1 Pre-Alpine basement

Rocks belonging to the pre-Alpine basement crop out only in small areas in the ACMB (Henjes-Kunst and Kreuzer 1982, Van der Maar and Jansen 1983), and were interpreted as the rocks on which the Mesozoic sedimentary sequence was deposited. Rocks belonging to this basement occur on Ios and possibly Naxos and Sikinos (Fig. 2.4). The metamorphic history of these rocks is complex.

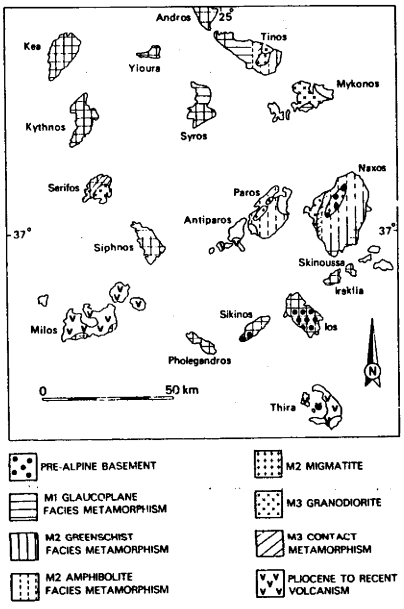

Figure 2.4. The petrology of the Cycladic Archipelago. (after Van der Maar 1981, Van der Maar and Jansen 1983).

Henjes-Kunst (1980) has found evidence on Ios for intrusion of small granodioritic to tonalitic plutons into metamorphic country rock of possible Precambrian age during the Early Palaeozoic (462 ± 48 Ma by the Rb-Sr whole rock isochron method). During the Hercynian Orogeny in the Late Palaeozoic, these rocks experienced amphibolite facies metamorphism. The age of this metamorphism was determined by the lower intercept of the discordia line in a U/Pb zircon concordia plot at 305-300 Ma and also by Rb-Sr muscovite-whole rock ages at about 290 Ma (Henjes-Kunst and Kreuzer 1982). During the Alpine Orogeny, basement on Ios was subjected to high pressure, low temperature metamorphism M_1, and overprinting at greenschist facies grade during M_2.

By analogy to the well documented case at Ios, this pre-Alpine basement is inferred for Naxos (Dürr et al. 1978, Van der Maar and Jansen 1983). Recent U/Pb work on zircons of rocks from Naxos, which are suspected to belong to the same unit as the basement of Ios, has yielded results which are comparable to the results obtained in the basement rocks of Ios (Andriessen 1983).

2.2.1.2. The metasedimentary sequence

The major unit in the Cycladic Archipelago is a metasedimentary sequence (Fig. 2.4). On Naxos, rocks of this unit occupy the major part of the surface area of the island. The sequence consists of dolomitic and calcitic marbles, pelitic schists, amphibolites, eclogite lenses, metabauxites and metaophiolites. The presence of metamorphic ultramafic lenses and eclogite lenses within the sequence indicates that the sequence is composed of tectonically stacked units. A Mesozoic sedimentary age was proposed by Dürr et al. (1978). From the marbles on Naxos, Dürr and Flügel (1979) reported an Upper Triassic sedimentation age on the basis of micropaleontological evidence. Andriessen (1978) found that the Sr-isotopic composition of the marbles on Naxos agreed with the inferred isotopic composition of ocean water during the early Mesozoic. If the correlation of the metamorphosed sequence of the ACMB with the sedimentary sequences in mainland Greece holds (Dürr et al. 1978), then the ophiolites are of Permo-Triassic age (Roddick et al. 1979). It is likely that tectonism leading to the incorporation of these ophiolites into the sedimentary sequence occurred before the M_1 metamorphism

for reason of similarities between the metamorphosed and unmetamorphosed sequences.

During the Miocene, a thermal dome developed in the metamorphic complex (see section 2.3.2), causing partial melting of the metapelitic units. Some small granite bodies are associated with this high temperature event. In some cases, these can be traced to their migmatite precursors. The mineralogy of these granites which includes muscovite and garnet, as well as the clear association with anatectic metapelites, suggests that they may be classified as S-type granites (Jansen 1977b, Chappell and White 1974, Altherr et al. 1982a).

2.2.2. The granitoids

Two types of granitoids have intruded the sedimentary sequence during the later stages of the Alpine orogeny. The first type is often associated with the high grade M_2 metamorphism. The second type is clearly intrusive and not related to a metamorphic event. Granitoids belonging to the first group have been classified as S-type granites, and those belonging to the second group have been classified as I-type granitoids (Altherr et al. 1982a, Altherr et al. 1982b). This classification (Chappell and White 1974) works in the ACMB, because of the differences in mineralogy and occurrence between the two groups.

2.2.2.1 S-type granites

Granites belonging to this group are confined to areas that reached upper amphibolite facies metamorphic grade during the M_2 metamorphism (Fig. 2.4). Jansen (1973, 1977b) mapped several small granite bodies on Naxos and related them to the formation of migmatites during culmination of the M_2 event and infers that emplacement was synchronous with the formation of the thermal dome. The actual size of these bodies may vary from the migmatitic leucosome which can be identified in outcrop scale to clearly intrusive bodies, the largest of which has a size of 4 km by 0.5 km. In hand specimen these granites are relatively fine grained, and contain muscovite and biotite. Altherr et al. (1982a) reported similar granites from Paros, Ikaria and Tinos (Fig. 2.1b, 2.4). Because emplacement took place during high

grade metamorphism, these intrusives lack obvious contact metamorphic aureoles.

2.2.2.2 I-type granitoids

I-type granitoids occur on Naxos, Myconos/Delos, Serifos, Tinos, Ikaria and Keros (Fig. 2.1b) (Altherr et al. 1982a, 1982b). These intrusives have caused contact metamorphism in the surrounding country rock. The granitoids vary in composition from granodiorites in the west of the ACMB to monzonites in the east of the ACMB (Altherr et al. 1982b). On Naxos, it can be inferred from the mineralogy of the contact zone that intrusion took place at pressures between 200 and 500 MPa (Jansen et al. 1977). This constrains the relative time of intrusion at synchronous to, or slightly post dating the high grade phase of M_2. Conventional K-Ar dating and Rb-Sr dating of minerals from I-type granitoids at Tinos and Myconos are very similar to those reported from the high grade metamorphic zones and to those found in the high grades zones on Naxos as well. Mineral ages from the granodiorite at Serifos are younger, K-Ar ages of hornblende and biotite are 9.5 Ma and 8.6 Ma respectively (Altherr et al. 1982a, 1982b). This pluton has suffered severe hydrothermal alteration, accompanied by massive skarn formation in the country rock (Salemink 1982).

2.2.3. Non-metamorphic rocks

Although the non-metamorphic rocks fall outside the scope of this study, they are of some importance as they constrain the younger time limit of the thermal history of the metamorphic complex. Two units are recognized, the older rocks are part of an allochthonous unit and the younger rocks are interpreted as autochthonous. The presence of the allochthonous unit indicates that the area remained tectonically active after the end of the metamorphic cycle. The autochthonous sediments are important in that they represent a time constraint for the youngest part of the metamorphic and uplift history.

2.2.3.1. The allochthonous unit

Rocks belonging to this unit have been reported from many of the Cycladic Islands (Jacobshagen et al. 1978). On Naxos they occupy only a minor part of the total surface area (Fig. 2.3). The major outcrop is along the northern half of the contact between the granodiorite and the metamorphic complex. A second outcrop is located at Cape Moutsouna on the east coast. Rocks from this unit include mafic igneous rocks, like serpentinites, gabbros and diabase, and sedimentary rocks, including sandstones, limestones and conglomerates of presumably Tertiary age (Jansen 1977b). The conglomerates do not contain any locally derived metamorphic clasts, but Permian and Mesozoic limestones, radiolarites and mafic igneous components dominate. This observation led to the recognition of nappe overthrusts in the Cycladic Archipelago (Jansen 1973). Andriessen et al. (1979) proposed on the basis of the K-Ar measurement of a pseudotachylite, that overthrusting of these rocks took place as long ago as 10 Ma.

2.2.3.2. Autochthonous sediments

A variety of autochthonous sediments can be found on Naxos. They range in age from Pliocene to Recent. The oldest, and for this study the most important units are fresh water limestones and cherts (Jansen 1977a, Roesler 1978). The fossils found in this unit indicate an Upper Pliocene sedimentation age. Conglomerates intercalated in this sequence indicate the erosion of local rock units. Close to the granodiorite, the pebbles are mainly granodioritic and near the metamorphic complex, the pebbles in the conglomerates are mainly metamorphic (Jansen 1977b), supporting the interpretation that these rocks are autochthonous. The estimated stratigraphic thickness of these sediments is about 200 m (Roesler 1978).

2.3 Petrology of the metamorphic complex on Naxos

Various studies into the geochemistry and the petrology of the metamorphic complex on Naxos have been carried out, or are still in progress. The petrology was originally described by Schuiling and Oostrom (1967) and revised by Jansen and Schuiling (1976). These studies describe a concentric pattern of metamorphic zones formed during the M_2 metamorphism around the central migmatites, based on mineral assemblages observed in pelitic schists and metabauxites. More detailed work is in progress on the phase relations in the metabauxites (Feenstra 1985) and in the siliceous dolomite system (Jansen et al. 1978, Van der Rijst et al. 1978). Studies of the stable isotope geochemistry of the metamorphic complex were carried out by Rye et al. (1976) and by Kreulen (1980). The Rb-Sr and K-Ar age relations in the granodiorite and the metamorphic complex were studied by Andriessen et al. (1979). Although by now more mineral reactions have been documented, the present study uses the division into mineral zones related to the M_2 metamorphism that was described by Jansen and Schuiling (1976).

2.3.1 The M_1 metamorphism

In rocks of the low grade M_2 zones, mineral assemblages formed during the M_1 metamorphism may still be preserved. Depending on the bulk composition, the observed mineral assemblages may include phengite, albite, glaucophane, calcite, epidote, chloritoid, chlorite and paragonite (Jansen et al. 1977). A more detailed study of the petrology of M_1 mineral assemblages was carried out on rocks from Ios and Sikinos (Van der Maar 1981, Van der Maar and Jansen 1983). Here, the M_1 event has produced a series of mineral assemblages, of which the earlier ones have recorded higher pressures and the later ones were formed at lower pressures. Typical mineral assemblages for the early stage of the M_1 event include according to Van der Maar (1981), omphacite-garnet-glaucophane-zoisite, garnet-phengite-rutile, garnet-glaucophane-chloritoid and garnet-phengite-zoisite-actinolite. Subsequently, in the metabasic rocks and the eclogites, crossite, barroisite, chloromelanite, albite, epidote and chlorite were formed. In the last stage of the M_1 event, crossite gives way to riebeckite and subsequently actinolite and

albite. The white micas become less phengitic.

On Syros, detailed structural analysis indicated that the M_1 metamorphism was accompanied by strong tectonism (Ridley 1982). Here the earlier phase of M_1 was found to be followed by low-angle thrusting. The later M_1 minerals grew at different angles to the foliation determined by the earlier M_1 minerals. Similar observations have been made on Evvia (Maluski et al. 1982).

The pelitic schists on Naxos in the zones which were least affected by the M_2 metamorphism contain predominantly quartz and phengite and some albite and chlorite. Inclusion patterns in the albite indicate that these minerals were either formed during a deformation phase, or between two deformation phases. The phengites in these rocks consistently show evidence for deformation of varying intensity. In the lowest grade M_2 metamorphic zones, this deformation has been the last major event that has affected the rocks. Toward higher M_2 metamorphic grade, the folded phengites become segmented into straight subgrains, suggesting that this deformation occurred before the M_2 metamorphism. In some rocks, chloritoid is part of the assemblage, showing lamellar twinning and chloritization along its margins. Some metapelites contain garnet and glaucophane as part of the mineral assemblage. The glaucophane is severely altered to a fine grained aggregate of chlorite and actinolite. In a deformed metabasic rock early glaucophanes and a younger phase of crossite occur.

In the metabauxites, the main aluminium phase is diaspore. Because the maximum temperature for the M_1 metamorphism was estimated at about 500 to 530 ^{o}C (Jansen et al. 1977), which is higher than the experimentally determined position of the reaction from diaspore to corundum (Haas 1972), corundum may have been the stable aluminium phase during the M_1 event. Feenstra (1985) suggested on the basis of microstructural arguments that diaspore belongs to an M_1 mineral assemblage, implying a maximum temperature of 450 ^{o}C for the M_1 metamorphism. As a result of the thermal gradient during the M_2 metamorphism, toward higher M_2 metamorphic grade corundum becomes the main aluminium phase in the metabauxites. The mineral assemblages in the metapelites change very little at first, but in the higher grade parts of

zone II (see Fig. 2.5, and section 2.3.2), chlorite and muscovite occur, which near the + biotite M_2 isograd start to react to form biotite. Although phengite, which is formed during the M_1 metamorphism, may be recognized in rocks in the low grade part of zone IV, where muscovite, biotite, garnet and staurolite are part of the stable M_2 mineral assemblage, the relative abundance of phengite in the rocks diminishes rapidly from the high grade parts of zone II toward higher M_2 metamorphic grade.

Pressure and temperature estimates for the M_1 metamorphism from the different parts of the Attic Cycladic Metamorphic Belt range from 900 to 1500 MPa and 450 to 530 ^{o}C. The mineralogy suggests that during the M_1 event mineral assemblages were formed while the system experienced a period of decompression. The very high pressure mineral assemblages, which are reported from rocks on Ios or Syros, do not occur on Naxos. Here, the maximum pressure which was reached during the M_1 metamorphism is estimated at about 900 MPa. This estimate is based of the mineral assemblage including chloritoid and glaucophane (Jansen et al. 1977). The composition of phengite (Si^{4+} = 7.0) suggests that if the metamorphic temperature is estimated at about 500 ^{o}C, these minerals must have formed at pressures in excess of 1000 MPa (Velde 1967, Massone 1981).

2.3.2 The M_2 metamorphism

Mapping of the metamorphic complex into concentric M_2 mineral zones around the central migmatites in the core of the domal structure was based on a sequence of mineral reactions that were recognized in the field and calibrated with results from experimental petrology (Schuiling and Oostrom 1967, Jansen 1973, Jansen and Schuiling 1976, Jansen et al. 1977). An internally consistent set of P-T estimates was derived, on which most of the subsequent work on the complex is based. The zones are (Fig. 2.5):

Zone I. The diaspore zone is the zone least affected by M_2. The zone is terminated at higher metamorphic grade by the reaction of diaspore to corundum in the metabauxitic compositions (+ corundum isograd). The temperature of the reaction was estimated by Jansen and Schuiling (1976) at 420-440 ^{o}C.

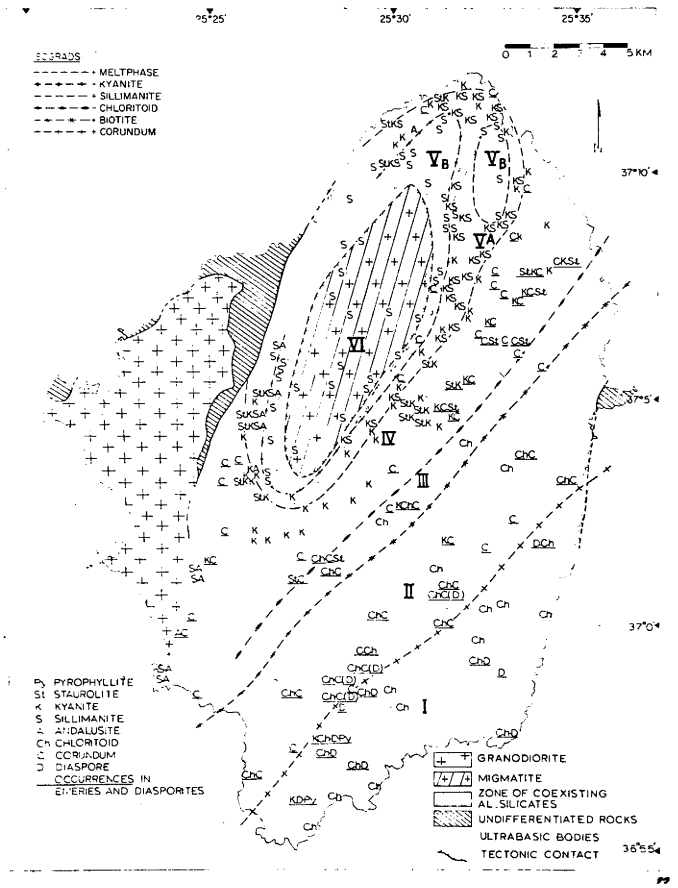

Figure 2.5. The petrology of the metamorphic dome on Naxos. (after Jansen and Schuiling 1976).

Zone II. The chlorite-sericite zone is based on the mineralogy of pelitic schists. The high temperature boundary of this zone is reached with the formation of biotite (+ biotite isograd). The temperature for the formation of biotite was estimated at about 500 ^{o}C.

Zone III. The biotite-chloritoid zone is based on mineral assemblages in the metabauxites and the pelitic schists. The high temperature boundary of this zone is the breakdown reaction of chloritoid (- chloritoid isograd). The temperature for this reaction was estimated at 540-580 ^{o}C.

Zone IV. The kyanite zone is based on mineral assemblages in the pelitic schists and the metabauxites. The high temperature boundary is reached when fibrolitic sillimanite is formed in the pelitic schists (the + sillimanite isograd). The temperature for this reaction to occur was estimated at 620 to 660 ^{o}C.

Zone V. The sillimanite zone can be divided into a lower grade part, where kyanite and sillimanite are both found in the pelitic schists and a higher grade part, where only sillimanite occurs. The high temperature boundary of the zone is determined by the first occurrence of anatexis in the pelitic schists. The temperature for this to occur was estimated at 660-690 ^{o}C.

Zone VI. The central zone is called the migmatite zone. It starts where evidence is found for anatexis in the metapelites. The metamorphic temperature in this zone is determined by the equilibria quartz-plagioclase-K-feldspar-liquid and quartz-biotite-plagioclase-liquid. This means that the temperature distribution throughout the migmatite zone must have been fairly uniform. A maximum temperature of 700-720 ^{o}C for the migmatite was estimated.

Relative to the position of these isograds, every location within the metamorphic complex may be assigned a maximum temperature reached during M_2 metamorphism. Within the metamorphic complex the M_2 metamorphic pressure, as indicated by the mineral assemblages, decreases slightly from east to west. This is best illustrated by the occurrence of polymorphs of the Al-silicates. On the east side of the dome the stable polymorphs are kyanite

and sillimanite and on the western side of the dome kyanite, andalusite and sillimanite occur. Both kyanite and andalusite appear to have crystallized earlier than the sillimanite, indicating increasing temperature, rather than decreasing pressure during the prograde part of the M_2 cycle. The metamorphic pressure during the M_2 event was estimated at 500 to 700 MPa (Jansen and Schuiling 1976, Jansen et al. 1977). In section 2.3.4 and 2.3.5 of this chapter, the temperature and pressure estimates for the M_2 metamorphism will be discussed in some detail.

2.3.3 Deformation in the metapelites

Tectonic activity in the Attic Cycladic Metamorphic Belt occurred throughout the recorded geologic history. The earliest evidence is found in ultramafic and eclogitic lenses which were included in the sedimentary sequence. In addition ultramafic lenses are found along the inferred tectonic windows where pre-Alpine basement is exposed. These inclusions in the metasedimentary sequence indicate an allochthonous origin for the sediments. On Syros there is evidence that major thrusting continued during the M_1 metamorphism (Ridley 1982). On Naxos, both schists and marbles show tight to isoclinal folding on a macroscopic scale. The large scale open folding shown on the 1:50000 map of Jansen (1973) is probably a late stage deformation (Dürr et al. 1978). On a microscopic scale, rocks containing M_1 minerals may show three phases of deformation (Wijbrans 1980). The first is responsible for the F_1 foliation defined by phengites and chlorites in orientations parallel to the alternating quartz and mica layers. A subsequent deformation, D_2, caused second foliation, F_2, at an angle to F_1. Locally the resulting crenulation cleavage is folded isoclinally during a third deformation event. Rocks containing predominantly M_2 minerals, may show two deformation phases. The first phase is related to the formation of quartz rich and mica rich bands, while during a second deformation isoclinal folds were formed. The muscovite and biotite crystals in the mica rich layers in the high grade M_2 zones show random orientation, indicating that the last major deformation preceded the peak of the M_2 metamorphic event.

Several different potassium white micas were recognized in the pelitic schists (Wijbrans 1981). The ones of relevance for this study are:

1. Phengites formed during the M_1 metamorphism occur as typically long, flat, often folded crystals. They are characterized on the basis of their chemical composition by a relatively high Si^{4+}, Fe_{tot} and Mg^{2+} content and a relatively low Al^{3+} content (Fig. 3.3).

2. Muscovites formed during the M_2 event. In rocks containing both phengite and muscovite, the muscovite crystals have different length-width ratios, are not deformed and often cut through the foliation formed by the phengites. From zone IV towards higher metamorphic grade, they form the dominant type of white mica in pelitic rocks.

The other types include a fine grained mica which occurs in zone I and II in association with the phengites and paragonites, and a muscovite in zone V and VI which occurs in pseudomorphs after kyanite and staurolite. The fine grained mica is either derived from phengites during post M_1 tectonism or is newly nucleated as a response to the M_2 metamorphism. The major element chemistry indicates a composition intermediate between phengite and M_2 muscovite. The sodium white mica, paragonite, occurs only in M_1 mineral assemblages in metavolcanic rocks. The calcium white mica, margarite, occurs quite abundantly in M_2 mineral assemblages in metabauxitic rocks (Jansen and Schuiling 1976). M_2 mineral assemblages in siliceous dolomites include a colourless phlogopite (Jansen et al. 1978).

In the metamorphic complex there is some post M_2 normal faulting which probably occurred during uplift. In the granodiorite there is evidence for sub-horizontal faulting which is probably related to overthrusting of non-metamorphic rocks of which remnants are located on Naxos close to the granodiorite.

2.3.4 Estimates of pressure and temperature

The physical conditions inferred for the M_2 metamorphism provide the basis for further thermal modelling of the system. It may be useful, therefore, to explore which factors influence the precision of the P-T estimates. The reactions involved in prograde metamorphism include:

- Dehydration reactions, for example the reaction of diaspore to corundum, the formation of biotite from chlorite and muscovite, and the breakdown of chloritoid.
- Solid-solid reactions between the polymorphs of Al_2SiO_5.
- Reactions which occur when partial melting of the rock starts in the metapelites. Anatectic melts, formed at this stage of the metamorphic evolution are likely to take water out of the metamorphic fluid.
- Exchange reactions may occur for example between phases containing Fe^{2+} and Mg^{2+} or Si^{4+} and Al^{3+}.

From experimental studies many of the dehydration reactions have been assigned a reaction temperature and pressure. Subsequently, these reactions have been used in the derivation of P-T grids in order to constrain the metamorphic pressure and temperature. A major uncertainty of such an approach is of course to what extent carefully controlled experimental conditions represent natural systems. It has been argued (e.g. Miyashiro 1973) that the location of a reaction line in a P-T field may be influenced by small amounts of contaminants in the reacting phases, which are always present in natural systems. In the case of dehydration reactions an additional uncertainty may be in the composition of the fluid phase during the reaction (Greenwood 1962, Thompson 1955). At the time that Jansen and Schuiling (1976) estimated the physical conditions for the mineral zonation around the thermal dome on Naxos, it was not yet known to what extent the metamorphic fluid during the M_2 metamorphism was dominated by CO_2. A study of fluid inclusions in syn-metamorphic quartz lenses suggested that the metamorphic fluid during the M_2 metamorphism on Naxos consisted of 50 to 90 percent CO_2 (Kreulen 1980). The effect of $P_{(H_2O)} < P(\text{total})$ on the position of a dehydration reaction in a P-T field can be profound. Hoschek (1969) reviewed the dependence of the position of the reaction line on $P_{(H_2O)}$ for a series of common dehydration reactions. His

conclusion was that for a system at 500 MPa and $a(H_2O) = 0.5$ the temperatures for reaction to occur are lowered by 85-115 °C. The $a(H_2O)$ in the syn-M_2 metamorphic fluid inclusions on Naxos is consistently lower than 0.5 (Kreulen 1980), implying that if the fluid composition in the fluid inclusions correctly represents the composition of the syn-M_2 metamorphic fluid, the temperatures estimated from dehydration reactions may be about 100 $\pm$ 15 °C lower than previously suggested (Jansen and Schuiling 1976, Kreulen and Van Beek 1983).

Reactions between polymorphs of the Al-silicates are solid-solid reactions. The phase transitions within the Al_2SiO_5 system are notoriously sluggish because of the small differences in chemical potential involved in the reactions. For an experimental petrologist this sluggishness presents severe problems (see Essene 1982 for a review), but for the field petrologist it may be useful. In metapelites during prograde metamorphism most of the Al-silicates are formed by dehydration of minerals like pyrophylite, chlorite, muscovite and biotite (see Winkler 1974). Assuming that the stable polymorph is formed by these dehydration reactions and the reaction from the one polymorph to the other is slow, a record of the P-T path followed by the rocks may be preserved. The thermal dome on Naxos where all three polymorphs occur, sometimes side by side, is a good example of such a case. The actual position of the triple point has been the focus of continued discussion. Jansen and Schuiling (1976), for the sake of internal consistency, proposed a relatively high estimate for the P and T of the triple point. Lower estimates for the pressure and temperature of the triple point are more widely accepted (Essene 1982). If the arguments discussed above hold, on Naxos a lower estimate for the triple point at about 400 MPa and 500-520 °C would fit very well for Naxos (cf. Schuiling 1957, 1962, Newton 1966, Holdaway 1971, Essene 1982). Consequently, the minimum estimate for the metamorphic pressure east of the dome on Naxos could be as low as 400 MPa.

Exchange reactions occur for example between K^+ and Na^+ in micas, or between Fe^{2+} and Mg^{2+} in chlorites, biotites, garnets and staurolites in metapelitic rocks, and may occur over wide temperature and pressure ranges without producing new mineral phases. Thus they can be very useful as geothermometers and geobarometers (Thompson et al. 1977, Ferry and Spear 1978, Spear et al. 1984, Chatterjee and Froese 1974). Temperatures for the M_2 metamorphism were calculated from the garnet-biotite data from Wijbrans (1980) using the calibration of Ferry and Spear (1978). Temperatures calculated according to this method are consistently lower than the temperature calculated from the M_2 isograds (Table 2.I). The K-Na substitution in M_2 muscovites was studied by Wijbrans (1980). It was concluded from comparison of the results with the experimental phase diagrams of Chatterjee and Froese (1974) that the M_2 muscovites may have been formed at a metamorphic pressure close to 400 MPa.

As stated above, the formation of a meltphase in the pelitic system is a water consuming reaction. This water may come from the breakdown of hydrous phases like muscovite and biotite or may be taken from the ambient metamorphic fluid (Thompson 1982). In both cases beginning anatexis will lower the partial water pressure in the metamorphic fluid. The effect of decreased water activity in the metamorphic fluid is twofold. Firstly, one may expect that when the water activity in the system decreases, the temperature for the melt producing reaction will increase (Jansen and Schuiling 1976). Secondly, it was argued that the composition of the metamorphic fluid is not mainly determined by local dehydration and decarbonation reactions, but by a more deepseated source (Rye et al. 1976, Schuiling and Kreulen 1979, and Kreulen 1980). If at the time of the peak of the M_2 event anatexis was more widespread in the rocks below the presently exposed erosion surface, then it is likely that the composition of the syn-M_2 metamorphic fluid will depend on anatectic reactions occurring at a lower level in the crust and consequently will be depleted in H_2O. The effect of a lowered $a(H_2O)$ in the metamorphic fluid on dehydration reactions has been described earlier in this section.

2.3.5 Discussion

Previous estimates of the P-T conditions experienced during the M_2 metamorphism on Naxos were mainly based on dehydration reactions with increasing temperature (Schuiling and Oostrom 1967, Jansen and Schuiling 1976, Jansen et al. 1977). Advances in the understanding of the metamorphic history of Naxos since that time, in combination with progress in geothermometry necessitate a revision of the original temperature calibration. Various systems suggest that the metamorphic temperature during the M_2 metamorphism in the metasedimentary sequence may have been lower than previously thought:

(1) Temperature calibration of the isograds in the M_2 mineral zonation with experimentally determined values should be corrected for the composition of the ambient metamorphic fluid. The composition of the syn-M_2 metamorphic fluid as determined by Kreulen (1980) consists of more than 50 percent CO_2. According to Hoschek (1969), the reaction temperature for dehydration reactions would decrease at least 100 ^{o}C with this proportion of CO_2.

(2) Oxygen isotope thermometry on muscovite-quartz and biotite-quartz pairs have yielded consistently lower temperatures than the isograd temperatures. In the amphibolite facies grade zones on Naxos the discrepancy between the two temperatures is about 100 ^{o}C (Rye et al. 1976). In the light of earlier interpretations of the M_2 metamorphism, which involved slow cooling after the peak of the M_2 event (Andriessen et al. 1979), the observed discrepancy was interpreted in terms of continued re-equilibration of the oxygen isotope system during cooling after the M_2 event. Presently, it is argued that the M_2 metamorphism was followed by a period of rapid cooling (see Chapter 3 and 4). In such an environment, because of exponential decrease of diffusion rates with decreasing temperatures, post-metamorphic re-equilibration may have been minor (Javoy 1977, Dodson 1979).

(3) Exchange thermometry of biotite-garnet pairs using the calibration of Ferry and Spear (1978) yielded temperatures which are between 50 and 100 ^{0}C lower than the temperature estimates by Jansen and Schuiling (1976). Because this thermometer also relies on diffusion of ionic species, it is expected that because of the period of rapid cooling which has followed the peak of the M_2

metamorphism, resetting during cooling has been minor.
(4) The calcite-graphite geothermometer was calibrated on Naxos using the original temperature estimates (Kreulen and Van Beek 1983). Comparison of data from Naxos with data from other areas indicates that the temperature calibration of Naxos data may be about 100 ^{o}C too high.
(5) The argon isotopic system in white micas from the upper greenschist facies grade and lower amphibolite facies grade zones were studied by Andriessen by the conventional K-Ar technique (Andriessen 1978) and by Wijbrans by the $^{40}Ar/^{39}Ar$ stepheat technique (see Chapter 3). Andriessen estimated the blocking temperature of muscovite for argon at 450 ^{o}C using the original temperature calibration. Temperature estimates from other terrains indicate that the blocking temperature would be closer to 350 ^{o}C (Purdy and Jäger 1976, Jäger 1979). A more detailed discussion of the isotopic systematics in white micas is presented by Wijbrans and McDougall (1985, see Appendix III).

Thus, modern geothermometers suggest lower temperatures in the amphibolite facies grade zones of the metamorphic dome on Naxos. For the present study an adapted temperature and pressure calibration will be used. The triple point of the Al-silicates according to Holdaway (1971), at a pressure of 376 MPa and a temperature of 501 ^{o}C is consistent with this new calibration. The occurrence of kyanite and sillimanite in the rocks on the southeastern side of the dome and all three polymorphs in rocks on the western side of the dome brackets the metamorphic pressure during M_2 between about 350 and 500 MPa. For the temperature of the + meltphase line, an estimate of about 720 ^{o}C will be used (Jansen and Schuiling 1976). The first appearance of fibrolitic sillimanite in the metapelites is estimated to have occurred at 540 to 580 ^{o}C. The disappearance of chloritoid from the metapelites is estimated to occur between 440 and 480 ^{o}C. Biotite formed in the metapelites at 400 to 420 ^{o}C and the reaction of diaspore to corundum occurred at a temperature of 320 to 340 ^{o}C.

The effect of this P-T calibration on the interpretation of the thermal gradient through the M_2 thermal dome is that in the zones near the migmatite zone the gradient becomes steeper and in the zones further away from the migmatite the gradient becomes shallower. This interpretation is consistent with models for the

M_2 metamorphism which require that a heatsource has acted upon the system from the outside (Schuiling and Kreulen 1979). It is supported by the fact that relict M_1 minerals occur in the rocks up to the kyanite zone (zone IV). Further implications for the thermal history of Naxos will be discussed in Chapter 4.

TABLE 2.I, Temperature estimates for some metapelites samples from Naxos

zone	code	location (lat/long)	isograd T	gar-bio T (°C)
IV	NJ41	37° 04' 17"/25° 30' 56"	550	450
IV	NJ38	37° 04' 39"/25° 30' 20"	605	510
IV	NJ10	37° 05' 08"/25° 30' 24"	620	570
V	NJ2	37° 05' 33"/25° 29' 40"	670	600

The isograd temperatures were estimated from the calibration of Jansen and Schuiling (1976), the gar-bio temperatures are calculated from the electron microprobe data of Wijbrans (1979) using the calibration of Ferry and Spear (1978). The zones were described in section 2.3.2.

Chapter 3

Dating the igneous and metamorphic events on Naxos

3.1 Introduction

3.1.1 Previous geochronological work

It was discussed in the previous chapter that an understanding of the timing of thermal events in the Attic Cycladic Metamorphic Belt (ACMB), of which Naxos is part, may provide constraints as to the tectonic and thermal evolution of the region. The application of geochronologic methods in the last decade has significantly altered interpretation of the geologic history of the area. In 1973 one could still essentially agree with Papavasiliou (1909) in suggesting that metamorphism on Naxos took place before the Alpine Orogeny (Schuiling 1973). This view was based on the occurrence of Permian sediments in the non-metamorphic rocks and the supposed analogy between the ACMB and the external massifs in the Swiss Alps where igneous and metamorphic rocks formed during the Hercynian Orogeny are exposed (Papavasiliou 1909). In the following years a quite different picture emerged (see Rye et al. 1976, Jansen and Schuiling 1976). Geochronological studies indicated that the metamorphic history of the ACMB took place during the Alpine Orogeny (Dürr et al. 1978, Bonneau et al. 1980, Altherr et al. 1979, Altherr et al. 1982a, Andriessen et al. 1979, Henjes-Kunst and Kreuzer 1982, Maluski et al. 1981).

On Naxos, mineral ages of white micas from zone I, the zone least affected by the M_2 metamorphism, were in the range of 40 to 48 Ma (Andriessen et al. 1979). These ages were related to the M_1 metamorphism. Similar ages have been recognized in adjacent islands (Altherr et al. 1979, Bonneau et al. 1980, Maluski et al. 1981). Towards the centre of Naxos the M_1 mineral assemblages become increasingly more overprinted by M_2 mineral assemblages. Concomitantly, the ages of the white micas were found to decrease until in the low grade part of zone IV the muscovite K-Ar ages were less than 15 Ma. From zone IV towards the central migmatite zone, ages decreased slightly until they reached values of 10 to 12 Ma. Hornblendes measured by Andriessen et al. (1979) gave K-Ar ages between 21 Ma in zone III to 18.8 Ma in zone VI. Some younger hornblende ages were recorded in the intermediate zones (Fig. 3.2). On the basis of these data Andriessen et al. (1979) proposed an essentially two stage metamorphic history in which

the early event (M_1), estimated at 45 ± 5 Ma, was followed by a subsequent metamorphism, M_2, focussed on the centre of the island. Following the model for regional high grade metamorphism in the Swiss Alps (Frey et al. 1974, and references therein), hornblende and white mica ages in rocks from zone III were interpreted as recording the peak of the M_2 event at 25 ± 5 Ma. The occurrence of mica and hornblende K-Ar ages as young as 10 Ma was explained in terms of slow cooling in the central part of the island. The intrusion of an I-type granodiorite and its associated contact aureole, which was designated M_3, was dated with a Rb-Sr whole rock isochron at 11.1 ± 0.7 Ma (initial $^{87}Sr/^{86}Sr$ ratio 0.7112). It was argued that, although the isochron age is controlled by aplites and pegmatites, it closely approximates the actual time of intrusion. Late retrograde overprinting, M_4, attributed to a phase of thrusting, was dated at 10 Ma by K-Ar dating of a pseudotachylite.

3.1.2 Aims of present study

Application of the $^{40}Ar/^{39}Ar$ stepheat method of dating minerals has the potential of significantly improving our understanding of the metamorphic evolution of the Attic Cycladic Metamorphic Belt. The aim of this work is to provide better constraints on the metamorphic and cooling history of the rocks on Naxos by study of the argon isotope system of selected minerals. Because the $^{40}Ar/^{39}Ar$ stepheat method can potentially identify ^{40}Ar diffusion gradients, it is possible to assess the relative importance of incorporation of excess argon ($^{40}Ar_{exc}$) into the minerals, or loss of radiogenic argon ($^{40}Ar^*$) from the minerals by volume diffusion. These problems cannot be readily addressed by the conventional K-Ar method. In the present study, the following problems will be examined:

- The scatter in the K-Ar ages of M_1 phengites in the lowest grade M_2 metamorphic rocks may be caused by diffusion of $^{40}Ar_{exc}$ into the crystals, by diffusion of $^{40}Ar^*$ out of the crystals, or by crystallization of a younger white mica subsequent to the M_1 metamorphism. For the correct interpretation of the metamorphic history of the ACMB on Naxos, it is important to know which process dominated.
- The major element chemistry and the petrology of white micas

Figure 3.1. Simplified geological map of Naxos (after Jansen 1973). The major lithologies are shown: (1) marble, (2) schist, (3) migmatite, (4) non-metamorphic rocks and (5) granodiorite. The mineral zones around the migmatite are separated by (a) + corundum isograd, (b) + biotite isograd, (c) - chloritoid isograd, (d) + sillimanite isograd, (e) - kyanite isograd, (f) + meltphase line. The locations for the samples used in the present study are given.

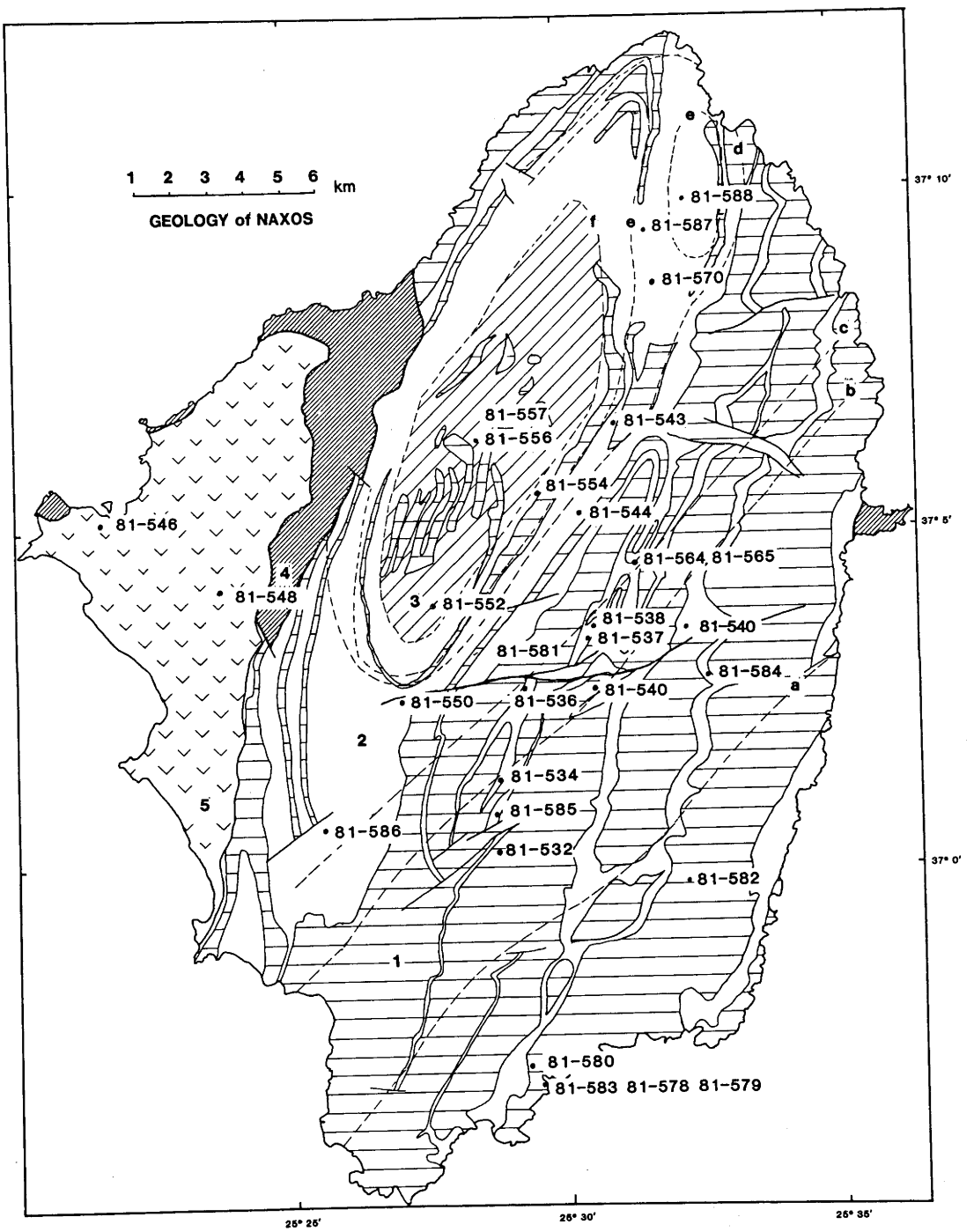
1 2 3 4 5 6 km
GEOLOGY of NAXOS
81-588
81-587
81-570
81-557
81-556
81-543
81-554
81-544
81-546
81-564
81-565
81-548
81-552
81-538
81-540
81-537
81-581
81-584
81-550
81-536
81-540
81-534
81-585
81-586
81-532
81-582
81-580
81-583 81-578 81-579
a
b
c
d
e
f
1
2
3
4
5
37° 10'
37° 5'
37° 0'
25° 25'
25° 30'
25° 35'

from metapelitic rocks indicates in a fairly wide zone on Naxos phengites, formed during M_1, and muscovites, formed during M_2, occur side by side. The K-Ar dating method applied to white micas from this area yielded intermediate ages between M_1 cooling ages and M_2 cooling ages (Fig. 3.2). A number of these white micas have been analyzed by the $^{40}Ar/^{39}Ar$ age spectrum method, to assess the effect of the crystallization of a new generation of mica at the expense of the earlier generation.

- As yet, relatively young metamorphic hornblendes have not often been studied using the $^{40}Ar/^{39}Ar$ stepheat method. Because of their low potassium concentrations and their young ages, these minerals contain relatively little $^{40}Ar^*$ and large quantities of atmospheric argon, $^{40}Ar_{atm}$. A study of these minerals will be a test of their usefulness for dating young metamorphic terrains.
- Hornblendes and actinolitic hornblendes were probably formed during the M_2 event. The scatter in their conventional K-Ar ages is large (i.e. between about 10 and 50 Ma). Consequently, interpretation of these ages as M_2 cooling ages, or crystallization ages caused by one single event is difficult. Although the petrology suggests that it is unlikely that these minerals crystallized during the M_1 event, this option cannot be excluded on the basis of K-Ar data alone. $^{40}Ar/^{39}Ar$ analysis may yield information as to the cause of the large range in conventional K-Ar ages of these minerals.

In summary, this work aims to identify the cause of the relatively large scatter in conventional K-Ar ages by $^{40}Ar/^{39}Ar$ stepheating analysis. Such an approach should improve our understanding of the timing of the thermal events experienced by the rocks. From estimates for the physical conditions during metamorphism it can be decided whether the isotopic ages may be interpreted as cooling ages, crystallization ages, or mixed ages originating from the effects of more than one thermal event on the rocks. Subsequently, in combination with estimates for the closure temperatures for argon, this information can be used to assess the thermal evolution of the rocks.

3.2 Experimental details

3.2.1 K-Ar dating

The potassium determination by wet chemical methods and the argon extraction in a high vacuum extraction line are standard laboratory procedures, which have been described elsewhere (Cooper 1963, McDougall and Schmincke 1977). Potassium was determined by flame photometry, using a lithium internal standard. In cases where hornblendes had a low potassium content, an isotope dilution technique was used for its measurement. Agreement between the two measurements was good. In order to extract the argon, the minerals are fused in an RF heated molybdenum crucible in a high vacuum line. After extraction, addition of a ^{38}Ar tracer and purification, the argon is measured isotopically in a mass spectrometer.

The mineral concentrates were prepared by standard mineral separation techniques, including heavy liquid separation and magnetic separation. The purity obtained was generally better then 99 percent.

3.2.2 Stepheating experiments

Procedures for $^{40}Ar/^{39}Ar$ dating, using the HIFAR reactor of the Australian Atomic Energy Commission, have been described by McDougall (1974) and McDougall and Roksandic (1974). The correction factors for interference by argon isotopes produced from calcium and potassium were given by Tetley et al. (1980). For this study, samples were irradiated for 120 hours in a facility next to core (positions X33 and X34). To minimize the effect of gradients in the fast neutron flux received by the sample, the sample containers were inverted after exactly 60 hours of irradiation. The fast neutron flux received by the samples was about $3.6 * 10^{12}$ $n/cm^2/sec$. Cadmium shielding was used to minimize the effect of thermal neutrons on the samples (Tetley et al. 1980).

After irradiation the isotopic composition of argon extracted from the flux monitor was determined. Laboratory standards biotite GA1550 (K-Ar age 97.9 Ma) and hornblende 77-600 (K-Ar age 414.2 Ma) have been used as flux monitors (McDougall and Roksandic 1974, Harrison 1981). Before the actual stepheating experiment, a split of the sample was measured by the direct fusion technique. Subsequently, a stepheating experiment was carried out on the remaining part of the sample. An experiment typically consists of 12 to 20 discrete steps of 30 minutes each at temperatures between about 400°C and fusion of the sample. The temperature of the sample was measured with an optical pyrometer on the upper inside wall of the molybdenum crucible and with a thermocouple in a cavity in the bottom of the crucible. The actual sample temperature was approximately equal to the average of the two measurements, which differed by about 120 °C.

The isotopic composition of argon extracted from the minerals was measured on a modified A.E.I. MS10 mass spectrometer. Subsequent data reduction was carried out on-line using an HP 1000E computer. The measured isotopic ratio is corrected for interferences by argon isotopes produced from calcium and potassium during irradiation, for radioactive decay of ^{39}Ar and ^{37}Ar, and for atmospheric argon, $^{40}Ar_{atm}$, which originates from the sample and the extraction line. To assess the proportion of $^{40}Ar_{atm}$ derived from the extraction line, lineblanks were measured at regular time intervals. The absolute amount of $^{40}Ar_{atm}$ derived from the lineblank may vary significantly between different stepheat experiments, but within single experiments the amount of $^{40}Ar_{atm}$ derived from the line decreases from typically 10^{-12} moles on the first day to about 10^{-14} moles on the fourth day of an experiment, indicating slow outgassing of the extraction line during the experiment.

The uncertainties in ages of individual steps were estimated by quadratical combination of the uncertainties in the measured isotopic ratios, and for the uncertainty in the irradiation parameter J (Dalrymple and Lanphere 1971). The uncertainty in the physical measurement of the $^{40}Ar^*/^{39}Ar_K$ ratio in an average step in a experiment on mica was about 0.2 to 0.5 percent. In a stepheating experiment on hornblende the uncertainty for an average step was about 1.0 to 5.0 percent, because of the lower

proportion of $^{40}Ar^{*}$ in the sample. The uncertainty in J was about 0.5 percent.

The results of $^{40}Ar/^{39}Ar$ stepheating experiments are displayed as age spectra, in which the apparent age of each step is given as a function of the total gas release (see Chapter 1). Integrated ages may be calculated over segments of the age spectrum, using either an average of the individual apparent ages, or from isotope correlation diagrams.

3.3 Conventional K-Ar dating

Numerous conventional K-Ar ages exist both for the metamorphic complex and the granodiorite on Naxos. The results of the present study are presented in Table 3.I. A compilation of all presently available K-Ar data is given in Figure 3.2 (Andriessen et al. 1979, Wijbrans and Andriessen 1980, Table 3.I).

White micas are important for this project, because they are found throughout the metamorphic complex. The highest K-Ar ages, 46.7 Ma and 48.3 Ma, were obtained from micas in zones I and II (Andriessen et al. 1979). The main difference between the results from zone I and zone II is that scatter towards lower ages becomes larger in zone II. In zone I, few K-Ar ages on white micas below 40 Ma were recorded, whereas in zone II ages as low as 24.3 Ma were obtained. Between the high grade part of zone II and the low grade part of zone IV, the highest recorded ages of the white micas decrease significantly from greater than 35 Ma to less than 15 Ma. From zone IV to the centre of the dome, white mica ages decrease slightly to values between 11.5 and 12.2 Ma.

Biotites are found in M_2 metamorphic mineral assemblages and in the granodiorite. Ages obtained with the K-Ar method range between 5.7 Ma and 13.3 Ma (Andriessen et al. 1979, Wijbrans 1980). Most biotites, however, yielded ages between 10 and 11 Ma (Fig 3.2), which are interpreted as recording cooling of the rocks below the closure temperature of biotite for argon (i.e. below about 300 ^{o}C). The age of 5.7 Ma was obtained from a biotite from a metapelite in the migmatite zone. Its age is substantially lower than all other biotite ages and regarded as anomalous. The biotite that yielded the age of 13.3 Ma is from a metapelite in zone III. The white mica from this sample yielded an age of 29.1 Ma (Wijbrans 1980). Biotite K-Ar ages may be slightly higher in zone III and the low grade part of zone IV, when compared to the more central and higher grade zones. This observation was interpreted as possibly caused by earlier cooling of the rocks which are further away from the thermal dome.

Figure 3.2. Summary of conventional K/Ar ages (Andriessen et al. 1979, Wijbrans 1980, this study). The individual ages are represented by the horizontal lines on the bars. PHE = phengite, PAR = paragonite, BIO = biotite MUS = muscovite, HBL = hornblende

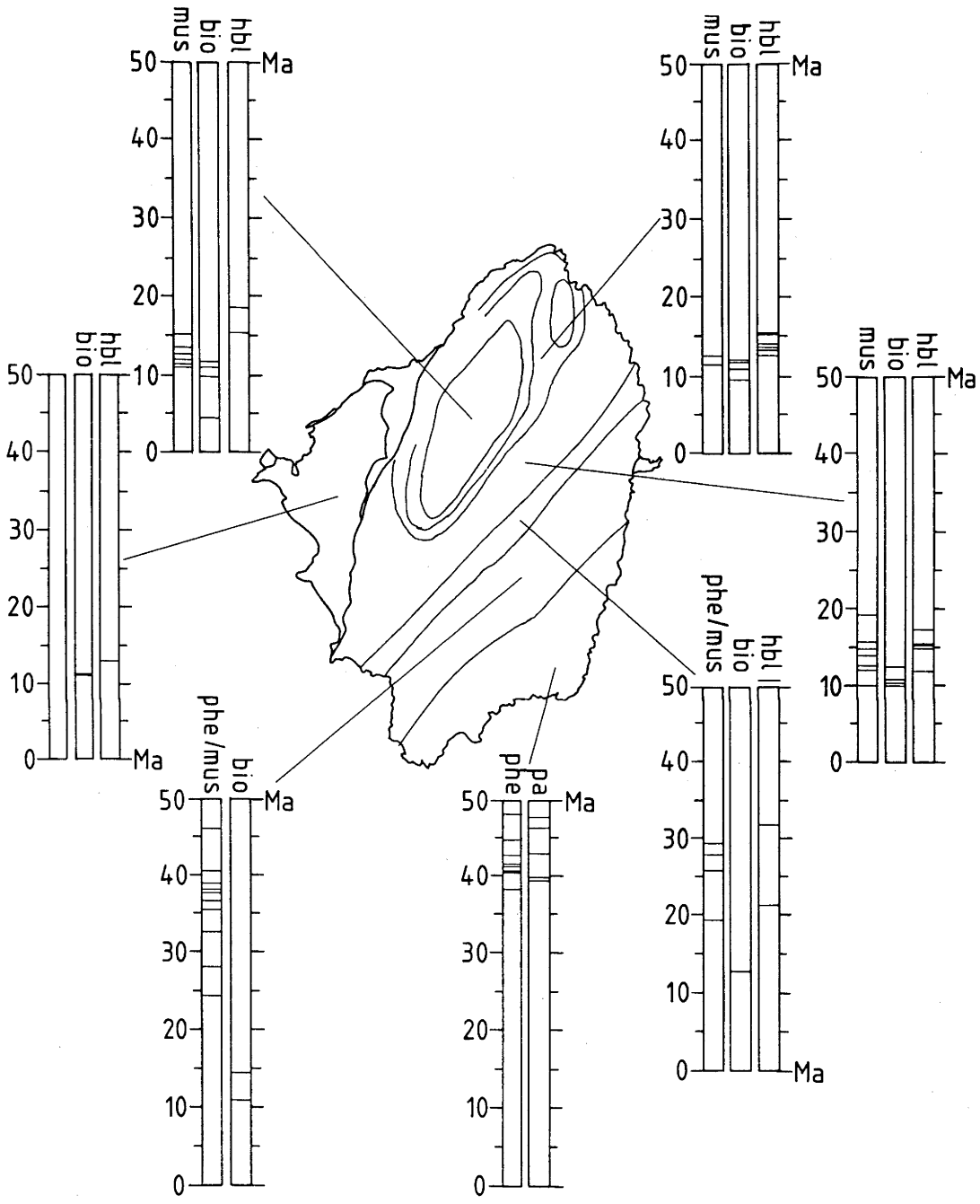

summary K/Ar data Naxos

Hornblendes from the amphibolites in the metamorphic complex range in composition from actinolitic to pargasitic hornblende (Fig. 3.4). In zone III some actinolite occurs as part of the greenschist assemblage chlorite-epidote-actinolite-albite, which is overprinted by an amphibolite facies assemblage including hornblende, calcic plagioclase and garnet. K-Ar ages on amphiboles range from 50.7 Ma in the low grade part of zone III, to about 12.7 Ma in an oval shaped thermal disturbance in zone V. In the migmatite, hornblende ages of 16.0 to 18.8 Ma are found. Andriessen (1978) reported some unexpectedly high ages for hornblendes from ultramafic lenses in zone V. These minerals have low potassium concentrations (less than 0.1 percent), and the ages were interpreted to be the result of the incorporation of excess argon in the crystals (Andriessen 1978).

Four mineral samples from the granodiorite have been measured. A biotite (81-546) has yielded an age of 11.2 Ma. A hornblende from the same sample yielded an age of 12.3 Ma. A biotite and a hornblende from another sample (81-548) yielded ages of 11.4 Ma and 13.5 Ma respectively. Repeated argon analyses of the two hornblendes have yielded ages between 12.1 and 13.5 Ma. Poor reproducibility was probably caused by sample inhomogeneiety. Nevertheless, all K-Ar determinations on hornblende yielded higher ages than the Rb-Sr whole rock isochron age of 11.1 $\pm$ 0.7 Ma reported by Andriessen et al. (1979). Because the Rb-Sr whole rock isochron age was determined by the analyses of aplites and pegmatites, the K-Ar ages of hornblendes are interpreted as a better estimate for the age of intrusion of the granodiorite.

3.3.1 Discussion

From the argon isotopic data on white micas, together with the major element chemical data (Fig. 3.3), and microstructural data, it was suggested that the white micas may be divided into two distinct groups (Andriessen 1978, Wijbrans 1980). In the low grade M_2 metamorphic zones the micas have ages up to 48.5 Ma. The chemical data show that in these zones phengitic mica dominates (Si^{4+}=6.7-7.0), these micas have experienced at least one deformation after crystallization. In the central region of Naxos, K-Ar ages of white micas range between 11.3 and 13.1 Ma.

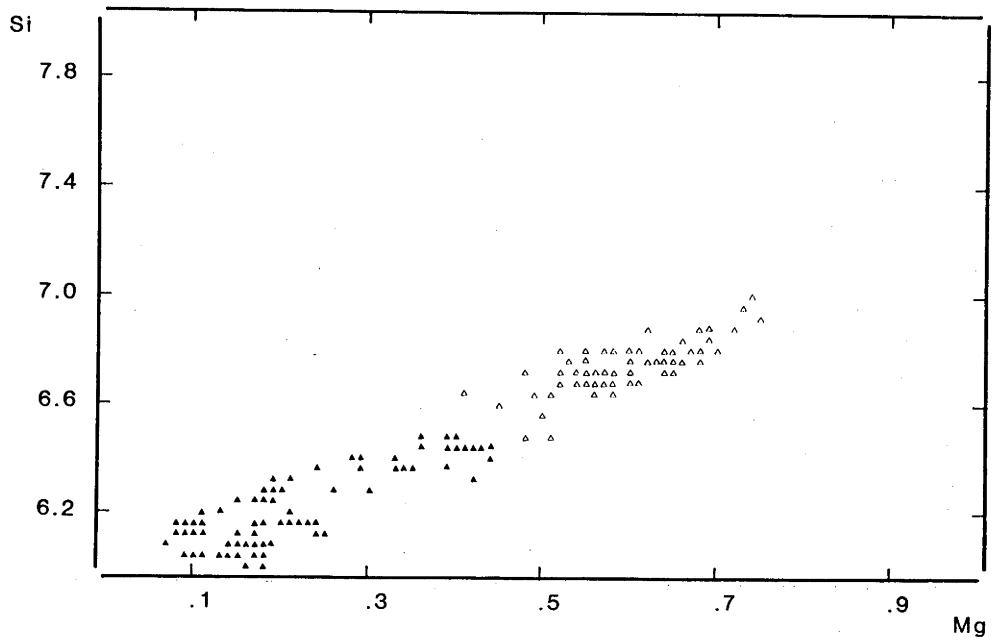

Figure 3.3. Summary of the major element chemistry of the white micas. The plot of Si against Mg (in coefficients of the structural formula based on 22-O) illustrates the transition of M_1 phengites to M_2 muscovites. The open symbols represent the phengites and the closed symbols represent the muscovites.

The chemistry of these micas indicates that muscovite (Si^{4+}=6.0-6.45) dominates. The phengites were formed during the M_1 metamorphism in the Eocene (Andriessen et al. 1979, timescale is according to Harland et al. 1982). The muscovites were formed in a subsequent thermal event during the Miocene. A consequence of the presence of two different groups of white micas on Naxos is that one must expect that along the thermal gradient caused by M_2 thermal dome metamorphism, the transition will occur from mineral assemblages containing mainly phengite to those containing mainly muscovite. This transition will cause mixed ages in white mica samples from this area.

In the centre of the island, the M_1 mineral assemblages were completely overprinted by mineral assemblages related to the M_2 metamorphism. During this second event biotite and muscovite were formed in the metapelites, and hornblende was formed in the amphibolites. Because the metamorphic temperatures during M_2 in zones V and VI are estimated to have exceeded 500 to 550 ^{o}C, the ages obtained from minerals in these zones probably record cooling of the rocks below the closure temperatures, T_c, of those minerals for argon. In the lower grade zones, M_2 minerals may have grown at temperatures close to or below their T_c for argon (cf. section 3.4.2.4, and Appendix III for a more detailed discussion).

The biotites and muscovites in the central zones yielded uniform K-Ar ages, recording a relatively simple cooling history after the peak of the M_2 event. The hornblendes, in contrast, show a range in ages of 38 Ma. It is difficult to interpret such a range in ages in terms of simple cooling after the M_2 event. A two stage history for the hornblendes is unlikely because the main amphibole developed during the M_1 event was glaucophane. Thus crystallization of actinolite and actinolitic hornblende is likely to have occurred after the M_1 event. It is possible that these minerals may have incorporated $^{40}Ar_{exc}$ during the M_2 event. This option will be explored further in sections 3.4.2.3 and 3.4.2.4.

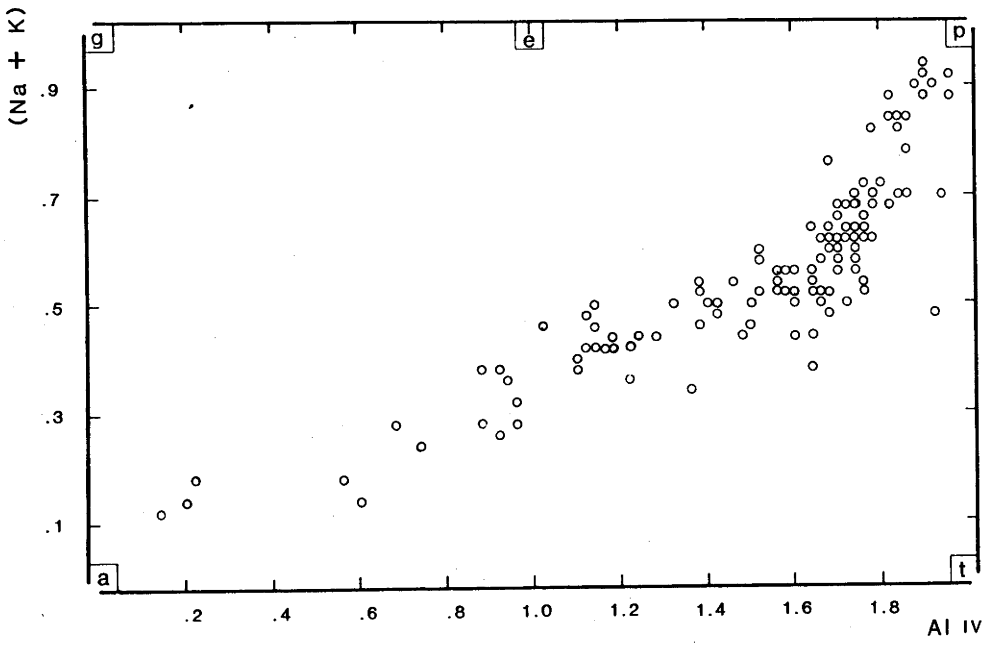

Figure 3.4. The chemistry of amphiboles. The transition of actinolites and actinolitic hornblendes in zone III to pargasite in zone VI is shown. Plot of (Na + K) against Al (in coefficients of the structural formula based on 23-O). a. actinolite, t. tschermakite, p. pargasite, e. edenite, g. glaucophane.

The K-Ar ages of biotites from the granodiorite are indistinguishable from those obtained from biotites from the metamorphic rocks. The hornblendes from the granodiorite yielded higher ages than biotites from the same samples, but slightly lower ages than hornblendes from the highest grade zones in the metamorphic complex. Because the age difference between hornblendes from the high grade M_2 metamorphic zones and the granodiorite is quite small (about 2 Ma), the granodiorite probably intruded shortly after the peak of the M_2 metamorphism. Thus the thermal histories of both rock units are very similar.

3.4 $^{40}Ar/^{39}Ar$ dating

3.4.1 Dating of the M_1 event

In order to date the M_1 metamorphism at Naxos more precisely, three phengites from zone I in the metamorphic complex were dated by the stepheat method (Table 3.II). The age spectra of phengites from this zone show low initial ages (about 20 to 25 Ma), followed by steep increases in the first part of the age spectrum, followed by a more gentle increase in ages (Fig. 3.5). For sample 81-582 there is a well developed horizontal segment in the spectrum, but in the case of 81-580 and 81-583 the ages increased throughout the experiment. Despite these differences, all three age spectra are very similar in appearance. Phengite 81-582 has yielded a conventional K-Ar age of 48.6 Ma. In the stepheating experiment, a integrated age of 49.5 $\pm$ 0.1 Ma was obtained over a horizontal segment of about 60 percent of the ^{39}Ar released (Fig. 3.5). This age is interpreted as recording cooling of the rock below the closure temperature of phengite for argon, i.e. about 360 to 410°C (see Chapter 1). As the maximum temperature for the M_1 metamorphism estimated from the mineralogy of the rocks was 500 - 530°C, the peak of the M_1 event must have occurred somewhat earlier than 49.5 Ma ago.

The other two stepheat experiments on phengites from zone I show continuously rising ages to a maximum of 44.5 Ma in 81-583 and 47.5 Ma in 81-580 (Fig. 3.5). If argon loss from white micas can be described in terms of a volume diffusion mechanism, as is suggested by the shape of the age spectra obtained from these phengites (Fig. 3.5), then the highest age reached in a continuously rising age spectrum must be interpreted as a minimum estimate for the original age. These three age spectra of M_1 phengites from zone I suggest that argon was lost from the minerals at some time subsequent to crystallization and that the sample yielding the highest K-Ar age was least disturbed. Therefore, the information obtained from these three age spectra from zone I, supports the interpretation that cooling of the rocks below the T_c of phengites for argon at about 50 Ma, and that the scatter observed in the K-Ar ages in this area was caused by argon loss from the original crystals.

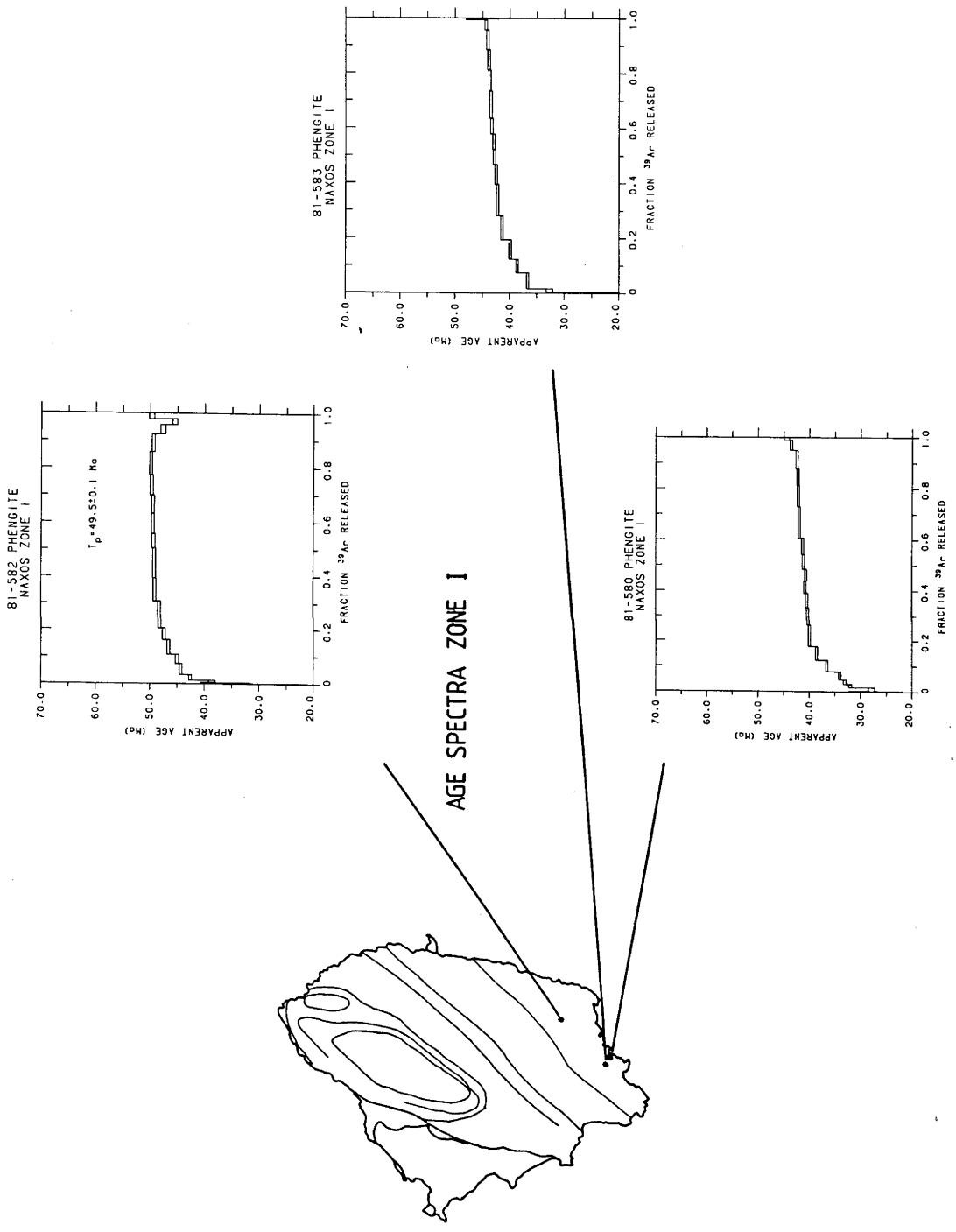

Figure 3.5. Age spectra of phengites in zone I.

3.4.1.1 Model calculations of diffusional loss of argon

The resemblance between the observed phengite age spectra and release patterns predicted from diffusion theory (Turner 1968), suggests that $^{40}Ar^{*}$ was lost from the crystals by volume diffusion. In 81-582 good agreement exists between the measured age spectrum and the predicted age distribution based on the model suggested by Turner (1968). The line shown in Figure 3.6a is based on a model with an initial age of 50 Ma and 3.5 percent of the accumulated argon lost during overprinting at 15 Ma. In the calculation, the equation for diffusional loss from an infinite cylinder was used, because this geometry best describes diffusion from mica crystals (Gilleti 1974). The models were calculated assuming a discrete grain size, because the samples are closely sized (see Table 3.II). Experimental work on phlogopite indicated a correlation between diffusion rate and grain size, suggesting that the effective diffusion radius is close to the radius of the actual grains (Giletti 1974).

For sample 81-583, three model release patterns have been calculated (Fig. 3.6b). Model 3, which assumes an original age of 45 Ma and 15 percent argon loss at 15 Ma, resembles the measured age spectrum best. This would suggest that cooling below the T_c of phengite for argon occurred slightly later in the area where phengites 81-580 and 81-583 were sampled, when compared with sample 81-582. Continuously rising age spectra, however, are not predicted by Turner's models if the fraction of gas released during overprinting is relatively small. The fact that samples from two different locations, about one kilometre apart, have yielded virtually identical age spectra, suggests that these age spectra have some geological meaning, rather than resulting from some experimental artifact.

Harrison and McDougall (1982) argued that minerals, which have cooled slowly through the temperature interval where the transition occurs from fully open to fully closed system behaviour with respect to argon, will not yield a horizontal segment, but continuously rising ages. The existence of such age spectra was demonstrated by experiments on K-feldspars from Separation Point, New Zealand which were known to have cooled

Figure 3.6. Model release patterns after Turner (1969), (a) Time(1)=50 Ma, Time(2)= 15 Ma, fraction of argon lost at Time(2) = 3.5 percent. (b) Three models are presented for the release of argon from 81-583, model three which is based on an initial age of 45 Ma and overprinting at 15 Ma describes the observed pattern best. The details of the models are discussed in the text.

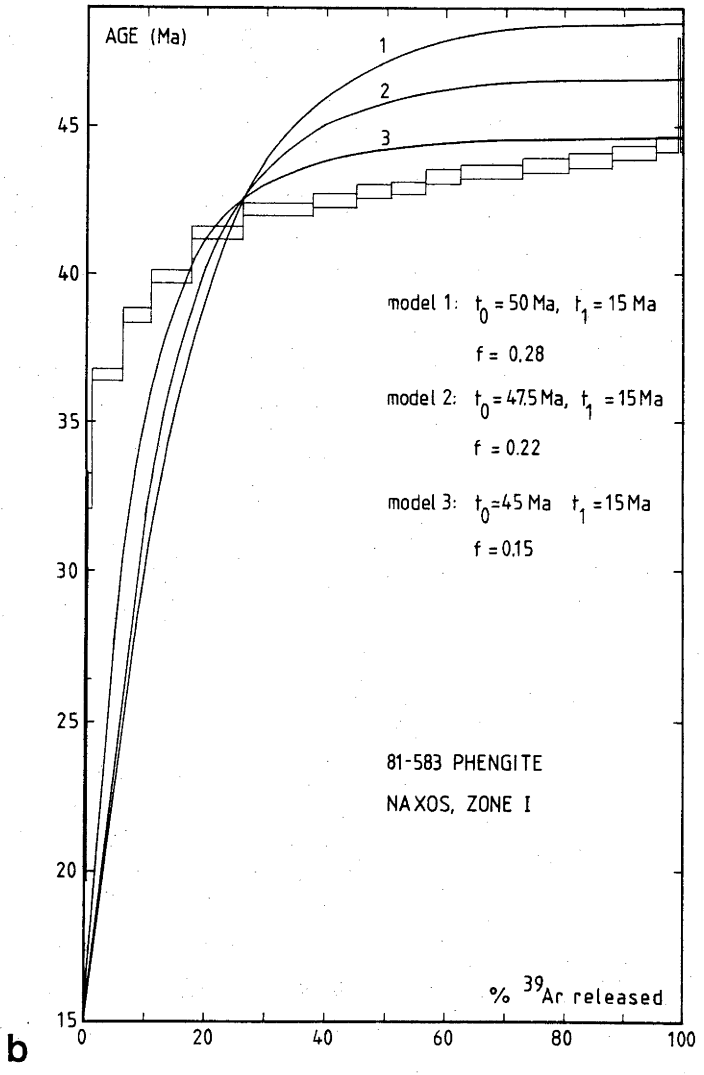
AGE (Ma)
1
2
3
model 1: t_0 = 50 Ma, t_1 = 15 Ma
f = 0.28
model 2: t_0 = 47.5 Ma, t_1 = 15 Ma
f = 0.22
model 3: t_0 = 45 Ma t_1 = 15 Ma
f = 0.15
81-583 PHENGITE
NAXOS, ZONE I
% ^{39}Ar released
15
20
25
30
35
40
45
0
20
40
60
80
100

b

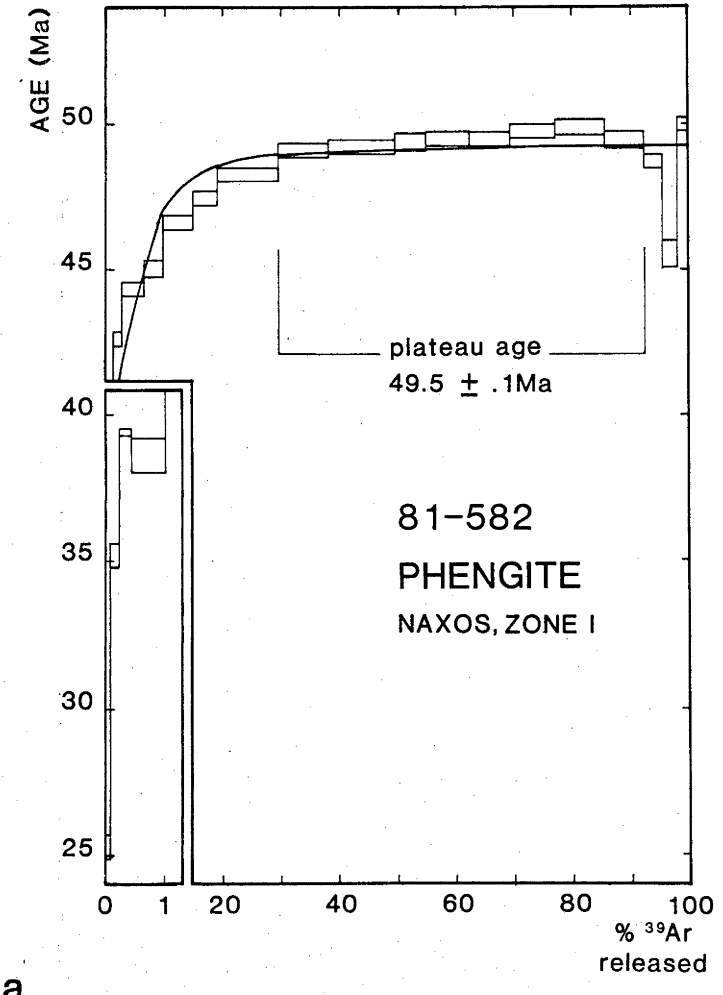
AGE (Ma)
50
45
40
35
30
25
plateau age
49.5 ± .1Ma
81-582
PHENGITE
NAXOS, ZONE I
0
1
20
40
60
80
100
% ^{39}Ar
released

a

slowly through this temperature interval. Calculation of cooling curves (see Chapter 4) for cooling after the M_1 metamorphism indicates that cooling through the 400 to 300 ^{o}C temperature interval (i.e. the temperature interval in which phengites start to accumulate argon) may have been slow. No geological data supports more complex thermal histories for the region, thus slow cooling of the rocks through the closure temperature of phengite for argon may be a possible interpretation of these age spectra.

3.4.2 Dating of the M_2 metamorphism

3.4.2.1 The migmatite zone

To establish the age of the M_2 event, the $^{40}Ar/^{39}Ar$ stepheat method was applied to a hornblende, a muscovite and a biotite from the central migmatite zone (Table 3.II). The muscovite and the biotite were from sample 81-556, and the hornblende was from amphibolite 81-557 sampled about 50 m from 81-556. It is unlikely that significant differences in thermal histories occur at this scale. These three samples may, therefore, be used to derive a cooling curve for this area. The cooling curve will be discussed in section 3.5.2. All three minerals have good flat age spectra (Fig. 3.7). The hornblende 81-557 has some minor structure in the low temperature steps, which may be the result of some diffusion of excess argon into the mineral during the early stages of cooling (see paragraph 3.4.2.3). A good integrated age of 15.0 $\pm$ 0.1 Ma was obtained for 95 percent of the gas release. The muscovite age spectrum has some minor structure in the first few percent of gas release, but shows a well developed horizontal segment for the major part of the age spectrum. The integrated age is 11.8 $\pm$ 0.1 Ma (Fig 3.7). The age spectrum of the biotite is similar to that of the muscovite in that it shows low initial ages and a horizontal segment over the bulk of the argon release. The integrated age of the biotite is 11.4 $\pm$ 0.1 Ma (Fig. 3.7). The low ages in the initial steps of both micas may indicate some loss of $^{40}Ar^{*}$ subsequent to beginning of argon accumulation. The integrated ages over the horizontal segments of hornblende 81-557 and muscovite 81-556 are in good agreement with ages of 14.9 $\pm$ 0.3 Ma and 11.7 $\pm$ 0.1 Ma respectively, calculated from $^{39}Ar/^{40}Ar$, $^{36}Ar/^{40}Ar$ correlation diagrams over the horizontal segments.

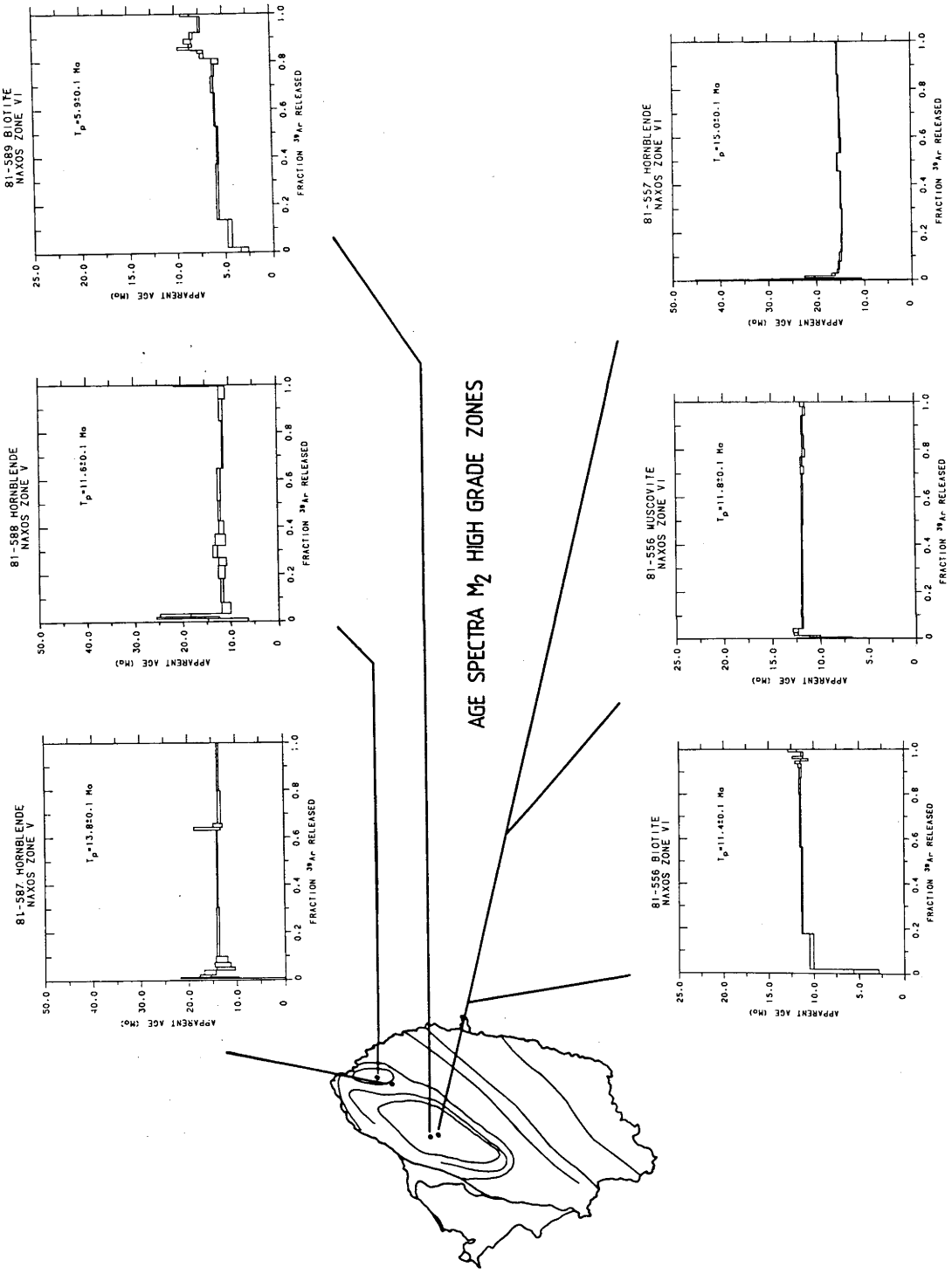

Figure 3.7. Age spectra of M_2 minerals in the centre of Naxos.

The petrology of these rocks suggests that the maximum temperature experienced during the M_2 metamorphism was about 700 ^{o}C. Therefore, the ages obtained from samples 81-556 and 81-557 are interpreted as recording cooling of the system below the closure temperatures of hornblende, muscovite and biotite for argon (i.e. below about 540 to 520^{o}C, 410 to 360^{o}C and 300^{o}C respectively (cf. Chapter 1)). Combination of these closure temperatures with the ages discussed above indicates that during this part of the cooling history, the rocks cooled at a rate of about 50^{o}C/Ma. Cooling rates of this order of magnitude are not uncommon in young metamorphic belts (Dodson 1979).

Biotite 81-589 from the migmatite zone yielded an exceptionally low K-Ar age (measured by Andriessen (1978) at 5.7 Ma). A $^{40}Ar/^{39}Ar$ stepheat experiment revealed a horizontal segment over about 50 percent of the gas release at 6.7 Ma, and in the high temperature steps some structure, indicating possibly a component of gas in the sample with an age similar to the ages of other biotites from Naxos. However, age spectra from biotites may not be very informative because of breakdown of biotites during stepheating in a vacuum extraction line (Roddick et al. 1980, Foland 1983). The stepheating experiment was carried out in an attempt to identify the cause of its anomalously low age. Although some evidence for an older component was found in the age spectrum, its shape is poorly understood.

3.4.2.2 The northern part of zone V

A slightly different cooling history was recorded by hornblendes from the northern part of the metamorphic complex. On the basis of differences in mineralogy, an oval shaped zone was mapped by Jansen (1973), where the metamorphic temperature during M_2 was somewhat higher than in the surrounding rocks. Two hornblendes from this zone were measured, 81-587 from the margin of this zone and 81-588 from the centre of this zone (Fig. 3.7). The age spectrum of hornblende 81-587 is essentially flat, with a integrated age of 13.8 Ma. The age spectrum of 81-588 yielded a integrated age of 11.6 Ma. Because the estimated metamorphic temperature (about 550 to 600 ^{o}C) during M_2 at the location of 81-588 probably exceeded the T_c of hornblende for argon, this age is assumed to record the cooling of the rock below the T_c of

hornblende for argon. In the case of hornblende 81-587, it is estimated that the metamorphic temperature (500 to 520 ^{o}C) during the M_2 event was close to the T_c of hornblende for argon. The observed age may be interpreted either as a crystallization age, or as a cooling age. The difference in time between crystallization and cooling below the T_c for argon was probably small, because the maximum estimated metamorphic temperature for this area was near the closure temperature of hornblende for argon, and it is inferred that the rocks experienced rapid uplift at this time (see Chapter 4).

These age spectra, supported by a K-Ar age of a hornblende 81-570 of 12.7 Ma, suggest that in this area cooling occurred somewhat later than in the centre of the metamorphic complex. In this particular area, pegmatites are more abundant than in rocks of similar metamophic grade elsewhere in the complex, possibly indicating local intrusive activity. Thus these younger ages may be the result of heating of the rocks caused by some igneous process below the presently exposed erosion surface during the waning stages of the M_2 event.

3.4.2.3 Excess argon in hornblendes

It was discussed in section 3.3 that conventional K-Ar ages of hornblendes in the centre of Naxos and towards the southeast formed during the M_2 metamorphism, show a rather large scatter. Although the petrology indicates that these minerals are part of M_2 mineral assemblages, their conventional K-Ar ages approach values which are compatible with crystallization during the M_1 metamorphism. Possibly, the observed increase in K-Ar ages in rocks from lower grade M_2 metamorphic grade was caused by excess ^{40}Ar in the crystals. To test this hypothesis, the $^{40}Ar/^{39}Ar$ stepheating method was applied to a series of hornblendes from zone III, the biotite-chloritoid zone, to zone VI, the migmatite zone in the M_2 metamorphic zonation.

The age spectra of these hornblendes show anomalously high ages in the low temperature steps, decreasing toward higher temperature steps. In hornblendes 81-557, 81-550, 81-564 and 81-536 the apparent ages decrease until an horizontal segment is reached. In hornblende 81-540, however, after a minimum was

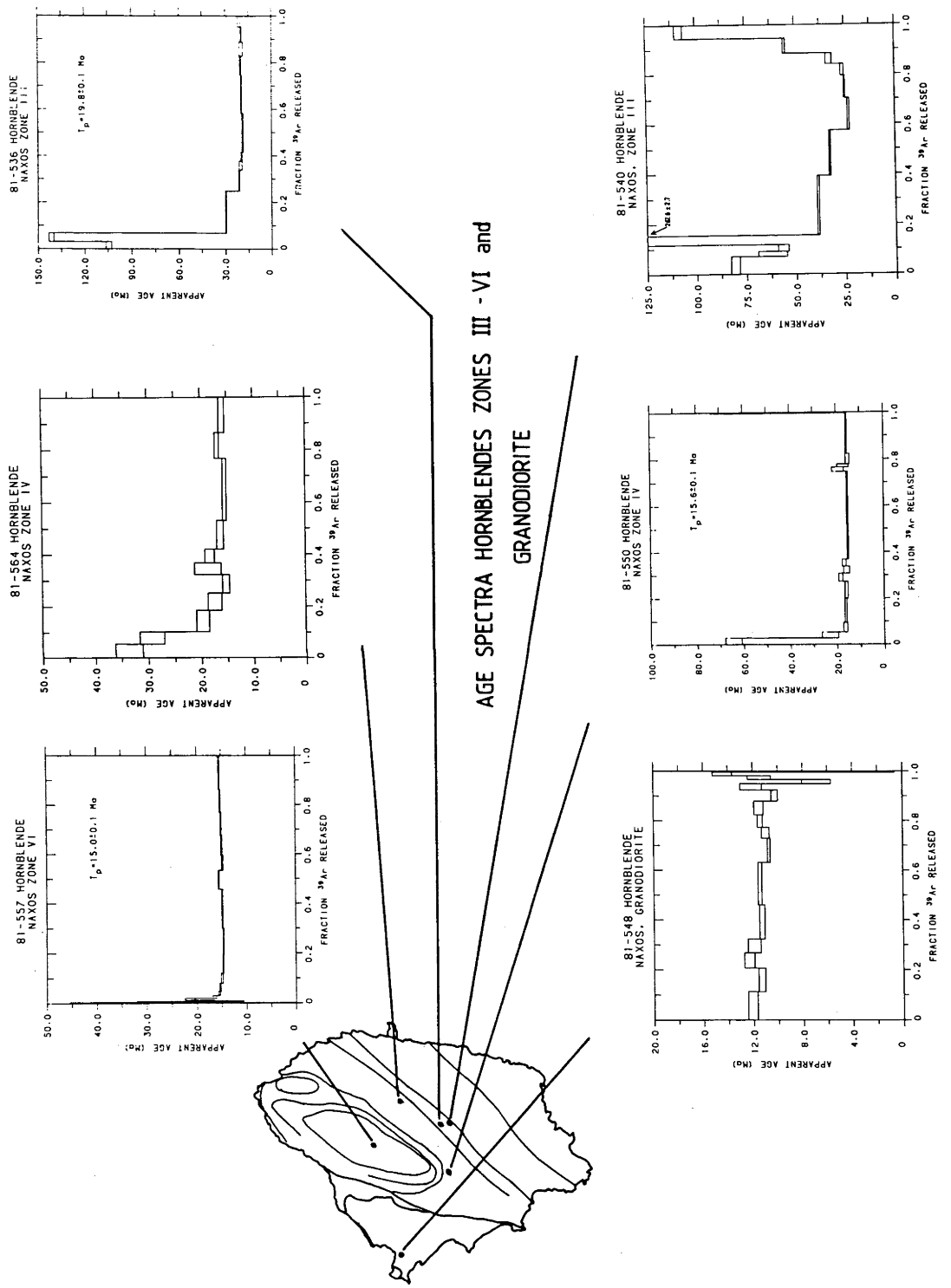

Figure 3.8. Age spectra of hornblendes with excess argon.

reached, the apparent ages increase again in the high temperature steps of the experiment (Fig. 3.8). The shape of age spectra 81-557, 81-550, 81-564 and 81-536 suggests simple volume diffusion of $^{40}Ar^{*}$ into the crystals subsequent to crystallization. Integrated ages over the sections of the age spectra yielding the lowest apparent ages agree well with ages obtained from $^{39}Ar/^{40}Ar$, $^{36}Ar/^{40}Ar$ correlation diagrams.

Diffusion of $^{40}Ar_{exc}$ into minerals will tend to raise the observed minimum ages recorded in age spectra (Lanphere and Dalrymple 1976, Harrison and McDougall 1982). Thus there is reason to assume that the apparent increase in minimum ages observed in these age spectra is related to the increased component of $^{40}Ar_{exc}$ in the samples. This relation is illustrated in Fig. 3.9. Model release curves in this diagram were calculated under the assumption that the diffusion equation describes both diffusion out of a body and diffusion into a body (Crank 1975). Instead of having a surface concentration of zero, as might be a usually accepted boundary condition for diffusion from a mineral, the surface concentration is set to a constant value. For convenience, this is represented in diagram 3.9 by the $^{40}Ar_{(* + exc)}/^{39}Ar_{K}$ ratio found in the initial gas released from the minerals. Thus, the arbitrary initial age of 60 Ma in Figure 3.9 represents a measure of the $^{40}Ar_{(* + exc)}$ concentration at the surface of the mineral. The fraction of excess argon in the minerals is calculated as a fraction of the total amount of gas at the beginning of the stepheat experiment. This diagram demonstrates that the recorded minimum age in an age spectrum affected by excess argon will be closer to the true age when the relative importance of $^{40}Ar_{exc}$ is small, and will deviate more from the true age when the proportion of $^{40}Ar_{exc}$ in the sample increases. In the argon loss model, the surface concentration of argon during overprinting is taken as zero (Turner 1968). In the excess argon model, the surface concentration of argon is an additional variable, which depends on the partial pressure of argon in the metamorphic fluid. Thus in minerals of equal age with equal amounts of excess argon, the sample with the highest surface concentration of argon will yield ages in the high temperature part of the experiments that are closer to the true age of the sample.

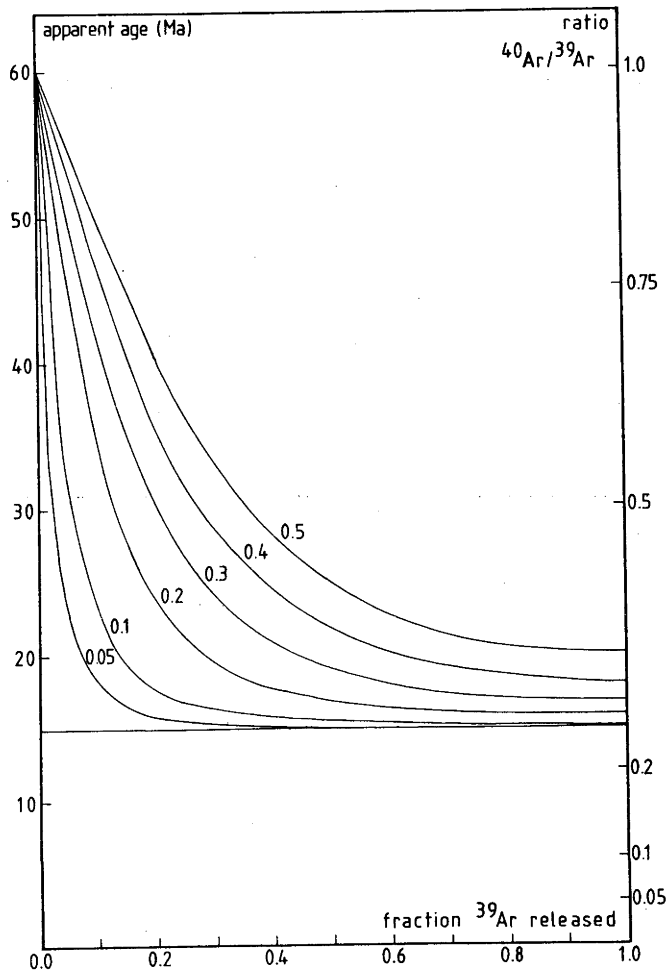

Figure 3.9. The diffusion of excess argon into minerals. The curves are based on 15 Ma old minerals, which contain presently 50 percent, 40 percent, 30 percent, 20 percent, 10 percent, 5 percent and 0 percent excess argon. The surface concentration of argon is represented by an apparent age of 60 Ma.

The age spectra of samples 81-557, 81-550, 81-564, and 81-536 indicate that towards lower M_2 metamorphic grade, the fraction of $^{40}Ar_{exc}$ in the samples becomes more important. Concomitantly, the apparent ages of the horizontal segments increase, as would be expected from the model discussed above. In the age spectra of 81-557 and 81-550, excess ^{40}Ar is restricted to the first few percent of the total gas released; therefore, the integrated ages of 15.0 Ma and 15.6 Ma, respectively, over the remaining part of the gas release are interpreted as reliably dating the beginning of accumulation of $^{40}Ar^*$ in these samples. The age spectrum of 81-564 yielded an integrated age over the plateau segment of 16.1 Ma. From a $^{39}Ar/^{40}Ar$, $^{36}Ar/^{40}Ar$ isotope correlation diagram over the same segment an age of 16.0 $\pm$ 1.1 Ma was obtained. Because of the fraction of excess ^{40}Ar is somewhat larger, this age spectrum may well be explained by the combination of excess ^{40}Ar and accumulation of radiogenic ^{40}Ar since 15 Ma ago. Sample 81-536 has an even larger fraction of excess ^{40}Ar and the age spectrum has still a shape which may be explained by diffusion of excess ^{40}Ar into the crystals. In this age spectrum an age of 19.8 $\pm$ 0.1 Ma was calculated (Fig. 3.8). The age obtained from a $^{39}Ar/^{40}Ar$, $^{36}Ar/^{40}Ar$ isotope correlation diagram was 19.6 $\pm$ 1.0 Ma. According to the excess argon model (Fig 3.9), the minimum age recorded in the experiment will be a maximum estimate for the true age of the sample. Because of the uniform ages of 15 Ma obtained from higher grade hornblendes and the large proportion of excess argon in the sample, it is suggested that in sample 81-536 argon accumulation may have started at some time significantly later than 19 Ma ago, possibly also near 15 Ma. Thus, $^{40}Ar/^{39}Ar$ age spectrum analyses show that despite their considerable scatter in conventional K-Ar ages, argon accumulation in all these hornblendes started during an time interval of less than 4 Ma.

In hornblende 81-540 high initial ages are recorded, decreasing monotonically to a minimum value of about 24 Ma and then in the last 30 percent of gas release, the apparent age increases again (Fig. 3.8). This type of age spectrum has been associated with $^{40}Ar_{exc}$ in the system (Lanphere and Dalrymple 1976). The sample comes from a rock in zone III, where the reaction occurs in the mafic rocks from a greenschist facies

assemblage containing actinolite-albite-epidote-chlorite, to an amphibolite facies assemblage containing hornblende-plagioclase-garnet. Both actinolite and actinolitic hornblende can be found in thin section. Saddle or U-shaped $^{40}Ar/^{39}Ar$ age spectra may be caused by differences in degassing of chemically different domains within the crystals, or degassing of different classes of lattice sites (Harrison and McDougall 1981, Claesson and Roddick 1982). Such a mechanism may possibly have caused the U-shaped age spectrum of hornblende 81-540 as well, because in the sample two different amphiboles were identified. Both the studies of Lanphere and Dalrymple (1976), and of Harrison and McDougall (1981) suggest that the minimum recorded ages in saddle shaped age spectra are higher than the true ages, and that the minimum ages deviate more from the true age with increased fractions of excess ^{40}Ar in the samples. Consequently, the age of 24 Ma of hornblende 81-540 must be interpreted as a maximum estimate for the beginning of argon accumulation. Considering the substantial amount of excess argon in this sample, its true age may well be close to that of the hornblendes discussed above, but apart from support for the interpretation of the K-Ar age of 50.7 Ma as a result of excess argon, little exact age information can be obtained from this age spectrum. The anomalous age of step four in this age spectrum is not well understood, but may possibly be the result of some disproportional release effect between ^{40}Ar and ^{39}Ar, or of sudden degassing of a reservoir of ^{40}Ar, for example from fluid inclusions.

It is proposed that for hornblendes from the major part of the M_2 metamorphic complex, argon accumulation started about 15 Ma ago, and that incorporation of excess argon occurred in the early stages of cooling after the peak of the M_2 event. Under this assumption, the absolute amounts of excess ^{40}Ar in the samples may be estimated. The amounts of $^{40}Ar_{exc}$ in the minerals are very similar (Table 3.III). Values range from $1.1*10^{-12}$ moles/g in 81-564 to $1.2*10^{-11}$ moles/g in 81-540, with a tendency to be higher in rocks from lower grade M_2 metamorphic zones. The effect of $^{40}Ar_{exc}$ on different age spectra is well illustrated by comparing samples 81-557 and 81-564. Both samples were estimated to contain similar amounts of excess argon, but have quite different potassium contents and cooling histories. As a result,

in 81-557 the excess argon shows only in the initial steps of the age spectrum, whereas in sample 81-564 a much larger part of the age spectrum was affected by excess argon.

3.4.2.4 Interpretation of hornblende ages

The interpretation of isotopic ages in a metamorphic terrain often may be somewhat ambiguous, because not all ages will record cooling of the system below the closure temperature, T_c, for argon, as will be the case for igneous rocks emplaced at high levels in the crust. Along the M_2 thermal gradient in the rocks on Naxos, the composition of the amphiboles changes gradually from actinolitic hornblende near the + biotite isograd to pargasite in the migmatite zone (Fig. 3.4). The estimated temperature of formation of these minerals ranges from about 400 ^{o}C to about 700 ^{o}C (see Chapter 2). Because the estimated closure temperature of hornblende for argon is about 520 to 540 ^{o}C for the conditions on Naxos, one must expect that along the M_2 thermal gradient the transition occurs from ages which record crystallization, to ages which record cooling of the rocks below the closure temperature for argon. Clearly, the interpretation of ages from hornblendes in such an area depends on reliable estimates of both T_c and the metamorphic temperature.

Accumulation of radiogenic ^{40}Ar in hornblendes was suggested to have started throughout much of Naxos at about 15 Ma ago. From the discussion in the previous paragraph it follows that along the M_2 thermal gradient the ages of hornblendes cannot be interpreted <u>only</u> as cooling ages, or <u>only</u> as crystallization ages. On the basis of a T_c of hornblende for argon of about 520 to 540 ^{o}C, it is suggested that the ages of 81-550 (M_2 metamorphic temperature, $T(M_2)$, is about 530 ^{o}C), 81-564 ($T(M_2)$ about 440 ^{o}C), 81-536 ($T(M_2)$ about 420 ^{o}C), and 81-540 ($T(M_2)$ about 400 ^{o}C) will record crystallization of the minerals, rather than cooling below the T_c of hornblende for argon. The age of hornblende 81-557 ($T(M_2)$ is about 700 ^{o}C) records cooling of the rocks below the T_c of hornblende for argon. Sample 81-564 is from a key locality on Naxos, because it was sampled virtually on the - chloritoid isograd. This sample was formed at a metamorphic temperature of about 440 ^{o}C (Chapter 2). From the same locality (within 20 m) a metapelite (81-565) was sampled that contains

chloritoid and staurolite side by side. The white mica in this rock has yielded a K-Ar age of 19.1 Ma, a mixed age caused by the presence of M_1 formed phengite as well as M_2 formed muscovite in the sample (see section 3.4.2.5.). The age spectrum of hornblende 81-564 has yielded an integrated age of 16.1 Ma over the steps least affected by excess argon. Because of the presence of excess argon in this sample, this age is interpreted as a maximum estimate for the true age of the sample. Further, because of the difference in diffusion parameters between hornblende and white mica, it is suggested that at temperatures where white micas are not fully open for argon, hornblendes are likely to retain their argon. Thus, the recorded age must be taken as a maximum estimate for the age of crystallization of the hornblende. This hornblende was formed during the peak of the M_2 metamorphism, thus the peak of the M_2 metamorphism must have occurred at some time later than 16 Ma ago. Consequently, in order to record a cooling age of 15.0 Ma for hornblende 81-557 in the migmatite zone, initial cooling from 700-720 ^{o}C to about 535 ^{o}C must have occurred at a rate of 150 to 200 ^{o}C/Ma. Cooling rates of this magnitude are commonly observed during the initial stages of cooling after the intrusion of magmas, but are not normally thought to be characteristic of regional metamorphic belts.

3.4.2.5 White micas from zone II, III and IV.

It was shown in section 3.4.1 that phengites in zone I have age spectra that closely resemble the predicted release patterns for episodic loss of argon in a thermal event subsequent to beginning of argon accumulation. Muscovite from central Naxos has yielded a perfectly flat release pattern (section 3.4.2.1). Age spectra of white mica samples from the M_2 mineral zones II, III and IV around the thermal dome (Fig. 3.1) are presented in Figure 3.10. They commonly show low initial ages, rising monotonically until a horizontal segment or a maximum age is reached. Apart from the age spectrum of 81-537, all age spectra show a decrease in ages in the high temperature steps. The shape of these age spectra will be called upward-convex (Foland 1983). Maximum recorded apparent ages decrease as the M_2 thermal dome is approached and range from 43.3 Ma in sample 81-585 (Fig. 3.10 curve a) from zone II to 17.15 Ma in sample 81-586 (Fig. 5 curve

Figure 3.10. Age spectra for white micas from the transition zone from M_1 formed phengites to M_2 formed muscovites. For sample locations see Figure 3.1. a : sample 81-585, b : sample 81-541, c : sample 81-534, d : sample 81-532, e : 81-537, f : sample 81-586.

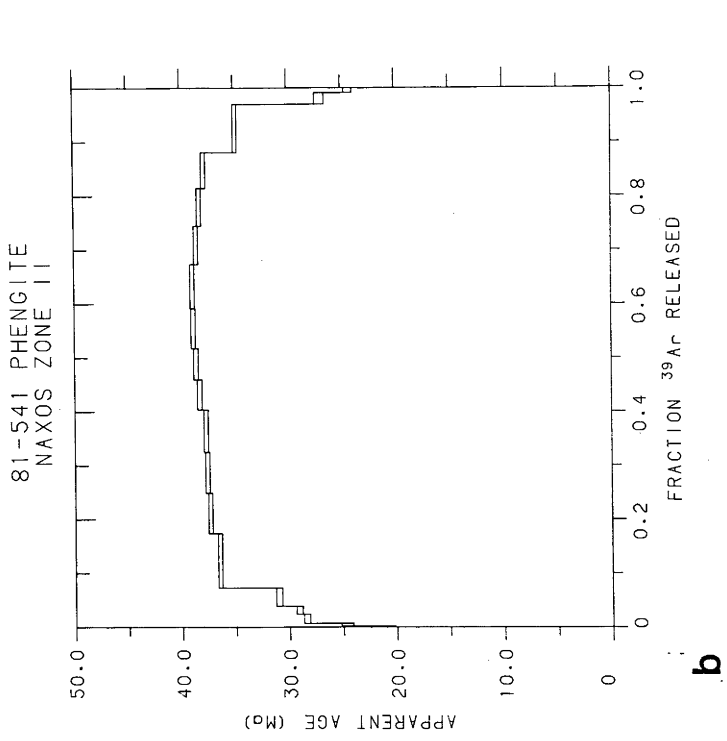
81-541 PHENGITE
NAXOS ZONE 11
APPARENT AGE (Ma)
50.0
40.0
30.0
20.0
10.0
0
0
0.2
0.4
0.6
0.8
1.0
FRACTION ^{39}Ar RELEASED
b

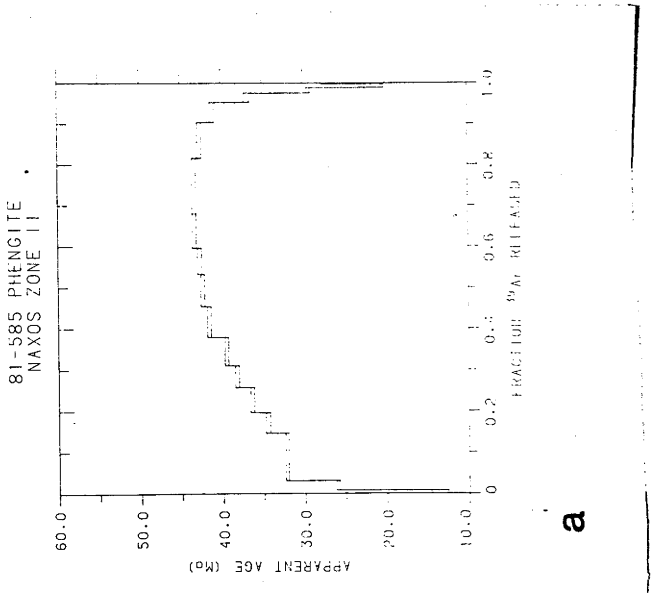
81-585 PHENGITE
NAXOS ZONE 11
APPARENT AGE (Ma)
60.0
50.0
40.0
30.0
0
a

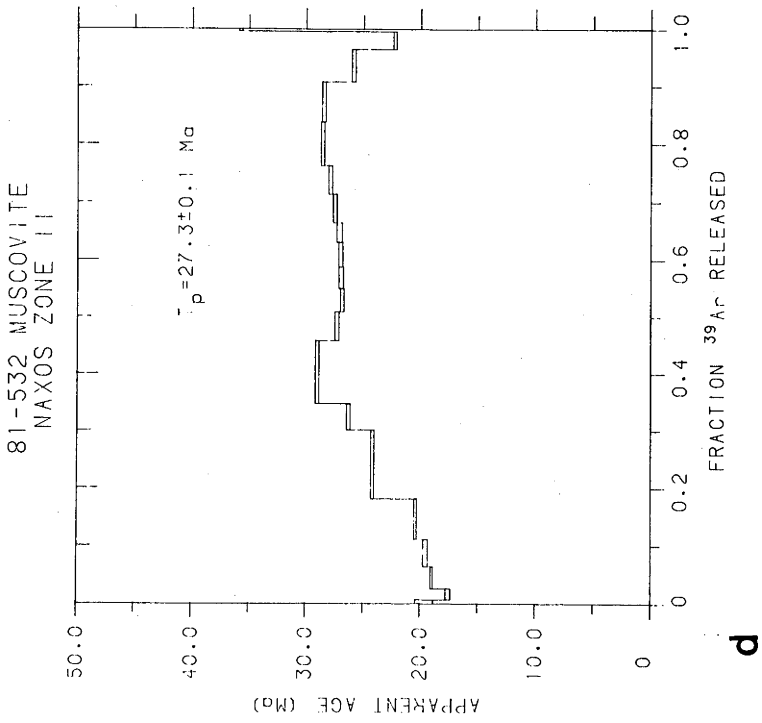
81-532 MUSCOVITE
NAXOS ZONE II
T_p=27.3±0.1 Ma
APPARENT AGE (Ma)
50.0
40.0
30.0
20.0
10.0
0
0
0.2
0.4
0.6
0.8
1.0
FRACTION ^{39}Ar RELEASED

d

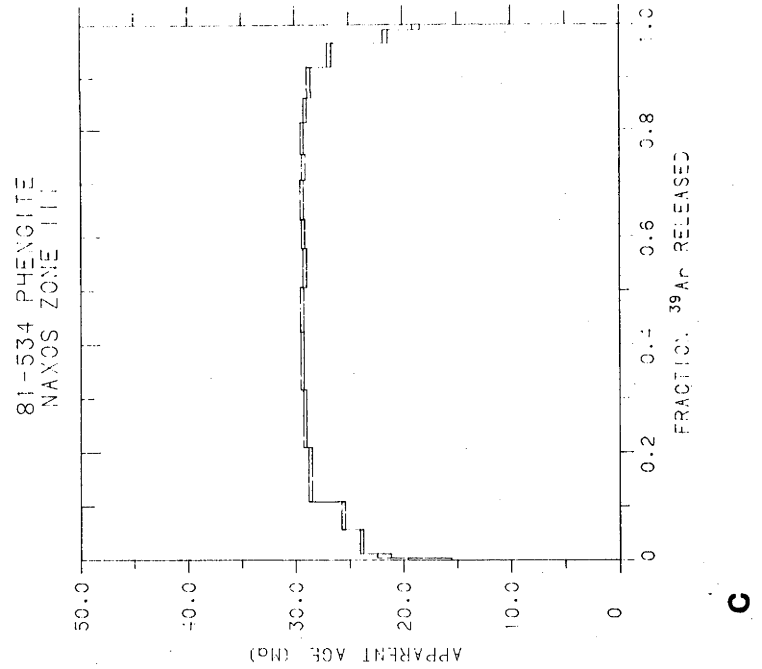
81-534 PHENGITE
NAXOS ZONE III
APPARENT AGE (Ma)
50.0
40.0
30.0
20.0
10.0
0
0
0.2
0.6
0.8
FRACTION ^{39}Ar RELEASED

c

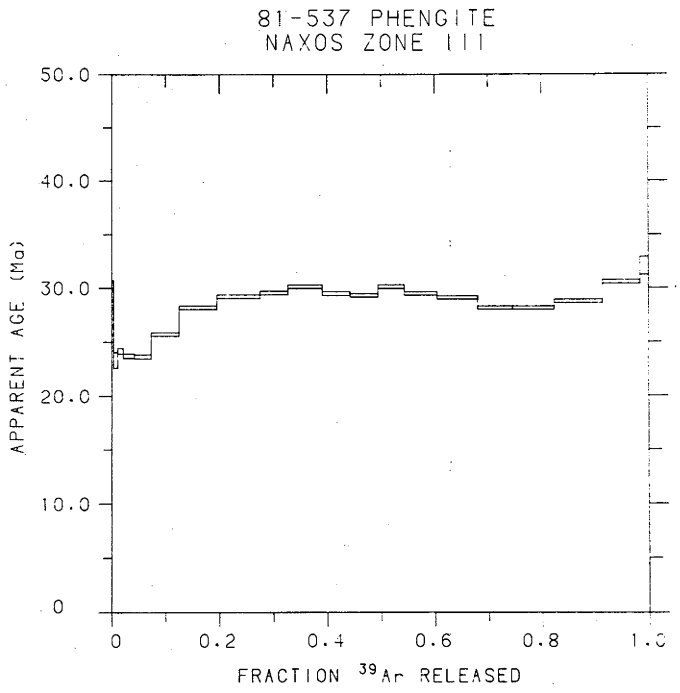
81-537 PHENGITE
NAXOS ZONE III
APPARENT AGE (Ma)
50.0
40.0
30.0
20.0
10.0
0
0
0.2
0.4
0.6
0.8
1.0
FRACTION ^{39}Ar RELEASED

e

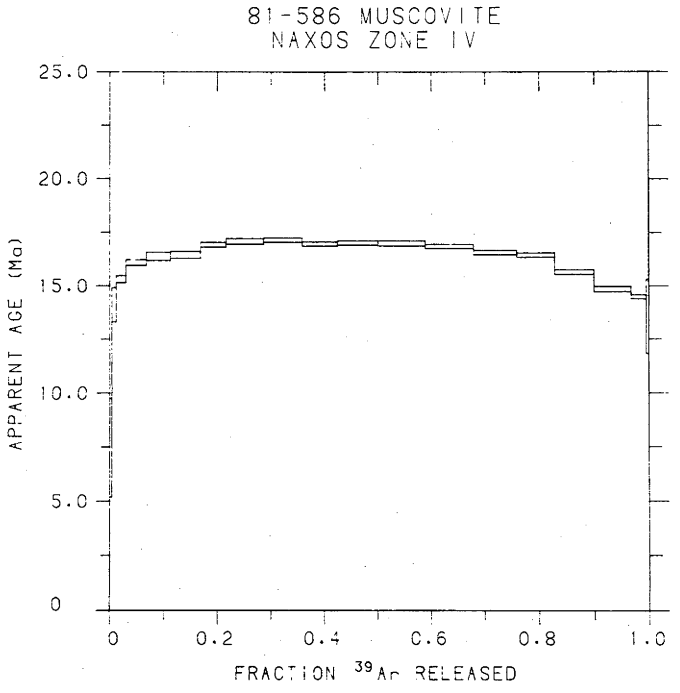
81-586 MUSCOVITE
NAXOS ZONE IV
APPARENT AGE (Ma)
25.0
20.0
15.0
10.0
5.0
0
0
0.2
0.4
0.6
0.8
1.0
FRACTION ^{39}Ar RELEASED

f

f) from zone IV. The low apparent ages in the initial steps are variable but may be as low as 8 Ma and the apparent ages in the high temperature part of the experiments are often only slightly higher.

The age spectrum of sample 81-532 (Fig. 3.10 curve d) is characterized by a progressive increase in apparent ages and a maximum apparent age of about 29 Ma. This is a substantially lower age than observed in other white micas from about the same metamorphic grade. In thin section it is observed that the mineral assemblage in this sample is profoundly recrystallized subsequent to the M_1 metamorphism. The ages of around 17 Ma in the initial steps of the age spectrum would suggest that overprinting may well have occurred during the M_2 metamorphism. It is noted that $^{40}Ar/^{39}Ar$ analysis indicates that argon derived from M_1 formed phengites contributes to the age spectrum, because of the similarity of this age specrum to age spectra of micas from less recrystallized rocks of similar metamorphic grade. In the case of full recrystallization during M_2 overprinting, a flat age spectrum similar to that of muscovite 81-556 would be expected. The age spectrum of sample 81-537 (Fig. 3.10 curve e) is difficult to interpret. It is disturbed, with low ages in the initial steps and slightly increasing ages in the high temperature steps of the age spectrum. The apparent ages of the bulk of the gas release suggest a poorly defined age of about 28 Ma.

Model for upward convex age spectra

Upward-convex age spectra have been reported in biotites which contain excess ^{40}Ar (Pankhurst et al. 1973, Foland 1983). No mechanism for the production of such age spectra was proposed. From comparison of the biotite ages with hornblende ages from the same area, it was suggested that the biotite ages are anomalously old, because of diffusion of excess ^{40}Ar into the crystals. Upward-convex age spectra in white micas were reported in rocks from the Swiss Alps (Hammerschmidt 1983); the presence of excess ^{40}Ar was also suggested in this case.

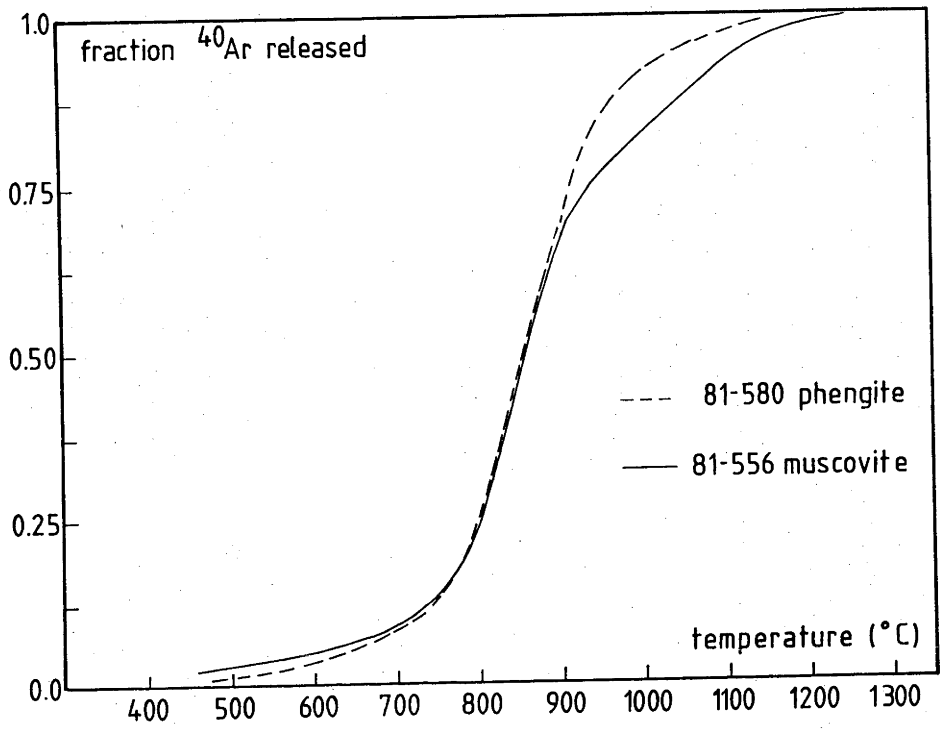

Figure 3.11. Fractional loss of ^{40}Ar during stepwise heating of white micas in an argon extraction line. The temperature of the sample was estimated from optical pyrometer and thermocouple measurements on the sample crucible. At low temperatures, argon is lost more readily from muscovite, but at high temperatures (i.e. in excess of 900 ^{0}C) phengite loses argon faster.

A mechanism which may explain upward-convex age spectra in white micas from Naxos is based on the following observations:

(1) The white mica population in these zones is known to contain both M_1 formed phengites and M_2 formed muscovites. Consequently, a mineral concentrate from these zones normally will contain both minerals.

(2) It was observed in stepheating experiments on muscovite and phengite that at high temperatures argon release from the pure M_2 muscovite lags slightly behind the release of argon from phengite (Fig. 3.11). This effect may be the result of differences in the chemistry of the two micas which causes small differences in diffusional behaviour at high temperature. Because this effect shows up at temperatures in excess of 900 ^{o}C in the experiments (Fig. 3.11), and dehydration of white mica in air occurs between 750 and 950 ^{o}C (Kiefer 1949), it is suggested that by the time the effect becomes prominent, the dehydration reaction in the mica is near to completion. Thus, the differences in argon release probably are caused by differences in physical properties of the anhydrous phases. From the release data of muscovite and phengite (Fig. 3.11) it can be seen that gas released from muscovite should start dominating the age spectra at temperatures higher than about 900 ^{o}C.

The effects of mixing are displayed schematically in Figure 3.12. This diagram shows in the upper curve the variation in $^{40}Ar^{*}/^{39}Ar_{K}$ ratio for an M_1 phengite that has lost some of its radiogenic argon during the M_2 metamorphism (as is the case in sample 81-580), and in the lower curve the $^{40}Ar^{*}/^{39}Ar_{K}$ ratio for an M_2 muscovite with an undisturbed argon distribution (as is the case in sample 81-556). The intermediate curve represents a model for a mixture of phengite and muscovite. The observation that muscovite retains argon at slightly higher temperatures than phengite is indicated by a broken line where the phengite is degassed and the muscovite still contains argon. This model suggests that gradients in the $^{40}Ar^{*}$ distribution in phengites can be resolved from a mixed sample, so that an estimate from the time of overprinting may be obtained from the initial ages, as is suggested from Turner's model (1968). It also indicates that the younger muscovite has an age which is approximated by the apparent ages in the highest temperature steps of the age

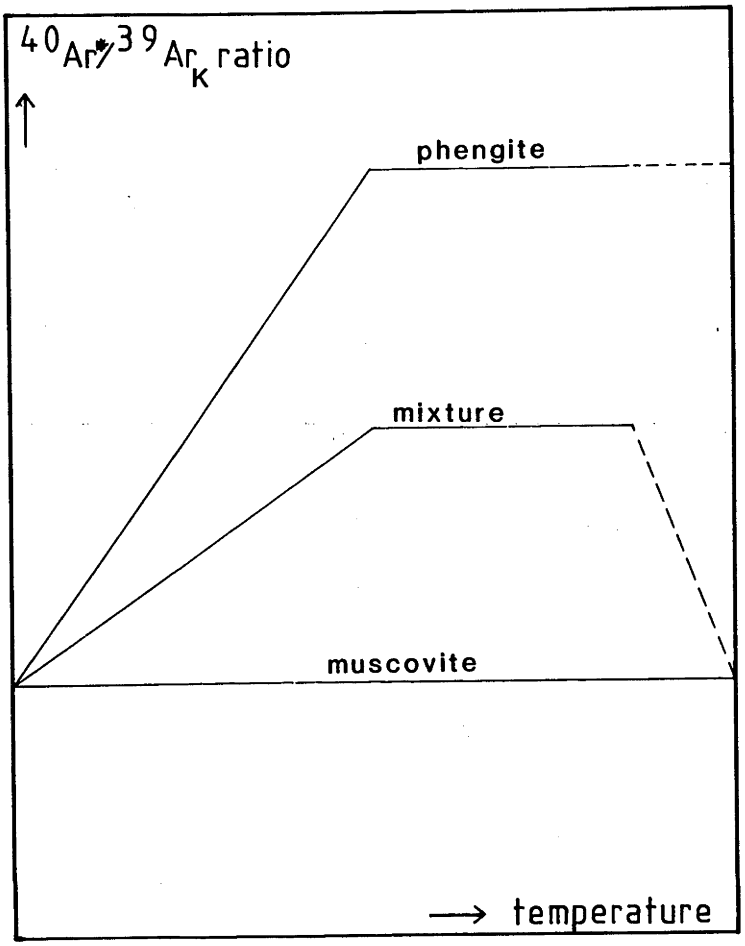

Figure 3.12. Schematic variation of $^{40}Ar^*/^{39}Ar_K$ ratios in a mixture of phengites and muscovites, as predicted from the fractional release data (Fig. 3.11). The line with the high ratio represents phengite, the line with the constant low ratio represents muscovite. A mixture will yield intermediate ratios. The dotted line in the upper curve represents the temperature interval where the phengite is essentially degassed, and the muscovite is still releasing argon. In the intermediate curve, the dotted line illustrates the shift from towards argon coming predominantly from muscovite. Note that although mixing lowers the $^{40}Ar/^{39}Ar$ ratio, the $^{40}Ar/^{39}Ar$ gradients remains preserved.

spectrum. The actual shape of the age spectrum will depend of on the amounts of muscovite and phengite in the sample and on the fraction of argon lost from the phengite during overprinting. The most important implication of this model is that in age spectra of white micas it is possible to have good horizontal segments of a meaningless intermediate age.

To test this model, a $^{40}Ar/^{39}Ar$ stepheating experiment was carried out on a mixture of pure muscovite (81-556), which has yielded an essentially flat age spectrum, and phengite (81-580), which showed a monotonically rising age spectrum. A mixture of 75 percent phengite and 25 percent muscovite was used. In Figure 3.13 the age spectra of the pure components and of the mixture are displayed. The age spectrum of the mixture follows that of the pure phengite in the early stages. Phengite derived argon dominates the age spectrum until a point is reached where the ages start to decrease. The ages in the highest temperature steps approximate the age of the muscovite component (Fig. 3.13). The resulting age spectrum is very similar to those observed in the low grade zones at Naxos. This experiment provides confirmation that the observed upward-convex age spectra are the result of the presence of two distinct generations of mica in the sample. This conclusion is in agreement with the petrological observations in rocks from zone II to IV in the M_2 mineral zone on Naxos.

Implications for the M_2 metamorphism at Naxos

The isotopic signature of phengites in age spectra can be traced along the M_2 thermal gradient to the low grade part of zone IV where the stable M_2 mineral assemblage includes biotite, staurolite and garnet (Fig. 3.1). The M_2 metamorphic temperature in this part of zone IV was estimated at 540 to 560 ^{o}C by Jansen and Schuiling (1976). It is unlikely that phengites will retain accumulated argon for any significant time at these temperatures (see Figure 3.14). The implication is that the temperatures reached in this part of zone IV are not as high as previously estimated, and indeed the presence of incompletely degassed phengites may be used to constrain the effective temperature reached during overprinting in the M_2 event.

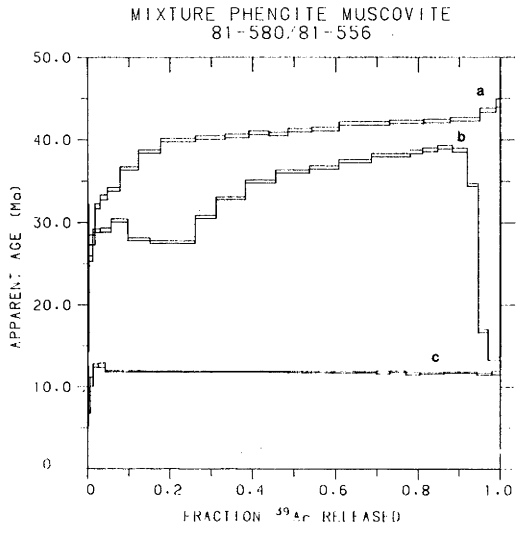

Figure 3.13. Experiment on an artificial mixture of 75 percent phengite and 25 percent muscovite. The result is an age spectrum which closely resembles the age spectra obtained from white micas in the zone between the + corundum isograd and the + sillimanite isograd (Figure 3.1). Curve a. is the age spectrum of phengite 81-580, curve b. is the age spectrum of the mixture, and curve c. is the age spectrum of muscovite 81-556. For sample locations see Figure 3.1.

The presence of staurolite in the M_2 mineral assemblage may be used to estimate the M_2 metamorphic temperature in zone IV. From such a temperature estimate, together with the argon isotopic data on phengites, it may be possible to obtain constraints on the duration of the M_2 thermal pulse. Experimental data on the stability of staurolite indicates that the mineral will be formed between 535 and 565 ^{o}C at pressures of 500 MPa and a metamorphic fluid of pure H_2O (Hoschek 1969). From a study of the fluid inclusions of syn-M_2 quartz lenses at Naxos, it was estimated that the fraction of CO_2 in the metamorphic fluid varied between 0.6 and 0.9 (Kreulen 1980). In this environment the temperature for the formation of staurolite would be lower, about 425 - 475 ^{o}C (Hoschek 1969, see also Chapter 2). Using this temperature estimate and diffusion theory it can be predicted how much time it would take for radiogenic ^{40}Ar to diffuse out of the mica crystals. The geometry of micas for diffusion of argon is best described by the infinite cylinder approximation (Giletti 1974). This means that argon mainly will move preferentially parallel to the (001) directions in the crystals.

The first term of the expression for diffusion from an infinite cylinder (Jost 1952) is a good approximation for cases of argon loss greater than F=0.9 (Fechtig and Kalbitzer 1966, Mussett 1969). If the resulting equation is solved for time (t), the following equation is obtained:

$$t = - \frac{a^2}{D(\alpha)_1^2} * \ln((1 - F)*\frac{(\alpha)_1^2}{4})$$

In this equation a is the effective diffusion radius of the mineral, D the diffusion rate at temperature T (calculated from the diffusion constant D_0 and the activation energy Q using the Arrhenius relation $D=D_0\exp(-Q/RT)$), F the fraction of argon lost by diffusion, and α_1 the first root of the Bessel function of the order zero. The solution of this equation for F=0.95 and the average grain radius $\bar{a}$=0.0085 cm is given in Figure 3.14. Fractional loss F=0.95 was used to approximate full resetting of the minerals. The average grain size in the separate was assumed to be representative for the grain size in the rock (i.e. fracturing of minerals during crushing was assumed to be minor). It was pointed out by Mussett (1969) that reliable diffusion data

Figure 3.14. Curves show the estimated times required to remove 95 percent of accumulated argon from white micas for a range of temperatures. The box at 550 ^{o}C represents the temperature interval over which the formation of staurolite takes place at P_{total} = 500 MPa and $a(H_2O)$ = 1.0, the box at 450 ^{o}C represents the formation reaction of staurolite at P_{total} = 500 MPa, and $a(H_2O)$ of the fluid is 0.5. t_1 and t_2 represent time estimates for white micas to reset based on muscovite diffusion data (D_0 = 6.03*10^{-7} cm^2/sec, Q = 40 kcal/mol), t_1' and t_2' are time estimates for white micas to reset based on phlogopite diffusion data (D_0 = 0.75 cm^2/sec, Q = 57.9 kcal/mol).

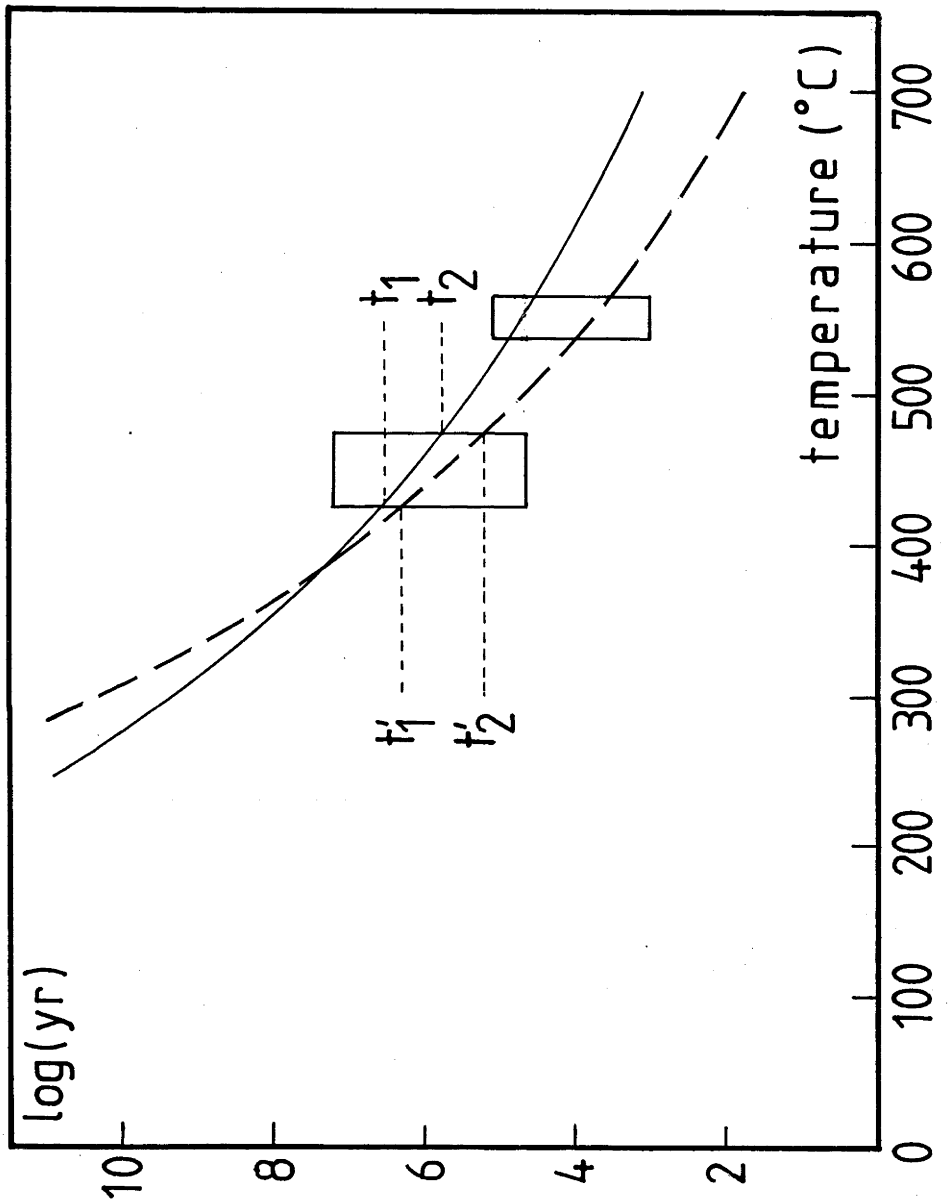
log(yr)
10
8
6
4
2
0
100
200
300
400
500
600
700
temperature (°C)
t1
t2
t'1
t'2

on micas are scarce, because in many experiments up to that time no attempts were made to assure that the minerals remained stable. Diffusion experiments where the minerals were kept stable in a hydrothermal apparatus were carried out subsequently by Giletti (1974) on phlogopite, and by Robbins (1972) on muscovite. Both the curves for muscovite and for phlogopite were plotted in Figure 3.14. Also plotted were the temperatures for the staurolite forming reaction according to Hoschek (1969) for $a(H_2O)$ in the metamorphic fluid is 1.0 and 0.5. From the curves in Figure 9 a time estimate for the duration the M_2 thermal pulse can be obtained (i.e. the time interval that the effective temperature of the system was at the temperature estimated from the formation of staurolite). Estimates assuming the $a(H_2O)$ of the ambient fluid was 0.5 range from the order of about 100000 years to about 3 Ma for both the phlogopite curve and the muscovite curve. These numbers suggest that the M_2 metamorphism on Naxos was caused by a short thermal pulse. This interpretation suggests that the event was caused by rapid input of heat into the system, rather than by a differential uplift and erosion mechanism as would be expected if the M_2 metamorphism was some form of regional metamorphism (England and Richardson 1977).

3.4.3 The granodiorite

Hornblende 81-548 from a sample of granodiorite on the west coast has been analyzed by the $^{40}Ar/^{39}Ar$ method (Table 3.II, Fig. 3.7). Its direct fusion age was 12.9 Ma, which agrees well with the conventional K-Ar ages. The stepheat experiment shows, despite some degree of scatter, an essentially flat release pattern. The integrated age over the total age spectrum is 11.4 $\pm$ 0.3 Ma which is lower than both the K-Ar ages and the $^{40}Ar/^{39}Ar$ direct fusion age for this sample. This age is similar to the K-Ar age of the biotite from this rock. The anomalously young integrated age over the age spectrum is not understood, and in order to date the granodiorite intrusion with more confidence the experiment should be repeated. Nevertheless, the $^{40}Ar/^{39}Ar$ direct fusion age and the K-Ar ages of hornblendes 81-546 and 81-548 suggest that cooling below the T_c of hornblende for argon occurred between 12.1 ans 13.5 Ma ago.

3.4.4 Summary

The present study of the argon isotopic system in minerals from the Attic Cycladic Metamorphic Belt supports earlier interpretations of the geology of this region in that two major phases of metamorphism were recognized (Andriessen 1978, Andriessen et al. 1979, Altherr et al. 1979). The first event, the M_1 metamorphism, caused a series of mineral assemblages indicating high to very high pressures and moderate temperatures (Van der Maar 1981). The results of the three stepheat experiments on white micas from zone I indicate that the peak of the M_1 metamorphism occurred before 50 Ma. Subsequent to the peak of this metamorphism the rocks cooled below the T_c of phengites for argon 49.5 Ma ago. It is virtually impossible to tell from the $^{40}Ar/^{39}Ar$ age spectra alone whether a mineral has experienced one or more phases of episodic loss of $^{40}Ar^*$ after beginning of argon accumulation in the crystal (Harrison 1983). Petrological information suggests that the M_1 metamorphism produced a series of mineral assemblages at a temperature of about 500 ^{o}C and pressures ranging from larger than 1200 MPa to about 700 MPa (Van der Maar 1981). There is no evidence for a complex thermal history of the rocks during the M_1 metamorphism. The marginal loss of $^{40}Ar^*$ from the three phengites measured in zone I is therefore interpreted as the result of overprinting during one single event. From the initial ages, which lie between 20 and 25 Ma, we estimate that this event occurred less than 20 Ma ago. This interpretation is consistent with the estimated age of the M_2 metamorphism at about 15 to 16 Ma ago in the centre of the island. The observed scatter in K-Ar ages of phengites in zone I is the result of diffusion of different amounts of $^{40}Ar^*$ from the minerals during the M_2 metamorphism. Possibly some scatter in ages was caused by slow cooling of the rocks through the temperature range where argon accumulation in phengites begins after the M_1 metamorphism.

The formation of a thermal dome in the centre of Naxos during the M_2 metamorphism has had a profound effect on the argon isotopic systems of the minerals. In the zones which were least affected by M_2 thermal overprinting, only limited diffusion of argon from the minerals is observed. Toward higher M_2 metamorphic

grade, a zone occurs where M_1 formed phengites and M_2 formed muscovites occur side by side. In this zone both ages obtained by the K-Ar method and horizontal segments in age spectra yielded ages which are intermediate between the ages of the M_1 and the M_2 metamorphism. In the central parts of the island, the M_2 metamorphism has reached upper amphibolite facies metamorphic grade. Mica ages in this area are interpreted as cooling ages. $^{40}Ar/^{39}Ar$ stepheating experiments have revealed well developed flat release patterns for both muscovite and biotite, suggesting that both $^{40}Ar/^{39}Ar$ data and K-Ar data on micas from this zone can be used with some confidence to derive a thermal history for the area. Hornblende ages in zone III and IV were interpreted as crystallization ages, and those from zone V and VI as recording cooling of the rocks below the T_c of hornblende for argon. However, an additional problem that affects hornblendes from the metamorphic complex is the incorporation of excess argon. Consequently, $^{40}Ar/^{39}Ar$ age spectra are likely to yield the most reliable ages on hornblendes. From the age spectra of hornblende 81-550 and 81-564, it is concluded that these minerals crystallized about 15 Ma ago. It was argued that in all hornblendes from the migmatite zone and the area south and east of it, argon accumulation commenced about 15 Ma ago.

The range in ages obtained on minerals in M_2 metamorphic assemblages and in the granodiorite is quite small. The biotite K-Ar ages from both areas are indistinguishable and hornblende ages from the granodiorite are only about 2 Ma younger than those from the main part of the metamorphic complex. This observation is clearly significant for the interpretation of the thermal and tectonic evolution of Naxos, as it suggests a close temporal relation between high grade metamorphism and intrusion of the granodiorite on the west coast of the island. It is noted that in a small area in the north of zone V in the metamorphic complex the ages on hornblendes are significantly lower than in the main part of the complex and in the granodiorite. It was suggested that these ages were caused by a late and local thermal disturbance below the presently exposed erosion surface. Abundant pegmatites in this area suggest the presence of a magma just below the presently exposed rocks.

3.5 Discussion

The two major metamorphisms of the ACMB on Naxos are reflected in the isotopic ages of minerals from the metamorphic complex, using the $^{40}Ar/^{39}Ar$ method (this study), the conventional K-Ar method (Andriessen et al. 1979, this study), and the Rb-Sr method (Andriessen 1978). Although in detail some difficulties exist with the interpretation of the Rb-Sr data (Andriessen 1978), both the argon isotopic data and the Rb-Sr data record the thermal evolution of the complex through the Tertiary. Similar histories were reported from studies of the metasediments at Siphnos (Altherr et al. 1979) and Ios (Henjes-Kunst 1980), but overprinting during the M_2 metamorphism was less severe on these islands. On Ios, Rb-Sr whole rock-mineral analyses of white micas from basement rocks have revealed pre-Alpine ages of about 290 Ma (Henjes-Kunst and Kreuzer 1982). On Naxos, neither Rb-Sr nor K-Ar analyses of white micas have revealed pre-Alpine ages. Because of the similarity in structure of the metamorphic complex on Ios and Naxos it is suggested that the area where pre-Alpine basement rocks might be exposed on Naxos, is located in the migmatite zone of the M_2 metamorphism, and, consequently, has experienced severe overprinting during the M_2 metamorphism (Van der Maar and Jansen 1983).

3.5.1 The M_1 metamorphism

The M_1 metamorphism has caused high pressure mineral assemblages throughout the ACMB. Conventional K-Ar dating of white micas supported an age of 45 $\pm$ 5 Ma (Andriessen et al. 1979, Altherr et al. 1979, this study section 3.3). The Rb-Sr whole rock-phengite ages of samples from areas which have experienced only minor overprinting during M_2 tend to be somewhat lower than the corresponding K-Ar ages (Andriessen 1978, Altherr et al. 1979). The present study using the $^{40}Ar/^{39}Ar$ method on phengites suggests that cooling below the T_c of phengites for argon occurred about 50 Ma ago. As Rb-Sr ages are consistently lower than the K-Ar ages, it seems that the Rb-Sr system was more severely reset during M_2 overprinting than the K-Ar system.

For blueschist belts to be preserved, a very low geotherm over a long time interval is required, or the processes related to subsidence and uplift need to proceed faster than the time necessary for the geotherm to re-equilibrate significantly (England and Richardson 1977). In a continental collision zone of the Alpine type, the second mechanism seems to be favoured. Thus, in order to preserve mineral assemblages formed at pressures in excess of 1000 MPa and temperatures of 500 ^{o}C or less, the processes of subsidence and subsequent uplift must have occurred well inside the time required to re-establish an equilibrium geotherm. For average continental lithosphere, substantial re-equilibration of the geotherm would occur in about 40 Ma (England and Richardson 1977). For Ios and southeast Naxos, Van der Maar and Jansen (1983) proposed on the basis of petrological observations that the M_1 event was followed by a period of essentially isothermal decompression, suggesting that the ACMB at Ios and southeast Naxos experienced a period of rapid uplift immediately after the M_1 metamorphism. Thus, if cooling below about 360 to 410 ^{o}C occurred about 50 Ma ago, then the peak temperature during the M_1 metamorphism probably was reached no earlier than about 60 Ma ago. In blueschist belts, because burial and uplift proceed relatively fast, it would be expected that the maximum pressure in the rocks was reached earlier than the maximum temperature was reached (England and Richardson 1977). The mineralogy of M_1 metamorphic rocks would support this view (Van der Maar 1981).

3.5.2 The M_2 metamorphism

For the discussion of the M_2 metamorphism it is useful to start with a summary of some basic observations which constrain the geological history.

(1) The domal structure and the thermal dome have approximately the same centre. In the north of the island there is a small angle between the the isograds and the strike direction of the schist-marble sequence (Jansen 1973).

(2) The thermal dome was formed later than the structural dome and after the last major penetrative deformation phase. This follows from the simple concentric mineral zonation around the central migmatites and from micro-structural observations in the

metapelites which indicate late grain boundary re-adjustment (Wijbrans 1980). Further, it is likely that the formation of the structural dome would have been accompanied by penetrative deformation of the rock. Because this is not observed, and because structural domes are reported elsewhere in the ACMB (e.g. on Ios) where they are not accompanied by a thermal event, the thermal dome may have formed somewhat later than the structural dome.

(3) The distribution of Al-silicates in the amphibolite facies rocks suggests a slight decrease in pressure from east to west in the complex (Jansen and Schuiling 1976). This may be interpreted as indicating slight tilting of the crustal block of Naxos to the west during uplift after the M_2 event, causing some asymmetry in the M_2 mineral zones (Fig 3.1).

Thus, it seems justified to assume that subsequent to the M_2 metamorphism, the metamorphic complex behaved as one single structural block, implying that it is possible to use data on the uplift history from the central parts of the island, in the granodiorite, and in the low grade rocks from southeast Naxos as well.

To preserve the signature of the M_1 metamorphism in the rocks from southeast Naxos, these rocks must have remained subsequently at a level in the crust where only little thermal overprinting occurred. It is estimated that at the time of the M_2 metamorphism the rocks of Naxos were at a level where the metamorphic pressure was just slightly higher than the pressure of the triple point of Al_2SiO_5, 376 MPa (Holdaway 1971), which corresponds to a depth of about 10 km. For the rocks in southeast Naxos, this must be taken as a minimum estimate for their depth during the M_2 metamorphism. Under these conditions, the argon isotopic system of phengites has remained closed for the diffusion of argon, thus constraining the maximum estimate for the geothermal gradient at this time to about 30 ^{o}C/km, on the basis of a closure temperature of phengite for argon of about 360 ^{o}C. Thus, it is suggested that the rocks were uplifted to a depth of about 10 km in the crust directly after the M_1 metamorphism, and remained at about that level until the beginning of the M_2 event. This interpretation and its tectonic implications will be discussed in Chapter 4.

In Figure 3.15 a family of cooling curves is given for the M_2 metamorphism and subsequent igneous activity. The curves are based on isotopic data in combination with estimates for the closure temperatures of various minerals (see Chapter 1). The cooling curve of the migmatite zone is based on Rb-Sr muscovite/whole rock data (Andriessen 1978), $^{40}Ar/^{39}Ar$ analyses on hornblende, muscovite, biotite and K-feldspar (this study, Zeitler personal communication), and on fission track ages of apatite (Altherr et al. 1982, Andriessen personal communication). The presence on Naxos of Pliocene sediments (Roesler 1978), indicates that the metamorphic rocks reached the earth's surface about 5 Ma ago. For the cooling curve of rocks near the - chloritoid isograd, it is assumed that hornblende 81-564 crystallized between 15 and 16 Ma ago at the time that the maximum M_2 temperature occurred. The cooling age of muscovite in this zone is not known from direct measurement, because of contamination of the sample with M_1 formed phengite, but is estimated to lie between the K-Ar age of biotite (81-538) and the lowest apparent age registered in the high temperature steps in the age spectrum of white mica 81-586, 12.5 Ma and 13.6 Ma respectively. Biotite K-Ar ages in this area range from 10.4 to 12.5 Ma. In the lower grade M_2 metamorphic rocks, cooling curves become less well constrained. In the area near the + biotite isograd a K-Ar age on biotite of 13.3 Ma is reported (Wijbrans 1980), but in lower grade zones reliable information on cooling after the M_2 event is not available. Cooling of the rocks from the thermal anomaly in the north of zone V is represented in Fig. 3.15, as well as the cooling curve of the granodiorite intrusive. These cooling curves illustrate the similarity of the thermal evolutions observed in the M_2 thermal dome and the granodiorite intrusive.

An earlier interpretation (Andriessen et al. 1979) of the M_2 metamorphism as a high temperature regional event which occurred at 25 $\pm$ 5 Ma and was followed by a period of very slow cooling, was based on the assumption that K-Ar ages on hornblendes and white micas in zone III recorded the peak of the M_2 metamorphism. Detailed $^{40}Ar/^{39}Ar$ analysis of minerals from M_2 mineral assemblages have shown that this assumption is incorrect. Hornblende K-Ar ages increase toward lower M_2 metamorphic grade

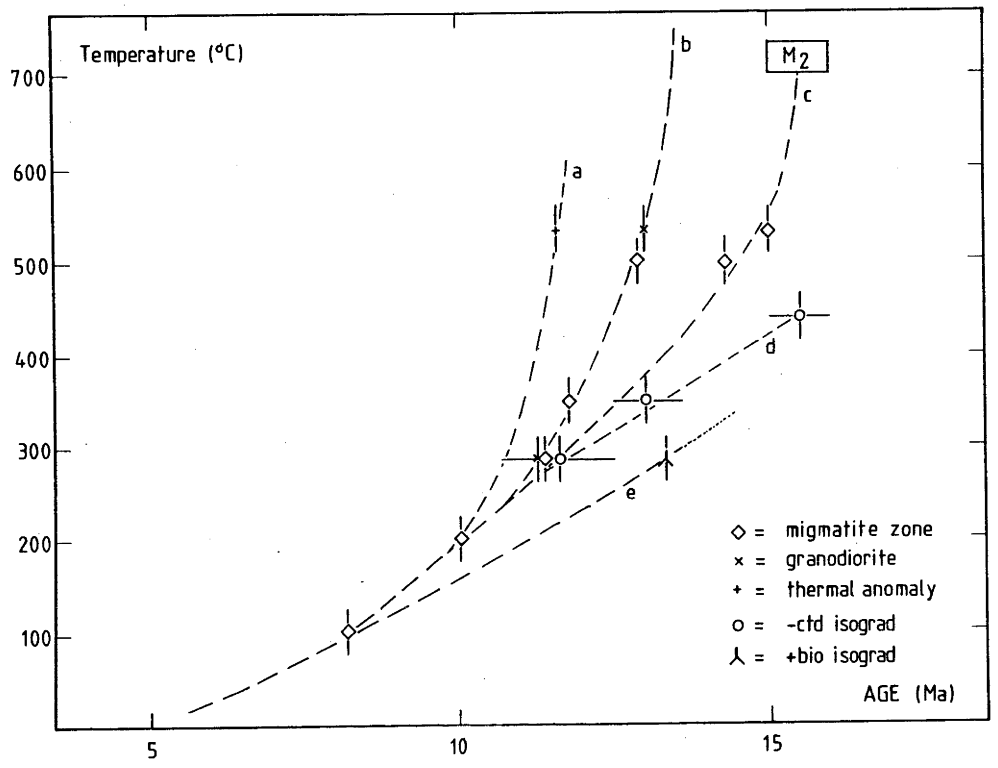

Figure 3.15. Cooling curves for different parts of the M_2 thermal dome and the adjacent granodiorite intrusive. The curves are based on available geochronological data, and estimates for closure temperatures as discussed in Chapter 1. (a) Cooling of the thermal anomaly in the north of zone V, (b) cooling of the granodiorite intrusive, (c) cooling of the central migmatite zone, (d) cooling of the region near the - chloritoid isograd, (e) cooling near the + biotite isograd. See section 3.5.2 for discussion.

because of an increase in $^{40}Ar_{exc}$ in the minerals. Muscovite samples from zone III were shown to be contaminated with M_1-formed phengite, which had not been fully degassed. Thus K-Ar ages on white mica samples from this area cannot be interpreted as crystallization ages of M_2 muscovites.

In addition to more precise ages of minerals, this study has provided two important constraints as to the thermal evolution of the ACMB on Naxos during the M_2 metamorphism:

(1) The peak of the M_2 metamorphism in the migmatite zone was followed by a period of rapid cooling, as suggested by the $^{40}Ar/^{39}Ar$ analyses of hornblendes and micas.

(2) Heating of the rocks during the M_2 event was probably of short duration, as interpreted from the $^{40}Ar/^{39}Ar$ analyses of white micas from zones II, III and IV in the metasedimentary sequence.

As a result, a quite different picture of the M_2 metamorphism at Naxos emerges. The event is characterized by a short period of elevated temperatures, followed by rapid cooling. In such an environment one may assume that the M_2 mineral assemblages reflect the physical conditions at the peak of the M_2 metamorphism (see section 2.4). Further, if heat was transported from a central source located in the migmatite zone into the sedimentary sequence by conduction, it is expected that heating of the complex would take significantly less than 1 Ma (Harrison and Clarke 1979, Chapter 4). If there is reason to suggest fluid convection in the complex as well, which may be concluded from the relative uniform composition of the syn-metamorphic fluid inclusions (Kreulen 1980), heating of the complex may have occurred even faster. Thus for the present discussion it is justified to assume that heating occurred synchronously throughout the complex. This means that if the ages of hornblendes 81-550 and 81-564 may be interpreted as recording the time of crystallization of these minerals, the peak temperature occurred between 15 and 16 Ma ago throughout the complex.

To establish the age of high grade metamorphism during the M_2 event, Andriessen attempted Rb-Sr whole rock analyses of rocks from the migmatite zone and the small S-type bodies which have intruded it during the M_2 event (Andriessen 1978). The results show that the Rb-Sr whole rock system was not fully re-equilibrated during the M_2 metamorphism, as the individual analyses scatter within an envelope which is bounded by reference lines equivalent to ages of 590 Ma and 57 Ma. Thus, in absence of reliable Rb-Sr whole rock isochron data on the migmatites, the best estimate for the age of the thermal dome were obtained from $^{40}Ar/^{39}Ar$ analyses of hornblendes from the migmatite zone and the lower grade M_2 metamorphic zones.

3.5.2.1 The formation of the M_2 thermal dome

To conclude this chapter, possible causes of the M_2 thermal dome will be discussed briefly. A more detailed discussion of the thermal and tectonic history of the area will be given in Chapter 4. The constraints on the thermal evolution, as were discussed in the previous paragraph, support the interpretation that the M_2 metamorphism was caused by significant input of heat into mid- to upper crustal levels, rather than as a case of regional metamorphism in the sense that the M_2 metamorphic zoning was caused by differential uplift and erosion (England and Richardson 1977). A second important finding of this study is the recognition of the close temporal relation between the M_2 metamorphism and the intrusion of an I-type granodiorite just west of the thermal dome. This may suggest that both events, intrusion and thermal dome metamorphism, are manifestations of one single thermal process. In recent publications on thermal domes, two mechanisms were proposed (Schuiling and Kreulen 1979, Vernon 1982, Tetley 1978), which attempt to identify a means of transporting relatively large amounts of heat into a small section of the crust.

The first mechanism involves the intrusion of a hot magma below the presently exposed erosion surface (Tetley 1978, Vernon 1982). This mechanism would satisfy the constraints from the present study because short thermal pulses and fast initial cooling are common in thermal contact aureoles. An important problem relates to the marked contrast in size between the

contact metamorphic zone of the granodiorite and the thermal dome. The granodiorite has produced a contact zone only about 200 to 500 m wide (Jansen 1973), whereas the metamorphic zoning around the migmatite dome is in excess of 5 km wide. Therefore, a hidden intrusive would have to carry a great deal more heat than the exposed granodiorite on the west coast. Thus, it would be unlikely that the M_2 thermal dome was caused by another granitoid similar in size to the granodiorite. The hidden intrusive would have to be either much larger than the granodiorite, or similar in size, but with a significantly higher temperature. If the hidden intrusive is much larger than the granodiorite, the question arises why this heat would be focussed on the relatively small migmatite zone in the complex. Heating of the rocks by conduction of an increased mantle heatflux, or of conduction from a large granitoid batholith in lower levels of the crust, would result in a more widespread thermal event. Concentration of heat could possibly occcur if it was transferred by metamorphic or hydrothermal fluids. The domal structure of the metamorphic complex on Naxos could then have caused concentration of fluid flow through the core of the dome, resulting in superposition of the thermal dome on the structural dome. It is unlikely that a large granitoid with a temperature of about 800 to 900 ^{o}C can cause extensive migmatization of the country rock (Jaeger 1964, 1968). The other option is that the hidden intrusive may be a relatively small body which is substantially hotter, and thus more mafic than a granitoid magma. A gabbroic magma with a temperature of about 1200 ^{o}C could probably represent enough heat to cause the M_2 thermal dome on Naxos. Although relatively small I-type granitoid plutons occur quite abundantly in the ACMB (Altherr et al. 1982a, 1982b), there is neither on Naxos, nor elsewhere in the ACMB evidence for mafic magmatism, which can be related to the M_2 metamorphism. As a consequence, there is some doubt whether a mafic intrusive could be responsible for the M_2 metamorphism on Naxos.

An alternative mechanism for the formation of the M_2 thermal dome was proposed by Schuiling and Kreulen (1979), who suggested that the M_2 metamorphism on Naxos was caused by the migration of hot fluids from an upper mantle environment into the complex. Focussing of the fluid stream on a relatively small area may have

been caused by the domal structure on the island, or a structural weakness in the crust. Le Pichon and Angelier (1979) contended that I-type intrusives in the ACMB originate from subduction of oceanic lithosphere from the Hellenic trenches, which they argued on the basis of plate motion and the present day length of the subducting slab to have started about 13 Ma ago. In such a tectonic setting the upper mantle may possibly be thermally and structurally unstable, and thus cause the process envisaged by Schuiling and Kreulen (1979). The suggestion of Le Pichon and Angelier (1979) that the ACMB was in an island arc setting between 20 and 10 Ma ago is supported by the occurrence of andesitic volcanic rocks of this age on Kos and along the west coast of Turkey just north of the ACMB (Innocenti et al. 1982). In subduction zones transport of volatiles present in the oceanic crust and its sediment cover into the upper mantle with the subducting slab is quite possible (Fyfe 1982, Wyllie 1983). During heating of the slab, together with partial melting of the oceanic crust at depths in excess of 100 km (Nicholls and Ringwood 1973, Nicholls 1974), these volatiles will tend to migrate through the overlying mantle wedge into the continental crust. This process may cause complex melting reactions in the mantle wedge and may also cause significantly increased heatfluxes into the continental crust. It was argued that in an island arc setting, the contribution of hot fluids from the upper mantle may contribute to the formation of migmatites and S-type granites in the overlying continental crust (Wyllie 1983). In the ACMB, there is evidence for andesitic volcanism, intrusion of I-type granitoids and high grade metamorphism in the period between 10 and 20 Ma ago. The present study indicates that these high temperature events occurred over about the same period of time. Considering the tectonic setting of the ACMB during the Miocene in the vicinity of an active Benioff zone, these high temperature events may well have been caused by subduction of oceanic lithosphere into the mantle below the ACMB. The geochronological data from the granodiorite intrusive and from the M_2 thermal dome suggest that subduction from the Hellenic trenches was operating about 15 Ma ago, which is essentially in agreement with the estimate of Le Pichon and Angelier (1979).

The data presented in this study suggest that the M_2 metamorphism was of short duration, was closely related in time to the intrusion of the granodiorite and was focussed on a small section of the crust. Both mechanisms discussed above would be capable of transporting heat into the complex and satisfying these contraints. The hidden intrusive mechanism would be able to explain the short duration of the M_2 metamorphism, but has the problem that it is hard to find field evidence in support of it. However, the invasion of mafic magmas into the lower crust in an island arc setting is certainly not impossible, and if it has occurred under the ACMB during the Miocene, it would contribute to an increase in the geothermal gradient of the region. The hot hydrothermal fluid model has the advantage that no hidden intrusive is needed and that fluid introduced into the crust would contribute in the formation of anatectic melts, as well as acting as a catalyst for M_2 metamorphic reactions. This mechanism would also be compatible with an island arc tectonic setting of the ACMB in the Miocene, because subduction of oceanic crust would introduce volatiles into the upper mantle under the ACMB. There is, however, very little data on the thermal effects of fluid flow in these environments (Fyfe et al. 1978, Schuiling and Kreulen 1979, Etheridge et al. 1983), and it is uncertain whether this mechanism could produce a short thermal pulse, as suggested from the isotopic data.

Table 3.I. K-Ar data.

Code	mineral	K percent		$^{40}Ar^*$ 10^{-10} mol/g	$^{40}Ar^*/^{40}Ar$ percent	Age Ma	uncertainty 1σ
Zone I							
81-579	phe/par	4.77	4.74	3.375	89.0	40.5	0.4
81-579	par	1.28	1.25	0.8755	63.5	39.5	0.4
				0.8662	63.2	39.1	0.4
81-578	phe	7.81	7.82	5.905	95.0	43.0	0.4
81-580	phe	8.39	8.34	5.652	95.7	38.5	0.4
81-583	phe	9.04	8.98	6.576	95.5	41.6	0.4
				6.596	95.1	41.7	0.4
81-582	phe	7.35	7.38	6.292	80.4	48.6	0.5
Zone II							
81-584	phe	9.25	9.19	6.269	88.0	38.8	0.4
81-585	phe	8.35	8.31	5.526	79.0	37.9	0.4
81-532	mus	6.72	6.57	2.825	97.2	24.3	0.4
81-534	phe	7.85	7.81	3.835	91.7	28.0	0.3
				3.871	84.8	28.3	0.3
81-534	bio	4.63	4.62	0.8799	43.1	10.9	0.1
81-541	phe	7.69	7.77	4.970	93.6	36.7	0.3
				5.119	88.2	37.8	0.3
Zone III							
81-540	hbl	0.19	0.19	0.1711	60.0	50.7	0.6
81-536	hbl	0.24	0.24	0.1342	61.5	31.6	0.4
81-537	phe	9.03	8.93	4.360	88.3	27.8	0.3
"A	phe/mus	7.92	7.90	2.858	89.4	20.7	0.2

"B	mus/phe	7.74	7.61	2.825	87.0	21.1	0.3
81-538	phe/mus	7.79	7.74	3.478	88.2	25.6	0.2
				3.472	75.5	25.6	0.2
81-538	bio	6.15	6.19	1.347	70.2	12.5	0.1
Zone IV							
81-564	hbl	0.16	0.16	0.0481	37.0	17.5	0.3
				0.0455	34.2	16.3	0.2
81-565	mus/phe	7.14	7.18	2.425	90.0	19.4	0.2
81-581	bio	7.32	7.33	1.349	88.9	10.6	0.1
81-586	mus	8.56	8.50	2.430	88.9	16.4	0.2
				2.356	30.2	15.9	0.2
81-544	mus	8.12	8.13	1.806	85.6	12.8	0.1
81-544	bio	7.24	7.22	1.283	49.7	10.2	0.1
				1.267	34.6	10.1	0.1
81-550	hbl	0.22	0.23	0.0623	5.8	15.9	0.8
Zone V							
81-588	hbl	0.29	0.29	0.0676	37.4	13.5	0.2
81-587	hbl	0.37	0.38	0.0932	52.0	14.3	0.2
81-570	hbl	0.55	0.54	0.1201	61.6	12.7	0.1
81-543	hbl	0.43	0.43	0.1153	58.3	15.5	0.2
				0.1114	56.6	14.9	0.2
81-554	mus	7.52	7.59	1.721	83.9	13.1	0.1
81-554	bio	7.18	7.22	1.337	62.9	10.7	0.1
Zone VI							
81-552	mus	8.63	8.62	1.822	81.8	12.2	0.1
81-556	mus	8.48	8.41	1.656	76.1	11.3	0.1
"A	mus	7.26	7.28	1.471	71.2	11.6	0.1
81-556	bio	7.41	7.47	1.440	73.5	11.1	0.1
				1.423	54.5	11.0	0.1

Granodiorite

81-546.bio	6.33 6.40	1.239	63.5	11.2	0.1
81-546 hbl	0.69 0.70	0.1493	41.9	12.3	0.2
		0.1467	43.3	12.1	0.1
81-548 bio	6.31 6.39	1.263	65.9	11.4	0.1
81-548 hbl	0.59 0.58	0.1299	43.4	12.8	0.2
		0.1380	39.0	13.6	0.2

The uncertainties in the ages are quoted at 1σ-level.
The abundance of $^{40}K/K_{total}$ = 1.167 x 10^{-4} mol/mol.
The decay constants for ^{40}K are: λ_{β^-} = 4.962 x 10^{-10} yr^{-1}.
$\lambda_{(e + e')}$ = 0.581 x 10^{-10} yr^{-1}.
$^{40}Ar^*/^{40}Ar$ is percentage radiogenic ^{40}Ar of the total measured amount of ^{40}Ar.

81-537 is the 0.420-0.250 mm fraction, 81-537A is a 0.125-0.180 mm magnetic fraction, 81-537B is a 0.125-0.180 mm non-magnetic fraction. 81-556 mus is a 0.420-0.250 mm fraction, 81-556A mus is a 0.250-0.125 mm fraction.

Table 3.II $^{40}Ar/^{39}Ar$ data.

Quoted temperatures are the average of thermocouple measurement on the bottom of the sample crucible, and optical pyrometer measurement on the upper inside wall of the sample crucible. The difference between the two measurements was typically 150 ^{o}C.

The ^{39}Ar and ^{37}Ar concentrations are corrected for radioactive decay during the period between irradiation and analysis.

Laboratory standard hornblende 77-600 (K/Ar age 414.2 Ma) and biotite GA1550 (K/Ar age 97.9 Ma) were used as flux monitors.

Reported absolute amounts were calculated from machine sensitivity (5.045×10^{-15} moles/mV), which was determined from regular measurement of standard minerals.

Uncertainties in apparent ages are quoted at 1σ-level, 0.5 percent error in parameter J is included. $\lambda = 5.543 \times 10^{-10}$ yr^{-1}.

T (°C)	^{36}Ar 10^{-15} moles	^{37}Ar 10^{-13} moles	^{38}Ar 10^{-13} moles	^{39}Ar 10^{-12} moles	^{40}Ar 10^{-12} moles	$^{40}Ar^*/^{40}Ar$ percent	Age Ma	1σ
81-556 White mica								
0.4085 g, J = 0.002403, 250-420 μm								
460	7.408	0.03788	0.0786	0.04413	2.280	4.0	8.9	3.7
560	5.495	0.02681	0.05646	0.1025	1.823	10.8	8.3	1.5
630	3.759	0.02710	0.01947	0.1818	1.562	28.6	10.6	0.6
680	4.289	-	0.01151	0.3338	2.249	43.3	12.6	1.4
730	5.021	0.01618	0.005795	0.4375	2.773	46.1	12.62	0.27
780	14.37	0.01998	6.321	2.204	10.38	58.5	11.90	0.08
820	14.77	0.01655	4.048	4.483	16.78	73.3	11.85	0.07
860	11.15	0.01581	4.357	4.824	16.66	79.4	11.86	0.06
880	4.532	0.008338	2.511	2.746	8.918	84.2	11.81	0.08
900	2.662	0.004990	1.476	1.532	5.012	83.5	11.80	0.09
920	3.231	0.004396	1.238	1.266	4.444	77.8	11.80	0.08
940	2.862	0.002510	1.103	0.8331	3.138	72.3	11.77	0.18
970	2.708	0.004129	1.036	1.006	3.587	76.9	11.86	0.09
1000	2.865	0.001556	0.9135	0.9013	3.292	73.6	11.61	0.15
1055	3.759	0.006143	1.444	1.529	5.281	78.2	11.67	0.09
1110	3.270	0.005426	1.915	2.070	6.651	84.6	11.75	0.08
1160	2.599	0.003724	0.9618	0.9736	3.056	85.0	11.54	0.11
FUSION	2.956	0.006849	0.5245	0.5117	2.276	61.0	11.72	0.23
SUM	97.706	0.2087	28.0206	25.9794	100.162	71.2	11.74	
FLUX MONITOR (0.0385 g)	19.68	0.3350	4.095	2.168	56.17	89.6		
FUSION (0.0580 g)	11.42	1.770	2.930	3.284	12.30	71.8	11.63	0.08
81-534 White mica								
0.3683 g, J = 0.002417, 250-420 μm								
490	6.841	-	0.09635	0.07981	2.347	13.8	17.6	2.0
590	4.929	1.888	0.1875	0.1828	2.363	38.9	21.8	0.6
660	5.738	3.827	1.041	0.9433	6.891	75.5	23.90	0.16
700	3.955	0.7019	0.8844	1.125	7.841	84.8	25.59	0.18
730	6.606	0.6420	2.020	2.149	16.22	87.6	28.63	0.16
750	8.437	-	2.075	2.278	17.88	85.7	29.10	0.16
770	5.271	-	2.080	2.266	16.99	90.5	29.34	0.16
790	3.766	0.1968	1.645	1.766	13.15	91.1	29.36	0.16
800	3.226	0.1384	1.449	1.547	11.41	91.3	29.11	0.17
810	2.739	0.09620	1.051	1.142	8.563	90.2	29.25	0.16
830	6.022	-	1.473	1.579	12.54	85.5	29.36	0.17
850	2.673	-	0.9512	1.022	7.712	89.4	29.19	0.17
870	3.009	0.4977	1.197	1.288	9.654	90.5	29.33	0.16
890	2.241	-	0.9062	0.9701	7.204	90.4	29.05	0.16
920	2.153	0.5433	1.162	1.257	8.994	92.6	28.67	0.18
950	1.784	0.5508	0.8758	0.9533	6.440	91.5	26.75	0.20
1000	1.129	-	0.4996	0.5434	3.052	88.6	21.56	0.24
FUSION	1.249	-	0.1925	0.2081	1.272	70.5	18.70	0.37
SUM	71.768	9.0821	19.7866	21.2998	160.523	86.8	28.20	
FLUX MONITOR (0.0462 g)	3.147	-	5.590	2.403	64.81	85.6		
FUSION (0.0451 g)	7.170	0.6355	2.134	2.346	17.40	87.5	28.09	0.16

T (°C)	^{36}Ar 10^{-15} moles	^{37}Ar 10^{-13} moles	^{38}Ar 10^{-13} moles	^{39}Ar 10^{-12} moles	^{40}Ar 10^{-12} moles	$^{40}Ar^*/^{40}Ar$ percent	Age Ma	1σ
81-580 White mica								
0.4725 g, J = 0.002483, 125-250 μm								
475	13.72	-	2.061	0.07719	4.524	10.4	27.0	5.2
575	13.61	-	0.2587	0.2730	5.742	29.8	27.9	0.6
645	21.37	1.420	0.9934	0.5041	9.947	36.5	31.97	0.31
695	9.875	0.6407	0.5902	0.5519	7.036	58.4	33.03	0.30
735	9.906	0.6068	0.7103	0.9343	10.11	70.8	34.01	0.23
765	9.841	-	1.366	1.349	14.06	79.1	36.53	0.20
785	8.183	-	1.413	1.593	16.33	84.9	38.59	0.21
805	7.904	0.4549	2.360	2.530	25.23	90.5	39.97	0.22
815	6.826	-	2.072	2.139	21.53	90.4	40.27	0.22
825	6.518	0.3202	1.618	1.729	17.76	88.9	40.46	0.23
835	10.05	-	1.390	1.463	16.40	81.7	40.83	0.23
845	5.684	0.3060	1.861	1.357	14.18	87.9	40.70	0.21
865	6.520	0.4204	1.644	1.760	18.33	89.2	41.16	0.21
885	4.902	-	1.857	1.935	19.55	92.3	41.30	0.22
905	6.648	0.6310	3.478	3.647	36.63	94.4	41.98	0.22
925	5.279	-	2.348	2.481	25.26	93.6	42.18	0.23
955	8.032	0.1032	1.793	1.930	20.86	88.4	42.28	0.23
1005	5.595	0.1436	1.876	2.163	22.48	92.4	42.49	0.22
1075	6.855	0.8288	1.068	1.164	13.51	84.8	43.58	0.25
FUSION	32.74	0.2359	0.4620	0.3293	12.99	25.5	44.46	0.55
SUM	200.058	6.115	31.2196	29.9098	332.459	82.2	40.37	
FLUX MONITOR (0.0424 g)	43.18	0.2690	5.595	2.145	60.99	79.0		
FUSION (0.0653 g)	21.06	-	3.301	3.557	38.78	83.7	40.42	0.22
81-556/81-580 Muscovite/Phengite mixture								
0.4390 g, J = 0.002056, 250-420 μm								
460	6.070	0.01783	0.09157	0.05968	0.2066	13.1	16.7	2.4
560	5.961	0.04557	0.3155	0.2148	0.3260	45.8	25.61	0.34
630	4.868	0.07896	0.4745	0.4181	0.4744	69.5	29.00	0.21
680	4.111	0.04465	0.6436	0.5860	0.5861	79.0	29.08	0.26
720	6.859	0.04215	1.128	0.9510	0.9874	79.2	30.25	0.20
750	7.999	0.02738	1.332	1.240	1.182	79.7	27.97	0.17
770	7.946	0.02802	2.579	2.483	2.105	88.5	27.63	0.16
780	2.032	0.01214	1.321	1.185	1.052	94.0	30.67	0.19
800	3.041	0.01370	1.701	1.632	1.557	93.9	32.94	0.17
810	3.232	0.01467	1.733	1.670	1.689	94.1	34.95	0.19
820	3.716	0.01642	2.004	1.885	1.971	94.2	36.18	0.19
840	4.020	0.01217	1.618	1.585	1.706	92.8	36.66	0.20
860	4.385	0.01588	1.901	1.830	2.000	93.3	37.42	0.20
880	5.808	0.05992	2.304	2.143	2.405	92.6	38.15	0.20
900	3.260	0.01731	0.7320	0.6929	0.8280	88.1	38.65	0.22
920	1.797	0.05039	0.8842	0.8381	0.9416	94.1	38.80	0.23
940	2.195	0.05659	0.8602	0.8245	0.9459	92.9	39.11	0.22
990	3.384	0.04710	0.8732	0.8252	0.9737	89.5	38.75	0.24
1020	2.110	0.05677	0.6722	0.6314	0.6581	90.3	34.57	0.18
1080	2.874	0.08038	0.5942	0.5430	0.3340	74.2	16.84	0.20
FUSION	2.436	0.1543	0.6973	0.6647	0.3159	76.7	13.47	0.19
SUM	88.098	0.8923	24.4595	22.9024	23.2447	88.8	33.03	
FLUX MONITOR (0.0344 g)	20.99	0.1636	3.871	1.633	5.053	87.6		
FUSION (0.0337 g)	8.971	0.06496	1.762	1.683	1.854	85.5	34.58	0.16

T (°C)	^{36}Ar 10^{-15} moles	^{37}Ar 10^{-13} moles	^{38}Ar 10^{-13} moles	^{39}Ar 10^{-12} moles	^{40}Ar 10^{-12} moles	$^{40}Ar^*/^{40}Ar$ percent	Age Ma	1σ
81-586 White mica								
0.2953 g, J = 0.002420, 125-250 μm								
470	15.48	0.9565	0.1601	0.07788	4.702	2.8	7.5	2.3
570	7.629	1.501	0.2784	0.1628	2.773	19.0	14.1	0.8
640	5.779	1.472	0.5356	0.3488	2.931	41.9	15.31	0.18
690	5.802	0.9352	1.087	0.7271	4.417	60.9	16.09	0.13
730	6.639	0.9573	1.283	0.8721	5.263	62.4	16.38	0.19
760	6.381	-	1.572	1.076	5.987	68.0	16.45	0.16
780	6.020	0.6174	1.340	0.9226	5.394	66.7	16.93	0.11
800	5.968	0.6699	1.909	1.331	7.033	74.4	17.09	0.14
820	6.084	-	2.017	1.414	7.416	75.2	17.15	0.11
840	5.305	0.8175	1.809	1.275	6.577	75.8	16.97	0.10
860	7.043	1.409	2.082	1.467	7.854	73.2	17.02	0.17
880	8.015	1.524	2.469	1.729	9.165	73.8	17.00	0.13
900	8.146	0.7705	2.460	1.732	9.169	73.3	16.86	0.10
920	7.592	0.5410	2.213	1.555	8.212	72.2	16.57	0.11
940	6.900	0.9854	1.910	1.344	7.154	71.1	16.49	0.10
970	7.181	1.075	1.944	1.371	7.087	69.7	15.66	0.12
1010	5.415	1.410	1.556	1.093	5.353	69.8	14.86	0.12
1070	2.454	0.4687	0.7845	0.5339	2.527	70.9	14.59	0.09
1170	0.9887	0.4980	0.1386	0.09053	0.5722	49.3	13.5	1.7
FUSION	1.717	0.6400	0.03028	0.007330	0.5313	5.6	17.7	10.6
SUM	126.5387	17.2484	27.5785	19.1300	110.1175	62.7	16.44	
FLUX MONITOR (0.0498 g)	35.00	-	5.499	2.653	71.52	85.4		
FUSION (0.0407 g)	10.98	2.694	2.592	1.793	10.13	67.7	16.63	0.11
81-541 White mica								
0.3755 g, J = 0.002474, 250-420 μm								
470	4.921	0.2734	0.08704	0.05292	1.707	14.9	21.3	1.1
570	3.100	1.223	0.1731	0.1039	1.485	38.9	24.7	0.6
640	3.801	2.538	0.3733	0.3723	3.499	68.3	29.01	0.29
690	2.262	1.057	0.3428	0.3509	2.974	77.5	29.10	0.31
720	3.500	0.6114	0.7168	0.7519	6.313	83.4	30.97	0.29
760	5.557	0.3391	2.077	2.257	20.33	91.6	36.48	0.19
780	3.970	0.1121	1.602	1.691	15.52	92.2	37.35	0.19
800	4.318	-	-	1.691	15.72	91.6	37.60	0.20
810	4.230	0.4504	1.624	1.773	16.43	92.1	37.72	0.20
820	2.564	-	1.182	1.124	11.54	93.1	38.29	0.22
830	2.275	0.2288	1.199	1.318	12.23	94.2	38.62	0.22
840	3.238	0.06746	1.542	1.646	15.49	93.5	38.86	0.20
860	3.429	0.3487	1.707	1.844	17.31	93.9	38.92	0.20
880	2.919	0.2509	1.511	1.577	14.67	93.8	38.55	0.20
900	2.934	0.4414	1.461	1.575	14.55	93.8	38.24	0.20
920	2.516	0.3010	1.368	1.468	13.34	94.1	37.80	0.20
950	3.567	0.07186	1.798	1.995	16.83	93.4	34.82	0.18
1000	1.163	0.01163	0.4468	0.4792	3.273	89.1	26.96	0.44
FUSION	2.227	0.2943	0.1941	0.1953	1.731	61.8	24.29	0.37
SUM	62.491	8.6205	19.4049	21.4708	204.942	92.4	38.25	
FLUX MONITOR (0.0336 g)	15.09	1.738	4.250	1.299	33.75	86.7		
FUSION (0.0514 g)	5.989	1.313	2.231	2.412	22.05	91.7	37.05	0.18

T (°C)	^{36}Ar 10^{-15} moles	^{37}Ar 10^{-13} moles	^{38}Ar 10^{-13} moles	^{39}Ar 10^{-12} moles	^{40}Ar 10^{-12} moles	$^{40}Ar^*/^{40}Ar$ percent	Age Ma	1σ
81-532 White mica								
0.4420 g, J = 0.002456, 125-250 μm								
480	10.89	0.02619	0.4258	0.1628	3.947	18.4	19.6	0.8
540	6.881	0.04260	0.4385	0.4147	3.696	44.7	17.55	0.21
610	4.441	0.03507	0.9715	0.8367	4.937	73.0	18.98	0.11
660	4.299	0.03824	1.178	1.019	5.814	77.7	19.52	0.20
700	5.293	0.03324	1.273	1.550	8.778	81.7	20.38	0.12
740	6.590	0.03068	2.419	2.636	16.48	87.8	24.15	0.14
770	5.244	0.01409	2.899	1.008	7.601	79.3	26.29	0.16
800	4.580	0.02688	2.262	2.456	17.60	91.9	28.95	0.16
810	3.675	0.02001	1.047	1.120	8.070	86.2	27.30	0.17
820	2.107	0.01715	0.8628	0.9062	6.183	89.5	26.86	0.16
840	2.368	0.01778	0.7660	0.8257	5.784	87.5	26.96	0.20
860	2.980	0.02848	0.8812	0.9468	6.721	86.5	27.00	0.18
880	1.724	0.02702	0.7179	0.7565	5.194	89.8	27.11	0.23
900	2.687	0.06770	1.001	1.075	7.546	89.1	27.49	0.16
920	3.194	0.08743	1.008	1.070	7.754	87.5	27.87	0.16
950	4.232	0.1317	1.558	1.661	12.08	89.3	28.55	0.15
980	3.057	0.04979	1.444	1.544	10.94	91.4	28.44	0.16
1030	2.555	0.002336	1.130	1.250	8.144	90.3	25.88	0.17
FUSION	2.115	0.009707	0.6346	0.6869	4.116	84.4	22.26	0.14
SUM	78.912	0.7060	22.9173	21.9253	151.385	84.6	25.58	
FLUX MONITOR (0.0427 g)	26.47	0.2239	5.830	2.312	60.38	86.9		
FUSION (0.0427 g)	22.93	1.218	1.562	2.637	22.46	69.5	26.03	0.14

T (°C)	^{36}Ar 10^{-15} moles	^{37}Ar 10^{-13} moles	^{38}Ar 10^{-13} moles	^{39}Ar 10^{-12} moles	^{40}Ar 10^{-12} moles	$^{40}Ar^*/^{40}Ar$ percent	Age Ma	1σ
81-537 White mica								
0.3654 g, J = 0.002484, 250-420 μm								
470	15.42	0.2281	0.1414	0.08079	5.077	10.2	28.6	2.1
570	6.998	-	0.1974	0.1807	3.019	31.3	23.3	0.7
640	5.255	-	0.2761	0.2577	2.958	47.3	24.16	0.27
690	7.052	-	0.5298	0.5372	4.959	57.7	23.70	0.20
730	6.423	0.3389	0.7578	0.7663	5.983	68.0	23.63	0.19
760	9.081	0.4981	1.275	1.301	10.23	73.5	25.71	0.16
780	9.010	0.8910	1.660	1.722	13.62	80.2	28.19	0.17
800	8.967	0.5372	1.929	1.990	15.77	82.9	29.21	0.17
810	5.688	2.659	1.358	1.317	10.44	83.8	29.55	0.17
820	5.820	-	1.517	1.576	12.45	85.8	30.12	0.17
830	5.234	0.3533	1.304	1.289	10.13	84.4	29.49	0.18
840	5.667	1.048	1.311	1.281	10.15	83.3	29.33	0.16
860	5.445	-	1.221	1.221	9.924	83.5	30.13	0.17
880	5.653	0.4626	1.495	1.525	11.82	85.6	29.49	0.16
900	6.319	-	1.842	1.897	14.34	86.6	29.11	0.15
920	3.893	0.2549	1.530	1.599	11.32	89.5	28.16	0.15
950	5.167	0.2503	1.849	1.957	13.97	88.7	28.15	0.16
1000	12.95	0.05376	2.082	2.228	18.31	78.8	28.77	0.17
1070	4.786	0.1074	1.519	1.589	12.40	88.2	30.58	0.18
FUSION	78.96	-	0.6413	0.4036	26.26	11.1	32.08	0.84
SUM	213.788	7.6826	24.4358	24.7183	223.130	71.7	28.66	
FLUX MONITOR (0.0349 g)	37.41	-	3.927	1.880	53.31	79.2		
FUSION (0.0484 g)	17.75	0.5048	2.916	3.082	25.47	79.1	29.05	0.16
81-585 White mica								
0.2509 g, J = 0.002420, 125-250 μm								
470	6.460	1.978	0.1960	0.1361	2.320	18.3	13.6	1.1
570	5.138	-	0.5799	0.4014	3.936	61.2	25.99	0.19
640	6.886	1.598	2.941	2.011	17.04	87.8	32.21	0.19
690	2.422	0.5164	1.298	0.8826	7.774	90.5	34.50	0.26
720	2.677	0.2846	1.546	1.056	9.679	91.1	36.39	0.23
740	2.343	-	1.346	0.9205	8.858	91.9	38.21	0.25
760	2.707	-	1.768	1.203	11.98	93.1	39.99	0.22
780	3.104	-	1.962	1.325	13.72	93.1	41.57	0.23
800	3.058	0.5116	1.977	1.348	14.17	93.4	42.36	0.25
820	3.005	-	1.664	1.130	12.10	92.4	42.72	0.24
840	4.328	-	2.134	1.453	15.91	91.7	43.33	0.24
860	5.281	-	3.484	2.381	25.54	93.6	43.34	0.24
880	3.205	-	2.221	1.542	16.23	93.9	42.66	0.24
900	1.930	1.106	1.279	0.8524	8.524	93.3	41.09	0.27
920	1.389	-	0.5883	0.3978	3.812	88.9	36.83	0.32
950	1.109	-	0.3484	0.2348	1.924	82.6	29.32	0.22
980	1.703	-	0.2433	0.1603	1.257	59.6	20.29	0.16
FUSION	0.8361	1.021	0.04575	0.02685	0.3941	39.5	25.9	2.5
SUM	57.5811	7.0156	25.5759	17.4618	175.1681	90.3	39.02	
FLUX MONITOR (0.0516 g)	79.58	-	5.255	1.352	77.76	69.7		
FUSION (0.0417 g)	58.99	-	3.255	2.099	35.75	51.1	37.58	0.24

T (°C)	^{36}Ar 10^{-15} moles	^{37}Ar 10^{-12} moles	^{38}Ar 10^{-13} moles	^{39}Ar 10^{-13} moles	^{40}Ar 10^{-12} moles	$^{40}Ar^*/^{40}Ar$ percent	Age Ma	1σ Uncertainty
81-557 Hornblende								
1.5067 g, J = 0.002513, 180-250 μm								
610	14.08	0.09637	2.904	0.3292	5.984	30.6	237	5.0
710	9.882	0.05938	0.1945	0.3397	3.221	9.5	40.3	5.0
760	7.295	0.06942	0.08971	0.4041	2.397	10.3	27.4	4.5
810	5.396	0.06536	0.09075	0.3175	1.679	5.3	12.7	2.1
860	7.456	0.1497	0.2485	0.5073	2.403	8.8	18.9	2.5
910	8.751	0.3368	0.3444	0.9683	3.019	15.3	21.5	1.0
950	5.336	0.6234	0.5921	1.744	2.160	29.4	16.47	0.37
980	4.144	0.8578	0.7953	2.413	1.982	41.8	15.54	0.18
1000	4.235	1.833	1.685	5.179	2.853	61.5	15.32	0.13
1020	3.608	2.137	1.977	6.092	2.903	69.4	14.96	0.21
1040	5.265	4.154	3.800	11.87	5.069	76.1	14.71	0.09
1060	5.645	5.645	5.064	16.16	6.417	81.3	14.61	0.08
1080	6.330	8.692	7.449	24.20	9.074	87.3	14.82	0.09
1090	3.722	4.179	3.710	11.69	4.647	83.8	15.07	0.11
1100	4.416	3.478	2.983	9.716	4.193	75.8	14.80	0.16
1110	3.654	4.437	3.792	12.37	4.797	85.2	14.95	0.15
1120	3.089	5.137	4.356	14.30	5.238	90.7	15.04	0.09
1140	3.273	5.138	4.363	14.36	5.371	89.9	15.22	0.10
1160	5.519	7.123	6.131	20.37	7.974	86.9	15.40	0.10
FUSION	10.82	0.3429	0.3444	0.9817	0.6271	53.6	15.48	0.22
SUM	112.178	54.21733	50.91366	154.3118	82.0081	59.6	15.65	
FLUX MONITOR (0.1428 g)	11.87	5.873	3.010	4.105	44.71	93.3		
0.1981 g, J = 0.002513, 180-250 μm								
FUSION	11.71	7.183	2.074	20.30	10.01	71.4	15.94	0.12
81-587 Hornblende								
1.4684 g, J = 0.002363, 125-250 μm								
550	9.278	0.02478	0.1058	0.05407	2.865	4.4	97	73
650	4.003	0.02233	0.1107	0.07720	1.271	7.0	49	42
735	4.745	0.03893	0.09872	0.09232	1.543	9.4	66	22
810	5.389	0.06512	0.09406	0.08390	1.608	1.3	11	32
855	4.225	0.1030	0.1040	0.09137	1.322	6.2	38.3	9.5
900	5.339	0.4075	0.1204	0.2721	1.641	6.1	15.7	6.1
925	5.174	0.7677	0.1525	0.5070	1.657	11.8	16.6	1.2
950	4.339	1.530	0.2624	1.005	1.512	24.2	15.6	1.2
970	3.284	0.9412	0.1581	0.6556	1.075	17.5	12.3	1.9
980	4.334	1.415	0.2484	1.000	1.457	20.7	12.9	1.7
1000	4.129	1.854	0.2832	1.320	1.460	27.7	13.1	1.2
1030	16.88	13.93	1.860	10.72	7.219	48.0	13.85	0.26
1080	26.34	20.64	2.925	16.94	11.38	47.6	13.71	0.14
1080	1.828	0.7192	0.1239	0.5588	0.6850	30.4	16.0	2.8
1100	2.917	1.131	0.1836	0.8940	1.049	27.3	13.7	1.0
1130	10.51	8.854	1.246	7.210	4.583	49.3	13.43	0.20
FUSION	12.95	12.68	1.787	10.48	6.048	55.2	13.66	0.19
SUM	125.664	65.32473	9.86378	51.96136	48.375	23.2	14.03	
FLUX MONITOR (0.1222 g)	16.79	5.527	2.226	3.940	47.01	90.5		
0.2372 g, J = 0.002363, 125-250 μm								
FUSION	20.17	11.25	1.392	8.945	10.25	51.5	25.25	0.18

T (°C)	^{36}Ar 10^{-15} moles	^{37}Ar 10^{-13} moles	^{38}Ar 10^{-13} moles	^{39}Ar 10^{-12} moles	^{40}Ar 10^{-12} moles	$^{40}Ar^{*}/^{40}Ar$ percent	Age Ma	1σ Uncertainty
81-583 White mica								
0.2850 g, J = 0.002437, 250-420 μm								
470	4.887	0.08812	0.1597	0.09590	1.882	23.1	19.9	1.4
560	3.710	0.02204	0.3779	0.2176	2.735	59.7	32.7	0.6
640	5.578	0.04305	1.606	1.166	11.58	85.4	36.64	0.20
730	2.644	0.02305	1.501	0.9683	9.402	91.4	38.61	0.24
770	4.159	0.02089	2.152	1.421	14.30	91.1	39.88	0.23
800	3.989	0.01931	2.634	1.714	17.55	93.0	41.40	0.22
830	4.514	0.01869	3.419	2.301	23.73	94.1	42.19	0.22
840	2.633	0.009658	2.174	1.433	14.82	94.5	42.48	0.25
850	1.844	0.009382	1.643	1.074	11.16	94.9	42.85	0.24
870	2.312	0.009074	1.736	1.129	11.86	94.0	42.91	0.22
890	2.020	0.006794	1.702	1.137	11.96	94.8	43.30	0.26
910	3.501	0.005026	2.906	1.972	20.82	94.8	43.47	0.25
940	2.855	0.008000	2.239	1.498	15.94	94.5	43.66	0.23
970	2.288	0.007044	1.972	1.324	14.09	94.9	43.87	0.26
1010	2.831	0.006419	2.173	1.440	15.49	94.3	44.08	0.24
1070	1.850	0.006734	1.053	0.7067	7.787	92.7	44.38	0.24
1120	0.4209	0.0008925	0.1570	0.09046	1.107	88.5	47.01	1.0
FUSION	1.794	0.002187	0.09921	0.05348	1.075	50.5	44.1	2.0
SUM	53.8299	0.3063605	29.70381	19.74144	207.288	92.3	42.01	
FLUX MONITOR (0.0541 g)	7.049	0.06101	2.168	0.6267	16.47	87.3		
0.0472 g, J = 0.002437, 250-420 μm								
FUSION	51.30	0.03399	4.967	3.205	46.47	67.2	42.35	0.24
81-582 White mica								
0.3111 g, J = 0.002391, 125-250 μm								
450	5.820	0.1071	0.08505	0.02173	1.848	6.9	25.3	4.1
510	8.448	0.5455	0.08687	0.03770	2.803	11.1	35.2	3.7
580	3.606	1.219	0.09770	0.04275	1.450	27.2	39.4	1.2
620	5.044	3.260	0.1958	0.1175	2.524	42.0	38.6	0.6
680	6.017	3.611	0.5077	0.3341	5.090	65.5	42.59	0.27
730	7.342	1.385	1.020	0.6727	9.158	76.2	44.24	0.25
770	14.88	0.2346	0.8812	0.5617	10.34	57.4	45.00	0.31
800	11.18	0.1939	1.369	0.8964	13.12	74.6	46.51	0.26
830	7.186	0.1113	1.075	0.7196	10.16	78.9	47.44	0.27
850	18.48	0.1698	2.549	1.723	25.05	78.0	48.26	0.26
870	13.09	0.08647	2.089	1.413	20.21	80.7	49.12	0.27
880	16.78	0.09351	2.743	1.841	26.30	81.0	49.22	0.26
900	7.855	0.03303	1.294	0.8688	12.42	81.1	49.37	0.30
920	11.75	0.03827	1.836	1.242	17.95	80.5	49.49	0.27
940	10.68	0.03115	1.6707	1.108	16.06	80.2	49.48	0.26
970	11.64	0.02577	1.785	1.233	17.87	80.6	49.75	0.28
1010	12.82	0.02551	2.048	1.402	20.26	81.1	49.88	0.26
1040	9.955	0.01956	1.559	1.067	15.31	80.6	49.23	0.29
1080	5.492	0.02483	0.8553	0.5881	8.223	80.1	47.67	0.26
1120	2.914	0.03213	0.5304	0.3469	4.575	81.0	45.49	0.45
FUSION	2.917	0.02522	0.5232	0.3443	4.896	82.2	49.74	0.47
SUM	193.896	11.56992	24.80812	16.58128	245.617	76.7	48.25	
FLUX MONITOR (0.0282 g)	29.61	0.3178	6.389	2.814	74.43	88.1		
0.0468 g, J = 0.002391, 125-250 μm								
FUSION	29.38	1.647	4.551	2.512	38.18	77.1	49.87	0.26

T (°C)	^{36}Ar 10^{-15} moles	^{37}Ar 10^{-13} moles	^{38}Ar 10^{-13} moles	^{39}Ar 10^{-12} moles	^{40}Ar 10^{-12} moles	$^{40}Ar^*/^{40}Ar$ percent	Age Ma	1σ Uncertainty
81-550 Hornblende								
1.4114 g, J = 0.002324, 180-250 μm								
735	33.74	5.898	0.3358	0.07240	10.96	9.5	64.3	3.5
835	16.95	7.618	0.3760	0.06197	5.255	5.9	22.9	2.5
915	12.84	15.64	0.6253	0.1030	4.022	9.1	16.27	0.83
965	10.31	48.04	0.4613	0.2607	3.507	26.1	16.08	0.43
995	7.199	32.92	0.3225	0.1815	2.463	25.5	15.83	0.68
1015	6.797	16.21	0.1881	0.08746	2.212	15.7	18.15	0.85
1035	5.487	13.62	0.1801	0.07352	1.753	14.4	15.74	1.27
1055	2.688	14.32	0.1448	0.07716	0.9479	29.7	16.66	0.79
1075	7.475	70.62	0.5557	0.3809	2.835	44.3	15.07	0.28
1095	9.538	101.7	0.8330	0.5576	3.773	49.3	15.25	0.29
1105	2.543	9.042	0.1065	0.04930	0.8782	23.6	19.21	2.49
1115	3.650	5.711	0.09676	0.03100	1.144	10.2	17.13	2.38
1135	5.632	20.32	0.1952	0.1119	1.852	19.9	15.07	0.82
SUM	124.849	361.659	3.386	2.04841	41.6021	11.3	16.36	
FLUX MONITOR (0.1023 g)	10.69	36.12	1.416	0.2574	29.04	90.2		
81-550 Hornblende								
0.1934 g, J = 0.002324, 180-250 μm								
FUSION	17.26	59.51	0.6096	0.3352	5.892	22.4	17.99	0.60
81-564 Hornblende								
1.2212 g, J = 0.002479, 180-250 μm								
760	35.66	15.67	0.3016	0.08273	11.02	5.6	33.6	7.6
860	16.66	17.35	0.1882	0.06849	5.212	8.5	29.3	2.3
960	16.58	30.25	0.2508	0.1196	5.147	10.1	19.6	1.2
1010	12.00	23.03	0.1935	0.09523	3.704	9.8	17.3	1.3
1040	11.54	25.44	0.1910	0.1030	3.529	9.8	15.2	0.7
1060	9.886	16.30	0.1364	0.06546	2.999	7.5	15.5	3.0
1080	6.510	19.20	0.5238	0.07724	2.030	13.7	16.3	1.6
1100	5.852	38.42	0.2038	0.1607	1.963	29.4	16.3	0.6
1120	7.012	80.52	0.3865	0.3442	2.525	46.4	15.4	0.4
1130	4.178	32.53	0.1784	0.1414	1.469	35.7	16.8	0.3
FUSION	10.71	45.01	0.2563	0.1953	3.449	19.9	15.9	0.5
SUM	136.688	343.72	2.8103	1.45335	43.047	6.2	17.84	
FLUX MONITOR (0.1390 g)	18.33	51.15	1.804	0.3636	42.44	88.3		
81-564 Hornblende								
0.1500 g, J = 0.002479, 180-250 μm								
FUSION	12.22	39.55	0.5184	0.1684	3.912	16.7	17.6	0.6

T (°C)	^{36}Ar 10^{-15} moles	^{37}Ar 10^{-13} moles	^{38}Ar 10^{-13} moles	^{39}Ar 10^{-12} moles	^{40}Ar 10^{-12} moles	$^{40}Ar^*/^{40}Ar$ percent	Age Ma	Uncertainty 1σ
81-556 Biotite								
0.4677 g, J = 0.002433, 250-420 μm								
470	172.7	-	0.7387	0.4914	51.53	0.9	4.2	1.8
570	154.4	-	3.187	4.086	55.31	17.3	10.24	0.22
640	62.04	-	10.04	10.04	46.56	58.2	11.30	0.07
690	16.62	-	6.091	6.188	21.33	76.2	11.49	0.07
710	4.813	0.4935	1.807	1.838	6.315	76.8	11.54	0.11
730	2.821	-	1.193	1.199	4.007	78.4	11.47	0.11
750	1.729	-	0.4777	0.4817	1.795	70.8	11.54	0.18
770	1.627	-	0.3224	0.3178	1.344	63.6	11.77	0.28
810	7.128	-	0.3031	0.2765	2.808	24.7	10.99	0.42
860	2.594	-	0.2625	0.2487	1.443	46.4	11.77	0.59
970	4.670	0.1723	0.5417	0.5353	2.772	49.8	11.28	0.12
FUSION	5.178	0.05651	0.2985	0.3007	2.387	35.5	12.35	0.48
SUM	436.32	0.72231	25.2626	26.0031	197.601	34.8	11.44	
FLUX MONITOR (0.0479 g)	28.89	0.8991	3.807	0.2332	62.05	86.2		
81-556 Biotite								
0.0583 g, J = 0.002433, 250-420 μm								
FUSION	43.88	0.08962	3.187	2.456	19.27	32.4	11.11	0.13

T (°C)	^{36}Ar 10^{-15} moles	^{37}Ar 10^{-13} moles	^{38}Ar 10^{-13} moles	^{39}Ar 10^{-12} moles	^{40}Ar 10^{-12} moles	$^{40}Ar^*/^{40}Ar_{total}$ percent	Age Ma	Uncertainty 1σ
81-589 Biotite								
0.4348 g, J = 0.002409, 125-250 μm								
450	31.33	-	0.6784	0.4253	9.566	3.1	3.02	0.41
550	131.7	0.2375	3.697	2.321	41.41	5.9	4.55	0.23
620	149.2	-	5.981	4.663	50.42	12.3	5.78	0.12
670	55.31	-	4.586	3.129	20.54	20.0	5.70	0.09
710	44.40	0.4740	4.112	2.780	17.01	22.4	5.96	0.07
740	24.70	0.3917	2.057	1.384	9.303	21.2	6.17	0.13
760	17.05	0.4547	1.400	1.014	6.472	21.8	6.04	0.11
780	8.299	-	0.7194	0.4812	3.110	20.7	5.81	0.37
800	9.322	0.2725	0.6994	0.4398	3.490	20.8	7.17	0.20
820	5.008	-	0.4033	0.2477	1.905	21.9	7.32	0.30
840	6.235	-	0.3743	0.2420	2.356	21.5	9.09	0.62
860	4.297	0.3231	0.4244	0.2761	1.805	29.4	8.33	0.18
880	9.912	0.4360	0.6427	0.4029	3.739	21.5	8.64	0.39
950	8.067	0.5426	0.8626	0.5784	3.492	31.4	8.23	0.17
1050	17.94	-	1.886	1.300	7.556	29.4	7.40	0.11
FUSION	5.764	-	0.3177	0.2083	2.135	20.0	8.87	0.47
SUM	528.534	3.1321	28.8412	19.8927	184.309	15.3	6.02	
FLUX MONITOR (0.0464 g)	38.47	1.692	3.590	2.147	61.10	81.3		
FUSION (0.0667 g)	52.68	2.921	2.155	1.441	17.62	11.5	6.08	0.22

T (°C)	^{36}Ar 10^{-14} moles	^{37}Ar 10^{-11} moles	^{38}Ar 10^{-13} moles	^{39}Ar 10^{-13} moles	^{40}Ar 10^{-11} moles	$^{40}Ar^*/^{40}Ar_{total}$ percent	Age Ma	Uncertainty 1σ
81-540 Hornblende								
1.1150 g, J = 0.002425, 180-250 μm								
650	2.216	0.05827	0.4713	1.047	0.8466	23.2	80.7	2.2
750	1.067	0.02168	0.2057	0.3199	0.3593	12.8	62.0	7.2
820	0.8427	0.07526	0.1848	0.3980	0.2939	17.6	56.6	2.7
880	0.8375	0.03657	0.1927	0.5829	0.5812	63.1	267.5	2.7
930	0.1239	0.4078	0.7220	2.294	0.2209	70.2	38.6	0.5
970	0.4047	0.4477	1.938	2.718	0.2813	71.6	32.5	0.4
1000	0.2410	0.2944	0.3560	1.935	0.1470	69.3	23.1	0.5
1030	0.1594	0.2166	0.2468	1.347	0.1043	73.3	24.9	0.3
1050	0.1239	0.1242	0.1323	0.6883	0.06626	61.4	26.0	0.8
1070	0.1778	0.1679	0.1278	0.6519	0.08568	56.2	32.6	1.5
1090	0.2720	0.3316	0.1690	0.9162	0.1647	69.3	55.1	0.6
1110	0.4847	0.3664	0.1735	0.8300	0.3151	65.0	108.2	2.0
SUM	6.9506	2.54838	4.9199	13.7282	3.46624	40.7	52.19	
FLUX MONITOR (0.0376 g)	0.5976	0.1211	0.5739	0.8637	1.076	84.6		
81-540 Hornblende								
0.1489 g, J = 0.002425, 180-250 μm								
FUSION	0.8738	0.3575	0.8199	1.700	0.4504	49.8	57.6	0.8
81-548 Hornblende								
1.2508 g, J = 0.002447, 125-250 μm								
700	4.712	0.05691	0.8658	6.069	1.555	10.7	12.07	0.38
800	1.806	0.02353	0.6603	5.064	0.6633	19.7	11.33	0.27
880	2.109	0.05367	0.4788	3.265	0.7106	12.9	12.32	0.41
930	1.438	0.2470	0.5078	3.014	0.4845	16.7	11.92	0.51
960	1.676	0.7506	1.586	7.406	0.6178	30.5	11.28	0.21
990	1.597	0.9318	1.772	9.275	0.6298	38.1	11.45	0.15
1000	0.8312	0.5292	1.060	5.287	0.3270	39.1	10.72	0.11
1020	0.4190	0.2417	0.3683	2.394	0.1620	36.7	10.99	0.31
1040	0.4107	0.2891	0.4320	2.741	0.1666	42.4	11.42	0.21
1060	0.4738	0.3394	0.4763	2.982	0.1876	41.3	11.52	0.37
1080	0.4159	0.2936	0.3931	2.420	0.1528	36.5	10.24	0.26
1090	0.2343	0.1775	0.2515	0.1400	0.09179	41.6	12.12	0.87
1100	0.1929	0.1224	0.1643	0.09110	0.06020	23.3	6.85	1.18
1150	0.1499	0.1195	0.1570	0.08252	0.05498	38.7	11.46	0.93
1190	0.2015	0.1278	0.1274	0.07925	0.07388	34.8	14.42	0.78
FUSION	0.2237	0.09572	0.05308	0.02545	0.06056	5.0	5.4	4.8
SUM	16.8909	4.39943	9.35368	50.33532	5.99842	16.8	12.24	
FLUX MONITOR (0.0622 g)	0.7259	0.2060	1.140	1.459	1.720	88.6		
81-548 Hornblende								
0.1441 g, J = 0.002447, 125-250 μm								
FUSION	1.597	0.4574	0.8551	5.548	0.5937	27.2	12.88	0.25

T (°C)	^{36}Ar 10^{-15} moles	^{37}Ar 10^{-13} moles	^{38}Ar 10^{-13} moles	^{39}Ar 10^{-12} moles	^{40}Ar 10^{-12} moles	$^{40}Ar^*/^{40}Ar$ percent	Age Ma	1σ Uncertainty
81-588 Hornblende								
1.4448 g, J = 0.002335, 125-250 μm								
710	16.04	3.573	0.1861	0.04290	4.815	2.2	10.5	4.2
805	12.16	1.599	0.1029	0.01996	3.668	2.5	19.0	6.6
905	24.13	7.764	0.1640	0.03933	7.260	2.7	21.5	3.2
975	13.99	21.94	0.2710	0.1402	4.299	8.4	10.9	1.0
1005	14.02	47.71	0.5058	0.3037	4.561	18.4	11.75	0.31
1025	9.005	25.82	0.2892	0.1661	2.893	15.9	11.79	0.70
1045	5.730	15.66	0.1747	0.1002	1.828	14.9	11.57	0.81
1065	7.957	23.82	0.2518	0.1540	2.616	18.2	13.12	0.49
1075	7.416	22.46	0.2485	0.1426	2.395	16.8	12.0	1.1
1085	5.933	26.06	0.2732	0.1686	1.988	23.4	11.73	0.54
1095	5.875	39.20	0.3978	0.2541	2.116	34.4	12.16	0.24
1115	8.037	63.66	0.6233	0.4116	2.993	39.5	12.19	0.34
1135	10.30	99.35	0.8828	0.6063	3.781	42.8	11.35	0.14
1155	10.76	48.66	0.4156	0.2738	3.496	21.4	11.64	0.38
1165	3.799	32.75	0.2553	0.1643	1.271	34.6	11.41	0.69
FUSION	5.458	4.495	0.03576	0.01478	1.634	3.8	18.0	3.6
SUM	160.61	484.521	5.0776	3.00247	51.614	8.0	11.96	
FLUX MONITOR (0.1757 g)	15.22	54.46	2.381	0.3890	46.59	91.4		
81-588 Hornblende								
0.2152 g, J = 0.002335, 125-250 μm								
FUSION	16.54	70.98	0.7832	0.4382	5.486	22.4	11.91	0.35
81-536 Hornblende								
1.2413 g, J = 0.002412, 180-250 μm								
770	19.85	9.437	0.1858	0.07183	7.540	23.3	104.4	1.8
870	13.34	22.86	0.2076	0.08803	6.660	43.9	141.5	1.6
970	13.04	74.16	0.5764	0.4156	6.017	46.9	29.69	0.29
1020	5.893	35.96	0.3006	0.2097	2.438	41.7	21.23	0.29
1050	3.717	15.45	0.1661	0.09128	1.385	30.6	20.33	0.93
1070	3.603	14.60	0.1451	0.08856	1.333	29.9	19.69	0.30
1090	2.211	14.82	0.1532	0.09252	0.9208	43.3	18.89	0.50
1110	4.719	46.20	0.3712	0.2937	2.260	56.4	19.02	0.39
1130	7.333	60.14	0.4740	0.3855	3.382	51.7	19.86	0.23
1140	4.638	29.36	0.2435	0.1902	1.996	44.4	20.40	0.35
1150	2.158	21.63	0.1819	0.1405	1.088	59.0	19.99	1.15
1170	2.260	22.60	0.1911	0.1470	1.073	62.1	19.86	0.22
FUSION	7.238	17.18	0.1639	0.1104	2.520	21.2	21.14	0.88
SUM	90.000	384.397	3.3602	2.32482	38.6138	31.1	29.0	
FLUX MONITOR (0.1123 g)	9.923	39.66	1.986	0.2809	32.33	92.0		
81-536 Hornblende								
0.2028 g, J = 0.002412, 180-250 μm								
FUSION	125.3	52.98	31.17	0.3525	39.40	7.2	35.1	2.0

TABLE 3.III Estimated amounts of excess ^{40}Ar in hornblendes

zone	code	K-Ar age (Ma)	$^{40}Ar_1$ 10^{-8} mole/g	$^{40}Ar_2$ 10^{-8} mole/g	$T(M_2)$ ^{o}C
III	81-540	50.7	17.11	11.88	400
III	81-536	31.6	13.42	7.31	420
IV	81-564	17.5	4.81	1.07	440
IV	81-550	15.9	6.23	1.39	530
VI	81-557	16.0	36.69	1.51	700

(1) radiogenic + excess argon.

(2) estimated amount of excess argon based on an initial age of 15 Ma.

$T(M_2)$: estimated metamorphic temperature during the M_2 event (cf. Chapter 2).

Chapter 4

The tectonic and thermal history of Naxos

4.1 Introduction

In this chapter data on the geochronology and the petrology of Naxos are used to derive a thermal and tectonic history for the area. The discussion will concentrate on the geologic history of Naxos, but it should be noted that because of the central position of Naxos in the Attic Cycladic Metamorphic Belt (ACMB), much of the discussion is pertinent to the surrounding parts of the belt as well. The present day tectonic setting of the ACMB was summarized in Chapter 2. The similarity in metamorphic evolution between the ACMB in the Aegean Sea and other areas affected by the Alpine Orogeny, as for example the Sesia Zone in western Alps was pointed out.

The two main metamorphisms, M_1 and M_2, in the ACMB took place in quite different crustal environments. The physical conditions during the M_1 metamorphism were estimated at about 1500 MPa and 450 ^{o}C on Syros and Siphnos, and at 900 to 1200 MPa and 470 to 530 ^{o}C on Ios and southeast Naxos (see Chapter 2). These data suggest that metamorphism took place at depths between 25 and 40 km, with a geothermal gradient of 10 to 20 ^{o}C/km. Limited overprinting of the very high pressure rocks (Altherr et al. 1979) and isothermal decompression after the M_1 event, as it was described on Ios (Van der Maar 1981), suggest that the M_1 metamorphism was followed by a period of rapid uplift. The M_2 metamorphism is a high temperature event which occurred at a pressure slightly in excess of the triple point of Al_2SiO_5. Maximum estimated temperatures of 700 ^{o}C and pressures of 400 to 500 MPa (see Chapter 2) indicate a geothermal gradient of 50 to 70 ^{o}C/km. These observations indicate clearly that the thermal structure of the crust on Naxos has changed profoundly in the 35 Ma which separate the two metamorphisms (see Jansen and Schuiling 1976).

The discussion of the metamorphic history of Naxos will concentrate on the following points:

(1) As the petrology indicates that the metamorphic conditions during the M_1 metamorphism were similar to those inferred for the Sesia Zone in Italy (Ernst 1971, 1973, Dal Piaz and Ernst 1975, Williams and Compagnoni 1983, Van der Maar 1981, Van der Maar and Jansen 1983, Maluski et al. 1981), it will be useful to compare

tectonic models for the two areas.

(2) The M_2 metamorphism was interpreted to be the result of a short thermal pulse. This interpretation is not compatible with a model involving differential uplift between central Naxos and the southeast coast as a cause for the metamorphic zonation on Naxos. Alternative interpretations suggest that an external heat source acted on the system. Possibilities include magmatic or deepseated hydrothermal processes as means of transporting heat into the system.

(3) The M_2 metamorphism was followed by a period of rapid cooling. During the initial stages of this cooling, the intrusion of the I-type granodiorite along the west coast of Naxos occurred. The similarities between cooling histories of the intrusive and the thermal dome were discussed in the previous chapter. Cooling of these rocks was strongly influenced by uplift to the earth's surface which occurred sometime earlier than about 5 Ma ago.

The discussion is supported by numerical calculations of thermal histories. These models are based on solutions of the heat flow equation (Carslaw and Jaeger 1959). Two different models have been used in this study. The M_1 metamorphism was modelled with a one dimensional model (UPLIFT2) developed by Parrish (1982). The thermal effects of heat transport into the system during the M_2 metamorphism were studied with a two dimensional model of an intrusive dyke (THERMAL) which was developed by Harrison and Clarke (1979). The application of numerical models may yield information on the importance of tectonic processes, and on the time spans necessary for these processes to occur (Clark and Jäger 1969, Oxburgh and Turcotte 1971, 1974, Bickle et al. 1975, Albarede 1976, England 1978, Harrison and Clarke 1979, Clark 1979, Draper and Bone 1981, Parrish 1982, Zeitler 1985). This approach is used to explore possible thermal histories for the area. Constraints for modelling were obtained from petrological data and from the geochronology study of rocks on Naxos.

During the geological history since the Late Mesozoic, the ACMB has experienced tectonic processes which occur near the margin of a continental plate. As this is the case for the M_1 metamorphism, the M_2 metamorphism and the period following the M_2 metamorphism until the present day, it is implied that the location of the ACMB on the southern margin of the Apulian-Anatolian Microplate can explain most aspects of its tectonic and thermal history. During the M_1 event the supracrustal rocks of the ACMB and their continental crustal basement were buried at deep levels in an anomalously thickened crust. In the numerical models it is envisaged that a segment, or segments of the margin of the continental plate are transported to great depth (i.e. greater than 30 km), thus producing thickened crust near the continental margin. As the rates at which these processes have occurred are not known, two limiting models have been considered. A first group of models (Group A) is calculated assuming that thickening of the crust occurred in a very short time interval, a second group of models (Group B) assumes slow burial. These models describe the tectonic history from initiation of subsidence until the present day. This approach is favoured because it allows some degree of thermal disequilibrium to be taken into account. During the M_2 event, parts of the ACMB in the centre and northeast of the Cyclades suffered high temperature metamorphism, while major parts in the western and northwestern segment of the belt escaped substantial overprinting. High temperature metamorphism was accompanied by the intrusion of I-type granitoids which suggests that the central to eastern part of the Cyclades was in an island arc tectonic setting at this time.

In summary, from the information on the pressure-temperature-time path, in combination with model thermal histories, constraints on the tectonic evolution of Naxos can be obtained. With this information a detailed picture of the thermal and tectonic evolution of the area during the Tertiary can be established.

4.1.1 The basis for modelling

The geodynamical evolution of the region between the African Plate and the Eurasian Plate was summarized in Figure 2.2. The microplate which moves independently in between is the Apulian-Anatolian Microplate. Several authors have suggested that the Apulian-Anatolian Microplate may be further divided into sub-plates which have moved independently at some stage of their history (Dewey et al. 1973, McKenzie 1978). Regions where high pressure metamorphism has occurred during the Alpine Orogeny are for example the Sesia Zone, located on the southern margin of the Eurasian Plate in northwestern Italy and the ACMB located near the southern margin of the Apulian-Anatolian Microplate in Greece.

Similarities in the geology of the ACMB and the Sesia Zone in the western Alps include:

(1) Both regions have experienced high to very high pressure metamorphism during the Alpine Orogeny.

(2) In both regions continental crust was exposed to these extreme physical conditions.

(3) Both regions experienced a period of uplift and cooling during the Early Tertiary.

Differences between the two regions are mainly in the tectonic setting and in the geochronology:

(1) The Sesia Zone is located on the southern margin of the Eurasian Plate and is thought to have resulted from collision between the Apulian-Anatolian Microplate and the Eurasian Plate. The ACMB, on the other hand, is located on the southern margin of the Apulian-Anatolian Microplate and has no obvious continental mass immediately to the south of it.

(2) On both its northern and southern margins, the ACMB has younger high pressure belts. Because of its limited exposure it is difficult to establish regional variations in metamorphic assemblages. Blake et al. (1981) distinguish two different trends in the ACMB. The first is a decrease in metamorphic pressure from the northwest to the southeast along the present day strike of the belt. The second trend is perpendicular to the first, and suggests increasing pressures in northeasterly directions. The Sesia Zone is asymmetrical with the most extreme physical

conditions on its southern margin and decreasing pressures toward the north.

(3) The Sesia Zone has experienced its highest pressures in Early Cretaceous times and has evidence for younger less extreme high pressure metamorphism in Late Cretaceous to Early Tertiary times. The ACMB, according to the presently available data, has experienced its most extreme conditions in Late Cretaceous to Early Tertiary times, and has on its margins some evidence for younger Oligocene to Miocene high pressure metamorphism.

(4) In the Italian and Swiss Alps the predominant direction of nappe emplacement is in a northerly direction. In the Apulian-Anatolian Microplate in Greece, the predominant direction of nappe emplacement is in a southerly direction (Jacobshagen et al. 1978).

As indicated by the petrology of M_1 mineral assemblages, the continental crust on the southern margin of the Apulian-Anatolian Microplate was significantly thickened at the time of metamorphism. One of the earlier plate tectonic models for the formation of blueschist belts suggests that this type of metamorphism occurs in the deepest levels of an accretionary wedge (Fig. 4.1). Deep sea sediments accumulated in the wedge are expected to be important rock types in belts formed in this way (Ernst 1971). This model is not applicable to the Alpine blueschist belts because in both belts mentioned above continental platform sediments as well as their continental crustal basement experienced high pressure metamorphism.

Models for the high pressure metamorphism in the Sesia Zone suggest that underthrusting of continental lithosphere of the Eurasian Plate occurred along a south dipping subduction zone beneath the continental crust of the Apulian-Anatolian Microplate (Ernst 1971, 1973, Dal Piaz and Ernst 1975, Rubie 1983). This interpretation is supported by the size of the area affected by high pressure metamorphism and the apparent decrease in metamorphic pressure towards the north. In the ACMB, there is presently no evidence for collision with a southern continent. Although it cannot be excluded that in the Cretaceous history of the Levantine Basin, small microplates of the size of Corsica-Sardinia existed and collided with the southern margin of the Apulian-Anatolian Microplate, there is at present little

Figure 4.1. (A) The accretionary wedge model for blueschist metamorphism (Ernst 1971). Under this model the sedimentary accretionary wedge will consist predominantly of deepsea sediments, with incorporation of a proportion of greywackes derived from the continental margin by gravity sliding.
(B) Model for thickening of the continental margin by faulting and subsequent subsidence of segments of the margin of the continental plate (modified after Rubie 1983).
(C) Thickening of continental crust along the margin of a continental plate by continental collision.

The last two models may be used to account for high pressure metamorphism in continental crustal rocks and can be taken as the tectonic model on which the thermal modelling of the M_1 metamorphism was based. Model (C) requires the presence of continental crust to the south of the ACMB. As there is little evidence for such a continental mass, model (B) is the preferred interpretation of the tectonic history of the Apulian Microplate.

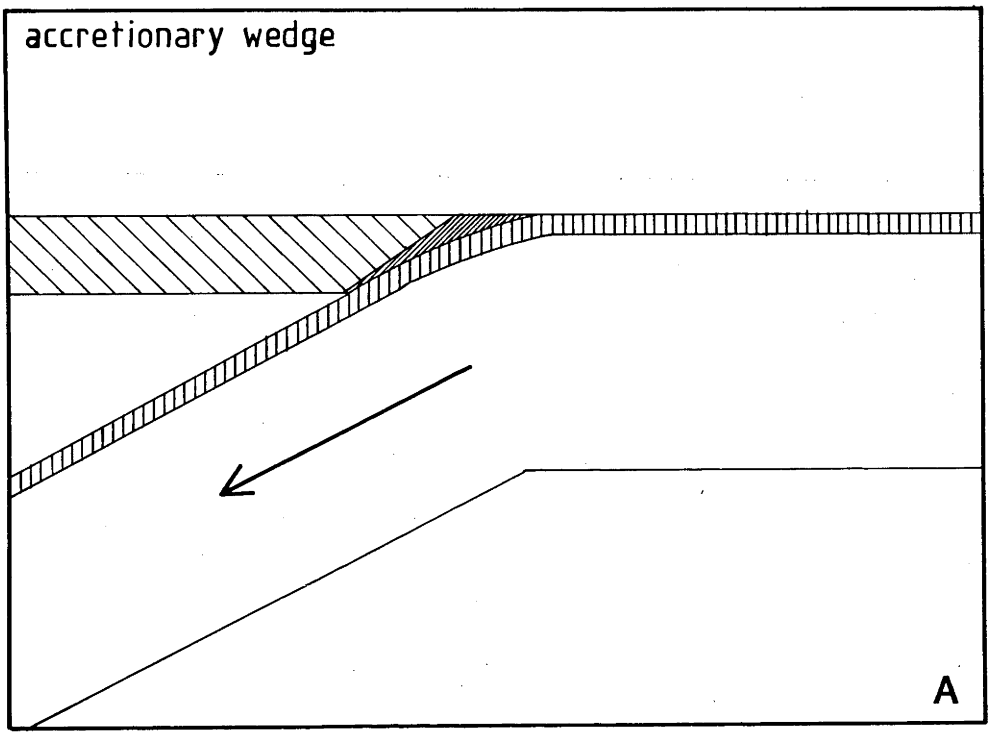
accretionary wedge
A

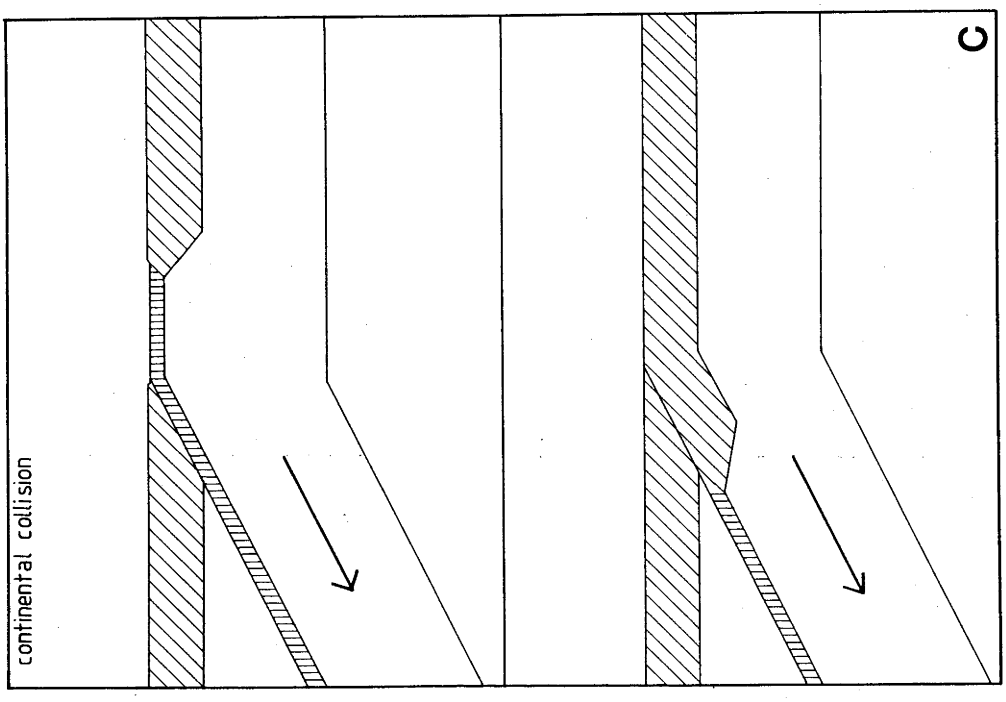
continental collision
C

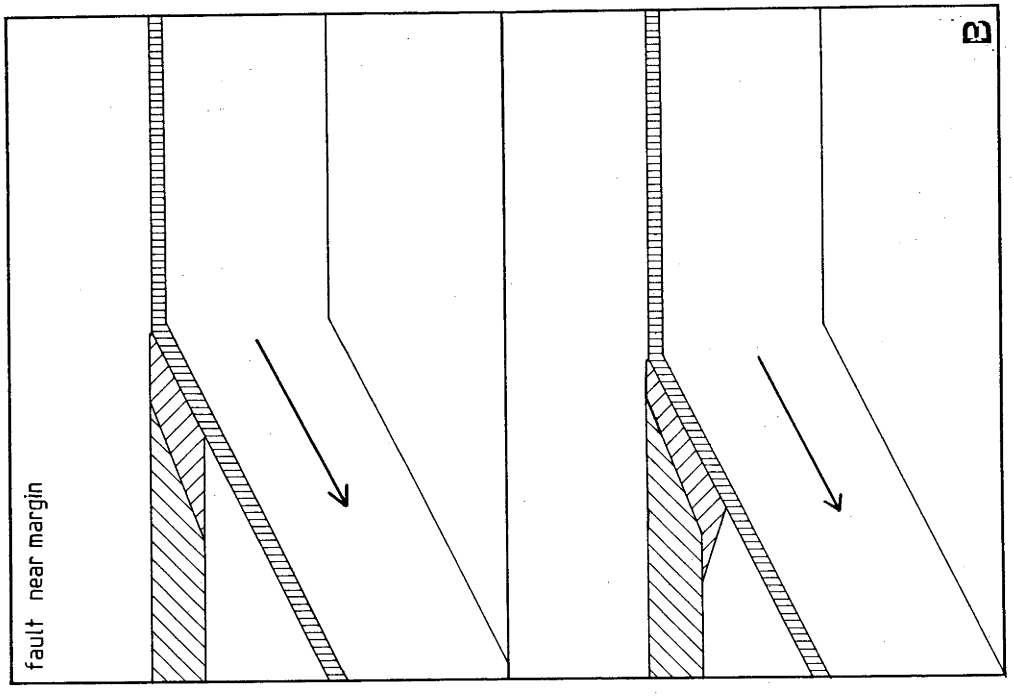
fault near margin
B

evidence for it. Thus, the continental collision model as proposed for the Italian Alps cannot readily be applied to the ACMB. A possible model for the ACMB is discussed in section 4 of this chapter. This model suggests that segments of the margin of a continental plate may be transported to depth by the action of the subducting oceanic plate (Fig 4.1 and its caption). When continental crustal segments are transported to considerable depths, the result will be a thickened continental crust near the margin of the plate. Because these crustal segments were originally positioned near the earth's surface, the geothermal gradient near the margin of the continental plate will be low. The simplest case, where only one segment of continental crust is transported down will be indistinguishable from the case where a small microplate collides with the main continental plate. Multiple fracturing and subsidence will result in a thickened crust near the continental margin, which lacks the chemical stratification inferred for normal continental crust.

In the next sections, first an outline of the numerical calculations and their parameters will be given. This section is followed by the application of the calculations to the thermal history of Naxos. This part of the chapter is organized in a way that per section a particular time interval is discussed (e.g. the pre-M_1 to M_1 period, the time interval between the M_1 and M_2 events, the M_2 metamorphism and subsequent cooling). Each of these sections begins with a summary of geological and geochronological constraints, which is followed by discussion of the model calculations.

4.2 Thermal models

Numerical models allow geological histories to be simulated. In this study, they are used to model the thermal effects of tectonic and magmatic processes. With constraints on the thermal history of an area from petrological and geochronological data, it should be possible to constrain the tectonic processes that produced these thermal effects. The models, which were used in this study, were discussed in detail in the papers where they were originally presented (Harrison and Clarke 1979, Parrish 1982). Here, the parameters and the application of the models to the metamorphic history of Naxos will be discussed.

4.2.1 Thermal model for uplift and burial of a crustal section

A model designed to calculate the effects of uplift and erosion on the thermal structure of the lithosphere can be based on the solution of the heat flow equation for one dimension:

$$\frac{\delta^2 T}{\delta z^2} - U/\kappa \cdot \frac{\delta T}{\delta z} - 1/\kappa \cdot \frac{\delta T}{\delta t} = - A_0/K \cdot e^{(-(z-U.t/DS))}$$

In this equation T stands for temperature, z for depth, U for uplift rate, κ for thermal diffusivity, t for time, A_0 for surface heat production, K for thermal conductivity, and DS for the depth scale factor which determines the decrease in radioactive heat generation in the crust. The model used in this chapter is based on a numerical solution of this equation using the Crank-Nicholson implicit method (see Crank 1975). The initial geotherm is defined by:

$$T(z,0) = T_0 + Q.z/K + DS^2.A_0/K \cdot (1 - e^{-z/DS})$$

The symboles in this equation are the same as those explained above, Q is reduced (mantle) heat flux. The advantage of using a numerical model, rather than the analytical solution, is that a numerical model is much more flexible. UPLIFT2 for example, allows variation of the factors for mantle heat flux and for the uplift rate with time. UPLIFT2 was tested against the analytical solution by Parrish (1982) and Zeitler (1983). Agreement between the two solutions was shown to be very close.

The boundary conditions for the model, as it is used in the following sections, include a constant surface temperature of 20 ^{o}C, a lithospheric thickness of 100 km with either a constant temperature, or a chosen heat flux at the lower boundary, and an exponentially decreasing heat production with increasing depth. Within the boundary conditions of the model, the method can be applied successfully. Because of the nature of the solution, the models should be limited to cases where:

(1) Heat transfer occurs predominantly by conduction and advection.

(2) The one dimensional solution of the heat flow equation is appropriate, i.e. horizontal variations in heat distribution are insignificant.

The derivation of very detailed thermal models can be frustrated as some of the parameters used in the models are poorly known, or the variation of these parameters with temperature is not well known. For example, the values for the thermal conductivity (K) and thermal diffusivity (κ) vary with temperature and also depend on the composition of the rocks (Čermak and Rybach 1981). Thermal models generally use average values for these parameters.

Further, the radioactive heat production (A(z)) depends on the distribution of the elements U, Th and K in the crust. It is generally accepted that these elements are concentrated in the upper part of the continental crust (Lachenbruch and Sass 1978, Taylor 1979, Taylor and McLennan 1981). Studies of surface heat flow suggest that the concentration of heat producing elements should decrease fairly rapidly with depth. The variation in concentration of heat producing elements through the crust is poorly known. Consequently estimates depend on the model for the crust that was used (England 1978, Taylor 1979, Sawka and Chappell 1985). A convenient way of expressing the variation in heat producing elements is by assuming that the decrease in radioactive heat production has an exponential form (Lachenbruch 1970, Lachenbruch and Sass 1978). The depth scale factor (DS) determines the rate of the exponential decrease of heat producing elements with depth. The estimated average value for the scale factor in the continental crust is 8.5 km (Oxburgh 1981). For the

models in this study, a factor of 10 km is used. This value was estimated by Lachenbruch and Sass for the western U.S.A. and may be more representative of orogenic belts near continental margins (Lachenbruch and Sass 1978).

Another parameter which strongly influences the thermal structure of the lithosphere is the mantle heat flux (Q). This parameter is defined as the surface heat flux reduced by the contribution of crustal heat production (Lachenbruch and Sass 1978). Values for the mantle heat flux vary from 20 mW/m^2 and less for cold lithospheric conditions for example near subduction zones, to about 34 mW/m^2 in orogenic belts (Blackwell 1971). In the models which will be discussed in the next sections, the mantle heat flux is kept at a constant value throughout the model. The reason for this choice is that the variation of the mantle heat flux with time is not well known in the Aegean. Thus, the models have been calculated for two different estimates for the mantle heat flux (30 and 40 mW/m^2). Because of the low rate of heat conduction through the lithosphere, sudden variations in mantle heat flux will be transmitted only slowly into the upper part of the crust which represents the segment of interest to this study.

4.2.1.1 Discussion of parameters

The parameters which determine the initial thermal structure of the lithosphere are given in Table 4.I. The values represent estimates for an average to warm continental lithosphere. This approach has been chosen because of lack of information on the initial thermal structure of the lithosphere in the area before subsidence started. Similar approaches have been used in other studies of thermal histories of orogenic belts (e.g. England 1978, Parrish 1982, Zeitler 1985, Rubie 1983). The effect of variation of individual parameters on the thermal structure of the lithosphere is given in Figure 4.2. The diagrams in Figure 4.2 (a,b,c,d) show an standard geotherm ($A_0 = 5.0*10^{-6}$ W/m^3, DS = 10 km, and HF = 30 mW/m^2), and in each diagram the effect of variation of the individual parameters. In Figure 4.2a and b the importance of variation in the concentration of radioactive heat producing elements for the geotherm is illustrated. In Figure 4.2a the surface heat production (A_0) is changed and in 4.2b the

Figure 4.2. The effect of variation of model parameters of UPLIFT2 on the geothermal gradient. The equilibrium geotherm is determined by: $A_0 = 5.0 * 10^{-6} W/m^3$, $T_0 = 20^oC$, HF = 30 mW/m^2, and depth scale DS = 10 km (A_0 = surface heat production, T_0 = surface temperature, HF = mantle heat flux, DS = the depth scale factor ($DS = -z/\ln A(z)/A_0$), thermal diffusivity: 32 km^2/Ma, thermal conductivity: 2.5 kW/km^oC).

a Equilibrium geotherms using the parameters listed above. A_0 is varied: curve (1) $A_0 = 1*10^{-6} W/m^3$, curve (2) $A_0 = 5*10^{-6} W/m^3$, curve (3) $A_0 = 10*10^{-6} W/m^3$.

b Equilibrium geotherms using parameters listed above. DS is varied: curve (1) DS = 5 km, curve (2) DS = 10 km, curve (3) DS = 20 km.

c Equilibrium geotherms using the parameters listed above. Mantle heat flux (Q) is varied: curve (1) 10 mW/m^2, curve (2) 20 mW/m^2, curve (3) 30 mW/m^2, curve (4) 40 mW/m^2.

d Transient geotherms on the basis of the equilibrium geotherm with parameters listed above (curve (3)). Curve (1) geotherm after subsidence of 2 mm/yr for 20 Ma, curve (2) geotherm after subsidence of 2 mm/yr over 10 Ma, curve (4) geotherm after uplift of 2 mm/yr over 10 Ma, curve (5) geotherm after uplift of 2 mm/yr over 20 Ma. The geotherms were calculated with a constant temperature at the bottom of the grid.

e Re-equilibration of the geothermal gradient after an instantaneous drop of 40 km. Mantle heatflux is 40 mW/m^2, $A_0 = 0.8*10^{-6} W/m^3$. The curves give the geothermal gradient in 10 Ma intervals from 0 to 50 Ma. The equilibrium geotherm is presented in curve g.

f Re-equilibration of the geothermal gradient, as in e but with a mantle heatflux of 30 mW/m^2. The equilibrium geotherm is given in curve g.

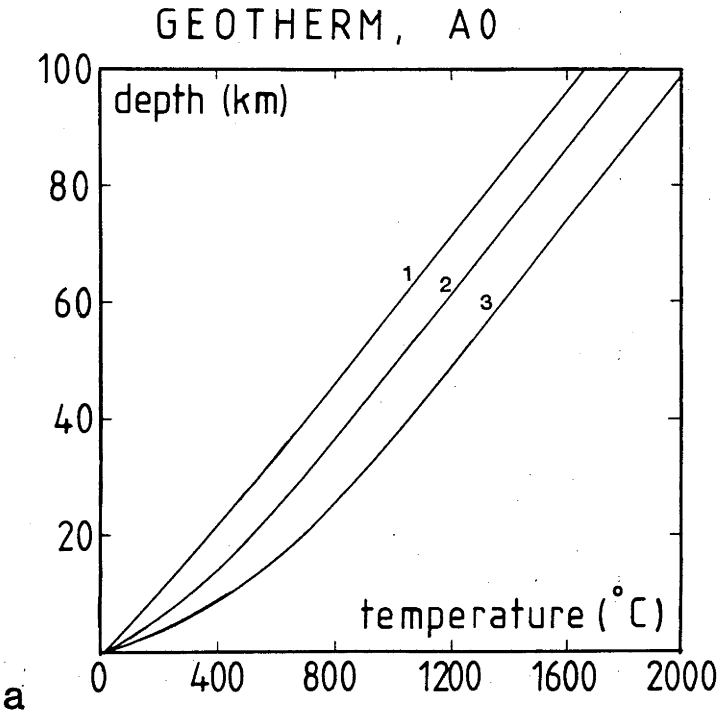
GEOTHERM, A0
depth (km)
temperature (°C)
100
80
60
40
20
0
400
800
1200
1600
2000
1
2
3

a

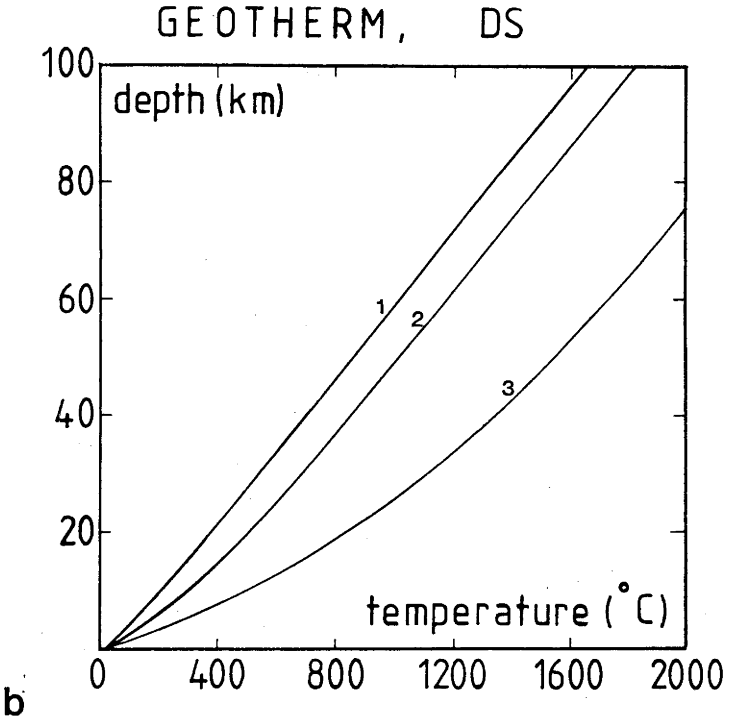
GEOTHERM, DS
depth (km)
temperature (°C)
100
80
60
40
20
0
400
800
1200
1600
2000
1
2
3

b

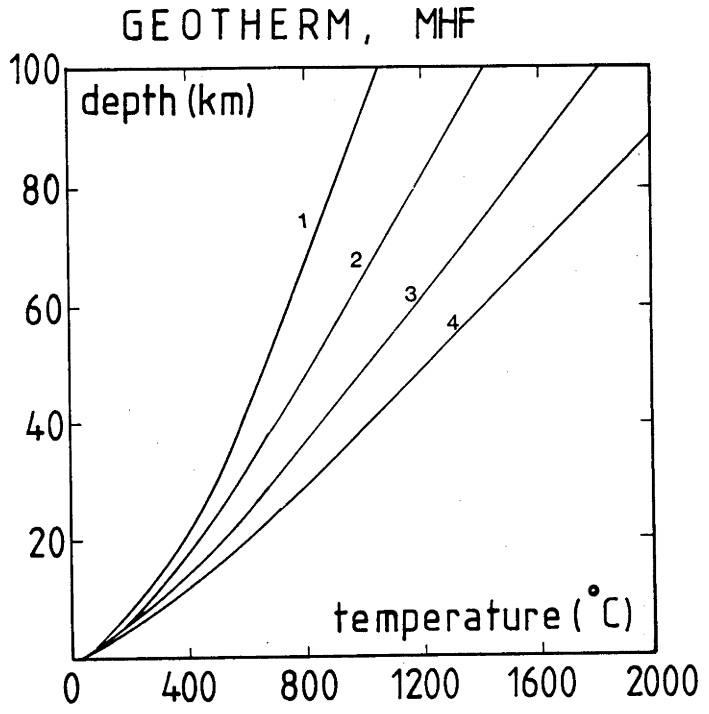
GEOTHERM, MHF
depth (km)
100
80
60
40
20
1
2
3
4
temperature (°C)
0
400
800
1200
1600
2000

c

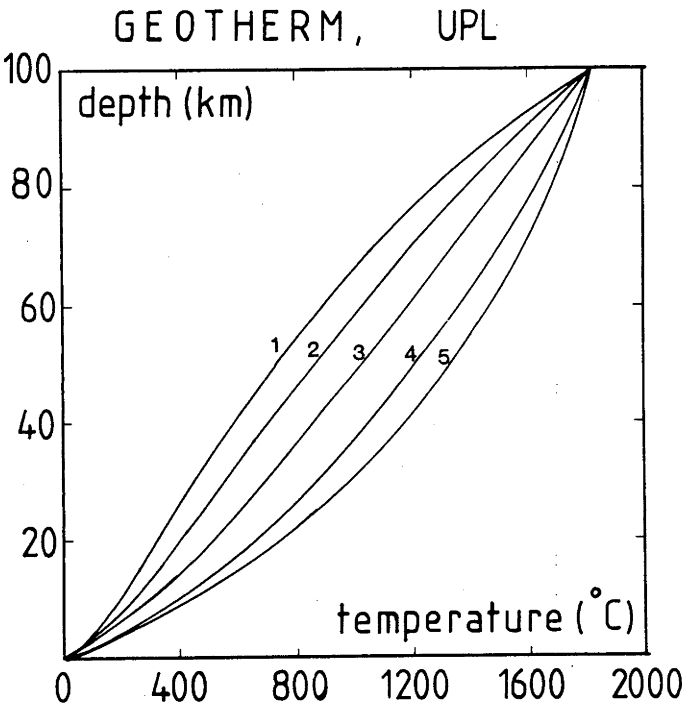
GEOTHERM, UPL
depth (km)
100
80
60
40
20
1
2
3
4
5
temperature (°C)
0
400
800
1200
1600
2000

d

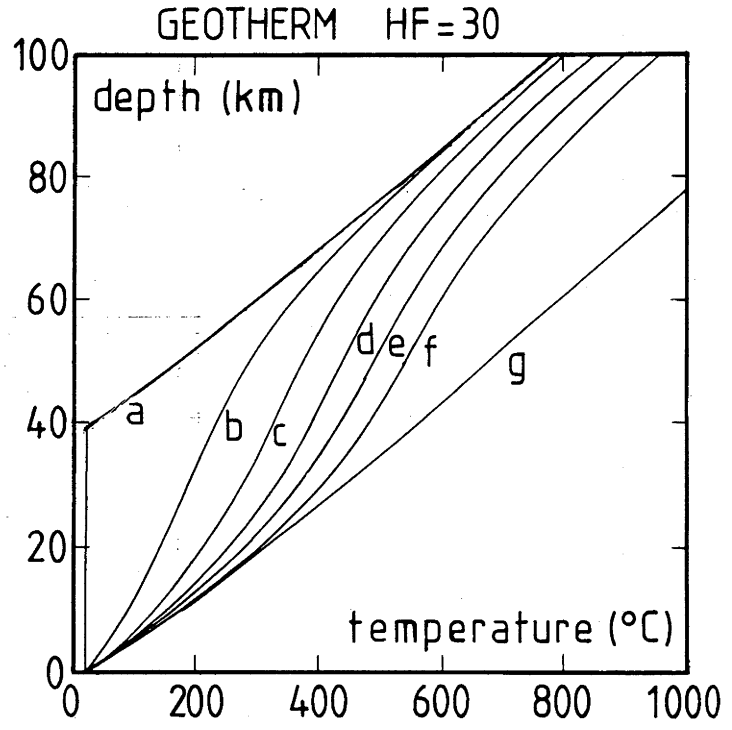
GEOTHERM HF=30
depth (km)
100
80
60
40
20
0
a
b
c
d
e
f
g
temperature (°C)
0
200
400
600
800
1000

e

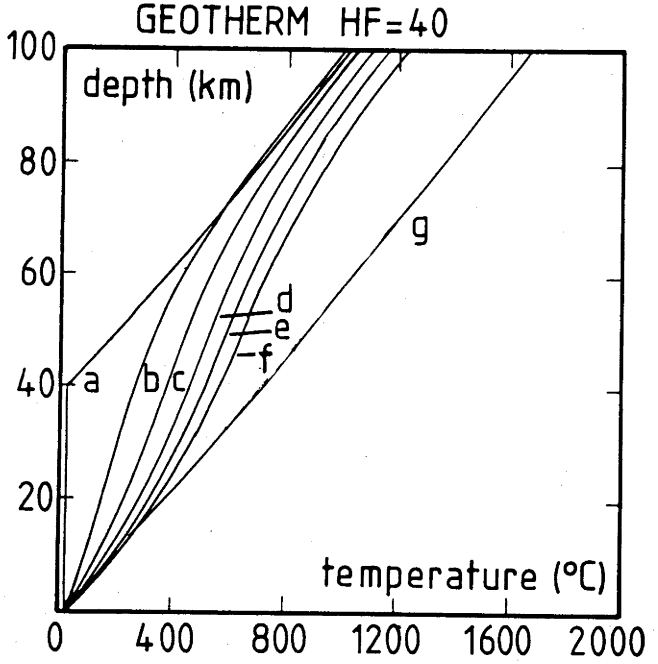
GEOTHERM HF=40
depth (km)
100
80
60
40
20
a
b
c
d
e
f
g
temperature (°C)
0
400
800
1200
1600
2000

f

depth scale factor DS is varied. Because the radioactive heat production is described in UPLIFT2 by an exponential relation, the geotherm is not very sensitive to variation of the surface heat production. The depth scale factor, which controls the slope of exponential decay with depth, has a much stronger influence on the geotherm. The contribution of a mantle heat flux (Q) also strongly influences the position of the geotherm. Normal values for a continental environment range between 20 and 30 mW/m^2, values higher than 30 mW/m^2 are characteristic for hot continental crustal sections.

In Figure 4.2d a continental crustal segment is modelled with the above mentioned standard geotherm. This crustal segment is exposed to uplift and erosion, and to burial at a rate of 2 mm/yr for 10 and 20 Ma. The temperature at the bottom of the grid (100 km) is kept constant. This diagram illustrates that uplift and burial can produce transient geotherms which may cause high temperature metamorphism, and high pressure, low temperature metamorphism respectively. In Figure 4.2e and f the effect of sudden rapid vertical movement on a section of continental crust is given. The curves a to f in both diagrams represent the degree of re-equilibration in 10 Ma intervals to 50 Ma. These diagrams indicate that significant re-equilibration of the geotherm occurs during the first 10's of million years, but that full re-equilibration may take much longer.

The contribution of radioactive heat production has an important effect on the geotherm. To model subsidence, one needs to make assumptions as to the distribution of heat producing elements in the part of the crust located above the section of interest. Two groups of models will be discussed. The difference between the two groups is in the rate of burial and in the distribution of heat producing elements.

In Group A rapid burial is modelled. The maximum rates of burial near a continental margin are limited by the rate of movement of the subducting slab. As plate speeds of 10 to 15 cm/yr were measured (e.g. Johnson 1982), subsidence rates along a 30^{o} dipping slab may be as high as 5 to 7.5 cm/yr. It is assumed that if segments of the continental crust are taken down at these speeds, the material on top of it will have a uniform heat

production rate comparable to supracrustal levels. Thus in the models a constant concentration is assumed in the upper 40 km of the crust, and an exponentially decreasing concentration further down (Fig 4.3). Further, because the maximum rate of burial at a continental margin can be in the order of centimeters per year, the times required for burial will be very small when compared with the times required for thermal re-equilibration (see Fig. 4.2. e and f). In the models, therefore, burial is assumed to be instantaneous. In Figure 4.2 e and f the effect of re-equilibration of the geotherm after rapid burial is given. The geotherms at 10 Ma intervals over the first 50 Ma after burial are presented.

In models of Group B subsidence is slow and continuous until the rocks reach their maximum depth of about 40 km. Uplift follows immediately after subsidence ceased, thus substantial heating must occur while the rocks are still subsiding. In these models the distribution of heat producing elements is kept constant with respect to the earth's surface. This implies that when the rocks move down into the earth, the heat producing elements migrate upwards. This assumption is clearly a simplification, but may be reasonable considering the high mobility of U (e.g. Langmuir 1976). Because the other two main heat producing elements, K and Th, are less mobile at low temperatures, the actual concentration of heat producing elements at depth may be underestimated. Therefore, times of heating obtained from this group of models are likely to be maximum estimates.

The models of Group A have a surface heat production (A_0) of $0.8*10^{-6}$ W/m^3. This value is appropriate for carbonate platform sediments consisting of limestone, sandstone and pelitic units. The models of Group B have a surface heat production (A_0) of $3.0*10^{-6}$ W/m^3, a value appropriate for average supracrustal rocks. This distribution compares favourably with estimates for the heat production through the crust (e.g. Oxburgh 1981) and is similar to the variation in heat production with depth as obtained from crustal sections as for example in the Vredefort Dome (Nicolaysen et al. 1981). As can be seen from Figure 4.3, these heat production distributions result in different heating characteristics of the crust. The exponentially decreasing

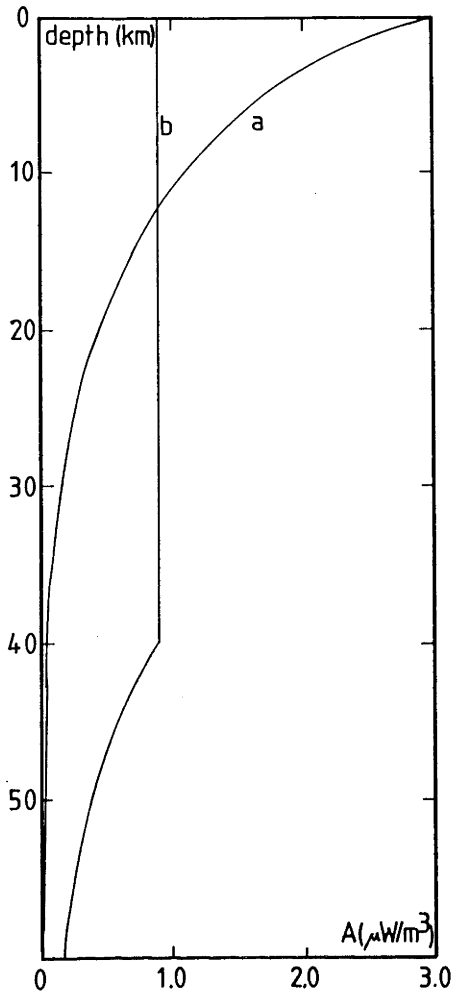

Figure 4.3. Distribution of heat producing elements used in UPLIFT2. (a) Exponential decreasing distribution, surface heat production A_0 = $3.0*10^{-6}W/m^3$, and depth scale DS = 10 km. (b) Constant concentration of heat producing elements over the upper 40 km (A_0 = $0.8*10^{-6}W/m^3$) followed by exponential decrease with DS = 10 km. Note that the total concentration of heat producing elements in both cases is approximately the same for the upper 60 km of the lithosphere, but curve (a) has its major concentration near the surface and curve (b) has a significantly higher concentration at depth. This difference will have implications for the heating rate of the sediments when buried to a depth of 40 km.

concentration of heat producing elements results in a large production of heat near the surface and very little heat production at depth (Fig 4.3). In the other distribution, substantially more heat is produced by radioactivity at depth of about 40 km (Fig 4.3). It is therefore likely that the models of Group A, which use this distribution, will tend to yield the younger time constants.

In the models, the state of thermal disequilibrium during orogeny was simulated by following the rocks through time from a near surface position until they reach the surface again after the metamorphic cycle. This approach illustrates that initially normal to warm continental crust can be taken down to an environment where high to very high pressure, low to medium temperature metamorphism can occur. Another consequence of such an approach is that it shows how the time factor becomes important. After the M_1 event which involved crustal thickening, and high pressure, low to medium temperature metamorphism, the crust of the ACMB needed a finite time to reach thermal equilibrium. The models indicate that at the time of the M_2 metamorphism, the geotherm has not yet fully reached equilibrium again. Consequently, it is difficult to understand the formation of the M_2 thermal dome from this model. In the following sections, the M_1 metamorphism, the M_2 metamorphism, and the periods between the two metamorphisms and subsequent to the M_2 metamorphism will be discussed. Because UPLIFT2 describes the whole of the history until the present time, parts of the models will be discussed in the following sections. ~~of the models will be discussed.~~

4.2.2 Thermal modelling of a transient heatsource

The second thermal model that has been used in this study is THERMAL which was developed by Harrison and Clarke (1979). It is based on a solution of the heat flow equation in two dimensions (Carslaw and Jaeger 1959).

$$\frac{\delta^2 T}{\delta x^2} + \frac{\delta^2 T}{\delta z^2} - U/\kappa . \frac{\delta T}{\delta z} - 1/\kappa . \frac{\delta t}{\delta t} = - A/K$$

The symboles of this equation are the same as those described in section 4.2.1; x is the variable describing the horizontal

distance from the centre of the dyke. The model predicts the thermal effect of an intrusive on the surrounding country rock and conductive cooling of the intrusive itself. The geometry of the intrusive is an infinite dyke with a vertical orientation. The initial temperature within the dyke can be chosen to fit the estimated temperature of a magma, and the initial temperature of the country rock is given by:

$$T(x,z,0) = T_0 + Q.z/K + A.z(Z-z/2)$$

In this equation is Z the lower grid boundary, the other symboles were discussed previously. This model has been used to explore the effects of a transient heat source on the rocks during the M_2 metamorphism. The model allows the choice of different values for heat production in the intrusive and in the country rock. Heat production is taken to have a constant value throughout the crust. Two time intervals with different uplift rates are allowed. The model parameters used for calculations relating to the M_2 metamorphism are shown in Table 4.I. With this set of parameters the initial temperature of the rocks was 325 ^{o}C. This value compares favourably with estimates of the pre-M_2 temperatures in zone I (see section 4.3.2).

By using this model for calculating the thermal effects of the M_2 metamorphism, it is implied that the heat source which caused the event was an intrusive dyke of a certain specified width and height and the crust has a well specified thickness. In reality, if there is an intrusive below Naxos, its shape is poorly known. If the thermal dome was caused by a hidden intrusive, it is difficult to determine the actual shape of such a body. On the other hand, if the intrusive mass is represented by the migmatite rocks which are found in the core of the dome, the actual shape of the body may be better approximated by a wedge or a cone rather than by a rectangular slab. These geometries represent larger volumes of intrusive material than the infinite dyke geometry and thus may have a larger effect on the country rock.

As was pointed out above for the one dimensional model, the calculations are restricted to the case where conductive heat transport dominates. If hydrothermal convection contributed to the distribution of heat subsequent to emplacement of the intrusive, it is expected that the top part of the contact aureole widens, and lower parts of the contact aureole would be narrower than predicted by the conductive solution (Parmentier and Schedl 1981).

4.3 The thermal evolution of Naxos

4.3.1 The M_1 metamorphism

As discussed in the previous chapter, cooling after the M_1 metamorphism through the temperature interval between 400 and 300 ^{o}C occurred on Naxos approximately 50 Ma ago. Despite considerable scatter caused by subsequent overprinting, the ages related to the M_1 metamorphism from various parts of the ACMB support the results obtained in southeast Naxos (Altherr et al. 1979, Bonneau et al. 1980, Blake et al. 1981, 1984, Maluski et al. 1981). Several authors have pointed to the similarities between the M_1 metamorphism in the ACMB and the high pressure metamorphism in the Sesia Zone in the western Alps (Van der Maar 1981, Maluski et al. 1981). Because the main high pressure event in the Sesia Zone occurred during the Early to Mid Cretaceous, it has been suggested that the ACMB may have experienced a major high pressure metamorphism during this period as well (Maluski et al. 1981, Rodgers 1984). As yet, no convincing geochronological evidence in support of this hypothesis exists. The high pressure belt of the ACMB is accompanied on its northern and on its southern margin by younger high pressure metamorphisms of Oligocene to Miocene age. The southern belt is exposed on Crete and the northern belt is found on Evvia (Seidel et al. 1982, Maluski et al. 1981). As these events have occurred in the period subsequent to the M_1 metamorphism, and outside the main part of the ACMB, they will not be discussed here, but will be mentioned briefly in the following section which deals with the period between the M_1 and the M_2 metamorphisms.

4.3.1.1 Thermal history

For the thermal history of the M_1 metamorphism on Naxos, there are the following constraints:

(1) Rocks of the schist-marble sequence affected by Alpine metamorphism were deposited in the Triassic on a continental basement in which evidence was found for igneous and metamorphic events during the Paleozoic (Dürr et al. 1978, Henjes-Kunst and Kreuzer 1982).

(2) The estimated maximum temperature during the M_1 metamorphism is 500 $\pm$ 30 ^{o}C for southeast Naxos and Ios (Jansen et al. 1977,

Van der Maar and Jansen 1983).

(3) The maximum pressure reached during the M_1 metamorphism in southeast Naxos and Ios is 900 to 1200 MPa (Jansen et al. 1977, Van der Maar and Jansen 1983, Chapter 2).

(4) Cooling below the closure temperature of phengite for argon occurred about 50 Ma ago.

(5) Isothermal decompression, as described on Ios, suggests that uplift after the peak of the M_1 metamorphism was rapid (Van der Maar and Jansen 1983).

Data on the metamorphic histories of other parts of the ACMB suggest that in more western and southern parts of the belt maximum pressures were somewhat higher (up to about 1500 MPa), and the accompanying metamorphic temperatures were somewhat lower (about 450 ^{o}C) (Altherr et al. 1979, Matthews and Schliestedt 1984)).

It was not possible to determine a cooling rate, or an apparent uplift rate for the M_1 metamorphism from the geochronology and closure temperatures, because the only minerals which date cooling after the M_1 event with some confidence are white micas. Paragonite K-Ar ages from southeast Naxos are indistinguishable from the K-Ar ages of phengites (Andriessen et al. 1979). This suggests that both minerals have similar closure temperatures for argon diffusion, and thus can not be used to determine a cooling rate.

In the model calculations for the M_1 metamorphism, it is assumed that the maximum depth reached by the rocks is equivalent to a pressure of 1500 MPa. As indicated by England and Richardson (1977) and by Draper and Bone (1981), some temperature increase must be expected in the initial stages of uplift. The magnitude of the temperature rise will mainly depend on the uplift rate and heat production. As a consequence, the maximum temperatures during metamorphism will occur at pressures which are less than the maximum pressure experienced by the system.

The models assume a thermal structure based on a single crustal section. Justification for this choice is based on the model which produced crustal thickening. The mechanism favoured by this study is a modification of that proposed by Rubie (1983), and will be discussed in section 4 of this chapter (Figure 4.1).

Because the large differences in temperature distribution caused by doubling of the crust level out relatively rapidly (see Draper and Bone 1981, Rubie 1983, Zeitler 1983), results from the present study do not differ significantly from those obtained from models of doubled continental crust.

The models of Group A describe the case where a segment of continental lithosphere goes down at approximately the same speed as the subducting slab. For the thermal calculations it was assumed that subsidence occurred instantaneously. On top of the subsiding crustal segment, material was deposited which consists mainly of sedimentary material. Thus, it is likely that the material on top of the segment has a uniform concentration of heat producing elements. A value of $0.8*10^{-6}$ W/m^3 was used. This value is considered to be representative for a sedimentary pile consisting of limestone, sandy units and pelites. In the model the value for the mantle heat flux is kept at a constant value. The values used in the calculations were 30 and 40 mW/m^2. In order to obtain temperatures of about 450 to 500 ^{o}C, the rocks need to remain at maximum depth for 30 and 50 Ma respectively.

The results of the calculations of Group B are presented by curves a and b in Figure 4.4. For a surface heat production of $3.0*10^{-6}$ W/m^3, and mantle heat fluxes of 30 and 40 mW/m^2, the times required for rocks transported from the earth's surface to a depth of about 40 km, to reach a temperature of 450 to 500 ^{o}C are 135 and 75 Ma respectively. Within the constraints from the petrology and geochronology, which suggest a maximum temperature of 450 to 500 ^{o}C and cooling of the rocks below about 350 ^{o}C about 50 Ma ago, this means that subsidence may have started 200 Ma or 140 Ma ago and has continued until about 65 Ma ago, when rapid uplift was initiated. In this model, rapid uplift immediately follows upon termination of subsidence. These models may be seen as maximum estimates for the duration of the M_1 metamorphic cycle, because more rapid burial followed by some time spent at depth will shorten the duration of the metamorphic cycle. Also, as discussed previously, the distribution of heat producing elements chosen for these models is likely to be a low estimate for the actual concentration.

Figure 4.4. Model thermal histories of zone I on Naxos calculated with program UPLIFT2. The variation of temperature with time (Figure A) and the variation of pressure and temperature (Figure B) are given. (a) Model I (burial at 0.31 mm/yr between 200 and 65 Ma ago), (b) model II (burial at 0.55 mm/yr between 140 and 65 Ma ago), (c) model III (instantaneous burial at 115 Ma ago), (d) model IV (intantaneous burial at 95 Ma ago). (See table I for model parameters). Models I and II used radioactive heat production as in Figure 4.3 curve a. Models III and IV used a radioactive heat production as in Figure 4.3 curve b. Comparison of figure A and B indicates that the peak temperature during the M_1 metamorphism occurred about 60 Ma ago, while the rocks experienced rapid decompression. Pressures associated with the highest temperatures are between 800 and 1200 Ma. Final uplift to the earth's surfaces occurred between 15 and 5 Ma ago. Time is given in Ma before present.
Figure C is based on model IV, but instead of rapid uplift after M_1, uplift was continuous between 65 Ma and 5 Ma. This model indicates that during the initial segment of a slow uplift history, temperatures in the rocks will rise.

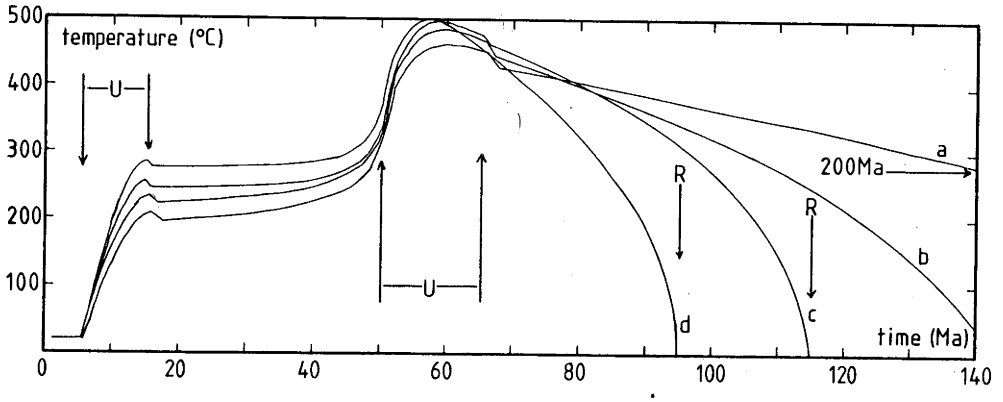
temperature (°C)
500
400
300
200
100
0
20
40
60
80
100
120
140
U
U
R
R
a
200Ma
b
c
d
time (Ma)

A

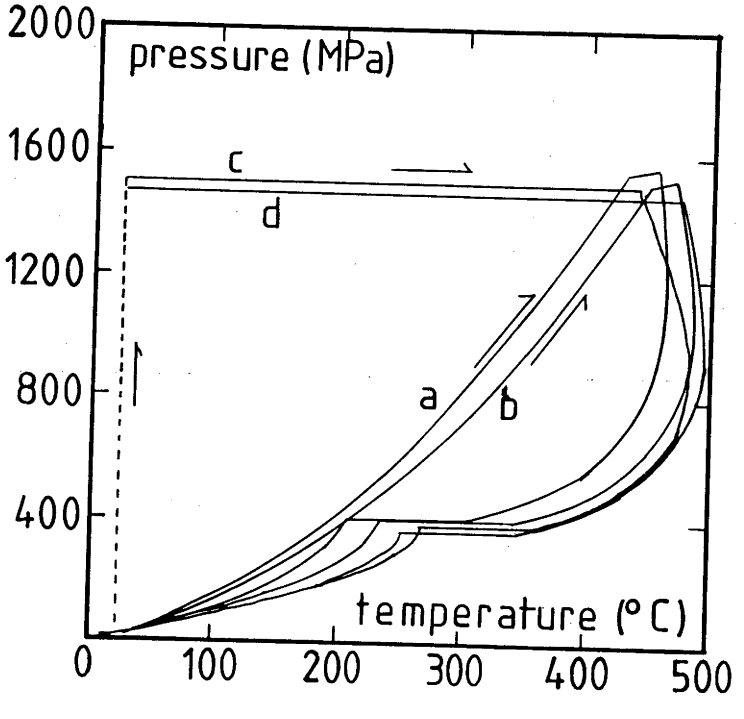
pressure (MPa)
2000
1600
1200
800
400
c
d
a
b
temperature (°C)
0
100
200
300
400
500

B

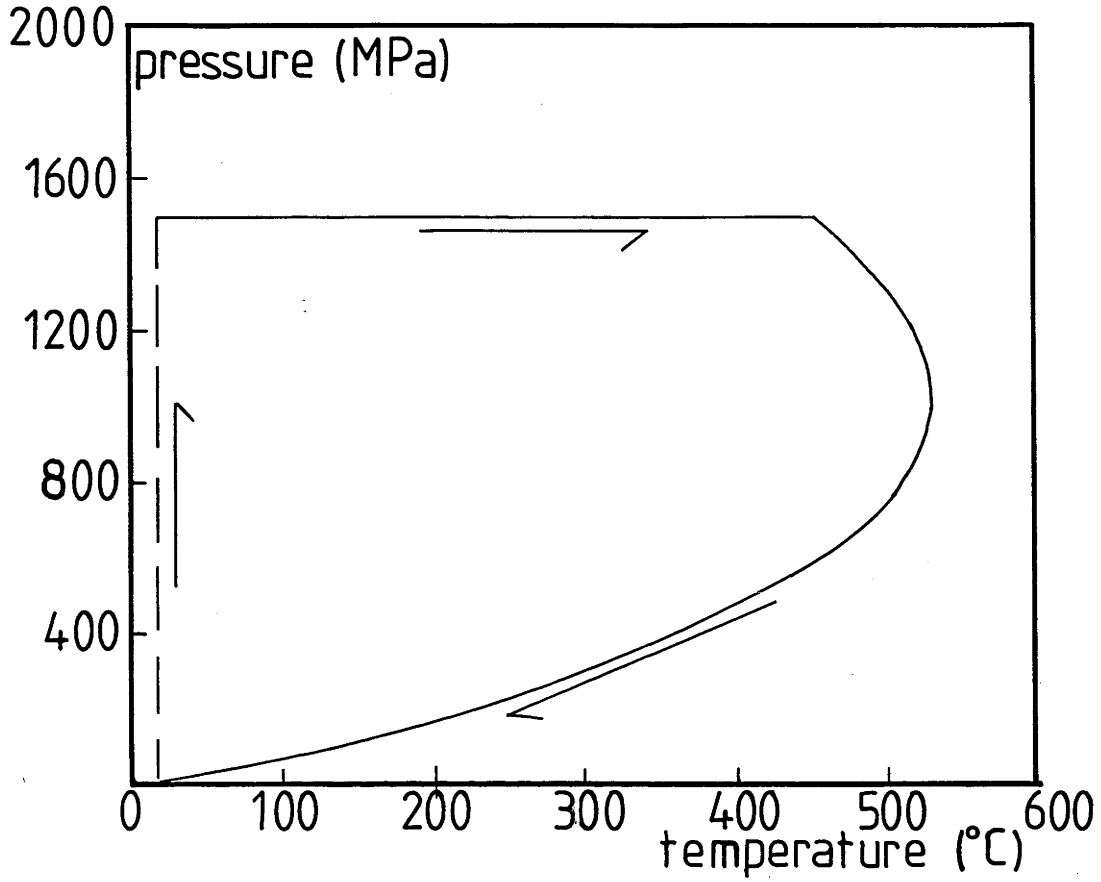
2000
pressure (MPa)
1600
1200
800
400
0
100
200
300
400
500
600
temperature (°C)

c

To check the importance of the distribution of heat producing elements in the crust on the calculated thermal histories, the models of Group A were also run using the distribution as in Figure 4.3a, the models of Group B with a distribution as in Figure 4.3b. This alteration caused shorter time spans for the rocks to reaches temperatures of about 500 °C in the models of Group B, and longer time spans for the models of Group A, thus emphasizing the critical importance of the distribution of heat producing elements for these models. In both sets of models, the uplift rates required to obtain cooling of the rocks below about 360 to 420 °C at about 50 Ma, are in the order of 2 mm/yr. Smaller values for the uplift rate will result in significant temperature increases during decompression (Draper and Bone 1981).

4.3.1.2 Discussion

The thermal calculations indicate that the geothermal structure of thickened continental crust is critically dependent on the distribution of heat producing elements through the crust and on the contribution of mantle heat flux (Fig. 4.2 a, b and c). Calculations by Rubie (1983) show that subduction of cool oceanic lithosphere directly adjacent to thickened crust may slow down heating inside the continental crust significantly as it decreases the contribution from the mantle heat flux, and transports cold lithosphere to deep levels in the earth. The effect of this factor is difficult to constrain and may introduce an extra uncertainty into the calculations. In the calculations on the thermal effects of the M_1 metamorphism this effect is ignored. The models for fast subsidence require that the rocks remained for a certain time at depth in order to generate temperatures in the order of 450 to 500 °C. The times required are calculated to be in the order of 30 to 50 Ma, depending on the thermal constants. As the continental crust will be out of isostatic equilibrium, it is debatable whether periods at depth as long as 50 Ma can be maintained. In the case of the slower subsidence models, no time is spent at depth but subsidence continues until the maximum depth is reached. As was noted previously, the time spans calculated for this case are likely to be maximum estimates for the duration of the metamorphic cycle,

as low estimates for distribution of heat producing elements were used. Higher concentrations of these elements may be incorporated in the sediments on top of the crustal segment of interest, thus reducing considerably the necessary time span for subsidence during the metamorphic cycle. The difference in estimated time spans between the two sets of models can partly be understood as the result of differences in distribution of heat producing elements, and partly from the difference in time spent at an effective depth of 40 km. In the first set of models, uplift immediately followed upon termination of subsidence. This is probably the more realistic model, but as only a very short time is spent at maximum depth, re-equilibration of the geotherm will be less efficient as a means of increasing the rock temperature in this case, when compared to the models of Group A.

Cooling after the M_1 event can be understood in terms of uplift. To obtain cooling from about 500 ^{o}C to 300 ^{o}C or less in the rocks, all models suggest that rapid uplift from maximum depth to about 10 to 13 km depth occurred within a period of 15 Ma after the peak of the M_1 event. This means that the transition from anomalously thickened continental crust to crust of about normal thickness occurred early in the history of the region. Modelling indicates that uplift rates of about 2 mm/yr are required in order to preserve blueschist assemblages. In Figure 4.4C the case is presented where M_1 metamorphism was followed by slow continuous uplift until the Present. This model illustrates that during slow decompression substantial temperature increases will occur. This model supports the interpretation that the M_1 event was followed by rapid uplift. It is noted that uplift rates of this magnitude are reported predominantly from orogenic belts along continental margins and in continental collision zones (Albarede 1976, Hollister 1979, Scholz et al. 1979, Mueller 1982, Zeitler 1983), consistent with the inferred geological situation of Naxos. Similar values were calculated by Draper and Bone (1981), who note that uplift rates of this magnitude are uncommon in present day mountain belts and very much higher than the erosion rates calculated from river sediments. They suggest that tectonic denudation, as for example nappe emplacement, is likely to have operated to allow uplift rates of this magnitude to be maintained over longer periods of time.

The modelling also indicates that slight differences in uplift history after the M_1 metamorphism may have caused the differences in metamorphic grade as observed in the different parts of the ACMB. Faster rates during early uplift would cause the preservation of higher metamorphic pressures and lower metamorphic temperatures. Conversely, in areas where initial uplift was slower, higher temperatures and lower pressures are likely to be recorded. In all models the maximum temperatures are recorded as the rocks experience decompression between 1200 and 900 MPa (Fig 4.4). This is in accordance with the petrological observations from Ios and southeast Naxos. The models are based on a simple tectonic history (see Table 4.I). Within these boundary conditions, the models with high estimates for the mantle heat flux tend to yield prograde temperature histories during decompression. To preserve the high pressure mineral assemblages, temperature rise during decompression must have been small. It is, therefore, not likely that a mantle heat flux of 40 mW/m^2 can be combined with estimates for crustal heat production which are higher than those presented in the models. The higher concentrations of heat producing elements would result in faster rising temperatures during the first stages of decompression, resulting in overprinting of the earlier high pressure mineral assemblages. It should be noted that in such conditions higher uplift rates would cause the desired cooling of the rocks. However, such a tectonic history would be substantially more complex, because to preserve the M_1 ages in the micas, the rocks would then have to be uplifted to higher levels in the crust than in the models presented in the previous section. This in turn would imply that the rocks need to have experienced renewed burial before the beginning of the M_2 metamorphism.

The timespans required for the M_1 metamorphic cycle, as estimated from thermal calculations are compatible with the time constraints as listed in the beginning of this section. From the geological constraints none of the modelled tectonic histories can be excluded. However, all calculated models imply that the M_1 metamorphism was followed by rapid uplift. Slower uplift rates would cause more substantial heating of the rocks, and thus prevent the preservation of high pressure mineral assemblages and M_1 $^{40}Ar/^{39}Ar$ and K-Ar ages. It is suggested that processes that

led to subsidence of rocks to blueschist facies metamorphic environments may have started as early as the end of the Jurassic, or as late as the Mid Cretaceous. The time spans required for the M_1 metamorphic cycle depend strongly on the thermal structure of the continental crust. Both factors which mainly control the thermal structure, mantle heat flux and radioactive heat production, are poorly known. But as a result of the tectonic processes near a continental margin they may differ considerably from normal values estimated for continental crust.

Geodynamic reconstructions of the eastern parts of the Mediterranean suggest opening of the Levantine Basin during the Triassic and subsequently during the Cretaceous a period of compression between the Eurasian and African Plates (Fig 2.2). This compressional phase occurred between about 100 and 60 Ma ago. If one may correlate this compressional phase with subduction at the plate boundary of the Apulian-Anatolian Microplate and the Levantine Basin and thus with subsidence of the rocks of the ACMB, the time constants calculated in the second set of models give the best agreement. This observation would support the model of fast subsidence of supracrustal rocks, followed by relatively fast thermal re-equilibration by radioactive heating in the sediments.

In conclusion, lack of adequate constraints on subsidence rates prevents us from rejecting any of the models calculated for the M_1 metamorphism. From geodynamic considerations, the shorter time constants seem to be the more realistic ones. To obtain isothermal decompression, higher concentrations of heat producing elements would necessarily have to be compensated for by faster uplift rates after the event. Although this may be another alternative, it would result in ambient rock temperatures in the period between the two metamorphisms which are too high to allow argon accumulation in the phengites, or in a considerably more complex tectonic history for which, as yet, no evidence exists. Cooling after the event suggests a phase of rapid uplift. In all models this is achieved by having the transition from thickened crust to a crust of normal thickness in the 15 Ma following the peak of the M_1 metamorphism.

4.3.2 The period between the M_1 and the M_2 metamorphism

It was shown in the previous chapter that the time gap between the M_1 and the M_2 metamorphisms is about 35 Ma. In the main part of the ACMB there is very little evidence for thermal disturbances during this period. However, rocks from the northern margin of the ACMB on Evvia, and rocks which probably were located at this time on the southern margin of the ACMB on Crete, experienced high pressure, low temperature metamorphism during the Oligocene and Miocene. In both areas this metamorphism may have continued to the Late Miocene (Seidel et al. 1982, Maluski et al. 1981).

It is assumed that in the main part of the ACMB, this period was relatively uneventful. Arguments in support of this view may come from thermal modelling. It was argued in the previous section that by the end of the M_1 event, the rocks of the ACMB were uplifted to a level of about 10 to 13 km below the earth's surface. Petrological observations in M_2 mineral assemblages indicate that during the M_2 metamorphism, the rocks were still at a level of 10 to 13 km (see Chapter 2). In the thermal models for M_2 metamorphic zone I, it was assumed that during this period no uplift or subsidence occurred. In Figure 4.4, it can be seen that this assumption results in ambient rock temperatures between 200 and 300 ^{o}C. As the closure temperature of phengite for argon is about 360 to 410 ^{o}C, it must be expected that prolonged times at temperatures higher than 300 ^{o}C will partly reset the argon isotopic ages. As only very limited overprinting caused by M_2 metamorphism occurred in rocks from zone I, it can be argued that the ambient rock temperature has not been in excess of 300 ^{o}C for significant amounts of time. It follows that it is unlikely that during this period any significant renewed subsidence occurred. Assuming about 10 km uplift in the post-M_2 period, and a present day crustal thickness of 30 to 32 km (Makris 1978), the pre-M_2 continental crust of the ACMB is likely to have had a thickness of 40 to 45 km. This is a crustal thickness which is similar to the present day crustal thickness of mainland Greece and Turkey, supporting the interpretation that the continental crust of the Aegean during this period was relatively stable.

Overprinting of M_1 mineral assemblages at greenschist facies metamorphic grade were described in many parts of the ACMB (see Altherr et al. 1979, Henjes-Kunst 1980, Van der Maar and Jansen 1983). Thermal models indicate that these events need not necessarily be related to the high grade M_2 metamorphism on Naxos and adjacent islands in the northeast of the Cycladic Archipelago. As the temperature of the rocks in zone I on Naxos is calculated at values between 200 and 300 ^{o}C, it is suggested that only relatively small differences in overburden, or local renewed subsidence, would increase the physical conditions of the rocks to greenschist facies metamorphic grade. In such an environment widespread resetting of argon isotopic ages in white micas may occur without the contribution of an external heat source. It should be noted that this argument does not apply to the two zones of Oligocene to Miocene high pressure metamorphism, located on Crete and on Evvia. To bring these rocks back into the glaucophane stability field (Carman and Gilbert 1983), a period of significant renewed subsidence, or increase in overburden must have occurred over a relatively short time interval.

Both these local greenschist facies grade zones and the zones of blueschist metamorphism on the margins of the ACMB on Crete and on Evvia are post-M_1 events. These events are probably not related to the high grade M_2 metamorphism, as it occurred on Naxos, Paros and parts of Tinos and Iraklea. It may lead to confusion to classify these post-M_1 metamorphisms under M_2, because the M_2 metamorphism, as it was defined on Naxos, is one distinct phase of high grade metamorphism, whereas greenschist and blueschist facies overprinting may not be as well defined in time.

4.3.3 The M_2 metamorphism

The M_2 metamorphism on Naxos caused the formation of a thermal dome. The constraints from the geochronology on the cooling history are illustrated in Figure 3.15. These data were interpreted as suggesting that the maximum temperatures in the dome were reached between 15 and 16 Ma ago. Cooling after the event was rapid, with initial rates similar to those expected for cooling of an intrusive body. The isotopic dating of M_2 minerals suggests that the event which caused the metamorphism was of

short duration. These two arguments suggested that the thermal dome was the result of transport of heat into the system (see previous chapter). The variation of M_2 metamorphic temperatures with distance from the central migmatites, as was estimated from the petrology, is given in curve a in Figure 4.5 (see Chapter 2). It is assumed that the temperature distribution through the migmatite was uniform.

The area in which an anatectic meltphase has been observed in metapelitic rocks has an oval shape, with longest axis of about 8 km and shortest axis of about 4 km. The longest axis is oriented along a NNE-SSW line. The estimated metamorphic temperature decreases to about 400 ^{o}C within 5 km from the + meltphase line. Thus, heat is concentrated in a small segment of the crust. The present day geometry of the dome suggests that the average dip in the metasedimentary envelope is about 30^{o}. As argued previously, from the excellent preservation of the M_2 metamorphic zoning it is suggested that after metamorphism no major tectonism has occurred within the complex. This means that the present day geometry may be used to calculate differences in structural level at the time of the M_2 metamorphism.

The granodiorite intrusive on the west coast of Naxos caused only a narrow thermal contact zone (about 200 to 500 m), and did not significantly influence the isograd pattern produced by the thermal dome. As mentioned in the previous chapter, the contact aureole of the granodiorite is about one tenth as wide as the mineral zones around the thermal dome. It was argued that it would be unlikely, therefore, that the M_2 thermal dome was caused by a granitoid intrusive similar in size to the granodiorite. Further, structural domes similar to the one found on Naxos occur also in the ACMB without being the focus of a high grade thermal event (see discussion in the previous chapter). This suggests that differences in uplift alone are not likely to have produced the M_2 thermal dome. Thermal modelling of the M_2 thermal dome supports the view that significant additional heat is required to produce the observed effects.

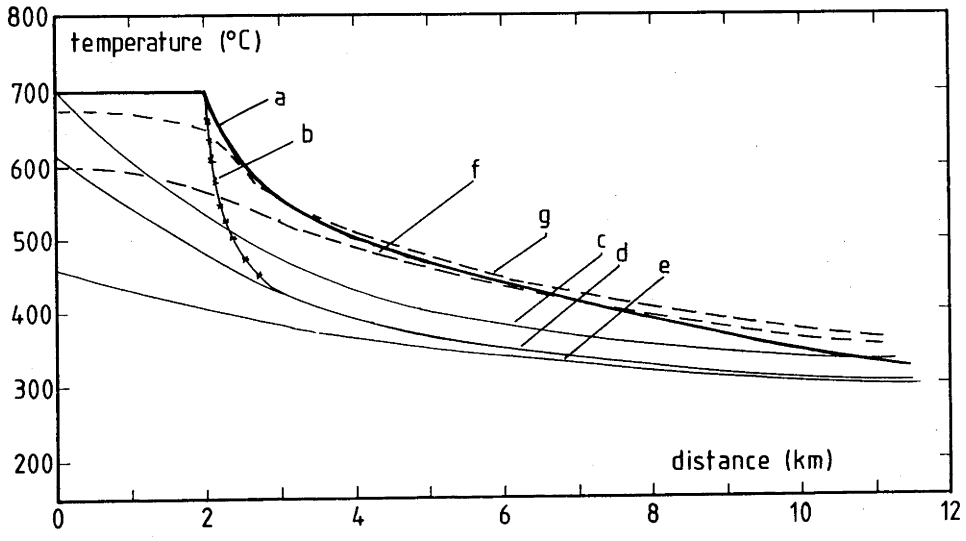

Figure 4.5. Maximum M_2 metamorphic temperatures as a function of distance from the centre of the migmatite zone toward the southeast. Curves b to f were calculated with THERMAL.
(a) The thick solid line represents the temperature estimates from the petrology (see chapter 2).
(b) The crossed line represents the temperature calculated with THERMAL for model A.
(c, d, e) The thin solid lines represent the temperatures for models B (1000 m), C (500 m) and D (100 m) respectively (calculated with THERMAL).
(f, g) The broken lines give the temperature distribution for models E and F respectively (calculated with THERMAL). (see table I).

4.3.3.1 Thermal calculations

One dimensional modelling of the thermal effects of the M_2 metamorphism with UPLIFT2 was carried out under the assumption that these rocks have experienced a tectonic history similar to that of the rocks from zone I before the M_2 metamorphism. This approach was chosen to take into account some degree of disequilibrium in the thermal structure of the crust caused by the M_1 metamorphic cycle. The model parameters used for the M_2 metamorphism were identical to those that were used to model the M_1 metamorphism as it is exposed in zone I. It is estimated from the geometry of the dome, that there could be a difference in structural level of 6.5 km between zone I and the core of the dome. Two models take into account the thermal effect of this extra uplift on the rocks. Curve a in Figure 4.6 makes use of model II (Group B) as the pre-M_2 history, and curve c has model IV (Group A) as a pre-M_2 history. The additional uplift of 6.5 km, which models the effect of differential uplift between zones I and VI, was assumed to have occurred between 20 and 15 Ma ago. Curve d shows the evolution in temperature assuming that 6.5 km uplift occurred between 50 and 15 Ma ago. The differences in time-temperature path between these to models illustrate that if differential uplift is to be a viable option, it must have occurred over a relatively short period of time. A longer period of differential uplift would increase temperatures over longer time intervals, which would lead to an inconsistency with the requirement that the M_2 metamorphism was of short duration.

The sort of processes needed to generate the very high temperatures associated with the M_2 metamorphism were investigated with models UPLIFT2 VI and THERMAL A. Model VI is represented by curve b in Figure 4.6. It is assumed in this model that the migmatites intruded into the sedimentary sequence, and originate from a depth of 10 km below the presently exposed erosion surface. Consequently, in the model 16.5 km uplift occurred in the period between 20 and 15 Ma ago. The pre-M_2 history used for this calculation is model II (Group B). The model is compatible with the inferred high M_2 temperatures and with the geochronological data for the M_2 event in zone VI in that it explains the M_2 cooling ages of hornblendes and micas between 15 and 11 Ma. A major problem with this model is however,

that the geology of the area does not support differential movements of this magnitude between the migmatite zone and the surrounding sedimentary sequence. This model history has been also investigated with THERMAL model A (Table 4.I). As discussed in a previous section, THERMAL can be used to calculate the effects of intrusion and subsequent conductive cooling on a section of the continental crust. In Figure 4.5, curve b shows the effect of the intrusion of a 700 ^{o}C intrusion on the country rock. Comparison of this model with the temperature estimates from the petrology (Fig. 4.5a) suggests quite clearly that conductive cooling of such a body cannot account for the formation of the M_2 metamorphic zonation.

Another set of models was calculated using THERMAL (Harrison and Clarke 1979). The parameters used for the calculations are listed in Table 4.I. These models explore heating of rocks during the M_2 metamorphism by a hot intrusive below the presently exposed erosion surface. Several possible solutions were calculated (Fig 4.5). These solutions are based on the assumption of a 1200 ^{o}C body and conductive heat transfer. The effect of latent heat is not taken into account. The effect of an intrusive with a half width of 2000 m was calculated for depths of intrusion of 1000 m, 500 m, and 100 m (Figure 4.5 c, d and e). Conductive cooling of such a body would have only a rather limited effect on the temperatures in the presently exposed crustal section. To cause the thermal effects as inferred from the petrology, the level of intrusion would have to be less than 100 m below the presently exposed erosion surface. It is unlikely that an intrusive would be present so near to the surface without finding some field evidence for it. Thus such an intrusion is unlikely to have caused the M_2 thermal dome. The alternative option is a larger intrusive (half width 4000 m), for which the thermal effects of intrusion at 1000 m and 500 m were calculated (Fig 4.5 f and g). It turns out that a pluton of this geometry and dimensions at a depth of 500 m below the erosion surface would cause a thermal effect which is very close to that estimated from the petrology of M_2 mineral assemblages. This model is more realistic than those discussed above, but still requires the intrusion of a magma at very shallow levels below the present erosion surface. These models illustrate quite

Figure 4.6. Model thermal histories calculated with model UPLIFT2 for the migmatite zone. These models are based on the assumption of differential uplift between zone I and zone VI. Thus they are based on models for the M_1 event in zone I as a pre-M_2 history. This means that uplift from a maximum depth started 65 Ma ago and continued until 50 Ma ago. After a quiet period which lasted until 15 Ma ago the rocks are transported to the earth surface. To model formation of the domal structure, it is assumed that differential uplift (6.5 km in (a), and (c), 16.5 kn in (b)) occurred between 20 and 15 Ma ago that is immediately before beginning of the M_2 metamorphism. Curve (d) is a variation on the model presented in curve a, where the additional 6.5 km uplift occurred between 50 and 15 Ma ago.

(a) The basic model (model V). It is based on model II as a 'prehistory', and has experienced 6.5 km extra uplift between 20 and 15 Ma ago.

(b) Model VI assumes an additional 10 km uplift, in order to model the diapiric rise of hot migmatites. All other parameters as in model V.

(c) Model VII is similar to model V, but has model IV as an M_1 'prehistory'.

(d) Model VIII has the same parameters as model V, but instead of having the 6.5 km additional uplift between 20 and 15 Ma, it occurs between 50 and 15 Ma ago. (see table I for the values of the parameters).

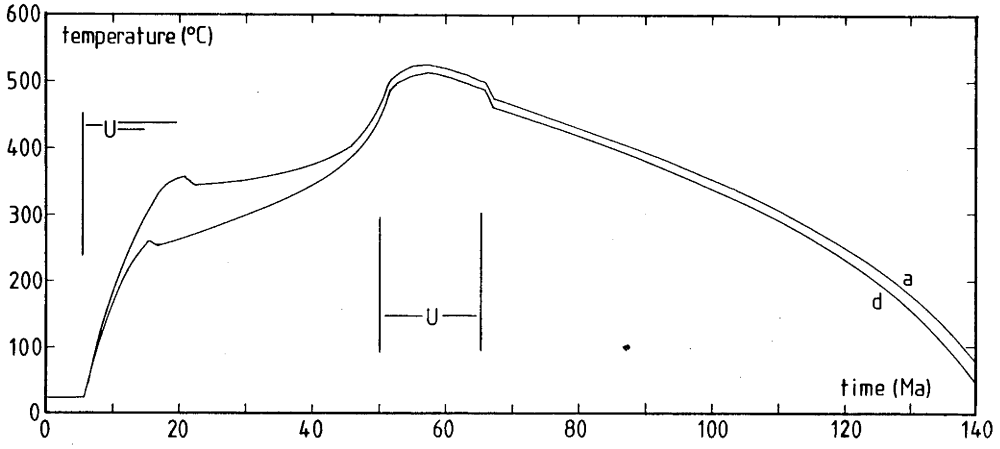
temperature (°C)
600
500
400
300
200
100
0
U
U
a
d
time (Ma)
0
20
40
60
80
100
120
140

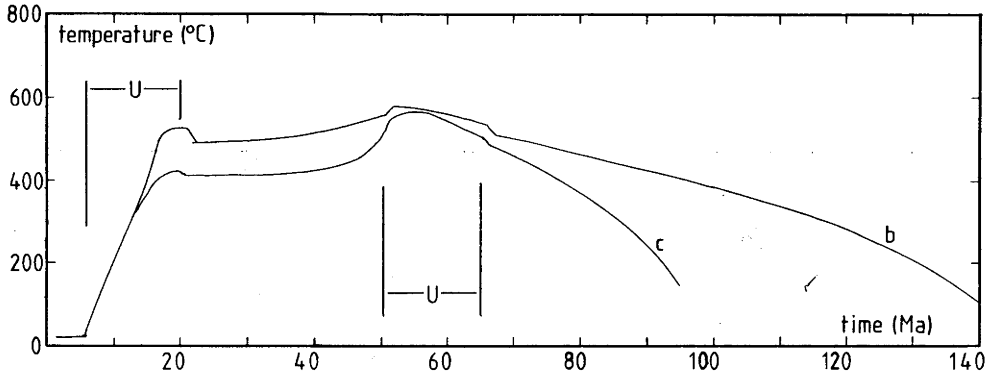
temperature (°C)
800
600
400
200
0
U
U
c
b
time (Ma)
20
40
60
80
100
120
140

clearly the amounts of heat necessary to produce a thermal dome as exposed on Naxos.

4.3.3.2 Discussion

The calculations with UPLIFT2 indicate clearly that the M_2 metamorphism cannot be the result of differences in uplift between zone I and zone VI. This conclusion is based on the following two observations. Firstly, the calculated temperature of the rocks is too low to have caused migmatization. Secondly, the maximum temperature is reached by the system at a time which is not compatible with the geochonological data. Further, although the cooling history of zone VI can be explained by a diapiric model assuming an additional 10 km uplift in this zone, field evidence and the calculation of the thermal effect of such a body on the surrounding country rock, do not support this option. The field evidence suggests that little or no differential movement has occurred between the migmatites and the country rock as migmatization has not only affected the core of the dome but also parts of the metasedimentary envelope directly adjacent to the core. In addition, structural analysis would document diapiric rise in the core of the dome. Analysis of the lineations in the dome suggests instead stretching along a north-south axis (Lister et al. 1984). These lineations are not compatible with diapiric rise.

From the models which assume a hidden intrusive, model F which suggests an intrusive dyke with a half width of 4000 m at a depth of 500 m below the presently exposed surface would introduce enough heat to form the observed metamorphic zonation (Fig 4.5 g). This solution is preferred to the solution where a smaller or cooler body would be positioned at shallower depth, as was calculated in models B, C and D (Fig 4.5 c, d and e), because such very shallow intrusions would probably be accompanied by pegmatitic activity that could be observed in the field.

Arguments in favour of a magmatic heat source for the M_2 metamorphism are mainly based on the results of the isotopic study.

(1) The focussing of heat on a small segment of the crust is well explained.

(2) The rapid cooling after the peak of the M_2 event is similar to cooling expected for an intrusive body (Fig 3.15) and is understood best by the intrusion and cooling of a hot magma below the presently exposed surface.
(3) The overprinting relations of M_1 formed white micas and M_2 formed white micas in the area of lower amphibolite metamorphic grade suggest a discrete short heating pulse.

Arguments against a simple contact metamorphic event are:
(1) The petrology of high grade metamorphic rocks suggests high fluid to rock ratios (Schuiling and Kreulen 1979, see also Etheridge et al. 1983).
(2) The high proportion of CO_2 of deep seated origin in the syn-metamorphic fluid (Rye et al. 1976, Kreulen 1980) is compatible with high grade metamorphism as is found in granulite facies terrains (Touret 1971, Swanenberg 1980).
(3) The homogeneity of fluid inclusions which were observed in the quartz lenses argues for either significant fluid convection, or for very large quantities of fluid (Kreulen 1980).
(4) The intrusion of small S-type granitic bodies, which are clearly derived from below the present day erosion surface, suggests that rocks similar to those exposed at the surface may occur at deeper levels as well.
These arguments led Schuiling and Kreulen (1979) to suggest that hot deep seated fluids could be the main source of heat for the formation of thermal domes. They suggested that the source for these fluids was a rising mantle dome below the Cyclades. However, it is, as yet, unclear whether high temperature metamorphic fluids can be focussed on a small segment of the crust, and whether such a process could occur within the time constraints discussed in Chapter 3.

The calculations of the thermal effect of intrusion, as presented above are limited to the case of conductive cooling. It was demonstrated quite clearly that large quantities of heat are required for the formation of a thermal dome. Some of the observations from the M_2 thermal dome are very well explained by magmatic transport of heat into mid to upper crustal levels. There is some regional gravity data which could be interpreted as support for a mafic intrusive under Naxos and Paros (Makris 1978), but the author is nor aware of more detailed observations

on Naxos that could constrain the extent of a sub-surface intrusion. Similar calculations to the ones described above by Parmentier and Schedl (1981) and by Carrigan (1983) explore the effects of hydrothermal convection on cooling of the intrusive and the effect of convection within the intrusive. Compared to the conductive solution, these processes are likely to transport more heat into the higher levels of the intrusive and into the contact zone directly above the intrusive. Also, in the calculations with THERMAL the effect of latent heat was ignored. Thus, it may be possible to obtain similar thermal effects from a slightly smaller, or cooler intrusion. Thus, the conclusion of this section must be that the M_2 thermal dome on Naxos was formed by an amount of heat equivalent to the heat transported into the system by conductive cooling of a 1200 ^{o}C mafic intrusive, with a half width of 4000 m, if it were emplaced 500 m below the presently exposed erosion surface.

4.4 Tectonic synthesis

The tectonic history of the ACMB since the initiation of Alpine orogenic activity in the Aegean is interpreted as a direct consequence of interactions between oceanic lithosphere belonging to the Levantine Basin and continental lithosphere of the Aegean part of the Apulian-Anatolian Microplate. This is the case for the M_1 metamorphism, it is the case for the neotectonic history during the last 5 Ma, and it is also likely to be the case for the M_2 metamorphism. The general configuration of oceanic basin, trench, subduction zone and continent as found today in the eastern Mediterranean need not have changed since the end of the Cretaceous. Because of the limited size of the area, it is considered unlikely that each of the high pressure events in the area is related to the closure of an oceanic basin, along separate subduction zones and followed by continent-continent collisions. It is proposed here that various interactions occurred between the continental crust of the Apulian-Anatolian Microplate and the subducting oceanic lithosphere belonging to the Levantine basin.

The present day structure of the Alpine Orogenic Belt in Greece is characterized by a series of sedimentary nappes which were emplaced from the north to the south (see Jacobshagen et al. 1978). At least part of the sedimentary units, which are presently located to the south of the metamorphic belt originate from an area further to the north of it. In the far northwest of the belt near Mount Olympos (Fig 2.1), there is some evidence for overthrusting of rocks belonging to the ACMB onto non-metamorphic sedimentary rocks (Godfriaux 1968, 1977). In the Cyclades and in Anatolia there is no evidence for similar relations. Therefore, it is assumed that in these areas the ACMB forms an autochthonous basement for the non-sedimentary nappes.

4.4.1 The M_1 metamorphism

From the petrology it is estimated that the thickness of the crust of the Apulian-Anatolian Microplate during the M_1 metamorphism was in excess of 60 km. As discussed in an earlier section of this chapter, depending on the rate of heating of the crust, which is determined by mantle heat flux and radioactive

heat production, it may take between 135 and 30 Ma to produce conditions suitable for blueschist metamorphism. The geodynamic history may be interpreted as supporting the shorter durations for this event, which may point to relatively high estimates for heating rates in the crust. As re-establishing of a normal crustal thickness is likely to have occurred in about 15 Ma following the peak of the M_1 event, the minimum time constant for a blueschist metamorphic cycle may be as short as 45 Ma.

The tectonic history of the ACMB may be described in a model which is similar to that proposed by Rubie for the Sesia Zone (Rubie 1983). The model suggests fracturing of the continental crust near the plate margin, with the development of fault planes parallel to the Benioff zone. Along these faults partial underthrusting of segments of continental crust occurs, caused by compression along the subduction zone (Fig 4.1). Multiple fracturing of the crust of the Apulian-Anatolian Microplate may have followed, which in turn may have caused thickening of continental crust near the convergent plate margin. By this process cool upper crustal rocks are transported to deep levels of the crust. Consequently, the geothermal gradient of the crust near the continental margin will be significantly lowered. Under this model high to very high pressure metamorphism of continental supracrustal rocks may occur in the continental side of a convergent plate margin. To explain subsequent high pressure events, it is suggested that during subsequent periods of compression faults may have been reactivated, resulting in multiple bands of high pressure metamorphism.

The geodynamic evolution of the ACMB was discussed by Blake et al. (1981, 1984), Bonneau (1982), Rodgers (1984), and Lister et al. (1984). Blake et al. (1981) note the existence of two different pressure trends in the M_1 metamorphic assemblages. The first trend is an increase in metamorphic pressure from southwest to northeast across the belt. The second trend is an apparent decrease in pressure from the northwest to the southeast along the present day strike of the belt. They interpret the observed pressure trends and apparent differences in lineation trends as being related to two different subduction zones at high angles with one another. Subsequent work on the neotectonic stresses within the Aegean, has revealed that the area was exposed to a

late extensional stress field which has caused thinning of the continental lithosphere and rotation of crustal blocks. These observations have led to the suggestion that one single subduction zone may have caused the high pressure metamorphism in the ACMB (Rodgers 1984, Blake et al. 1984, see also Nur and Ben-Avraham 1982). Rodgers (1984) suggests also that at least since the Miocene the tectonics of the Aegean Sea were dominated by the subduction of oceanic crust of the Levantine Basin from the Hellenic Trenches (see Fig 2.1, The Hellenic Trenches consist of a series of en echelon trenches, of which the main ones are the Ionian Trench, the Plini Trench and the Strabo Trench).

It is suggested here that subduction from the Hellenic Trenches may have occurred during the M_1 metamorphism in the ACMB as well. Bonneau (1982) suggests that blueschist metamorphism in the ACMB is the result of subduction along the northern margin of a separate oceanic basin which closed some 30 Ma ago. Uplift of the high pressure rocks of the ACMB occurred according to this interpretation between 40 and 30 Ma ago. From the present study it was concluded that this phase of uplift occurred earlier, between 65 and 50 Ma ago. It is suggested that the southern part of the Apulian-Anatolian Microplate has been substantially affected by crustal extension since the Late Miocene (McKenzie 1978, Le Pichon and Angelier 1979, Angelier et al. 1982). Pre-extension reconstructions suggest that there was a close relation between Crete and the ACMB in the Miocene. Thus there is little evidence in the Aegean for a separate oceanic basin. The simpler interpretation is to position the ACMB near the southern margin of the Apulian-Anatolian Microplate since the beginning of the Tertiary. After uplift ceased at about 50 Ma ago, phases of increased compression may have reactivated earlier faults related to the original subsidence phase before the M_1 event. During this period very little is recorded in the ACMB on Naxos and Ios in terms of thermal events. It is therefore interesting to note that directly to the north and to the south of the ACMB, blueschist metamorphism occurred during this period and may have continued until the rocks were uplifted to the earth's surface between 15 and 5 Ma ago (Maluski et al. 1981, Seidel et al. 1982). These events may represent evidence for thrust tectonics during a compressional phase prior to the M_2 metamorphism. As the ages

associated with this high pressure event are similar to the cooling ages of M_2 high grade minerals from the central parts of the ACMB (Seidel et al. 1982, Maluski et al. 1981), uplift in these areas may have been synchronous to post-M_2 uplift in the central parts of the belt.

4.4.2 The M_2 metamorphism

High temperature metamorphism is restricted to a relatively small part of the belt located in the central to northeastern parts of the Cycladic Archipelago, i.e. on the islands Naxos, Paros, Tinos, Myconos and Iraklea (Altherr et al. 1982). This metamorphism occurred at mid to upper crustal levels (between 15 and 10 km) while the Aegean continental crust entered an extensional stress regime which was related to processes at the Hellenic Trenches (McKenzie 1978, Le Pichon and Angelier 1979). As already briefly mentioned in the previous chapter, there is some evidence in the Aegean for migration of the magmatic arc which is related to subduction of oceanic lithosphere from the Hellenic trench system, in a southerly direction since the Early Miocene. The present day location of the arc is immediately to the south of the ACMB (Fig 2.1). K-Ar dating of volcanism suggests that this position of the arc is relatively young. The earliest volcanism is probably just over 3.0 Ma old (Fytikas et al. 1976). There is, however, evidence for earlier arc related volcanism and magmatism further to the north (Fig 2.1). In the ACMB, because of substantial uplift, no extrusive volcanism is exposed, but I-type magmatism which is suggested to be of arc related origin, occurred between 8 and 15 Ma ago (Altherr et al. 1982). Directly on the northern margin of the ACMB, in western Anatolia, andesitic volcanism occurs of similar age (Innocenti et al. 1982). Toward the northeast the age of these volcanics increases to about 25 Ma (Fig 2.1). Along the northern margin of the Aegean Sea, this volcanism is accompanied by granitic magmatism between 25 and 30 Ma old (Innocenti et al. 1982, Dürr et al. 1978). This age pattern, together with the observed extensional stress field in the area over the last 15 Ma, suggests relative movement of the trench arc system to the south with respect to the Aegean segment of the Apulian-Anatolian Microplate. As the inferred position of the magmatic arc

coincides with the position of the ACMB during M_2 metamorphism and intrusion of I-type granitic magmas, it seems justified to propose that the high heat flow environment related to the development of the thermal dome on Naxos occurred in a magmatic arc tectonic setting. The high heatflow can be modelled successfully by assuming mafic magmatism at lower levels in the crust. Based on conductive heat transfer alone it is estimated that intrusion below Naxos occurred to a shallow depth of about 500 m below the present erosion surface. However, if more efficient heat transfer occurred by fluid movement, as suggested by Schuiling and Kreulen (1979), mafic magmatism may have been restricted to significantly deeper levels in the crust.

Structural analysis of the thermal dome on Naxos suggests that the rocks of Naxos were in an extensional regime during the M_2 metamorphism (Lister et al. 1984), that is about 15 to 16 Ma ago. Neotectonic arguments relate the extensional stress field in the Aegean to subduction of oceanic lithosphere from the Hellenic Trench system (McKenzie 1978, Le Pichon and Angelier 1979, Angelier et al. 1982, De Bremaecker et al. 1982). Consequently, it is suggested that subduction from the Hellenic Trenches was already going on at this time (Lister et al. 1984). In an extensional regime uplift of the ACMB may be described by models which were developed for the metamorphic core complexes in the Basin and Range Province in western USA (Davis 1983, Wernicke 1981, Spencer 1983). These models suggest extension of the lithosphere, which caused fracturing and thinning of the brittle non-metamorphic upper crust. Seismic studies would suggest that listric faulting occurs in the upper crust. In the zone where the upper crust is thinned, uplift of the lower part of the crust occurs, bringing igneous and metamorphic rocks to the surface. Lister et al. (1984) proposed such a model for the structural domes at Naxos and Ios. They mentioned the following similarities between the domes on Ios and Naxos and the North American core complexes: (1) a major ductile shear zone with mylonitic rocks, (2) elongated domes over which stretching lineation warps, (3) igneous activity associated with uplift, (4) progressive mylonitization during uplift, and (5) low angle faults overlain by unmetamorphosed rocks. The initiation of the extensional stress field must have occurred somewhat before the time that the

M_2 thermal dome developed on Naxos. The arguments cited by Lister et al. (1984) in support of the interpretation of the domes of Naxos and Paros as metamorphic core complexes are likely to hold for the ACMB as a whole, because of the tectonic relation between the metamorphic rocks and the overlying sedimentary units.

This mechanism may explain the rapid uplift in the period between 15 and 5 Ma ago, when the rocks of the ACMB were brought from upper to mid crustal levels to the earth's surface. This period of rapid uplift was terminated about 5 Ma ago. This sudden termination of uplift in the ACMB may mark the shift of the focus of extensional forces from the ACMB to the Sea of Crete, which is located immediately south of it. Evidence in support of the extension of the Sea of Crete in the period between 5 Ma ago and the Present comes from a paleomagnetic study of rocks from the Peloponesos in southern Greece, which indicates rotation in response to the opening of the Sea of Crete in this time interval (Laj et al. 1982).

4.5 Conclusions

The present study indicates that blueschist metamorphism on the margins of continental plates may be the result of thickening of the continental crust over periods between 150 and 45 Ma. The actual length of such a metamorphic cycle is mainly determined by the rate of heating of the crust. The parameters which dictate heating are mantle heatflux and radioactive heat production within the crust. Unfortunately, both parameters are poorly constrained in the region affected by Alpine metamorphism.

The transition from thickened crust to normal crustal thicknesses is necessarily short, 15 Ma is suggested for the ACMB. Prolonged residence at depth would induce overprinting of the original high pressure mineral assemblages by lower pressure higher temperature assemblages (England and Richardson 1977, Draper and Bone 1981).

As we calculate ambient rock temperatures at 200 to 300 ^{o}C for the period between the two major metamorphisms, based on the assumption of a stable crustal level throughout this period, it is suggested that renewed subsidence during this period has been minor. Existing differences in tectonic overburden are likely to have caused the different degrees of overprinting of M_1 mineral assemblages by later greenschist facies assemblages.

During the Miocene, probably before 15 to 16 Ma, the hinge of the subducting oceanic lithosphere at the Hellenic Trenches started moving to the south with respect to the Eurasian Plate. This process had a number of important consequences for the geology of the Aegean Sea:

(1) The southern part of the Apulian-Anatolian Microplate is placed in an extensional stress field.

(2) As the relative movement of the trench is in a southerly direction, the magmatic arc related to subduction of oceanic lithosphere beneath the Aegean continental crust migrates to the south as well. Its original position about 25 to 30 Ma ago is along the northeastern margin of the Aegean Sea, its final position is on the southern margin of the ACMB (Fig 2.1).

(3) The high temperature events in the ACMB, which include high temperature metamorphism (M_2), closely followed in time by the intrusion of I-type granitoids, may be related to the passing of

the magmatic arc through the ACMB. During this time the lower crust may have been intruded by mafic magmas, which caused local high heat fluxes into the mid to upper crust, either by individual plutons, or by focussing of fluid flow on certain favourable sections of the crust. This option is broadly supported by the results of gravity surveys (Makris 1978), but detailed gravity constraints to support this interpretation were not available.

(4) As the extensional stress thinned the lithosphere, the brittle upper crust became thinner by listric faulting. This process may have caused local uplift of the crystalline basement because of isostatic rebound. The period of rapid uplift is terminated when the focus of crustal extension moved from the ACMB to the Sea of Crete about 5 Ma ago (see Chapter 2).

Thus, many aspects of the tectonic and thermal history of the Aegean part of the Alpine Orogenic Belt can be explained by the interaction of oceanic lithosphere of the Levantine Basin and continental crust of the southern margin of the Apulian-Anatolian Microplate.

Table 4.I

program UPLIFT2 model:	I	II	III	IV
initial surface heat production (kW/km^3)	3.0	3.0	0.8	0.8
thermal conductivity ($kW/km*^oC$)	2.5	2.5	2.5	2.5
thermal diffusivity (km^2/Ma)	32	32	32	32
scale depth heat production (km)	10	10	10	10
mantle heatflux (kW/km^2)	30	40	30	40
surface temperature (^oC)	20	20	20	20
base of grid (km)	100	100	100	100
runtime model (Ma)	200	140	115	95
depth interval (DZ)	1.0	1.0	1.0	1.0
time step (DT)	2.0	1.4	1.15	0.95
time switch uplift rate 1 to rate 2 (Ma)	65	65	65	65
rate 2 to rate 3 (Ma)	50	50	50	50
rate 3 to rate 4 (Ma)	20	20	20	20
rate 4 to rate 5 (Ma)	15	15	15	15
rate 5 to rate 6 (Ma)	5	5	5	5
rate 6 to rate 7 (Ma)	0	0	0	0
rate 1 (mm/yr) (+)	0.31	0.55	0.0	0.0
rate 2 (mm/yr) (-)	2.02	2.02	2.02	2.02
rate 3 (mm/yr) (-)	0.0	0.0	0.0	0.0
rate 4 (mm/yr) (-)	0.0	0.0	0.0	0.0
rate 5 (mm/yr) (-)	1.1	1.1	1.1	1.1
rate 6 (mm/yr) (-)	0.0	0.0	0.0	0.0

program UPLIFT2 model:	V	VI	VII	VIII
initial surface heat production (kW/km^3)	3.0	3.0	0.8	3.0
thermal conductivity ($kW/km*^oC$)	2.5	2.5	2.5	2.5
thermal diffusivity (km^2/Ma)	32	32	32	32
scale depth heat production (km)	10	10	10	10
surface temperature (^oC)	20	20	20	20
base of grid (km)	100	100	100	100
runtime model (Ma)	140	140	95	140
depth interval (DZ)	1.0	1.0	1.0	1.0
time step (DT)	1.4	1.4	0.95	1.4
time switch uplift rate 1 to rate 2 (Ma)	65	65	65	65
rate 2 to rate 3 (Ma)	50	50	50	50
rate 3 to rate 4 (Ma)	20	20	20	15
rate 4 to rate 5 (Ma)	15	15	15	5
rate 5 to rate 6 (Ma)	5	5	5	3
rate 7 to rate 7 (Ma)	0	0	0	0
rate 1 (mm/yr) (+)	0.64	0.77	0.0	0.64
rate 2 (mm/yr) (-)	2.02	2.02	2.02	2.02
rate 3 (mm/yr) (-)	0.0	0.0	0.0	0.19
rate 4 (mm/yr) (-)	1.3	3.3	1.3	1.1
rate 5 (mm/yr) (-)	1.1	1.1	1.1	0.0
rate 6 (mm/yr) (-)	0.0	0.0	0.0	0.0

program THERMAL model:	A	B	C	D	E	F
surface T (^{o}C)	20	20	20	20	20	20
initial T intrusive (^{o}C)	700	1200	1200	1200	1200	1200
mantle heatflux (mW/m^2)	40	40	40	40	40	40
thermal conductivity ($W/m*^{o}C$)	3.0	3.0	3.0	3.0	3.0	3.0
thermal diffusivity ($10^{-4}m^2/s$)	1.28	1.28	1.28	1.28	1.28	1.28
halfwidth dyke (m)	2000	2000	2000	2000	4000	4000
depth top dyke (km)	14.0	16.0	15.5	15.1	16.0	15.5
base grid (km)	25	25	25	25	25	25
heat production host ($10^{-6}W/M^3$)	0.4	0.4	0.4	0.4	0.4	0.4
heat production dyke ($10^{-6}W/m^3$)	0.19	0.19	0.19	0.19	0.19	0.19
run time (Ma)	15	15	15	15	15	15
switch uplift rates (Ma)	5	5	5	5	5	5
uplift rate (mm/yr)	1.5	1.5	1.5	1.5	1.5	1.5
initial depth (km)	15	15	15	15	15	15
grid:						
horizontal (m)	250	250	250	250	250	250
vertical (m)	250	250	250	250	250	250
length (km)	25	25	25	25	25	25
depth (km)	25	25	25	25	25	25

CHAPTER 5

The metamorphic history of the Western Shaw Greenstone Belt Pilbara region, Western Australia

5.1 Introduction

In the Pilbara region in the northwest of Western Australia an Archaean granitoid-greenstone terrain is exposed. The Pilbara Archaean Block is located between the Indian Ocean and the Tropic of Capricorn (Fig 5.1). It is for most of its area a typical granitoid-greenstone terrain. The geology is characterized by large roughly oval shaped composite granitoid-gneiss domes, locally referred to as batholiths, separated by narrow synclinal greenstone belts (Fig. 5.2; Hickman 1980, 1983). The greenstone belts are dominated by mafic volcanic units, but also contain ultramafic volcanics, felsic volcanics and sediments in general as minor components. The granitoid-gneiss domes are complex structures, consisting of several generations of intrusive granitoids. Formation of the domal structure observed in the granitoid gneiss terrains probably took place late in the Archaean tectonic history. The older granitoids are often deformed to grey gneisses, and may be migmatized. The intrusion of younger granitoids continued until after the last major tectonic event (Hickman 1981, 1983).

Early work on the geochronology of the region by Compston and Arriens (1968) yielded ages in excess of 3.0 Ga, which suggested that Early Archaean crust was preserved. Subsequent studies have documented geological events during the interval between 3.6 Ga (Hamilton et al. 1981) and 1.2 Ga (De Laeter et al. 1975), thus illustrating the complexity of the geological history of the area. Because the main objective of these studies has been to decipher the primary igneous history of the area, the isotopic systems applied until now have included Rb-Sr, U-Pb on zircon, Sm-Nd and Pb-Pb. This effort has yielded a good, although as yet incomplete temporal frame for the area.

5.1.1 Aims of the present study

The area chosen for study is located in the southeastern part of the Pilbara region, in the Western Shaw Greenstone Belt and the two adjacent granitoid-gneiss terrains, the Yule Batholith and the Shaw Batholith (Fig. 5.2). The geology is covered by the Marble Bar sheet of the 1:250,000 geological map of W. Australia (Hickman and Lipple 1978). In this part of the Pilbara Block, the

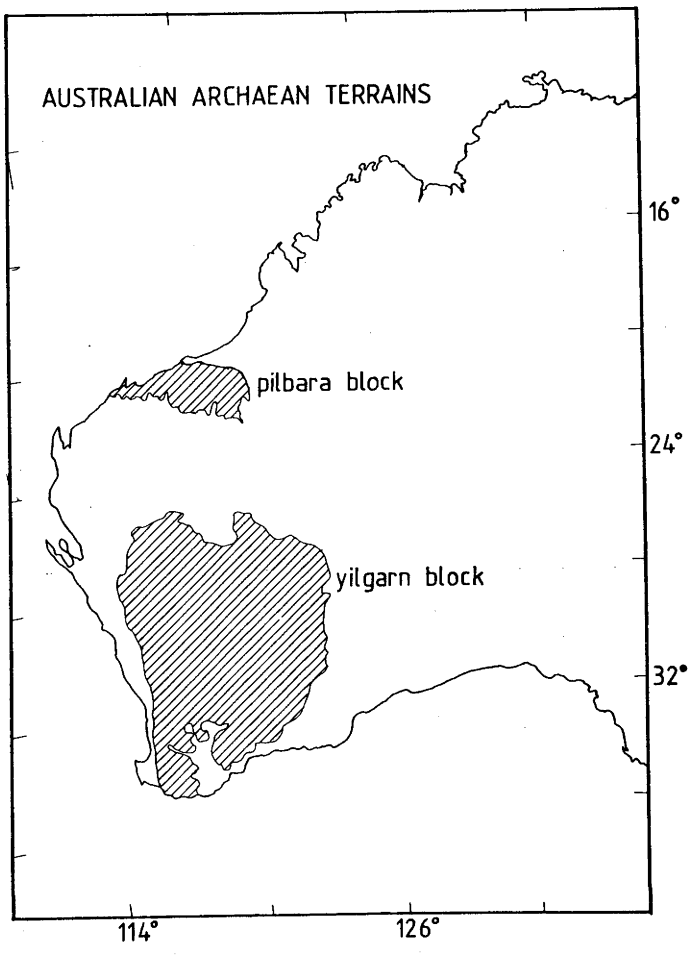

Figure 5.1 The location of Archaean Terrains in Western Australia. The Pilbara Block and the Yilgarn Block are separated by the Proterozoic rocks of the Hamersley Province.

early regional metamorphism has been more severe than further to the north, and it has been described, therefore, as intermediate between 'classic' Archaean granitoid-greenstone terrains and Archaean high grade gneiss terrains (Bettenay et al. 1981). During this early metamorphism minerals including hornblende, muscovite and biotite were formed. The present study applies the $^{40}Ar/^{39}Ar$ age spectrum method to metamorphic minerals formed during various events in the Archaean history of the Pilbara block. Because data obtained by the $^{40}Ar/^{39}Ar$ stepheating method can be more readily interpreted when the method is applied to discrete mineral phases, the possibility of establishing a reliable thermal history for the region is enhanced.

One of the main reasons for the selection of the Western Shaw area was the availability of detailed information on the tectonic and metamorphic history (Hickman 1978, 1980, 1981, 1983, Hickman and Lipple 1978, Bettenay et al. 1981, Bickle et al. 1980, 1983, 1984, Morant 1984), and the existence of a reasonably detailed geochronological database (Compston and Arriens 1968, De Laeter and Blockley 1972, Oversby 1976, De Laeter et al. 1975, Pidgeon 1978a, b, De Laeter et al. 1981, Richards and Blockley 1984, Richards et al. 1981, Richards 1977, Collerson and McCulloch 1982, 1983, Cooper et al. 1982, Bickle et al. 1983).

Most of the presently available data suggests that the major updoming event associated with the granitoid-gneiss domes occurred late in the Archaean tectonic history. On the basis of Pb-Pb isochron data from gneisses from the southeast of the Pilbara region, which clustered around 2.95 Ga, Oversby (1976) contended that at this time a major metamorphism occurred. A similar argument was put foreward by Pidgeon (1978b), who noted that much of the Rb-Sr data on gneisses from this region clustered around a 3.07 Ga reference line. These ages were argued by Hickman (1981) to be associated with the metamorphism that accompanied the formation of the granitoid-gneiss domes.

The possibility of obtaining pre-updoming argon isotopic ages from the greenstone belts depends wholly on the character and extent of the thermal effect which accompanied updoming. As most of the previous isotopic work was carried out on rocks from the granitoid-gneiss terrains, little is known about the thermal

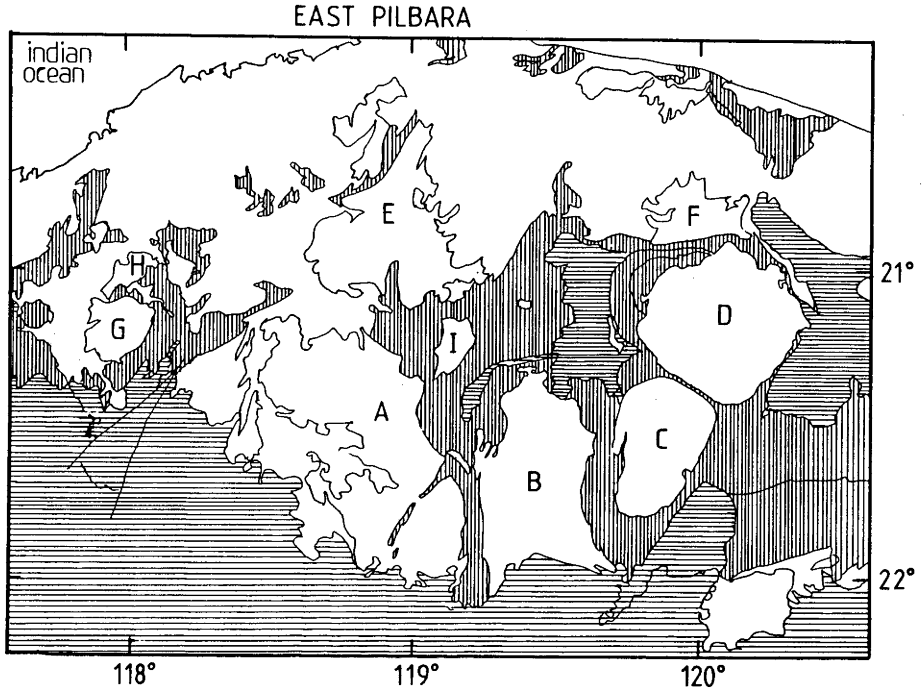

Figure 5.2 Simplified geology of the eastern section of the Pilbara Archaean Block. Horizontally shaded areas indicate the location of overlying Proterozoic rocks belonging to the Mount Bruce Supergroup. Vertically shaded are Archaean supracrustal rocks. The main Archaean granitoid-gneiss terrains are indicated: A Yule Batholith, B Shaw Batholith, C Corunna Downs Batholith, D Mt Edgar Batholith, E Carlindi Batholith, F Muccan Batholith, G Satirist Granite, H Peewah Granodiorite, I North Pole Dome. Areas covered with alluvial sand are unshaded.

evolution of the metavolcanic rocks in the greenstone belts. Structural work in the Western Shaw Greenstone Belt suggests that the early metamorphic mineralogy was affected by a deformation phase prior to the one associated with formation of the granitoid-gneiss domes (Bettenay et al. 1981). The implication is that metamorphic assemblages may be preserved that were formed before the main event recorded in the granitoid-gneiss domes.

The present study concentrates on an area which includes only a limited part of the southeast Pilbara. The justification for this approach lies in the sensitivity of the $^{40}Ar/^{39}Ar$ stepheating method to thermal disturbances. From the available geochronological data it was clear that the Pilbara Block has had a complex history. Looking superficially at a large area would, therefore, very likely yield information which may be hard to interpret, because it is the reflection of that complex history. Thus by limiting the study to a smaller area, it was hoped that relating the argon isotopic data to identified geological events would improve. During the last 15 years the Shaw Batholith area has become a focus of attention for study of Archaean granitoid-greenstone terrains. For this reason alone, it is of great importance to know the geologic history of this area in as much detail as possible.

The second main aim of the present study was to investigate the suitability of the argon isotopic system for dating thermal events in the Archaean. The number of studies using the $^{40}Ar/^{39}Ar$ stepheating method on problems related to Archaean geology is still very small. The Archaean rocks from the Godthaab district in western Greenland were studied by Pankhurst et al. (1973). Dallmeyer (1982) studied the effect of Grenvillian overprinting of Archaean gneisses in southwest Labrador that had already experienced earlier resetting. Martinez et al. (1984) described stepheating experiments on wholerock komatiite and komatiitic basalt samples from Barberton in South Africa. In the present study, the emphasis is on the metamorphic history of a greenstone sequence. As stated above, in the Western Shaw Greenstone Belt, it is possible to study the metamorphic history by $^{40}Ar/^{39}Ar$ stepheating experiments on mineral separates. The mineral used predominantly in the following study is hornblende. Hornblende is the most retentive mineral commonly used for argon dating,

therefore hornblendes may have preserved an isotopic signature of the early history of the area. Further, $^{40}Ar^{*}$ distribution gradients in hornblendes may be resolved by $^{40}Ar/^{39}Ar$ stepheating experiments (Harrison and McDougall 1980), and hornblendes are abundantly available in the mafic lithologies of the greenstone sequence.

In contrast with earlier studies, which have concentrated on the isotopic ages of rocks belonging to the granitoid-gneiss terrains, the emphasis of this study is on the thermal evolution of the rocks within the greenstone belts. Because of the high concentrations of argon in the minerals, there is the potential of obtaining very precise results. Also, because the method used in this study is based on the concentration of the noble gas argon which, in comparison with other isotopic systems, has a very favourable partitioning of isotopic daughter product into the metamorphic fluid, the results of this study may be more readily correlated with the thermal events experienced by the rocks through time.

5.2 An outline of the geology and geochronology

5.2.1 The geological setting of the Pilbara Block

The geology of the area has been mapped recently (Hickman and Lipple 1978, Hickman 1980), and a detailed account of the geology of the Pilbara was published in 1983 (Hickman 1983). This work contains a detailed description of the stratigraphy of the greenstone succession, the geology of the granitoids and gneisses in the batholiths, a tectonic history and the economic geology. An important result of this large mapping effort was the recognition that many units could be traced through various greenstone belts. This has important implications:

(1) By using a number of key units it was possible to propose a detailed stratigraphy which is applicable to the whole of the Pilbara Block.

(2) Because of the continuity of the lithology throughout the Pilbara Block it was suggested that the Archaean supracrustal succession was deposited in one big basin, as essentially flat units, rather than being deposited in several narrow basins. As a consequence, it was suggested that the narrow synclinal greenstone belts were secondary structures.

The second point places some severe constraints on models proposed for the genesis of greenstone belt volcanics. Some of these models are discussed elsewhere in this chapter. Here some aspects of the stratigraphy and geochronology of the supracrustal succession will be discussed.

5.2.2 The greenstone succession

The Archaean greenstone succession in the Pilbara is divided into three groups which together comprise the Pilbara Supergroup (Hickman 1983). The oldest group is the Warrawoona Group, which is overlain by the Gorge Creek Group and the Whim Creek Group (see Fig. 5.4). A major unconformity, accompanied by a change in tectonic style separates the Archaean succession from the overlying volcanics belonging to the Proterozoic Mount Bruce Supergroup. Rocks belonging to this supergroup crop out south of the Pilbara in the Hamersley Ranges (Trendall 1983), and in isolated outcrops in the Pilbara region. These rocks consist

Figure 5.3 Simplified geological map of the Western Shaw Greenstone Belt. Granitoid-gneiss terrains are unshaded, greenstone belts are horizontally shaded, posttectonic granites are diagonally shaded, Proterozoic cover is shaded with two sets of diagonal lines, Proterozoic dolerite dyke are indicated in black (after Hickman and Lipple 1978). The location of sample points for the K/Ar study are indicated.

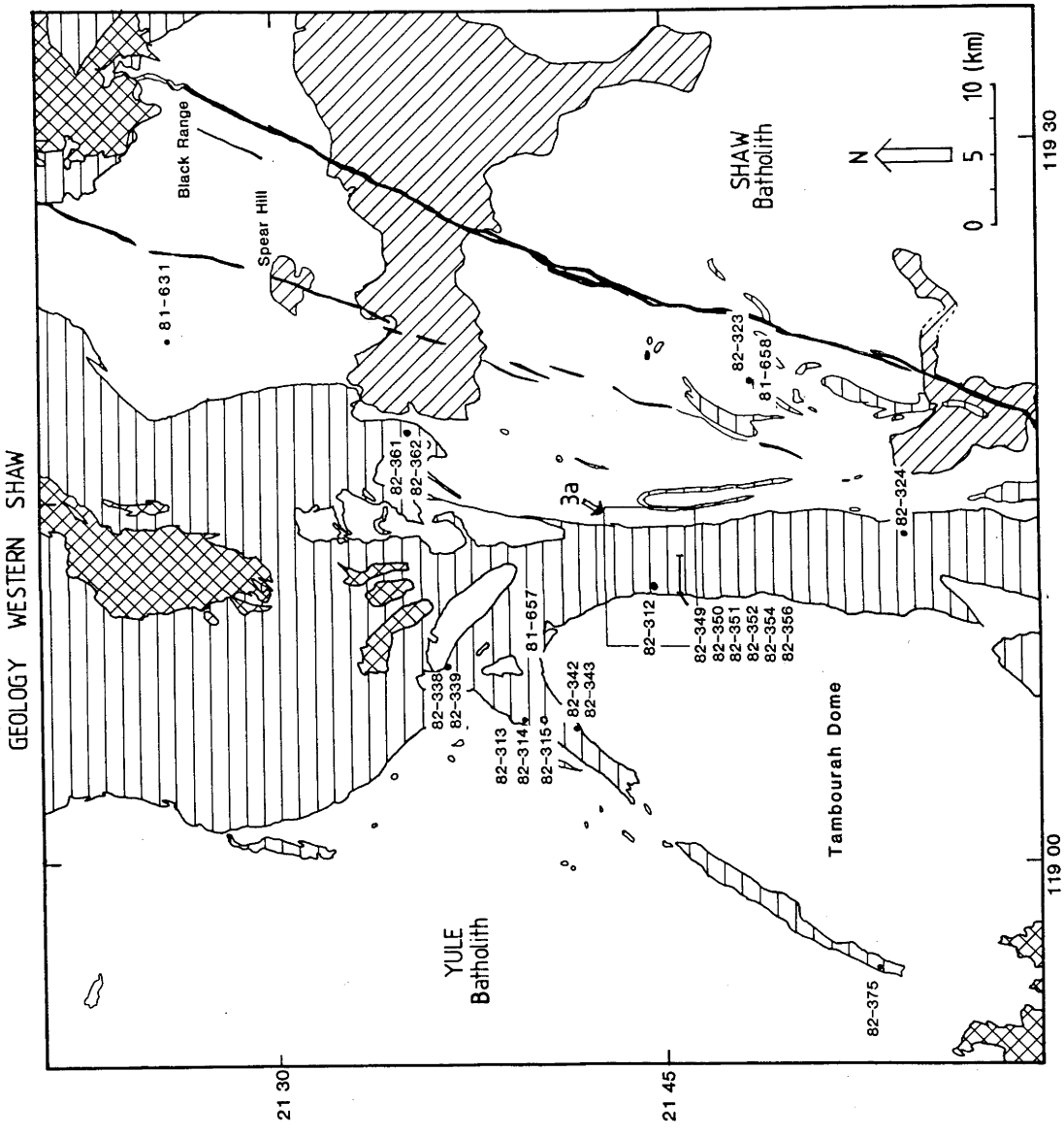
GEOLOGY WESTERN SHAW
Black Range
Spear Hill
SHAW Batholith
YULE Batholith
Tambourah Dome
3a
81-631
82-361
82-362
82-338
82-339
82-313
82-314
82-315
81-657
82-342
82-343
82-312
82-349
82-350
82-351
82-352
82-354
82-356
82-323
81-658
82-324
82-375
N
0 5 10 (km)
21 30
21 45
119 00
119 30

mainly of flatlying to gently folded volcanics and banded iron formations. Rocks of the Mount Bruce Supergroup show only very minor metamorphism. The grade of metamorphism and the degree of deformation of the rocks belonging to the Pilbara Supergroup may vary from minor, to complete recrystallization at upper amphibolites facies grade accompanied by thorough shearing. This variation is not a function of stratigraphic level, but seems to be related to geographic position relative to the granitoid-gneiss domes.

The stratigraphically oldest unit of the Warrawoona Group, the Talga Talga Subgroup, consists of basaltic to ultramafic extrusives (Fig. 5.4). Some pillow lavas are recognized in the succession. The ultramafic units are severely altered. The mafic volcanics of the Talga Talga Subgroup are separated from those of the Salgash Subgroup by a unit consisting of felsic volcanics called the Duffer Formation. In the Salgash Subgroup two important marker horizons exist which have allowed stratigraphic correlation over long distances. The lowest of these, the Towers Formation, consists of two, and in some areas three major chert units, separated by pillow lavas. The second marker horizon is the Panorama Formation which consists of felsic volcanics, and some chert, shale and sandstone. This unit separates the two major mafic volcanic units of the Salgash Subgroup, the Apex Basalt and the Euro Basalt. The Wyman Formation, which consists mainly of rhyolites, marks the top of the Warrawoona Group. The total stratigraphic thickness is about 20 km. Because of lateral variations in thickness, the actual thickness in a given area is always smaller.

The lower part of the overlying Gorge Creek Group is marked by two sedimentary units, the Corboy Formation and the Clearville Formation, separated by mafic volcanics of the Charteris Formation. Together these three units form the Soansville Subgroup. The upper part of the Gorge Creek Group consists mainly of sedimentary rocks, of which the Lalla Rookh Sandstone is the most prominent member. These sediments were interpreted to represent the debris from erosion of the granitoid-gneiss terrains, which were uplifted during a major tectonic event at about 2.95 Ga ago (Hickman 1981, 1983). The top of the Archaean succession in the Pilbara consists of sediments and mainly felsic

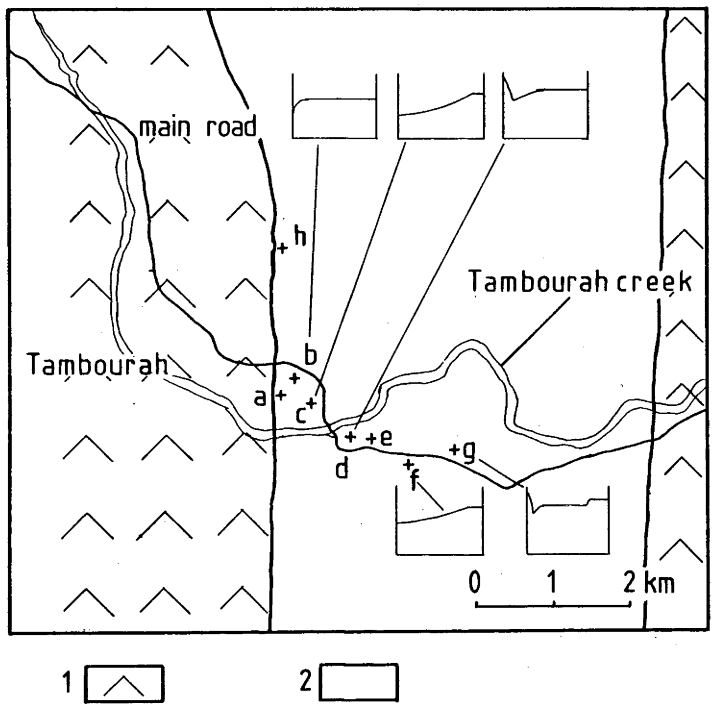

Figure 3a. Sample locations within the Tambourah Section, Western Shaw Greenstone Belt. a. 82-349, b. 82-350, c. 82-351, d. 82-352, e. 82-353, f. 82-354, g. 82-356, h. 82-312. 1 : granitoids, 2 : greenstones.

volcanics belonging to the Whim Creek Group, and two separate formations, the Louden Volcanics and the Negri Volcanics, which consist of mafic to ultramafic units (Fig. 5.4). According to Hickman (1983) the justification for assigning these two units to the Archaean succession is the fact that they were deformed in a Late Archaean event which is not recorded in the lowest units of the overlying Fortescue Group of the Mount Bruce Supergroup.

In the Western Shaw Greenstone Belt, Hickman (1980) recognized from west to east the Apex Basalt, the Euro Basalt and the Wyman Formation belonging to the Warrawoona Group, and the Corboy and Clearville Formations from the Gorge Creek Group. The eastern margin was interpreted as in fault contact with the Shaw Batholith. The greenstone units in the Western Shaw greenstone belt are metamorphosed at medium grade and display a pronounced early (i.e. D_2 according to Bickle et al. 1980, 1984) foliation.

The relation between the metavolcanic rocks in the greenstone belts and the mafic enclaves found within the granitoid-gneiss terrains has been given various interpretations in different models for crustal evolution of the region (Glikson 1979, Hickman 1981, 1983, Bickle et al. 1980, see also section 5.4). Many of the rocks in these enclaves are of supracrustal origin, because they contain metapelitic rocks as well as amphibolites. They were incorporated into the granitoid-gneiss terrain by two processes: some were included tectonically (Bickle et al. 1980), others are found mainly in interdomal synclinal structures where rocks occur which commonly consist of about equal proportions of granitoid and amphibolite (Hickman's Agmx lithology (Hickman and Lipple 1978)). This second set was interpreted to be remnants of greenstone belts partly absorbed by syn-D_2 intrusive granitoid (Hickman 1981, 1983).

Geochronologic control of the stratigraphy is still imperfect. The Archaean succession is bracketed by the dating of the North Star Basalt, which is the lowest unit in the Warrawoona Group, at 3560 $\pm$ 32 Ma (Sm/Nd wholerock isochron by Hamilton et al. 1981). Jahn et al. (1981) reported Sm/Nd ages on the same unit ranging from 3590 $\pm$ 100 Ma to 3460 $\pm$ 120 Ma, essentially in agreement with the results of Hamilton et al. (1981). The younger age limit on the Archaean succession comes from U/Pb dating of

MBS	F	Fortescue Group		2768 ± 16^{3}, 2760 ± 30^{5}
PS		Negri Volcanics	A,B	
PS		Louden Volcanics	B,UM	
PS	WC	Whim Creek Group	B,FV,S	2937, 2940^{6} 2950 ± 104^{4}
PS	GC	Mosquito Creek Formation	S	
PS	GC	Lalla Rookh Formation	S	
PS	GC	Honeyeater Basalt	B	
PS	GC So	Clearville Formation	BIF	
PS	GC So	Chartris Basalt	B	
PS	GC So	Corboy Formation	S	
PS	WW	Wyman Formation	R,T	
PS	WW Sa	Euro Basalt	B,D	
PS	WW Sa	Panorama Formation	FV,S	3370^{6}
PS	WW Sa	Apex Basalt	B	
PS	WW Sa	Towers Formation	B,C	3460, 3470^{6}
PS	WW	Duffer Formation	FV	3452 ± 16^{2}, 3440, 3480^{6}
PS	WW Tt	Mount Ada Basalt	B	
PS	WW Tt	McPhee Formation	C,UM	
PS	WW Tt	North Star	B,D	3560 ± 32^{1}

MBS = Mount Bruce Supergroup, F = Fortescue Group, PS = Pilbara Supergroup, WC = Whim Creek Group, GC = Gorge Creek Group, WW = Warrawoona Group, So = Soansville Subgroup, Sa = Salgash Subgroup, Tt = Talga Talga Subgroup.
B = basalt, UM = ultramafic volcanics, FV = felsic volcanics, S = sedimentary unit (pelites, sandstone), BIF = banded iron formation, R = rhyolite, T = tuff, D = dolerite.
1. Hamilton et al. 1981, 2. Pidgeon 1978a, 3. Pidgeon 1984, 4. Compston and Arriens 1968, 5. Richards and Blockley 1984, 6 Richards et al. 1981.

Figure 5.4 Stratigraphy of the Pilbara Group (after Hickman (1981)).

zircons from the Spinaway Porphyry, an intrusive into the base of the Fortescue Group at 2768 ± 16 Ma (Pidgeon 1984). This age is supported by Pb/Pb model ages of 2760 ± 30 Ma on galenas from one of the lowest units of the Fortescue Group, the Kylena Basalt (Richards and Blockley 1984). These ages suggest that deposition of the Fortescue Group started about 2.76 Ga ago. Interestingly, these studies indicate that the Fortescue Group, which is the oldest part of the succession allocated to the Proterozoic in the Pilbara, was in fact deposited in what is formally part of the Late Archaean (Richards 1984, Pidgeon 1984, James 1978), and is coeval with parts of the greenstone succession in the Yilgarn Block (e.g. Roddick et al. 1976). The lowest unit of the Archaean succession dated by U/Pb on zircon is a dacite from the Duffer Formation which yielded an age of 3452 ± 16 Ma (Pidgeon 1978a). Additional stratigraphic control comes from Pb/Pb model ages on galenas from the Duffer Formation, the Towers Formation, the Apex Basalt, and the Panorama Formation ranging from 3470 to 3200 Ma.

5.2.3 The granitoid terrains

The granitoid terrains as exposed in the Yule Batholith and the Shaw Batholith are best described as composite granitoid-gneiss domes. Their plutonic and tectonic histories are complex, spanning about 1000 Ma between the earliest and last plutonic phase. They were mapped originally by Hickman as older granitoids, syntectonic granitoids and younger granitoids. This division is made with respect to his D_2 event which is associated with the formation of the domes (Hickman 1981, 1983). In the more deformed parts of the domes, grey gneisses and migmatites occur. Several generations of pegmatites are observed in the gneisses, suggesting either a single prolonged thermal event, or several individual thermal phases. The foliation in the margins of the batholiths is parallel to the greenstone-gneiss contact and was attributed to the D_2 event. In the gneisses an earlier D_1 event is recognized which includes all the pre-D_2 structures (Hickman 1983). The early granitoids have been studied by Bickle et al. (1983) in the north of the Shaw Batholith, where they are relatively little deformed. The chemistry indicates that these rocks are granodiorites with a calcalkaline affinity. Bickle et al. (1983) presented a precise Pb/Pb isochron on a suite of rocks

from the north Shaw area indicating an age of 3499 ± 22 Ma. These granites were interpreted as intrusive into the lower part of the greenstone succession (Hickman 1983). The grey gneisses of the Shaw Batholith are currently interpreted to be the more deformed equivalents of these granitoids. The ages obtained by U/Pb on zircons and Sm/Nd model ages on the grey gneisses are indistinguishable from the age of the less deformed granitoids, which was interpreted as recording emplacement of these rocks (Bickle et al. 1983, Collerson and McCulloch 1982, 1983, Williams et al. 1982, 1983). A Pb/Pb isochron on a suite of grey gneisses showed significantly more scatter around the 3500 Ma reference line (Bickle et al. 1983). It was argued that because of the great age of the rocks in this area, the apparent differences in age between the different determinations and between the results by different methods may be negligible, thus implying that results from the granitoid terrains and from the lower units of the Warrawoona Group in fact record one major phase of crustal generation.

Granitoids yielding U/Pb ages on zircons of 3280 ± 20 Ma were reported from the Mount Edgar Batholith (Fig. 5.2) (Pidgeon 1978b). Granitic rocks of the same age have not yet been demonstrated from the Shaw Batholith, or the Yule Batholith. In the Tambourah Dome, which is a part of the Yule Batholith (Fig. 5.2, 5.3, 5.3a), Cooper et al. (1982) identified a pretectonic fine grained adamellite yielding a Rb-Sr whole rock isochron age of 3087 ± 54 Ma. A similar age was obtained by Oversby on banded migmatite gneiss from Tambourah by a Pb/Pb isochron on selected samples (3070 ± 12 Ma, Oversby 1976). Both results were interpreted by the authors as primary, i.e. as reflecting the age of emplacement of granitoids. However, because of evidence for metamorphic resetting of the Rb-Sr system (Cooper et al. 1982), and because of evidence for high grade metamorphism related to dome formation at about 2.95 Ga presented in the present study, the ages of these granitoids may not be well known.

Syntectonic granitoids intrude the greenstone belts and may partly assimilate amphibolitic enclaves that occur in the gneisses. These granitoids are also found in synclinal zones within the domes where they have invaded greenstone belts. A group of posttectonic granitoids is intrusive into the granitoid-

gneiss terrains and into the greenstone belts. These younger granitoids are associated with tin and tantalum mineralization. A Rb-Sr wholerock isochron age of 2551 ± 128 Ma was obtained for one of these granitoids (De Laeter et al. 1975). Pidgeon, on the basis of Rb-Sr model ages on muscovites from pegmatites belonging to this event, proposed an age of about 2830 ± 30 Ma for this event (Pidgeon 1978b). Another posttectonic granitoid at Spear Hill (Fig. 5.3) yielded a Pb/Pb isochron age of 2847 ± 34 Ma (Blake and McNaughton 1984). It was observed by Trendall (1983) that the geochronology may indicate that some of these younger granitoids post-date the deposition of the Fortescue Group. There is, however, no direct contact between the two groups of rocks which may constrain their relative age.

5.2.4 Summary of previous geochronology

In the previous sections some of the relevant previous geochronology has been mentioned to reinforce the outline of the geology. Geochronological studies in the Pilbara region in the past have concentrated on the granitoid-gneiss terrains, and much less on the stratigraphy of the Pilbara Supergroup (see Blake and McNaughton 1984 for a comprehensive listing and review of all available previous data).

The temporal frame of the stratigraphy is essentially limited to the Sm/Nd whole rock isochron age of 3560 ± 32 Ma on the lowest unit of the Warrawoona Group (Hamilton et al. 1981), the age of 3452 ± 16 Ma obtained by U/Pb on zircons from the Duffer Formation (Pidgeon 1978a), and the U/Pb age of zircons from the Spinaway Porphyry which intruded into the base of the Fortescue Group, and thus constraining the age of the top of the Archaean succession (2768 ± 16 Ma, Pidgeon Some stratigraphic control was obtained from Pb/Pb model ages on galenas (Richards 1977, Richards et al. 1981, Richards and Blockley 1984). Where model independent control on the age of the rocks is available, as is the case for example for galenas from the Duffer Formation, or for galenas from the base of the Fortescue Group, the calculated Pb/Pb model ages are in good agreement, giving some confidence in the ages obtained for rocks where such control is lacking. This method does not date primary extrusion of the volcanic unit, but subsequent invasion by hydrothermal fluids, therefore it may not

be certain that in all cases primary ages are obtained.

The database on rocks from granitoid-gneiss terrains is much more extensive. Ages interpreted as recording early igneous events in the Shaw Batholith range from 3499 ± 22 Ma (Pb/Pb whole rock isochron, Bickle et al. 1983), and 3485 ± 30 Ma (U/Pb zircon ion microprobe spot analysis, Williams et al. 1982, 1983), to 3417 ± 40 Ma (conventional U/Pb analysis of zircons, Pidgeon 1978b). Both in the Yule Batholith and in the Shaw Batholith many Pb/Pb whole rock and mineral isochron ages were determined (Oversby 1976, Blake and McNaughton 1984). Most ages fall in the range from about 3100 to about 2850 Ma, and were interpreted as metamorphic ages, because they were determined on foliated rocks. A posttectonic granitoid at Spear Hill in the Shaw Batholith was dated at 2847 ± 34 Ma by the Pb/Pb isochron method (Blake and McNaughton 1984). Rb-Sr wholerock isochron determinations on rocks from the granitoid-gneiss terrains generally yield poorly defined isochrons, and in cases where both the Pb/Pb isochron and the Rb-Sr isochron methods were applied to the same rocks (see Oversby 1976, Blake and McNaughton 1984), the Rb-Sr ages were consistently lower and less precise than the Pb/Pb ages. Some Sm/Nd model ages on gneisses from the Shaw Batholith reported by Collerson and McCulloch (1982, 1983) range from 3460 to 3260 Ma.

Following Hickman (1981) and Bickle et al. (1983), the previous geochronology for the Shaw and Yule Batholith area is interpreted in terms of a major period of crustal formation at about 3500 Ma ago, followed by a complex metamorphic and tectonic history which is best documented in the granitoid-gneiss terrains and lasted until about 2950 Ma ago. The last phase of posttectonic granitoids probably intruded in the period between 2.850 and 2550 Ma ago (Blake and McNaughton 1984, De Laeter et al. 1975).

5.2.5 Metamorphism

A detailed study of the metamorphic petrology of the Shaw Batholith area was carried out by Morant (1984, see also Bickle et al. 1984). This study concentrated on the Shaw Batholith, and the Western Shaw Greenstone Belt. As the present study into the metamorphic history by argon dating concentrates on the Western Shaw Greenstone Belt, the adjacent Tambourah Dome and the western margin of the Shaw Batholith, there is considerable overlap between the two studies. Thus Morant's findings can be used as a petrological background for the present study. Briefly, the highest metamorphic grade rocks are found within the granitoid-gneiss domes. Metamorphism has affected both the granitoids and the greenstone enclaves within them. Within the greenstone belts, the recorded metamorphic temperature drops steeply with increasing distance from the contact with the granitoid-gneiss dome. Also, slightly higher pressure mineral assemblages occur within the greenstone belts, compared with the pressures recorded at the contacts with the granitoid-gneiss terrain. Because of the complex tectonic history of the Shaw Batholith and the Western Shaw Greenstone Belt, it was difficult to propose one definitive interpretation of the petrological observations (Morant 1984, Bickle et al. 1984).

For the Western Shaw Belt, the estimated metamorphic pressure is 400 to 450 MPa, at temperatures which decrease from 600 ^{o}C at the contact with the dome to less than 500 ^{o}C at about 2 km from the contact. The metamorphic facies trend was interpreted as Stonehavian (i.e. intermediate between the classic Barrovian and Abukuma trends). Along a section from the Western Shaw Greenstone Belt toward the centre of the Shaw Batholith, the physical conditions experienced by the rocks evolved from the stability field of kyanite through the stability field of andalusite, into the stability field of sillimanite (Fig. 5.5). It was argued that constraints on the metamorphic pressure are ambiguous, and because the exact location of some of the isograds was obscured by subsequent tectonism, pressure jumps along the section from the greenstone belt into the Shaw Batholith could not be ruled out (Morant 1984). There is some evidence in the southern part of the Western Shaw Belt near Garden Creek for overprinting of the kyanite bearing assemblage by younger andalusite and sillimanite

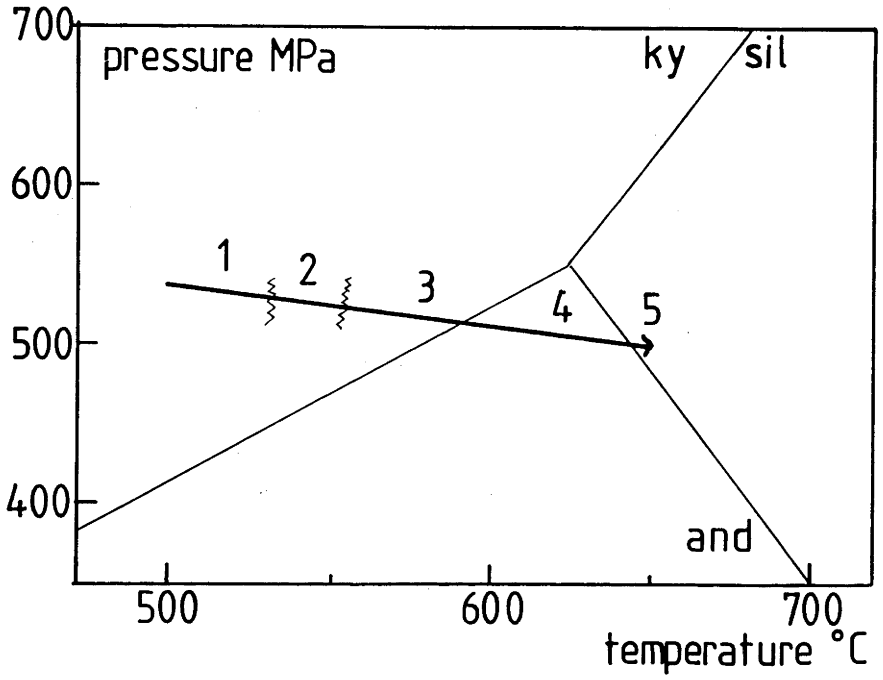

Figure 5.5 P-T evolution of the Shaw Batholith and Western Shaw Greenstone Belt (simplified after Morant 1984, Bickle et al. 1984). The arrow indicates the inferred metamorphic trend from the Western Shaw Greenstone Belt into the Shaw Batholith. Zone 1 is the chloritoid zone, zone 2 is the transition zone between the staurolite in isograd and the chloritoid out isograd, zone 3 is the staurolite-kyanite zone, zone 4 is the kyanite-andalusite zone, zone 5 is the andalusite sillimanite zone. The triple point of Al-silicates is from Richardson et al. (1969).

owing to the emplacement of a syntectonic granitoid. This observation may be interpreted as an argument against a single metamorphic facies trend, as discussed above. If the kyanite bearing mineral assemblage does not belong to the same metamorphism as the andalusite and sillimanite bearing assemblages, then there is no basis for proposing a single metamorphic facies trend. In his discussion, Morant (1984) considers both possibilities, and expresses a preference for the single stage metamorphic history.

Toward the more central parts of the Shaw Batholith, the estimated metamorphic pressure increases to values in excess of 600 MPa, accompanied by temperatures slightly higher than 650 ^{o}C. These conditions allow the formation of migmatites in the appropriate compositions. The estimates were based on geothermometry with garnet-biotite pairs, the stability fields of andalusite and sillimanite (according to Richardson et al. 1969), and on thermometry and barometry based on garnet-cordierite pairs (Morant 1984, Bickle et al. 1984).

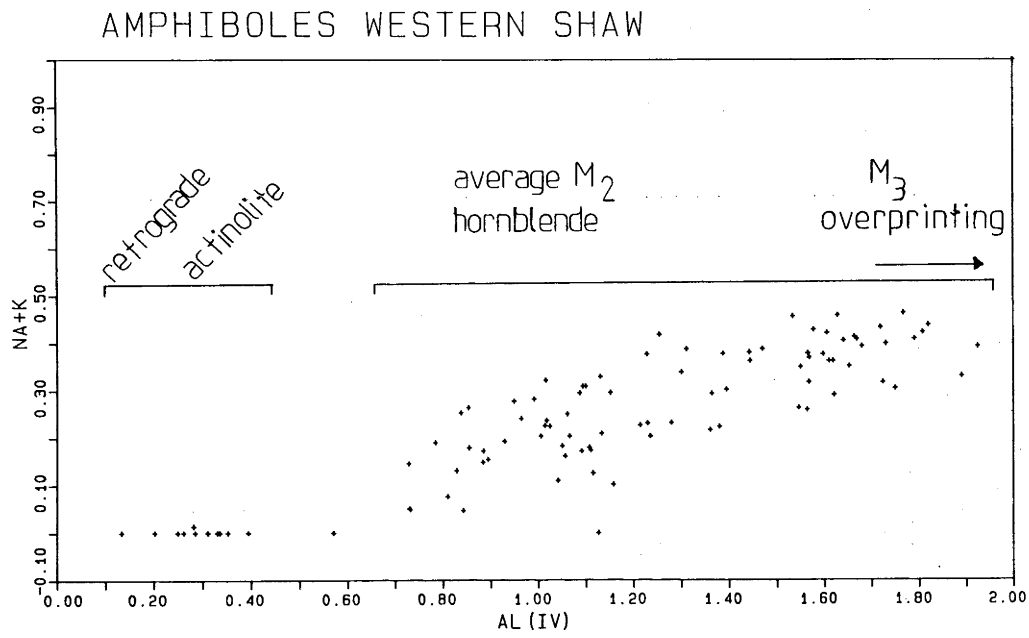

Figure 5.6 Compositional variation of hornblendes from the Tambourah Section in the Western Shaw Greenstone Belt. The indicated trends are towards lower silica and higher Al(IV) and higher Na+K for the overprinting high grade hornblendes, and overprinting by actinolites probably during the Mid Proterozoic. Data are presented as the coefficients of the structural formula of amphibole based on 23 oxygens, and the data were calculated following the method discussed by Laird and Albee (1981).

fine grained olive-green hornblende, which contains more aluminium and less silica than the blue-green hornblendes from rocks more to the centre of the greenstone belt (Fig. 5.6).

In the greenstone belt along the northwestern margin of the Tambourah Dome, the lower amphibolite facies assemblage in the metavolcanic rocks is clearly pretectonic with respect to D_3, the last major deformation associated with the formation of the granitoid-gneiss domes. Here, metapelitic rocks and a quartz-muscovite schist also were found. The metapelitic rocks contain biotite, garnet, staurolite, andalusite, and sillimanite. The plagioclase in these rocks is often severely sericitized. The staurolite is texturally early, because it occurs as inclusions in both the garnet and the andalusite. The sillimanite is often, but not always, fibrolitic and is texturally the younger mineral. Because grain boundary readjustment and growth of fibrolite continued until after the last tectonism (D_3 according to Bettenay et al. 1981), this mineral assemblage must be related to thermal overprinting accompanying the dome forming event (D_3). Temperatures calculated from biotite-garnet pairs, using the calibration of Ferry and Spear (1978), were generally lower than expected from the mineralogy. This suggests that the minerals have experienced some re-equilibration since the peak of the metamorphism. A muscovite-quartz schist from the same section reveals a foliation defined by quartz-rich and muscovite-rich layers. The foliation is folded at thin section scale, and within the folds, the muscovites have recrystallized with serated grain boundaries, and subgrains within the folded minerals, suggesting that a tectonic event was followed by a thermal pulse. The muscovite is low in silica (Si^{4+}=6.15), as would be expected for overprinting at a relatively high temperature.

The metamorphism is interpreted to have occurred in several different, possibly unrelated phases. This was one of the possible interpretations discussed by Morant (1984, see also section 5.4). It was also indicated by the pre- and posttectonic textures of rocks from the greenstone belts described in the present study, and will be demonstrated subsequently by $^{40}Ar/^{39}Ar$ stepheating experiments on hornblendes from metavolcanic units in the greenstone belts and from greenstone enclaves within the granitoid-gneiss terrains. The thermal effect of the doming event

on rocks in the greenstone belts seems to be limited, as it only caused overprinting adjacent to the contacts. Some of the thermal effect may be due to syntectonic granitoid mobility, because it is noticed that the greenstone rocks most intimately associated with syntectonic granitoids (in Hickman's Agmx lithology), display the highest metamorphic grades, followed by slightly lower grades in the greenstones near the margins of the belts. The thermal effect of doming on the mineralogy of the greenstones within the interiors of the belt seems to have been minimal.

5.3.2 Argon dating

5.3.2.1 Technique

The experimental procedures for the K-Ar experiments and for the $^{40}Ar/^{39}Ar$ experiments has been discussed in some detail in previous sections of this thesis. The only modification for the present study was a substantial increase in irradiation time, necessary in order produce sufficient ^{39}Ar so that the $^{40}Ar/^{39}Ar$ ratios could be measured in the very old samples used. The samples were irradiated in facility X-33, or X-34, for two full cycles of the HIFAR reactor of the Australian Atomic Energy Commission (one operational cycle has a duration of 21 days). The $^{40}Ar/^{39}Ar$ ratios obtained were typically in the order of 200. To minimize the effect of gradients in the fast neutron flux, the samples were inverted half way through each cycle.

Owing to problems in the reactor, the samples used for the present study were left out of the reactor for two full cycles between the two irradiation periods. Upon analysis of the samples it became clear that the correction factor for radioactive decay of ^{37}Ar and ^{39}Ar, as was published by Dalrymple et al. (1981) for multiple irradiations, was not appropriate in the case where the time gap between irradiations becomes significant with respect to the half life of ^{37}Ar (the half life of ^{37}Ar is 35.1 days). A modified equation for the correction for radioactive decay of isotopes during multiple irradiation was derived:

$$^{37}Ar_0 = {}^{37}Ar_m * \sum_{i=1}^{n} t_i \; / \; \sum_{i=1}^{n} ((1-e^{-\lambda t_i}) \; / \; \lambda e^{\lambda t'_i})$$

In this equation $^{37}Ar_m$ is the measured amount of ^{37}Ar, $^{37}Ar_0$ is the original amount of ^{37}Ar, t_i is the time in the reactor for irradation segment i, t'_i is the time between the end of

irradiation segment i and analysis of the sample, n is the total number of irradiation segments and λ is the decay constant for the decaying isotope. For hornblendes, which contain substantial amounts of calcium, the correction for interfering isotopes produced from isotopes of calcium based on measurement of the ^{37}Ar content of the sample is of critical importance. The discrepancy in the correction factor obtained from the equation of Dalrymple et al (1981), compared with the equation presented above, for the minerals used in the present study, was about 50 percent. This resulted in apparent $^{40}Ar/^{39}Ar$ ages that were about 7 to 10 percent too low.

5.3.2.2 The composition of atmospheric argon

To calculate an age from argon isotopic data, the measured amount of ^{40}Ar needs to be corrected for contamination by atmospheric argon. Because atmospheric argon presently has a constant $^{40}Ar/^{36}Ar$ ratio of 295.5, standard practice is to measure the ^{36}Ar content of the sample and to subtract the measured ^{40}Ar content by 295.5 times this amount. When measuring K-Ar ages and $^{40}Ar/^{39}Ar$ ages on minerals from Archaean rocks, one should consider the validity of this correction. Because of the continuous production of ^{40}Ar by radioactive decay of ^{40}K, it is likely that the composition of atmospheric argon has increased through time. Although the evolution of the isotopic composition of atmospheric argon with time is poorly known, the isotopic composition of Archaean atmospheric argon is likely to be less than 295.5. Models for the evolution of atmospheric argon include those assuming continuous degassing of the earth (e.g. Turekian 1959, Armstrong 1981), and those assuming rapid initial degassing of the earth (e.g. Schwartzman 1973, Cadogan 1977). The continuous degassing models predict the largest deviations from the present day compositions. In any case, by ignoring this problem, one may to overcorrect the $^{40}Ar^{*}$ concentration of the sample and consequently get a systematically lower age. However, the effect of this systematic error will in most cases be very small because (1) in addition to an Archaean atmospheric gas component, an atmospheric gas component of present day composition from the extraction line and from the sample itself cannot be avoided, and (2) from the data tables it can be seen

that in many cases the percentage of radiogenic ^{40}Ar is higher than 98 percent, when only the present day atmospheric argon correction is applied. If it is assumed that in these cases 50 percent of the non-radiogenic ^{40}Ar is of present day atmospheric origin, the error in the ^{40}Ar concentration will be less than 1 percent, and the effect on the calculated age even less. In cases where the radiogenic ^{40}Ar fraction is less than 98 percent, the additional contaminant is often of present day composition (caused by a poor line blank, or by gas adsorbtion on the minerals). Therefore, data presented in this study are corrected for modern atmospheric argon contamination only.

5.3.2.3 Results of the $^{40}Ar/^{39}Ar$ study

To select the samples most suitable for the $^{40}Ar/^{39}Ar$ study, conventional K-Ar measurements were undertaken initially, as results can be obtained relatively quickly on a large set of samples with the conventional method. Subsequently, by applying the more elaborate and time consuming stepheating technique, additional detailed information is obtained on selected minerals. The results of the K-Ar study are tabulated in Table 5.I and their locations can be seen in Fig 5.3(a). Superficially the results illustrate the reason why earlier attempts to apply the K-Ar method to dating in the Archaean were abandoned: the range in ages in table 5.I spans a time interval larger than one billion years. Nevertheless, because of the approach used in the present study, it can be demonstrated that some broad divisions can be made. The clearest group of ages is from hornblendes from the upper amphibolite grade rocks. The K-Ar ages of these minerals range between 2.75 and 2.9 Ga. One well crystallized muscovite also fell within this range. A muscovite from a post tectonic pegmatite with crystals in the range of 0.5 and 1 cm yielded an age of 2.67 Ga. Ages on blue-green hornblendes from within the greenstone belts yielded ages ranging between 2.0 and 3.18 Ga. This spread in ages is particularly well documented in samples from the Tambourah section, where it occurs in a series of samples from localities less than a kilometre apart (Fig. 5.3a).

On the basis of the K-Ar ages, the samples for the stepheating study were selected. Because of the exploratory nature of this study, and the aim to obtain as much detail as possible, the criteria for sample selection for the $^{40}Ar/^{39}Ar$ stepheating study included: (1) verification of the extremes obtained in the conventional K-Ar study; (2) quantification of the differences in ages between the granitoid-gneiss terrains and the greenstone belts; and (3) keeping the number of external factors small by concentrating on a limited area. This last point also helps to add significance to the variation in age spectra from samples located small distances from each other. The results of the stepheating experiments will be discussed in two groups. The first group is formed by those samples formed by, or recrystallized by high temperature metamorphism near, or within the granitoid gneiss domes. Their microstructure indicates that the mineralogy of these samples was formed after the last major deformation event (D_3, after Bettenay et al. 1981), and their petrology suggested crystallization at higher grade than the samples belonging to the early metamorphic mineralogy (M_2 in Fig. 5.18), as found within the greenstone belts. The second group consists of blue-green hornblendes from within the greenstone belts. These minerals come from assemblages which show evidence of deformation, and their chemical compositions indicate a lower metamorphic grade (Fig. 5.6).

Four stepheating experiments are pertinent to the thermal evolution of the granitoid-gneiss terrain. Hornblende 81-658 comes from a greenstone enclave in the Shaw Batholith near Garden Creek, hornblende 81-657 is from the Western Shaw Greenstone Belt where the greenstone sequence is intruded by syntectonic granitoids, hornblende 82-350 is from the margin off the greenstone belt at Tambourah and close to a deformed adamellite dated by Cooper et al. (1982), and finally, muscovite 82-315 is from the greenstone belt on the northwestern margin of the Tambourah Dome (Fig. 5.3). As this muscovite was produced by metamorphism subsequent to the last major deformation event (D_3 according to Bettenay et al. 1981), its age is related to the doming event. The age spectra of these minerals suggest that only limited loss of radiogenic argon occurred from the margins of the crystals. Hornblende 81-658, from the Shaw Batholith yielded a

maximum age of 2840 Ma, with some evidence for subsequent argon loss (Fig. 5.10). The time at which this argon loss occurred is not well constrained from this experiment because of some minor structure in the first steps. Although it is only a very minor effect, the apparent ages of the high temperature fractions increase slightly until all the gas is released. Under Turner's episodic loss model (Turner et al. 1966) this may indicate that the highest age reached in the age spectrum appoximates to, or is a minimum estimate for the original age of crystallization. Hornblende 81-657 has yielded an excellent flat age spectrum over more than 90 percent of the gas release (Fig. 5.9). Some minor structure in the first 3 percent may indicate a mild overprinting at possibly about 1500 Ma ago. The plateau is very well defined with an integrated age of 2865 $\pm$ 9 Ma. The age that was calculated from a $^{39}Ar/^{40}Ar$, $^{36}Ar/^{40}Ar$ isotope correlation diagram was 2866 $\pm$ 5 Ma, which is in excellent agreement with the integrated age over the plateau. The age spectrum of hornblende 82-350 yielded apparent ages increasing slowly to a maximum of 2965 Ma in the highest temperature steps, with some evidence for marginal argon loss during overprinting in the Mid Proterozoic (Fig. 5.12). Muscovite 82-315 shows evidence for some minor marginal loss during overprinting in the Mid Proterozoic, and apparent ages creeping up to a maximum age of 2940 Ma (Fig. 5.8).

The age spectra obtained in these four experiments display very regular shapes. Therefore, they may be interpreted with some confidence to be related to high grade events confined to the granitoid-gneiss domes and their margins. The uncertainties associated with the individual steps are consistently some 7 to 8 Ma. Because of the regular patterns and because of the error contraction which occurs when the integrated age over the plateaus is calculated, the ages obtained from the plateaus date events with very good precision (often better than 0.1 percent). The K/Ca ratios for the individual steps of the experiments were calculated from the $^{39}Ar_K/^{37}Ar$ ratios. On the basis of the chemical composition of the standard hornblende 77-600, and repeated analysis of its K/Ca ratio a conversion factor of 0.53 was found ($K/Ca = 0.53 * {}^{39}Ar_K/{}^{37}Ar$). The K/Ca ratio is a parameter which may yield information on the chemistry of the part of the crystals from which the argon gas is extracted. The

K/Ca ratios of hornblendes 81-657, 81-658, and 82-350 are nearly constant over the total of ^{39}Ar release and yielded values which agree well with those expected for pure hornblende concentrates. Isochron correlation diagrams on the plateau segments of the age spectra yielded results which agree with the calculated ages, although, because of the low air contamination, the intercepts giving the non-radiogenic argon compositions were not very well defined.

The $^{40}Ar/^{39}Ar$ stepheating experiments on blue-green hornblendes belonging to the earlier metamorphic mineralogy within the greenstone belts was focussed along the Tambourah section. In addition, a hornblende (82-361) from the Western Shaw Belt further to the north, and a hornblende (82-314) from the greenstone belt on the northwestern margin of the Tambourah Dome were measured (Fig. 5.17, 5.7). As was expected from the conventional K-Ar results, the argon isotope systematics of the hornblendes from within the greenstone belts are somewhat more complex than those described above. The earliest recognizable metamorphism is supported by age spectra from four blue-green hornblendes. The most convincing information comes from age spectra from samples 82-352 and 82-361, which show, apart from some minor excess argon in the initial steps, almost textbook examples of diffusional loss patterns, consistently rising from a partly obscured minimum value to maximum values of 3179 and 3100 Ma respectively (Fig. 5.14, 5.17). The age of this metamorphism is also supported by the slightly more irregular spectra of samples 82-314 and 82-356. Hornblende 82-314 yielded an integrated age of 3144 Ma over the segment that was not disturbed by excess argon and hornblende 81-356 had a maximum age of 3234 Ma in the high temperature fractions of the age spectrum (Fig. 5.7, 5.16). Under the models for episodic loss of argon during a subsequent thermal pulse developed by Turner et al. (1966), the maximum ages obtained from the highest temperature steps can be interpreted as minimum estimates for the original ages of these minerals. The observed scatter in conventional K-Ar ages is investigated by stepheating experiments on hornblendes 82-351 and 82-354. The age spectra indicate that these samples were much more severely overprinted by the inferred Mid Proterozoic greenschist facies event than the other samples analyzed in this

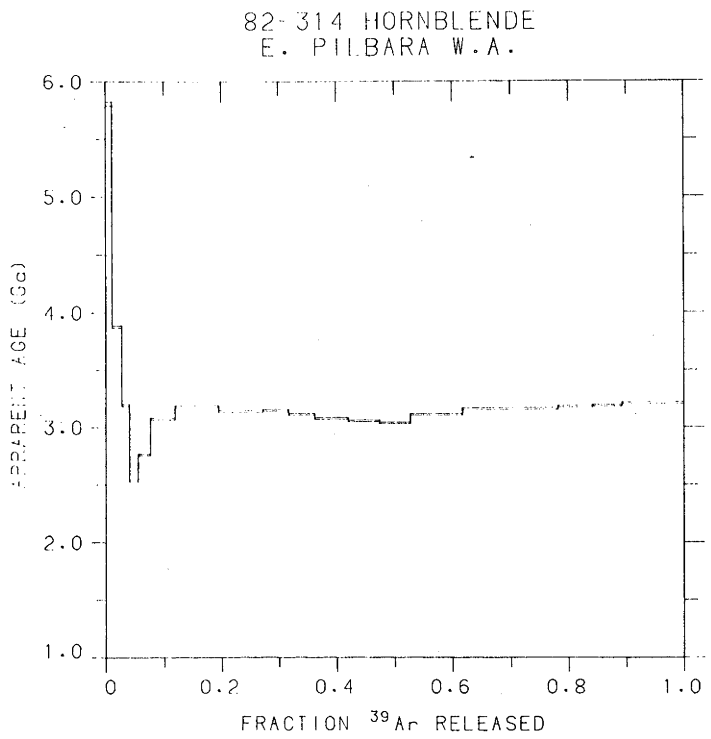

Figure 5.7 Hornblende 82-314

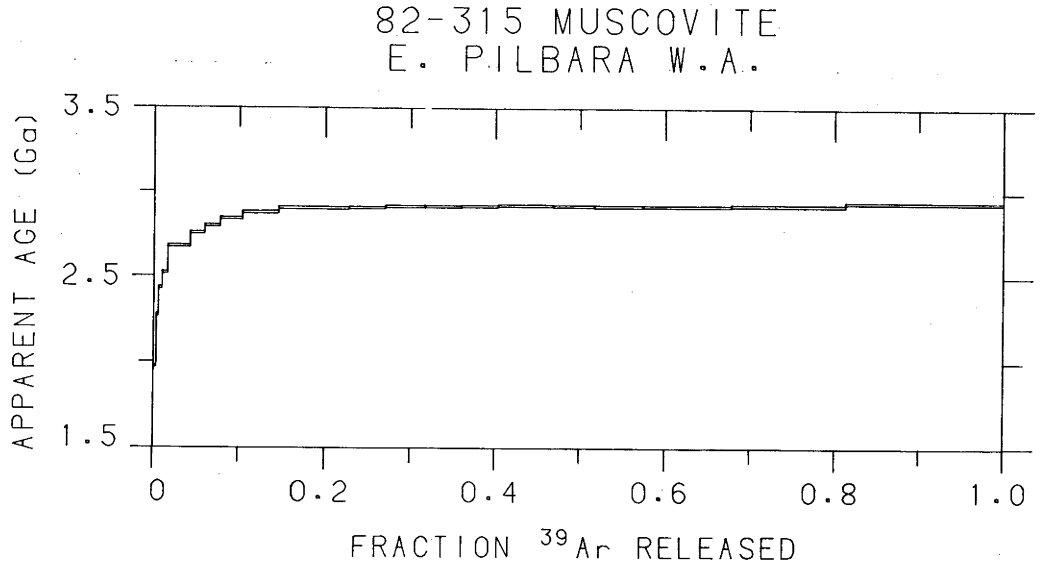

Figure 5.8 Muscovite 82-315

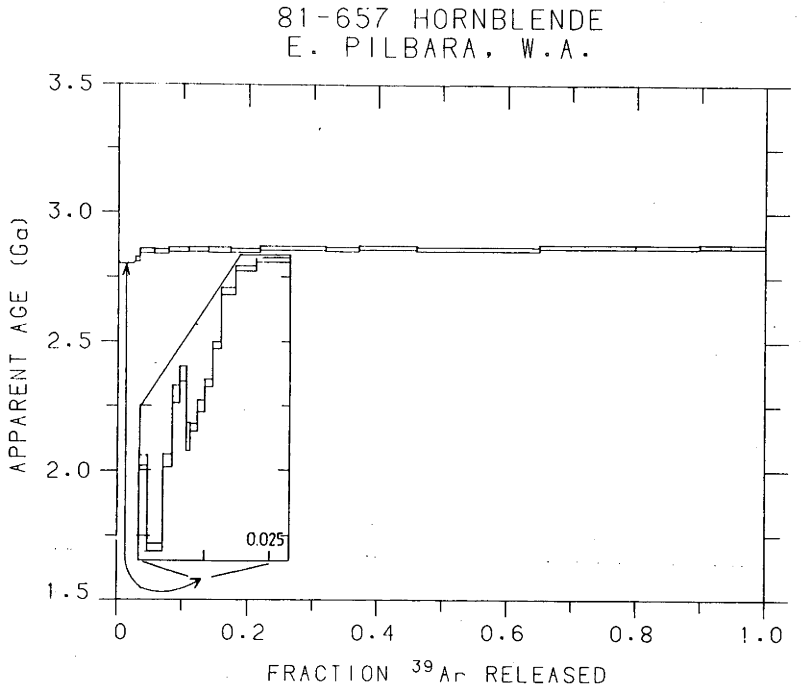

Figure 5.9 Hornblende 81-657

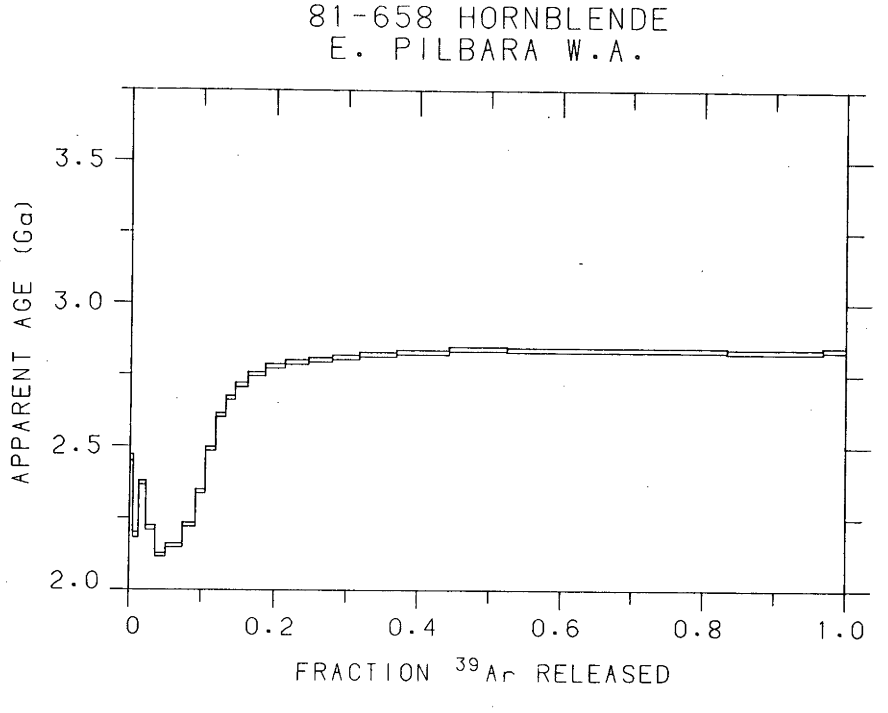

Figure 5.10 Hornblende 81-658

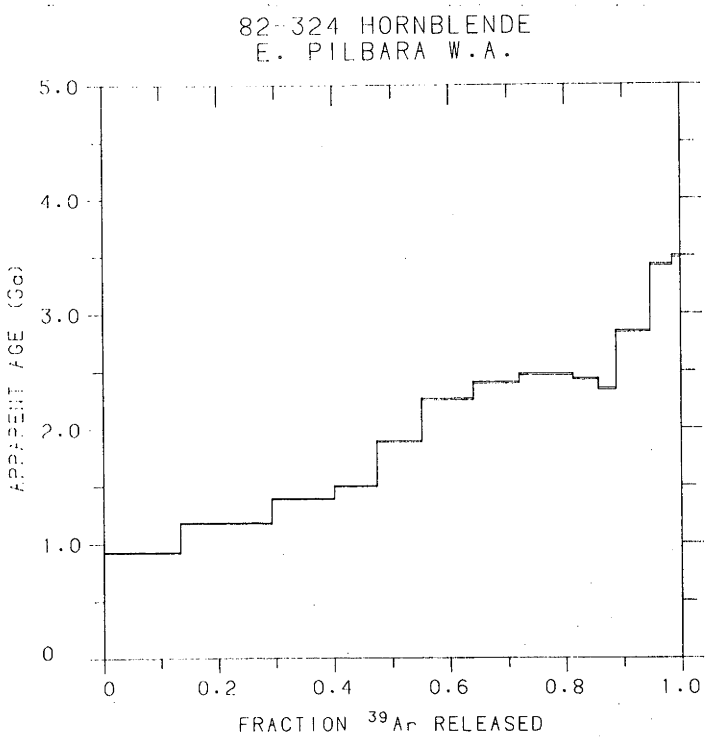

Figure 5.11 Actinolite 82-324

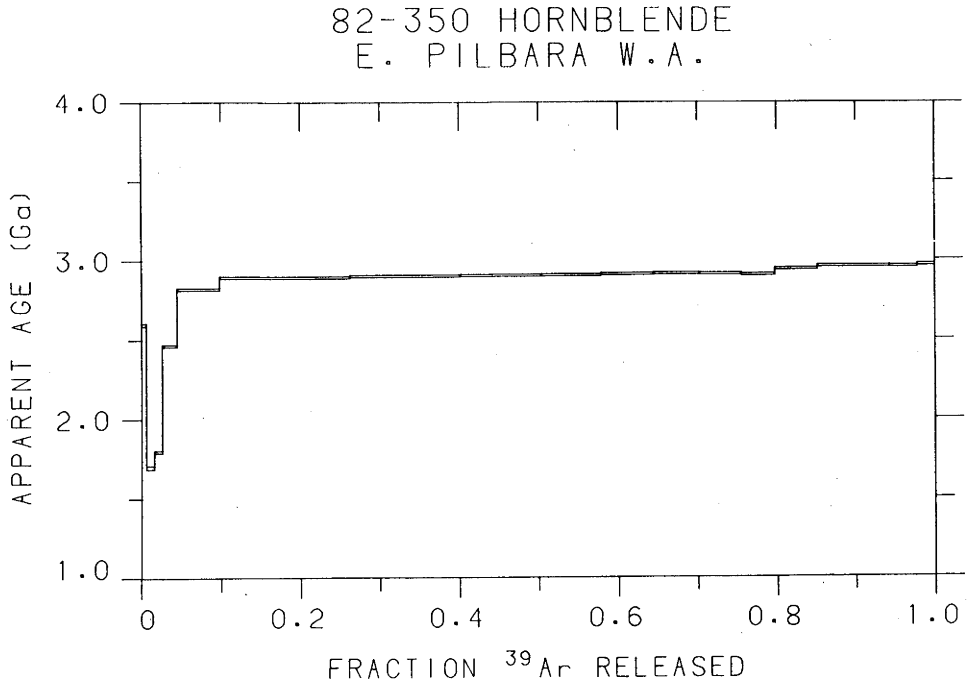

Figure 5.12 Hornblende 82-350

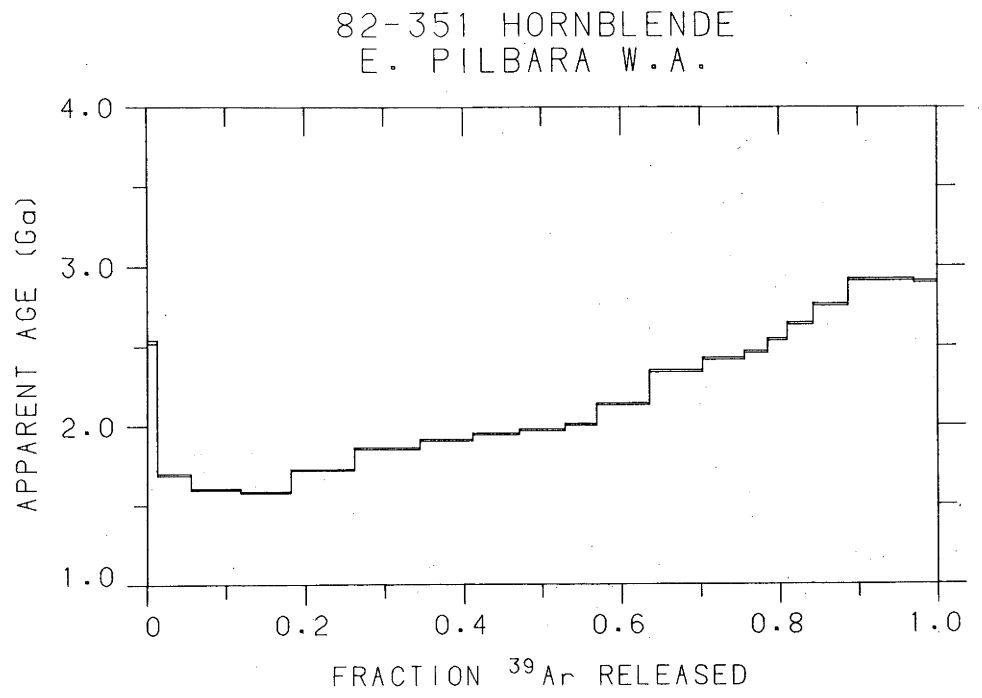

Figure 5.14 Hornblende 82-352

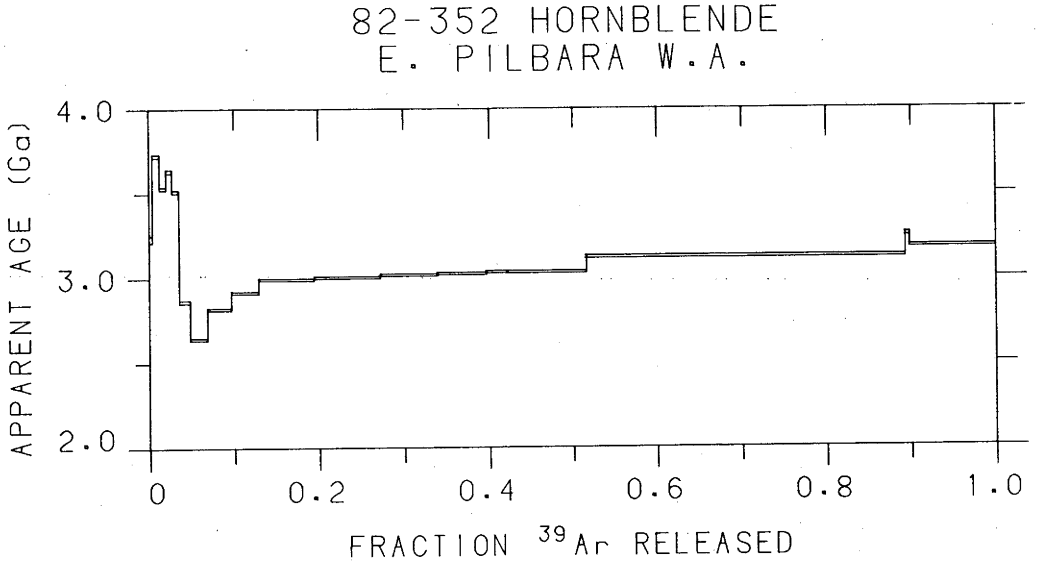

Figure 5.13 Hornblende 82-351

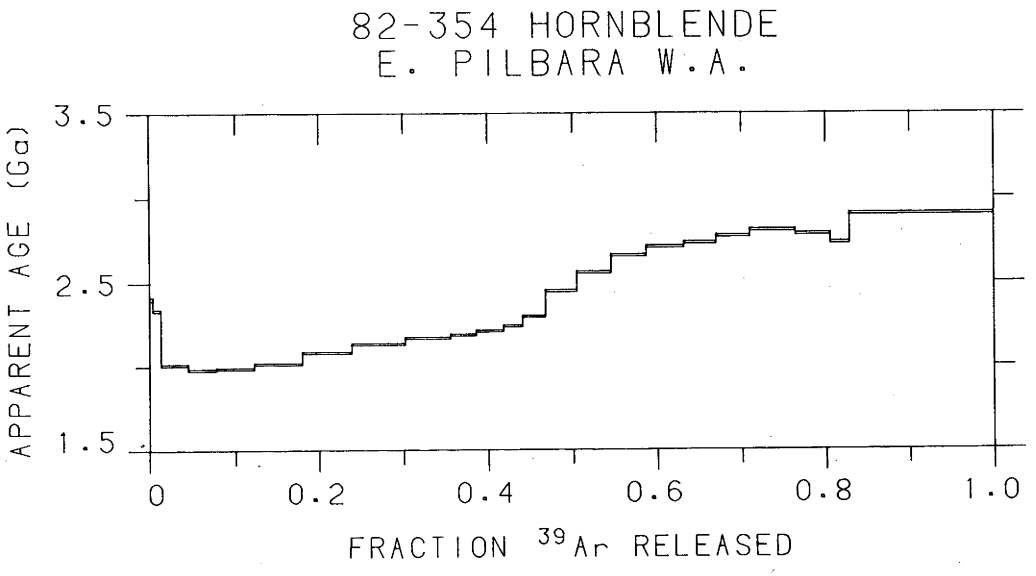

Figure 5.15 Hornblende 82-354

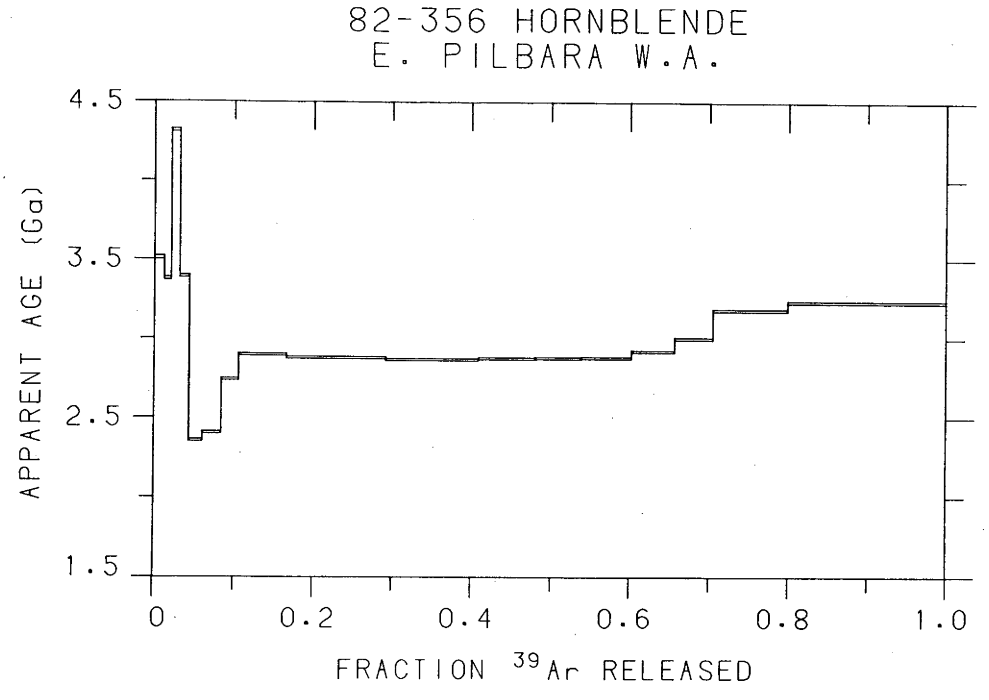

Figure 5.16 Hornblende 82-356

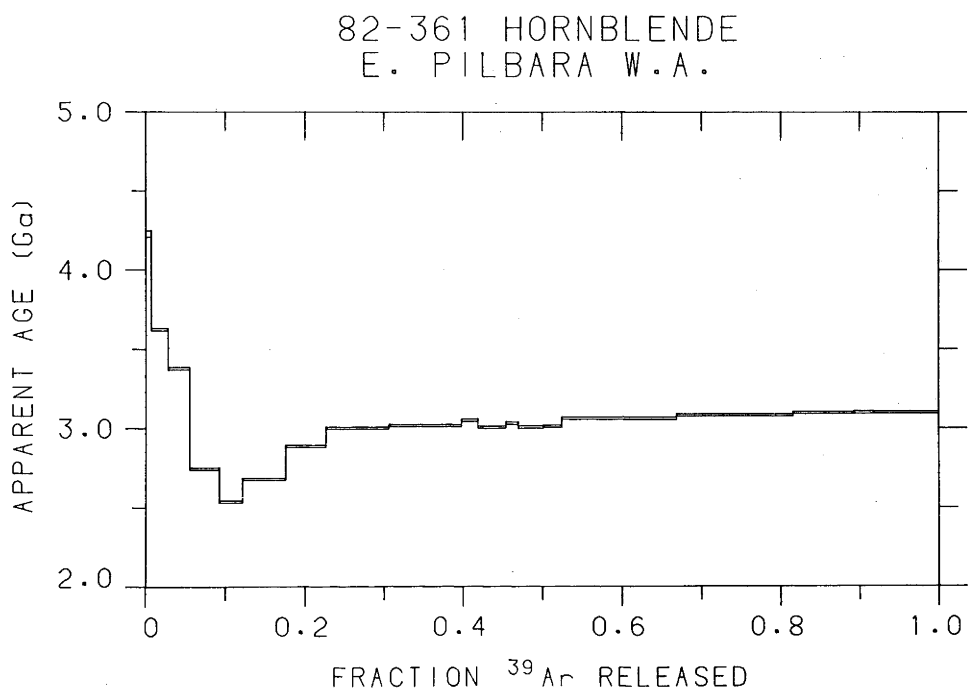

Figure 5.17 Hornblende 82-361

project (Fig. 5.13, 5.15). Both age spectra are very similar, and resemble the model release patterns calculated by Turner et al. (1966) for gas release from a sample with a lognormal grain size distribution. The maximum ages recorded in the high temperature steps are, under this model, substantially lower than the original crystallization ages, as the age spectra suggest argon losses in excess of 60 percent.

Only two of the samples (82-351, 82-354) from the Tambourah section show more severe overprinting. It is expected that on the scale of sampling, temperature differences were small during a thermal event which was probably caused by burial. Consequently, the probable cause for the differences in the shapes of age spectra lies within the minerals. Data on the diffusion of argon in hornblende suggest that the dependence of diffusion rate on the chemical composition of hornblende is small (Harrison 1983). It is suggested that the observed differences in the age spectra were probably caused by differences in the effective diffusion radii between minerals in different samples, possibly resulting from chemical exsolution within the crystals (Harrison and FitzGerald 1985). The K/Ca ratios in the undisturbed samples 82-352 and 82-356 have values typical of normal undisturbed hornblende, whereas the K/Ca ratios of samples 82-351 and 82-354 in the first 30 to 50 percent of the total gas release yielded values that are about an order of magnitude larger than those expected for undisturbed hornblende. This may possibly suggest that these hornblendes contain some kind of exsolved phase with a different calcium and potassium content compared with normal hornblende. However, no evidence for exsolution was observed in thin section.

Sample 82-324 (Fig. 5.11), from the Garden Creek area in the Western Shaw Belt was collected in order to constrain the post-metamorphic history of the belt. It was a fresh looking undeformed mafic dyke which is intrusive into the greenstones. This type of dyke occurs abundantly throughout the studied area, and may vary in thickness from about 10 cm to 150 m (Black Range). Upon microscopic examination it turned out that this sample was quite severely altered at greenschist facies grade. Consequently, the sample was analyzed with the intention to constrain the time of greenschist facies overprinting of the

rocks. In this sample, retrograde actinolite (Fig. 5.6) has partly replaced the original igneous amphibole as the dominant mafic mineral. The age spectrum is not readily interpreted under diffusional loss models, possibly because of the presence of two minerals in the sample. The high apparent ages obtained in the high temperature steps which approach 3.5 Ga clearly cannot be interpreted in terms of a thermal history, because this sample is from a dyke which intruded after the main metamorphism. If it is assumed that this effect is caused by excess argon, the poorly defined shoulder at about 2.5 Ga may be interpreted as being caused by the influence of the partly degassed original igneous minerals, while the thin metamorphic actinolite needles may contribute predominantly to the lower temperature segment of the age spectrum. This interpretation would suggest that greenschist facies overprinting occurred at about 1000 Ma ago, a value which is broadly supported by the loss patterns of the metamorphic hornblendes and muscovite described earlier. It should be stressed, however, that this interpretation is somewhat speculative because it is not firmly based on a well understood model for argon release.

5.3.2.4 Excess argon

Most hornblendes show some evidence for incorporation of excess argon into the margins of the crystals. This effect shows up as anomalously high apparent ages in the low temperature steps of the age spectra. Apparent ages as high as 4.3 Ga and 5.89 Ga in 82-361 and 82-314 (Fig. 5.17, 5.7) respectively, clearly indicate that no relevant geochronological information can be obtained from the low temperature steps in these experiments. Marginal excess argon is found in several other hornblendes. It should be noted, however, that excess argon seems to be confined to the first 5 to 10 percent of the total gas release. No U-, or saddle-shaped age spectra are observed. The age spectra provide some constraints as to timing of incorporation of excess argon. It is observed that the excess argon profiles are generally superimposed on $^{40}Ar^{*}$ loss patterns, produced by overprinting during the Mid Proterozoic, as can be inferred from the age spectra not being significantly affected by marginal excess argon. This leads to the suggestion that diffusion of argon into

the margins of the crystals occurred after the diffusional loss patterns were developed. Consequently it is most likely that it happened in the late stages of the Mid Proterozoic greenschist facies event.

5.3.3 Model release patterns

The age spectra of hornblendes 82-350, 82-352 and 82-361, as well as muscovite 82-315, can be compared with model release patterns (see Turner et al. 1966). These samples have yielded remarkably regular age spectra, and it is proposed that our understanding of thermal processes might be increased if the shape of these curves could be modelled on the basis of diffusion theory. The model originally proposed by Turner et al. (1966) assumes that an undisturbed mineral will yield a perfectly flat age spectrum. Subsequent thermal overprinting causes diffusion of $^{40}Ar^{*}$ from the crystals, resulting in the production of a $^{40}Ar^{*}$ concentration gradient within the crystals. On the basis of diffusion theory the shape of the age spectrum can be predicted for assumed amounts of argon loss. For hornblendes it is assumed that spherical diffusion geometry is appropriate. For micas the equations are easy modified to account for a cylindrical diffusion geometry.

If one wishes to apply a relatively simple single stage episodic loss model, the validity of such a model should first be discussed. It is recognized that such a model cannot take into account more intricate thermal histories, as for example slow cooling, multiple episodic loss, or a long, but poorly defined period of heating. In the Western Shaw area there is little constraint as to cooling rates. Because of the great age of the area, the subtle differences in age between different minerals as a result of cooling after one event would be difficult, although not impossible to measure. A more important consideration is that in terrains which have suffered several thermal events, the isotopic systems of different minerals may have been affected by overprinting to different degrees. This effect would make estimates of cooling rates from the isotopic systems virtually impossible. The information obtained in this study suggests that several discrete thermal pulses can be distinguished. Consequently, an episodic loss model is considered appropriate.

Figure 5.17 Model release patterns, after Turner et al. (1966). For explanation of the models see paragraph 5.3.3.

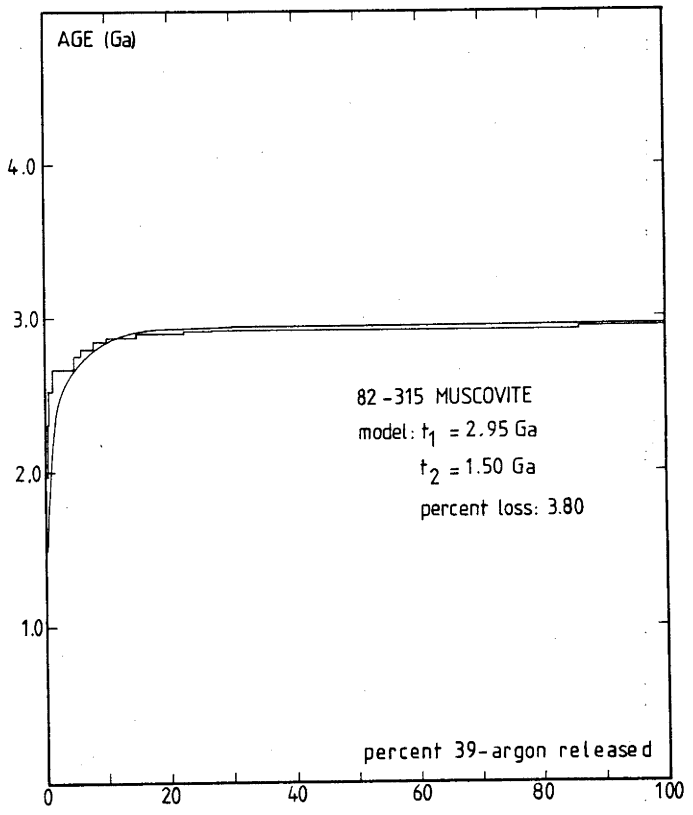
AGE (Ga)
4.0
3.0
2.0
1.0
82-315 MUSCOVITE
model: t_1 = 2.95 Ga
t_2 = 1.50 Ga
percent loss: 3.80
percent 39-argon released
0
20
40
60
80
100

a

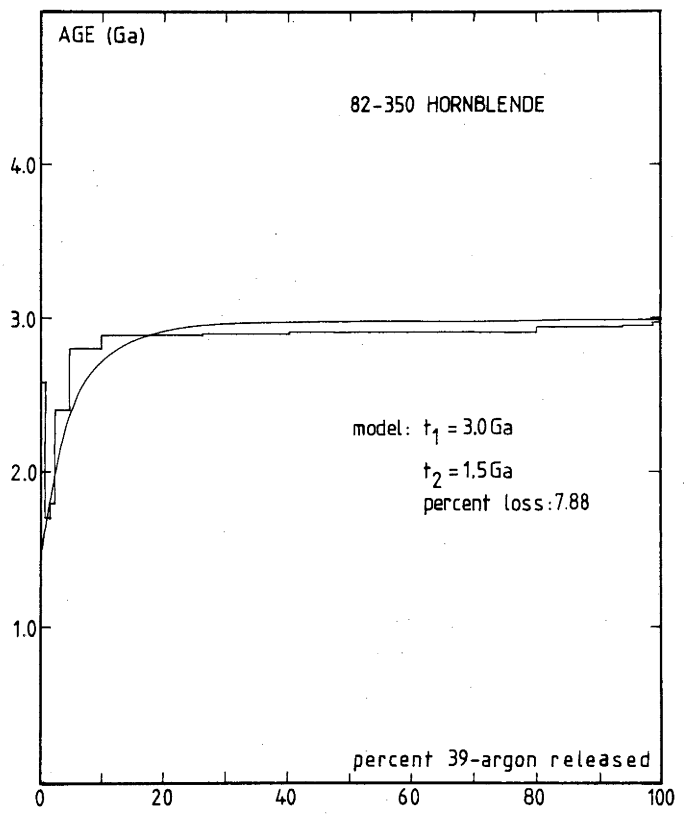
AGE (Ga)
82-350 HORNBLENDE
4.0
3.0
2.0
1.0
model: t_1 = 3.0 Ga
t_2 = 1.5 Ga
percent loss: 7.88
percent 39-argon released
0
20
40
60
80
100

b

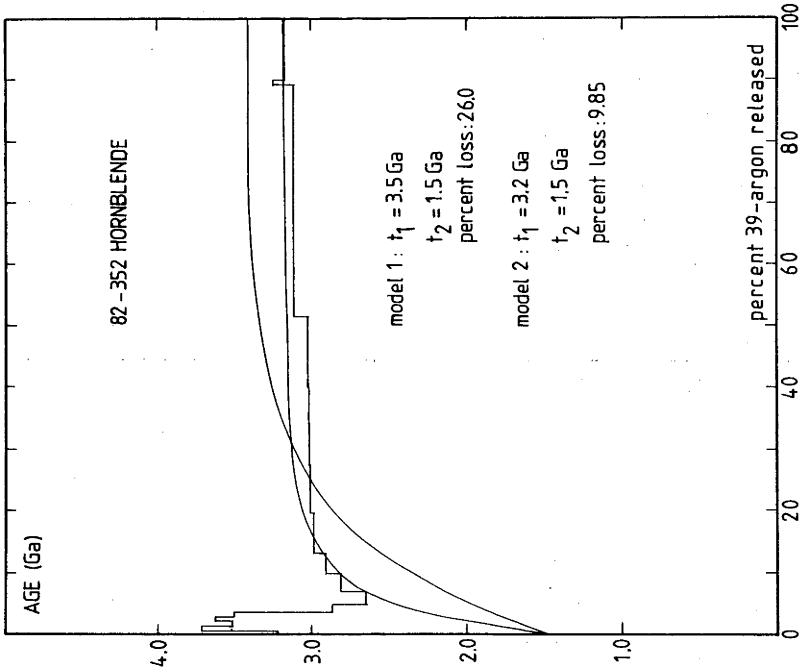
82-352 HORNBLENDE
AGE (Ga)
model 1 : t_1 = 3.5 Ga
t_2 = 1.5 Ga
percent loss: 26.0
model 2 : t_1 = 3.2 Ga
t_2 = 1.5 Ga
percent loss: 9.85
percent 39-argon released
4.0
3.0
2.0
1.0
0
20
40
60
80
100

c

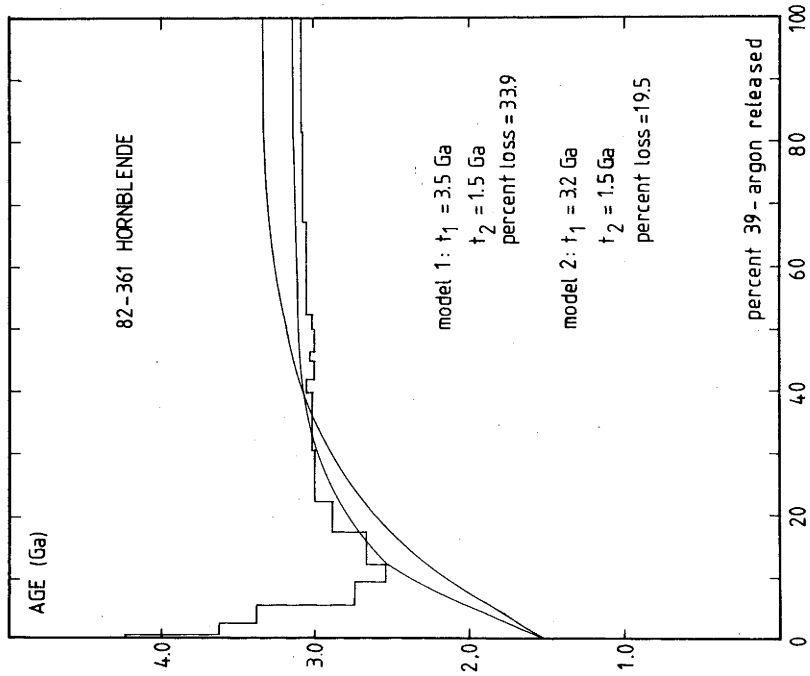
82-361 HORNBLENDE
AGE (Ga)
model 1: t_1 = 3.5 Ga
t_2 = 1.5 Ga
percent loss = 33.9
model 2: t_1 = 3.2 Ga
t_2 = 1.5 Ga
percent loss = 19.5
percent 39-argon released
4.0
3.0
2,0
1.0
0
20
40
60
80
100

d

Further, multiple episodic loss is a difficult problem to assess from the age spectra alone. It was demonstrated by Harrison (1983) that the predicted model release patterns in the case of two stages of episodic loss can be very similar to the curves expected for single stage episodic loss. Consequently, even in the case of very well resolved $^{40}Ar^*$ diffusion gradients it will be very hard to decide whether a single stage, or a multiple stage thermal history has occurred. In the case of hornblendes 82-352 and 82-361, the apparent ages in the high temperature part of the experiment increase slightly until a maximum age is reached in the last step. The choice for these age spectra is whether they are the result from two overprinting events, or from only one. In the first case, there is a possibility that the minerals were formed at 3.5 Ga, lost a substantial fraction of their accumulated argon during an event before 3.0 Ga, and then finally some marginal loss might have occurred at about 1.5 Ga. The other option is that the minerals were formed during a metamorphism between 3.5 and 3.0 Ga, and lost some amount of argon at 1.5 Ga. The mineralogy of the rocks yielding the 3.2 Ga ages suggests that the dual stage episodic loss model is the more unlikely alternative. If the primary metamorphic mineralogy was formed at 3.5 Ga, it would be expected that it is the result of contact metamorphism caused by intrusion of the early granodiorites. The mineralogy, which includes kyanite in the metapelites, does not suggest such a history. Also, if substantial resetting occurred subsequently, the temperatures involved would be of a magnitude that some recrystallization would be expected. The more likely alternative is that the early metamorphic mineralogy was formed during some regional event. It will be discussed in section 5.4 that this mineralogy was probably formed during the D_2 event recognized by Bickle et al. (1980). If this is the case, a single stage episodic loss model may be appropriate for the interpretation of the age spectra.

The present modelling has two objectives: (1) to constrain the age of the early metamorphism, and (2) to constrain the timing of formation of the Tambourah Dome. Hornblendes 82-352 and 82-361 yield information on the first event. Two models were calculated in order to make a choice between crystallization at 3.5 Ga or at 3.2 Ga. Subsequent overprinting was modelled to have

occurred at 1.5 Ga. As discussed above, this last point is a simplification, because the exact timing of this event is not well constrained, and there is the possibility that some argon loss occurred in earlier events. However, it seems that the effect of the thermal events documented in the granitoid-gneiss terrains has been limited in the greenstone belt away from the contacts with the gneiss terrain. It may be justified, therefore, to assume one single stage overprinting event. Both age spectra show some evidence for the incorporation of excess argon into the margins of the crystals. Although this effect is minor, a correction was made assuming that all steps affected by excess argon had an apparent age equivalent to an age of 2.0 Ga. As some of the early steps were likely to yield apparent ages somewhat lower than 2.0 Ga, and the subsequent steps ages somewhat higher than 2.0 Ga, an estimated average of 2.0 Ga over all steps containing excess argon was considered justified. Both the age spectra of hornblende 81-352 and 82-361 are best explained by assuming an initial age of 3.2 Ga (see Fig 5.17). These results support the interpretation that these hornblendes were formed during a regional metamorphism at about 3200 Ma ago, which was inferred previously on the basis of structural considerations, but for which until now no age constraints existed.

The second model was calculated to constrain the time of formation of the Tambourah Dome, located to the west of the Western Shaw Greenstone Belt, and part of the larger Yule Batholith (Fig 5.2, Fig 5.3). For hornblende 82-350 a model was calculated assuming a primary age of 3.0 Ga and overprinting at 1.5 Ga. For muscovite 82-315 a model was calculated assuming a primary age of 2.95 Ga, and overprinting at 1.5 Ga. Both models compare very well with the measured age spectra (Fig. 5.17), thus constraining the age of metamorphism, which accompanied the formation of the dome to the interval between 3.0 and 2.95 Ga.

5.3.4 Summary of results

The presentation of results in the previous section was organized in a way that samples, which are related geographically and petrologically, were discussed together. This approach was taken to facilitate discussion of the results. The division of samples into these groups was based on a combination of

microstructural, petrographical and chemical criteria. The present results are the first to date metamorphic mineral assemblages from Archaean greenstone belts with the $^{40}Ar/^{39}Ar$ age spectrum method. It is demonstrated that it is possible to date very ancient hornblendes and muscovites with considerable precision using this technique. This study confirms the Archaean age of the region, and results can be interpreted within the temporal frame based on previous geochronology.

As discussed previously, the dominant mineralogy within the greenstone belts is of upper greenschist facies to lower amphibolite facies metamorphic grade. The amphiboles belonging to this mineralogy are blue-green hornblendes, which were formed before D_3 (nomenclature according to Bettenay et al. 1981). The age spectra of hornblendes from this group (82-314, 82-351, 82-352, 82-354, 82-356, and 82-361) indicate complex histories, with evidence in some cases for substantial argon losses, as well as incorporation of excess ^{40}Ar into the margins of some minerals. The least disturbed age spectra indicate that argon accumulation in these metamorphic minerals started about 3200 Ma ago. The exact time of metamorphism is difficult to constrain, because all hornblende age spectra with ages attributed to this event have experienced substantial argon loss, and thus will only give a minimum estimate for the age of this event. Nevertheless, diffusion modelling supports the interpretation that the event occurred close to 3200 Ma ago, rather than at a substantially earlier time. Hornblendes belonging to this early metamorphic mineralogy (labelled M_2 in Figure 5.18) and which have yielded younger K-Ar ages, were shown by $^{40}Ar/^{39}Ar$ stepheating experiments to have lost substantial amounts of radiogenic argon (82-351, 82-354). This is consistent with the interpretation that they are part of the M_2 metamorphic mineralogy. The identification of pre-2950 Ma ages in hornblendes belonging to mineral assemblages from the Western Shaw Greenstone Belt is one of the major new findings of the present study. It indicates that metamorphism of the greenstone belts took place some 200 to 250 Ma before the mineral assemblages within the granitoid-gneiss domes cooled below the T_c of hornblende for argon. On the basis of structural arguments it was argued previously that mineral assemblages from within the greenstone belts predated the

formation of the granitoid-gneiss domes (Bettenay et al. 1981). Our data, however, is the first to constrain the absolute age of this event.

The second broad group consists of minerals formed during thermal overprinting near, or within the granitoid-gneiss terrains. Sample 82-350, an olive-green hornblende from the contact between the Western Shaw Greenstone Belt and the Tambourah Dome, muscovite 82-315 which was recrystallized at amphibolite grade after D_3, and hornblendes 81-657 and 81-658 which are both of upper amphibolite facies metamorphic grade belong to this group. The ages of minerals in this group span slightly more than 100 Ma, from 2960 to 2840 Ma. These results agree well with the previously interpreted age for the last major dome forming event (Hickman 1981). However, the quality of the data presented in this study allows further divisions to be made. Firstly, high temperatures affected the margins of the greenstone belts around the Tambourah Dome between 2965 and 2940 Ma. Because the mineralogy suggests that the minerals (hornblende 82-350 and muscovite 82-315) were formed after the last major penetrative deformation (D_3), their ages are interpreted to reflect cooling of the rocks after thermal metamorphism that accompanied the formation of the granitoid-gneiss domes. The age spectrum of hornblende 81-657 yielded a very well defined age of 2866 $\pm$ 5 Ma. This sample is from the margin of the Tambourah Dome about halfway between the locations of samples 82-315 and 82-350 (Fig. 5.3, 3a). The hornblende is from a high grade rock, in intimate contact with intrusive granite (Agmx lithology, Hickman and Lipple 1978). Because the evidence from muscovite 82-315 indicates that the Tambourah Dome area cooled below the closure temperature of muscovite for argon (i.e. about 350 ^{o}C) at 2940 Ma, it is suggested that the intrusion of granite to form the Agmx lithology was a later event, the thermal effect of which only overprinted those rocks in direct contact with the intrusive.

The age of sample 81-658 from the Garden Creek area in the Shaw Batholith yielded an age of 2840 Ma, which is very similar to the age of sample 81-657 from the Tambourah Dome. This age is interpreted as a cooling age, recording cooling after the last major phase of metamorphism in the more central parts of the

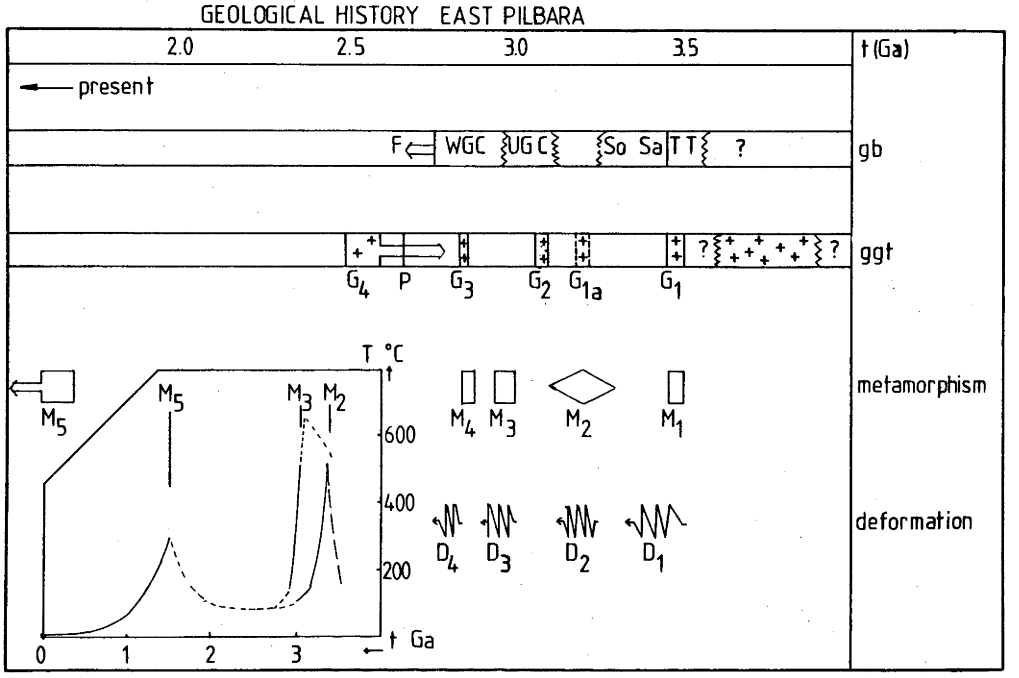
GEOLOGICAL HISTORY EAST PILBARA
2.0
2.5
3.0
3.5
t (Ga)
present
F
WGC
UGC
So Sa
TT
?
gb
ggt
G4
P
G3
G2
G1a
G1
T °C
600
400
200
0
1
2
3
t Ga
M5
M3
M2
M4
M3
M2
M1
metamorphism
D4
D3
D2
D1
deformation

batholith. It agrees well with the results of Rb-Sr whole rock isochron work and Pb-Pb isochron work reported by Blake and McNaughton (1984) from the Garden Creek area, and with the Pb/Pb isochron age of the Spear Hill posttectonic granite.

It is an important observation that the 2.8 to 2.9 Ga events in the granitoid-gneiss terrains which were associated with dome formation, have not severely influenced the rocks from within the greenstone belts. The dominant mineral assemblage within the greenstone belts is older, possibly with an age of about 3200 Ma, and overprinting seems to be confined to an event in the Mid Proterozoic. It is often difficult to decide from the age spectra whether episodic loss subsequent to crystallization occurred in one or more thermal pulses (Harrison 1983). However, it is clear that the Mid Proterozoic event has affected hornblendes from within the greenstone belts more profoundly than those associated with the high grade metamorphism in the granitoid-gneiss terrains. Constraints on the age of Mid Proterozoic overprinting are poor; from the low temperature steps in the age spectra one may argue that it occurred at some time between 1.0 and 1.5 Ga.

Younger ages obtained in the present study include an age spectrum on amphibole from a late mafic dyke (82-324, Fig. 5.11), a K-Ar age on pegmatitic muscovite of 2670 Ma, and a K-Ar age of a biotite from the North Shaw Granodiorite of 2650 Ma (81-631). The age of this biotite is difficult to interpret in terms of a metamorphic history. Either it records cooling after the last metamorphism, or partial resetting during the Mid Proterozoic greenschist facies metamorphism.

Thus, on the basis of the present study early regional metamorphism, M_2, occurred before about 3200 Ma (Fig. 5.18). In the labelling of metamorphic events, M_1 is reserved for the thermal aureole produced by intrusion of the early granodiorites at 3499 $\pm$ 22 Ma (Bickle et al. 1983). This event may be preserved in some of the greenstone belts, but was not identified by $^{40}Ar/^{39}Ar$ experiments in the present study. The M_2 event was followed in the granitoid-gneiss terrains by M_3, which occurred 2960 to 2940 Ma ago, and by M_4, which is interpreted as a local effect in the Tambourah Dome at 2860 Ma. Within the central parts of the Shaw Batholith no distinction between M_3 and M_4 could be

made. The greenstone belts have escaped substantial overprinting during the M_3 and M_4 events, but were more strongly affected by the Mid Proterozoic greenschist facies overprinting, labelled M_5. The present study does not indicate substantial thermal overprinting during the time interval between 2840 and 1500 Ma ago. If such an event had occurred in the area, it most certainly would have affected the age spectrum of muscovite 82-315.

5.4 Discussion

The following discussion is divided into two broad sections. First, a brief review of current ideas as to Archaean crustal evolution will be given. This section will be followed by a more detailed discussion of the results of the present study in terms of models put forward for the crustal evolution of the Pilbara Block. Justification for this approach is that in this manner the relevance of our work for the understanding of Archaean crustal evolution is best pointed out. For example, our data indicates that at the time of formation of the granitoid-gneiss domes in the eastern Pilbara, the metamorphic geotherms of the Western Shaw Greenstone Belt and the adjacent granitoid-gneiss terrain were grossly out of equilibrium. This observation has clear implications for the rate of tectonic processes during the Archaean. Presently, the importance of uplift- and subsidence rates for the generation of particular metamorphic facies trends is widely accepted in modern mountain belts, as for example the Alpine Orogenic Belt of southern Europe (see for example chapter 4 of this thesis). However, the application of this concept to metamorphism during the Archaean is still quite new (see for example England and Bickle 1984). It is important for the interpretation of the results of the present study, to discuss them in the light of current ideas as to Archaean crustal thickness, thermal structure and depositional environments for greenstone sequences.

5.4.1 Archaean continental crust

Archaean blocks or nucleii of varying size have been identified on all continents (Windley 1977). This is an important observation because it indicates that continental crust was already widespread during the Archaean. The geology of these Archaean nucleii can be divided into two broadly defined groups: (1) the high grade terrains which consist of granodioritic to tonalitic gneisses and minor supracrustal rocks, and (2) the low grade terrains which consist of mafic volcanics and sediments in greenstone belts, and granitoid domes. The high grade terrains are generally metamorphosed at granulite facies grade, whereas the low grade terrains are metamorphosed at greenschist facies grade and in some cases to amphibolite facies grade.

Geobarometric studies of Archaean granulite terrains suggest that the thickness of the crust in these nucleii was probably not less than the average thickness of the present day continental crust (Condie 1973, O'Hara 1977, Wells 1979, 1980, Newton and Perkins 1982). Similar conclusions were reached from consideration of the petrology of Archaean greenstone terrains (England and Bickle 1984).

An important problem with the interpretation of geological environment during the Archaean is that subsequent tectonism, probably including plate tectonic processes, has prevented the assessment of the relative positions of these blocks to each other during the Archaean. Further, modern tectonic models for orogeny require knowledge of the geology of the continental crust, as well as the oceanic crust. The problem in applying such models to the Archaean is that unless oceanic crust was incorporated in the continental crustal masses, subsequent plate tectonic processes have erased the evidence for such oceanic crust. Also, the study of the earliest history of the earth's crust is made difficult by the often complex tectonic and thermal history of the rocks in the Archaean blocks. These factors contribute to the incompleteness of knowledge of the geological history of the earth during the Archaean.

For the discussion of the structure and physical properties of the Archaean continental crust the following observations are of importance:

(1) Gross heat production in the earth during the Archaean must have been higher by a factor of at least two to three in comparison with the present (e.g. Lambert 1976).

(2) Petrological investigations have revealed that apart from the expected high temperature, low pressure metamorphic facies trends, many Archaean metamorphic terrains show medium pressure, low to medium temperature metamorphic facies trends (Grambling 1981, England and Bickle 1984).

(3) Geochemical studies suggest that the chemical composition of new additions to the continental crust has changed at about the Archaean-Proterozoic boundary, i.e. between about 3000 and 2500 Ma ago (e.g. Taylor and McLennan 1981, Veizer and Compston 1976, Veizer and Jansen 1979). In addition, there is some evidence that during this period vast amounts of new material was added to the

continental crust.

(4) As clastic sediments and pillow lavas were recognized in the earliest supracrustal sequences (Windley 1977, Hickman 1983), the average surface temperature is unlikely to have been very different from that observed today.

(5) Systematic assessment of heatflow data from the continental crust exposed in the Archaean nucleii, and from post-Archaean continental crust, indicates that the present-day heatflow from the Archaean nucleii is lower than that from younger continental crust (Morgan 1984, Morgan and Sass, 1984).

Because the contribution of radioactive heating during the Archaean was higher, it follows that if the Archaean continental crust was about as thick as that of the present day, and its chemical composition was also similar, then the Archaean continental geotherm must have been significantly different from the present day continental geotherm. Neither the petrological data, nor the geochemical data convincingly support the suggestion that the Archaean continental crust was hotter than the modern continental crust. Comparison of pressure and temperature estimates obtained from metamorphic mineral assemblages in Archaean and in Proterozoic rocks has revealed that the differences in physical conditions experienced by those rocks from different periods in the Earth's history are only very small (Grambling 1981). This argument can be used as support for interpretations in terms of a uniformitarian view point for continental evolution (e.g. Windley 1976, 1977, Armstrong 1968, 1981). Large scale geochemical investigation of Archaean and Proterozoic rocks (as carried out by Taylor and McLennan 1981), as well as isotope geochemical considerations (Veizer and Compston 1976, De Paolo and Wasserburg 1976, 1979, McCulloch and Wasserburg 1978, Moorbath 1976, 1977), and continental heatflow studies (e.g. Morgan 1984, Morgan and Sass, 1984), point to a significant change in chemistry of newly formed continental crust during the period between 3.0 and 2.5 Ga ago. During this period substantial amounts of mass were added to the continental crust. The chemistry of these new additions to the crust had a higher concentration of heat producing elements. The implication is that the thermal structure of the post-Archaean continental crust could have been quite different from the Archaean continental

crust. A consequence of such a major chemical change is that the bulk of the heat loss from the Archaean Earth took place outside the continental nucleii, and consequently that the thermal structure of the continental crust was cooler than expected, possibly similar to that of the present day.

Because it is uncertain that plate tectonic processes were operative during the Archaean (see Kröner 1981), or even that oceanic basins similar to the present day oceans existed, it is debated whether mid-ocean ridges similar to the present ones could account for the inferred heat loss. Possibly an increased length of Archaean ocean ridges compared with the present ridges, or a mechanism involving heat loss from abundant hot spots could be invoked to explain higher rates of heat loss through the Archaean oceanic crust. Mantle convection during the Archaean was probably more vigorous (Bickle 1978); thus as a means transport of heat to the earth's surface it may have been more efficient. Calculations by Davies (1979) indicate that more vigorous convection may result in a geotherm only about 150 ^{o}C higher than observed today. Consequently, if the mantle geotherm in the Archaean was only slightly higher than today, the mantle heatflux contribution to the Archaean continental geotherm may have been only marginally higher than that inferred for present day continents. A different argument was presented by Wells (1981) and by Dewey and Windley (1981) who contended that the continental lithosphere in the Archaean may have been already quite thick (about 200 km), and may have acted effectively as a heat shield between the continental crust and the more vigorously convecting mantle below it. Heatflow data from Archaean terrains support the view that a thick and old lithosphere is present below the crust of the Archaean nucleii (Morgan and Sass 1984).

5.4.1.1 Models for greenstone deposition

The depositional environment of most greenstone sequences, and the structural relation between the greenstone and gneiss terrains has been a topic of lengthy discussion. Models that seems viable can be divided into two main groups: (1) those involving tectonic processes of the kind active on earth today, and (2) those suggesting some unique Archaean tectonic setting. In the actualistic models, the depositional environment of

greenstone belts is seen to be related to subduction zones like those at modern plate margins. In these models, greenstone belts are positioned in back-arc basins on thinned continental type crust, because of the self destructing nature of the actual margins (e.g. Windley 1976, 1977). Phanerozoic analogues of greenstone belt volcanism in a plate tectonic setting in south Chile and in Newfoundland were discussed by Tarney et al. (1976), and by Burke et al. (1976).

Non-actualistic models include Glickson's model of an originally mafic crust (Glikson and Lambert 1973, Glikson 1979), and Green's extra-terrestrial model (Green 1972). The first of these models suggests that the lower units of the greenstone sequences were part of an early mafic crust, and was developed on the basis of observations in the Western Australian Archaean terrains. The granitoid-gneiss terrains were argued to be the result of subsequent intrusions by granitoid plutons, derived from partial melting of the lower sections of that early mafic crust. Glikson's (1979) model, as put foreward for the Pilbara Archaean Block, was rejected by Hickman (1981), and by Bettenay et al. (1981), who favour the view that the greenstone sequence in the Pilbara region is underlain by a sialic basement. However, despite considerable effort in recent years, geochronological investigations have as yet failed to reveal a pre-greenstone sialic basement in this area. The grey gneisses of the Shaw Batholith in the eastern Pilbara were suggested by Hickman (1981) as possible areas where remnants of the early crust could have survived. However, U/Pb ages of zircons, Sm-Nd model ages and Pb/Pb ages of samples from these grey gneisses were indistinguishable from the age found for the less deformed granodiorite pluton which was interpreted as intrusive into, but broadly coeval with the lower greenstone units of the Warrawoona Group at about 3.5 Ga (Bickle et al. 1983, Collerson and McCulloch 1982, 1983, Williams et al. 1982, 1983). Thus, these multiply deformed grey gneisses probably are best interpreted as the gneissified and migmatized equivalents of this pluton.

Although the basement problem is not yet resolved in the Pilbara, there are some considerations relating to the presence of a basement, and on its chemical nature as well. Firstly, the presence of sialic rocks with ages at least 400, and possibly 700 Ma older than the Pilbara greenstone volcanics are known or postulated in Western Australia (Froude et al. 1983, Kinny et al. 1985, De Laeter et al. 1985). Although the geographical position of these rocks in the northern Yilgarn Block (Fig. 5.1) in relation to the Pilbara Block during the Archaean is not well constrained, it illustrates that sialic basement did exist at the time of the extrusion of the earliest Warrawoona Group lavas. These recent findings cast some doubt on Glikson's suggestion that the greenstone belts of western Australia represent the oldest crust (see Glikson 1979).

A second argument was discussed by Kröner (1984), who contended that Archaean greenstone belts are quite unlike oceanic crust because of their often excellent preservation. If the greenstone belts were part of, or deposited on hot oceanic lithosphere, they would have been prone to vigorous hydrothermal alteration, as is observed in modern ocean floor basalts. The fact that alteration in many cases was relatively minor (see also Martinez et al. 1984), suggests that they were deposited subaerially, or in shallow water on a cold basement. Further, the observation that some greenstone sequences overlie granitoid-gneiss units in southern Africa (Bickle et al. 1975, J.F. Wilson pers comm. in Kröner 1984, Bickle unpublished data in Nisbet 1982), suggests that a similar tectonic setting may be inferred for the Pilbara as well.

Green's E.T. model equates the terrestrial greenstone belts to the lunar maria, which were formed as the results of vigorous meteorite bombardment which occurred on the moon before 3.9 Ga ago. The argument was that, because of the closeness of the Moon to the Earth, the Earth was unlikely to have escaped a similar meteorite bombardment. A meteorite impact would fracture the thin early Archaean crust, opening a way for mafic to ultramafic magmas to reach the surface. This model has run into problems as more detailed geochronological data have become available in recent years. It is now recognized that the earliest known continental crustal sections, such as exposed in the Isua and

Godthaab districts in Greenland and in the Western Gneiss Terrain of the Yilgarn Block, do not contain any significant amount of greenstone rocks. Consequently there is a time gap of some 300 to 400 Ma between the ending of the period of meteorite bombardment and the beginning of deposition of the earliest greenstone volcanics, making an extraterrestrial origin for greenstone volcanics unlikely.

A possible alternative model was discussed by Kröner (1984), who made the point that plate tectonics as observed today is unlikely to have been operative during the Archaean. Kröner contended that subduction of the kind observed today was unlikely, because the higher temperatures of the crustal plates would preclude the density contrasts necessary to allow oceanic crust to be subducted. However, because of the higher heat production in the Archaean mantle, it would be likely that vigorous mantle convection was occurring. Thus motion of crustal segments surely would be expected. These arguments led Kröner (1984) to suggest that modern plate tectonic models could not be applied to Archaean greenstone belts. Instead, Kröner argues that greenstone basins were positioned in continental rift zones. Models for the development of greenstone belts based on continental rifting were also discussed by Achibald et al. (1978), and in Kröner (1981). An important consideration for the geology of the Pilbara is that such models allow relatively large basins to develop. This tectonic setting would also agree with the propositions of field geologists that greenstone belts developed in large basins and were generally deposited on some kind of sialic basement (see for example Bickle et al. 1975, Hickman 1981, Gee et al. 1981). Archaean greenstone sequences were argued to be similar to younger continental flood basalts such as the Early Proterozoic Ventersdorp and Hamersley volcanics, and the Mesozoic sequences of Gondwanaland. Exploring this analogy further it should be noted that the Fortescue Group volcanics of the Hamersley Basin were attributed to the Early Proterozoic, but appear to be contemporaneous with Late Archaean greenstone belts of the Yilgarn Block (see for example Roddick et al. 1976, Pidgeon 1984, Richards and Blockley 1984). An important difference between the Archaean greenstone belts and the subsequent continental flood basalts is the degree of

deformation: whereas the Archaean greenstone sequences are often folded into narrow synclinal belts, the post-Archaean analogues have suffered only very minor deformation or metamorphism (Trendall 1983). This difference in degree of deformation, and metamorphism may have been caused by differences in strength of the continental crust on which the volcanic sequences were deposited. The continental rift model predicts that greenstone terrains are flanked by older sialic blocks. Such an arrangement is observed in the Yilgarn Block, where the older Western Gneiss Province is found on the western margin of the block, and younger greenstone provinces more to the east. In the Pilbara a similar arrangement of crustal sections cannot be distinguished. Perhaps a difficulty with this model is the fact that rifting is not easily reconciled with relatively low heatflow, as was inferred for the Archaean greenstone belts (England and Bickle 1984). Present day rift zones with associated volcanism are accompanied by higher than average continental heatflow. These rift models suggest that the mafic greenstone volcanism was caused by rising hot mantle plumes, and was accompanied by underplating of the continental crust by mafic magma. Models proposed for Archaean accretion by mafic underplating also suggest relatively high heatflow (Wells 1980, 1981).

5.4.1.2 Archaean metamorphic geotherms

After discussing more general models for the Archaean continental crust, the thermal structure of greenstone terrains needs to be addressed in somewhat more detail. Firstly, as already discussed, studies of metamorphic assemblages in high grade Archaean terrains suggest continental crustal thicknesses which are not significantly different from those inferred for the continents today (Condie 1973, Wells 1979, 1980, 1981, O'Hara 1977, Newton and Perkins 1982, see also England and Bickle 1984). Secondly, although all Archaean greenstone sequences are metamorphosed, it is argued that substantial areas have suffered remarkably little metamorphic alteration. This point is illustrated by the preservation of primary igneous features like pillow lavas, spinifex and quenching textures in many komatiites and komatiitic basalts (Arndt and Nisbet 1982, Hickman 1983). A similar indication is obtained from the $^{40}Ar/^{39}Ar$ wholerock work

of Martinez et al. (1984), who argued that the rocks they studied were metamorphosed in very low grade greenschist facies grade immediately upon extrusion and have not been altered since.

For the Pilbara Supergroup from the base up to the Clearville Formation, Hickman (1981,1983) suggest a total stratigraphic thickness of about 20 km. Allowing for lateral changes in thickness, and some degree of tectonic thickening, the bottom of the sequence has been at a depth of about 10 to 15 km. As the base of the Warrawoona Group has been metamorphosed only to lower greenschist grade, possibly to a temperature of about 300 ^{o}C, one could infer a thermal gradient of less than 30 $^{o}C/km$. The two main parameters which determine an equilibrium geotherm are the mantle heatflux and crustal heat production by radioactive decay. In a rough calculation to assess the approximate value for the mantle heatflux the contribution of radioactive heat production from within the mafic volcanics of the greenstone stratigraphic sequence may be neglected. Thus it is assumed that heating occurred by heatflow into the greenstone sequence from the rocks below, which may include a sialic basement and subcontinental lithosphere. This value will be called here the reduced heatflow. If the base of the sequence remained buried for significant times, thermal conditions should approach the equilibrium geotherm. The reduced heatflow can be calculated using the data mentioned above and an average value for the thermal conductivity (2.5 $W/m.^{o}C$), and may have been in the order of 50 to 75 mW/m^2 for a temperature estimate of 300 ^{o}C at the base of the sequence. For a metamorphic temperature at the base of the sequence of about 400 ^{o}C, values of 67 to 100 mW/m^2 would be obtained. The values calculated for the reduced heatflux, ignoring the minor amount of heat produced within the volcanics, are quite similar to the average present day mantle heatflux in continental areas, which is about 40 mW/m^2. Such a crude calculation seems to indicate that a reduced heatflux, of about the magnitude of the present day average mantle heatflux would be sufficient to produce the thermal overprinting observed in the basal units of Archaean greenstone sequences. Because the reduced heatflux, as defined above consists of contributions from an Archaean mantle heatflux and from a sialic basement, the conclusion is that if the Archaean mantle heatflux had a similar value to that of the

present day, the contribution of heat produced in a sialic basement was marginal. This would either mean that if a sialic basement existed, it was very thin, or significantly depleted in heat producing elements compared with present day sialic material.

P-T data obtained from petrological observations cannot be used to establish an equilibrium geotherm during the Archaean. This point was made for Phanerozoic orogenic belts by England and Richardson (1977), and illustrated by the decrease in abundance of high pressure, low temperature belts in orogenic zones from the present toward the Late Precambrian. Instead of invoking increased thermal gradients, they proposed a mechanism involving differences in erosion rates: if uplift and erosion is rapid, high pressure, low temperature belts will be exposed, but be destroyed quickly by erosion. If, on the other hand, uplift and erosion was slow, older metamorphic belts could still be exposed on the earth's surface, but because of slow erosion rates the high pressure assemblages, which may have been present, are likely to be overprinted by lower pressure, higher temperature assemblages. The same arguments hold, in principle, for the Archaean as well. As a consequence, if information on the equilibrium thermal structure of the Archaean continental crust were available, the degree of dis-equilibrium obtained from petrology might enable one to constrain the rates of tectonic and thermal processes.

5.4.2 The application of the $^{40}Ar/^{39}Ar$ technique to Archaean rocks

The present study demonstrates that the $^{40}Ar/^{39}Ar$ step heating method of dating may contribute significant new data on the thermal evolution of an Archaean granitoid-greenstone terrain. Earlier studies applying the method to Archaean rocks have concentrated either on the study of minerals from high grade terrains, or on wholerock samples from low grade greenstones. The studies of Pankhurst et al. (1973), and Dallmeyer (1982) concentrate on the gneissic terrains. Working on rocks from Greenland and from Labrador respectively, they show clearly the complexity of the thermal evolution in these terrains. The most important observation of both studies is the difficulty in

interpreting the $^{40}Ar/^{39}Ar$ data of biotites in this type of terrain. Biotites in some cases yielded ages that were too old to fit readily in a reasonable interpretation, yielding patterns in the age spectra that seemed undisturbed. Hornblendes analyzed by Pankhurst et al. (1973) did yield ages that could be interpreted in terms of a thermal evolution. Consequently, it was concluded that hornblendes may yield more useful information than biotites.

Martinez et al. (1984) concentrated on metavolcanic rocks from greenstone belts from Barberton in southern Africa. Their work is especially noteworthy, as they describe ages of 3.45 Ga on whole rock samples of lower greenschist facies metamorphic grade. They argued that because the results from argon isotopic dating and from Sm/Nd isotopic dating are not significantly different, lower greenschist facies metamorphism must have occurred very early in the history of these rocks. Of equal importance is the implication that the greenstones of this part of Barberton Mountainland must have remained at temperatures below those encountered at greenschist facies metamorphic grade since 3.45 Ga. These observations contrast with the results from the present study on greenstone volcanics from the southeast Pilbara, which have had a more complex thermal evolution.

It has been recognized for sometime that results obtained from Rb-Sr wholerock dating gave lower ages than expected for a primary igneous event. For the interpretation of Rb-Sr wholerock isochron ages from the Pilbara Archaean Block, De Laeter et al. (1981) applied a rigorous test to available data, thus rejecting more than 90 percent. In more recent reviews of the geochronology of the Pilbara region, Trendall (1983) and Blake and McNaughton (1984) argued that Rb-Sr wholerock isochron data should not be used to establish a primary geochronology. The present study by the $^{40}Ar/^{39}Ar$ technique again emphasizes the problems with the Rb-Sr data, because where direct comparisons can be made, the results from $^{40}Ar/^{39}Ar$ analyses on hornblendes agree well with the data obtained by the Pb/Pb isochron method, but Rb-Sr wholerock and wholerock/mineral isochron data often yielded lower ages. In the previous sections, a quite detailed thermal history of the Tambourah Dome was established, indicating that cooling after high grade regional metamorphism occurred about 2950 Ma ago, and was followed by minor local granite intrusion at about

2870 Ma. Rb-Sr wholerock mineral isochrons on banded gneisses from the Tambourah Dome yielded ages of 2610 ± 14 Ma and 2698 ± 14 Ma (Oversby 1976), whereas Rb-Sr wholerock isochron ages of banded gneisses from the same area yielded ages of 2995 ± 95 Ma and 2799 ± 35 Ma (Cooper et al. 1982). These data suggest that Rb-Sr wholerock/mineral isochrons do not reliably date high grade metamorphism, and that Rb-Sr wholerock isochrons may also give results which are younger than Pb/Pb isochron ages and $^{40}Ar/^{39}Ar$ ages, and cannot be readily understood in terms of a cooling history for the area.

The argon system is possibly more useful in metamorphic rocks, firstly because the radiogenic daughter isotope is the neutral, chemically inert noble gas argon. Argon loss from minerals occurs predominantly by thermally induced volume diffusion, and once outside the minerals, partitioning between fluid and solid phase is heavily in favour of the fluid. Thus once the argon has diffused out of the minerals it is in most cases lost from the system. Secondly, because a stepwise heating technique can be used, useful information can be obtained even in partly disturbed terrains.

5.4.3 Metamorphism and the age of the Warrawoona Group

The volcanics and the sediments of the Pilbara Supergroup probably were deposited as essentially flatlying units in one large basin (Hickman 1983). This conclusion was based on the coherence of the stratigraphy of the Archaean supracrustal rocks throughout the Pilbara region. Hickman assigns the rocks from the Western Shaw Belt to the Apex Basalt of the Warrawoona Group up to the Clearville Formation in the Gorge Creek Group (Hickman 1980, 1983, Hickman and Lipple 1978). The rocks of the Western Shaw Belt have suffered from various metamorphisms, accompanied by substantial deformation, making correlation with less metamorphosed equivalent units difficult. Nevertheless, if the succession up to the Clearville Formation is present in this area, regional metamorphism at about 3.2 Ga places a time constraint on the deposition of the Soansville Subgroup. This observation may suggest two points. Firstly, it was recognized that within the Archaean stratigraphy the older units had suffered various degrees of metamorphism, whereas the younger

units were substantially less metamorphosed. Therefore, it was inferred that at some time a metamorphic discontinuity occurred in the Archaean sequence. In the Western Shaw Belt there is some evidence that this metamorphic discontinuity occurred within the Gorge Creek Group after deposition of the Soansville Subgroup. Secondly the upper units in the Gorge Creek Group, of which the most prominent is the Lalla Rookh Sandstone Formation, are generally regarded as the products of rapid erosion of granitoid-gneiss material derived from the domes, that were formed about 2.95 Ga ago. Thus, it was argued that these units must be younger than 2.95 Ga (Hickman 1983). If these inferences are right, there would have been a major hiatus in the Gorge Creek Group between about 3.2 Ga and 2.95 Ga. However, as long as no constraints on the deposition of the upper part of the Gorge Creek Group exist, the significance of this inferred hiatus may be minor.

5.4.4 Models for the crustal evolution of the Western Shaw Belt

As discussed previously, various models exist for the crustal evolution of the Archaean Pilbara Block (Hickman and Lipple 1975, Glikson 1979, Hickman 1981, 1983, Bickle et al. 1980, 1983, 1984, Bettenay et al. 1981, Morant 1984). The findings of the present study provide important constraints on the tectonic and metamorphic evolution of the area.

(1) Lateral variations in metamorphic geotherms between the granitoid-gneiss terrains and the Western Shaw Greenstone Belt existed over short distances.

(2) Tectonism related to dome formation occurred prior to 2940 Ma.

(3) Local high grade metamorphism continued until about 2850 Ma ago.

From the investigations into the structural evolution of the Western Shaw Greenstone Belt reported by Bickle et al. (1980, 1984), and by Bettenay et al. (1981), and from the present study it is clear that the simpler models of greenstone evolution cannot adequately explain the geology of the Western Shaw area. The earlier models which regard the granitoid-gneiss terrains as batholiths, i.e. the intrusion of many individual plutons (e.g. Glikson and Lambert 1973, Glikson 1979), imply that metamorphism of greenstone belts must be interpreted as the result of a series

of superimposed thermal contact events. According to this view, the greenstone xenoliths found in the granitoid-gneiss terrains represent screens of supracrustals which separate the individual plutons of the batholith. Bickle et al. (1984) have argued that the structural relation between the greenstones and the granitoid-gneiss terrains is more complex, with various tectonic events documented.

The interpreted age of M_2 metamorphism, about 3.2 Ga, cannot readily be attributed to the intrusion of magma in either the Shaw Batholith or the Yule Batholith, because evidence for granitoids of this age is lacking. Further, the metamorphic petrology of the pre-D_3 mineral assemblages, as reported by Morant (1984) and in the present study, indicate that the early event, M_2, was of a medium pressure, low to medium temperature type, and therefore not easily reconciled with thermal overprinting caused by intrusion of granite. Indeed, it is suggested that the early metamorphic mineralogy was formed during a phase of metamorphism, characterized by lowering of the equilibrium geotherm by rapid thickening of the crust. Consequently, the early metamorphism is best interpreted as a regional event.

The model proposed by Hickman (1981) explains the crustal evolution of the area in some detail. Central to his model is the view that the greenstone sequence was deposited on a sialic basement, and that careful investigation of the granitoid-gneiss terrains, for example the Shaw Batholith, may reveal the existence of this basement. In Hickman's model the greenstone xenoliths, or enclaves, are part of an earlier generation of greenstone deposition, which may be older than the Warrawoona Group. This opinion is in contrast with the findings of Bickle et al. (1980) that the greenstones in the enclaves were likely to be of the same generation as those within the greenstone belts, because they could in some cases be traced from the granitoid-gneiss terrain into the greenstone belt. In Hickman's model, uplift of granitoid-gneiss material, and concomitant subsidence of greenstone rocks is a gradual process, which operated semi-continuously throughout the period between 3.6 Ga and 2.95 Ga. All deformation, earlier than the main phase of uplift was grouped together under D_1 (Hickmans nomenclature (1981)),

although it was recognized that D_1 consisted of a complex group of tectonic structures. Thus gradual uplift of the granitoid-gneiss terrains caused both the D_1 and D_2 structures and culminated in the 2.95 Ga event recognized in the Pb/Pb study of granitoids by Oversby (1976).

The present argon data is not readily explained by continuous uplift over a period in excess of 500 Ma. The argon data suggests that thermal disequilibrium occurred during at least two separate metamorphisms. Thermal disequilibrium cannot be explained in terms of gradual uplift over long time intervals. Consequently it is suggested that tectonic activity occurred in a series of short well defined episodes. The first event recognized here is in relation to the M_2 regional metamorphism, which we argue from the $^{40}Ar/^{39}Ar$ ages of blue-green hornblendes must have occurred before about 3200 Ma. The second tectonic event is related to the M_3 metamorphism, and involved significant thermal disequilibrium about 2950 Ma ago.

5.4.4.1 Towards a tectonic model

The concept of thermal disequilibrium tectonics also plays a role in the models proposed by Bickle et al. (1980, 1984), Bettenay et al. (1981), and Morant (1984). Consequently, these models have the potential to explain the argon isotopic data best. Two models were proposed for the Shaw Batholith and Western Shaw Greenstone Belt which take into account the complex tectonic evolution of the rocks. The first model, preferred by Bettenay et al. (1981), emphasizes the complex tectonic history of the area before the granitoid-gneiss domes were formed.. They proposed major tectonism, involving subhorizontal faulting and the incorporation of enclaves of greenstone material into the granitoid-gneiss units. Tectonic considerations led them to suggest that this event occurred before the domes were formed, possibly during an unrelated event. Morant (1984) argued that on the basis of the petrology alone, it is unnecessary to suggest two different events. The metamorphic mineral assemblages in the metapelitic units can be interpreted by assuming one single metamorphic facies trend from the greenstone belts into the Shaw Batholith, without proposing a major hiatus. Although discussing the possibly more complex history, the apparently simple

metamorphic facies trend led Morant (1984) and Bickle et al. (1984) to suggest that the inferred tectonic history was accompanied by one metamorphic event.

Our data contributes to the understanding of the geology of the area, in that it indicates that the metamorphic assemblages in the greenstone belt were formed significantly earlier than those in the granitoid-gneiss terrains. On the basis of structural considerations, the earlier metamorphic assemblages must be related to the pre-domal phase of tectonism reported by Bickle et al. (1980, 1984). The P-T conditions during this event are not very well constrained. The mineralogy suggests physical conditions near the greenschist facies - amphibolite facies boundary, within the stability field of kyanite (Morant 1984). Such conditions would require a fairly low metamorphic geotherm, which is consistent with an event involving tectonic thickening followed by subsequent erosion (Morant 1984). The texturally late mineral assemblages including andalusite and sillimanite were probably caused by the events related to dome formation. This observation is quite unequivocal in the greenstones in contact with the Tambourah Dome (see section 5.3.1), and was also suggested to be the case by Morant (1984) for the southern part of the Western Shaw Belt. The mineralogy of the rocks within the greenstone belts is likely to reflect the physical conditions of the early metamorphism at 3.2 Ga. The implication is that the metamorphic facies trend proposed by Morant (1984, see also Bickle et al. 1984) may be the result of two metamorphisms separated in time by at least 300 Ma.

The second major tectonic and metamorphic event also involved thermal disequilibrium. To preserve the isotopic signature of the first metamorphism, it is required that the mineralogy did not recrystallize or lose argon by volume diffusion, implying low temperatures and some degree of tectonic stability. The second regional metamorphism (M_3, M_4) in the granitoid-gneiss terrain was accompanied by temperatures in excess of 600 ^{o}C and local granitoid magmatism. It was argued by Hickman (1981, 1983) that during this event the presently observed configuration of granitoids and greenstone belts was formed. This suggetion is supported by the observation of posttectonic (D_3 nomenclature according to Bettenay et al. 1981) minerals yielding $^{40}Ar/^{39}Ar$

ages of 2965 to 2940 Ma. To explain the preservation of an earlier metamorphic signature within the rocks from the Western Shaw Greenstone Belt, which is only about 5 km wide and in intimate contact with the granitoid-gneiss domes which experienced high grade metamorphism until about 2950 Ma ago, it is necessary to postulate that dome formation at about 2950 Ma occurred over a short time interval. Uplift and erosion of the whole crustal section probably cooled the granitoid gneiss terrains sufficiently quickly to preserve thermal disequilibrium.

From the present work into the thermal history of the Archaean Pilbara Block by the $^{40}Ar/^{39}Ar$ age spectrum technique, reinforced by petrological studies (Morant 1984, Bickle et al. 1984), a revised picture of the continental crustal evolution of Archaean granitoid-greenstone terrains emerges. Metamorphism in the Archaean greenstone belts of the eastern Pilbara took place in several distinct phases, accompanied by discrete phases of rapid tectonism. Only during the second phase of regional metamorphism (M_3 and M_4 in the gneiss domes) is there some evidence that the metamorphic temperature of the greenstone belts was affected by the higher ambient temperatures in the granitoid-gneiss domes. But overprinting of the greenstone belt mineralogy during this event was only minor, and limited to relatively small areas near the contacts with the granitoid-gneiss domes. This model is in contrast with earlier interpretations which imply that thermal metamorphism of the greenstone belts was mainly the result of intrusion of granitoids (Glikson 1979), or which emphasize gradual processes (Hickman 1981, 1983). Instead, the main metamorphism of rocks in the greenstone belts is of lower amphibolite metamorphic grade, within the stability field of kyanite, and occurred before about 3200 Ma ago. In contrast, continued high grade metamorphism until about 2950 Ma in the granitoid-gneiss domes is interpreted as the result from prolonged residence at depth (i.e. below the supracrustal sequences), in combination with significantly higher concentrations of heat producing elements, compared to the greenstone supracrustal rocks (see Bickle et al. 1983). The posttectonic granites related to high grade M_4 metamorphism yielded Nd_{CHUR} ages in excess of 3100 Ma, which implies that at least a component of these granite magmas was derived from

melting of existing continental crust (Collerson and McCulloch 1982, 1983).

In this model the regional extent of the 2.85 to 2.95 Ga events is limited to the granitoid-gneiss domes, because widespread regional metamorphism would almost certainly fully have reset the argon isotopic system throughout the southeast Pilbara. As this has not happened, it must be concluded that after 2.95 Ga, igneous activity, although it occurred in a number of cases, was minor and did not affect the thermal history of the east Pilbara on a regional scale.

The current interpretation of the relation between granitoids and greenstones in the Pilbara is that the earliest greenstone extrusives and the earliest granitoid intrusives are essentially contemporaneous at about 3.6 to 3.45 Ga. Formation of the domes is regarded as a relatively late event which occurred just before 2.95 Ga. Thus dome formation occurred while the gneissic rocks experienced upper amphibolite facies metamorphism, but were still essentially in solid state. Structural observations argue against fold interference as a mechanism (Hickman 1981, 1983). Detailed structural work in the Shaw area has as yet failed to demonstrate the radial structures which are expected to accompany solid state diapirism (Bickle et al. 1984). Nevertheless, considering the substantial degree of gravitational instability between the relatively dense greenstone metavolcanics, and the lighter granitoids positioned below it, some sort of solid state diapirism, or alternatively, subsidence of greenstone supracrustals into synclinal troughs, seems to be inevitable.

5.5 Conclusion

Returning now to the aims set for this study, it ~~was~~ has been? demonstrated that the $^{40}Ar/^{39}Ar$ stepheating method of dating can be applied successfully to the tectonic and metamorphic evolution of early Archaean greenstone rocks. Precise ages of local posttectonic granites were obtained by measuring hornblendes from rocks thermally overprinted during intrusion. Further, new data on the timing of metamorphism within the Western Shaw Greenstone Belt were obtained.

There are still many questions concerning the thermal evolution of greenstone belts that need to be addressed. Some problems related to the interpretation of data from Archaean terrains were discussed in an earlier section of this chapter. The central problem is the tectonic environment in which greenstone belts were deposited, and the identification of the geological processes which allowed the formation of these impressive volcanic sequences. Current models which place the greenstone belts in marginal basins, or in continental rift environments are not easily reconciled with low heat flow, which is required to explain the often very good preservation of these rocks. Study of the metamorphic evolution of these rocks forms an important key to understanding the thermal regime of the crust during the Archaean.

Recently, in a theoretical study set against the background of field studies in Western Australia, England and Bickle (1984) have argued that the Archaean continental crust had a thermal structure similar to that of the present day. As the thickness of the crust at this time could very well have been similar to the present day crustal thickness, the physical properties of the crust were argued to have been similar to those in the present day crust as well. The implication is that orogenic activity during the Archaean may be explained by models similar to those proposed for Phanerozoic orogenic belts. Detailed geochronology can support petrological and tectonic models for the development of greenstone belts. It is demonstrated by this study that $^{40}Ar/^{39}Ar$ stepheating experiments can help to provide such detailed information. In addition, constraints as to the thermal state of the crust can be obtained. This is illustrated by the

observed presence of significant inhomogeneities in the temperature distribution between greenstone belts and gneiss terrains.

In conclusion, the $^{40}Ar/^{39}Ar$ method has the capacity to yield important new information on the metamorphic history of Archaean terrains. This kind of information is necessary for the understanding of crustal processes during the Archaean.

Table I. K-Ar data.

Code	mineral	K percent	$^{40}Ar^*$ 10^{-10} mol/g	$^{40}Ar^*/^{40}Ar$ percent	Age Ma	uncertainty 1σ
81-631	bio	6.043, 6.003	631.4	100.0	2652	25
81-631	hbl	1.304, 1.304	162.0	99.9	2892	26
81-657	hbl	0.677, 0.677	80.47	99.4	2829	26
			80.83	99.7	2836	26
81-658	hbl	0.511, 0.515	58.20	99.3	2764	25
82-312	hbl	0.177, 0.176	22.27	98.6	2915	26
82-313	mus	8.79, 8.74	931.4	99.9	2671	25
82-314	hbl	0.255, 0.253	38.25	99.2	3175	29
			38.35	99.3	3179	29
82-315	mus	7.26, 7.20	843.2	100.0	2802	28
			878.3	100.0	2861	26
82-323	hbl	0.690, 0.695	78.31	99.7	2758	25
82-324	hbl	0.111, 0.113	7.231	95.0	2020	29
82-338	hbl	0.311, 0.311	38.09	99.8	2871	26
82-339	hbl	1.22, 1.22	136.9	99.8	2746	25
82-342	hbl	0.439, 0.440	54.21	99.5	2883	26
82-343	hbl	0.678, 0.674	77.24	99.4	2773	25
82-349	hbl	0.873, 0.874	105.8	99.7	2857	26
82-350	hbl	0.224, 0.225	27.27	99.1	2859	26
			27.44	99.3	2868	26
82-351	hbl	0.175, 0.180	12.99	98.1	2176	42
			12.56	96.9	2133	42
82-352	hbl	0.146, 0.146	20.32	98.9	3058	28
			20.27	98.4	3053	28
			20.25	98.7	3052	28
82-353	hbl	0.174, 0.173	19.55	98.9	2753	25
82-354	hbl	0.332, 0.329	29.71	99.1	2442	22
			30.81	99.1	2491	23
82-356	hbl	0.162, 0.162	21.95	98.4	3020	27
			22.26	98.7	3041	28
82-361	hbl	0.196, 0.198	26.67	98.6	3018	27
82-362	hbl	0.281, 0.283	28.20	99.3	2587	23
82-375	hbl	0.388, 0.389	46.65	99.7	2844	26

The uncertainties in the ages are quoted at 1σ-level.

The abundance of $^{40}K/K_{total} = 1.167 \times 10^{-4}$ mol/mol.

The decay constants for ^{40}K are: $\lambda_{\beta^-} = 4.962 \times 10^{-10}$ yr^{-1}. $\lambda_{(e + e')} = 0.581 \times 10^{-10}$ yr^{-1}.

$^{40}Ar^*/^{40}Ar$ is percentage radiogenic ^{40}Ar of the total measured amount of ^{40}Ar.

Potassium was determined by flame photometry, using lithium as an internal standard.

hbl = hornblende, mus = muscovite, bio = biotite.

Table II $^{40}Ar/^{39}Ar$ data.

Quoted temperatures are the average of thermocouple measurement on the bottom of the sample crucible, and optical pyrometer measurement on the upper inside wall of the sample crucible. The difference between the two measurements was typically 150 ^{o}C.

The ^{39}Ar and ^{37}Ar concentrations are corrected for radioactive decay during the period between irradiation and analysis.

Laboratory standard hornblende 77-600 (K/Ar age 414.2 Ma) was used as a flux monitor for the experiments on hornblendes, laboratory standard biotite GA1550 (K/Ar age 97.9 Ma) was used as a flux monitor for the experiment on muscovite.

Reported absolute amounts were calculated from machine sensitivity (5.045×10^{-15} moles/mV), which was determined from regular measurement of standard minerals.

Uncertainties in apparent ages are quoted at 1σ-level, 0.5 percent error in parameter J is included. $\lambda = 5.543 \times 10^{-10}$ yr^{-1}.

The line blank was typically in the range between 10^{-12} to 10^{-14} moles ^{40}Ar.

T (°C)	^{36}Ar 10^{-15} moles	^{37}Ar 10^{-12} moles	^{38}Ar 10^{-13} moles	^{39}Ar 10^{-13} moles	^{40}Ar 10^{-11} moles	$^{40}Ar^*/^{40}Ar_{total}$ percent	Age Ma	Uncertainty 1σ
82-314 Hornblende								
0.4349 g, J = 0.01960, 180-250 μm								
550	18.33	0.6150	1.028	0.6579	8.527	93.7	5805	18
650	8.826	1.163	0.6765	0.9818	4.014	93.8	3878	9
740	7.383	1.997	0.3488	0.8119	2.179	90.8	3191	8
800	6.378	1.466	0.2245	0.8808	1.537	88.6	2531	7
840	7.702	1.510	0.3992	1.273	2.544	91.6	2760	8
880	10.39	3.913	0.4991	2.559	6.074	95.5	3073	8
910	13.19	8.586	0.4791	4.626	11.56	97.3	3180	8
960	11.99	8.619	0.5078	4.737	11.47	97.6	3139	8
980	6.152	4.553	0.4979	2.670	6.502	97.8	3149	8
1000	5.260	4.664	0.5085	2.766	6.546	98.3	3113	8
1020	5.842	5.839	0.5031	3.541	8.163	98.5	3077	8
1040	5.111	5.119	0.5209	3.269	7.415	98.6	3054	8
1060	4.208	5.008	0.5194	3.219	7.191	98.9	3036	8
1080	6.061	8.903	0.5115	5.473	12.81	99.2	3110	8
1090	11.61	16.83	0.5115	9.979	24.14	99.2	3160	8
1100	4.065	6.314	0.5113	3.654	8.941	99.3	3179	8
1140	3.913	5.313	0.6044	3.076	7.587	99.1	3188	8
FUSION	11.78	11.27	0.4756	6.514	16.40	98.5	3209	8
SUM	153.399	101.682	9.3271	60.688	153.600	97.0	3203	
FLUX MONITOR (0.0447 g)	12.50	10.19	0.7420	7.902	1.310	78.7		
FUSION (0.0474 g)	16.41	11.10	1.966	6.571	16.41	97.6	3183	8
82-324 Hornblende								
0.3347 g, J = 0.01936, 180-250 μm								
590	29.39	1.301	0.5801	2.607	1.752	51.0	921	5
690	10.40	0.5649	0.4635	3.107	1.776	82.9	1176	5
780	4.177	0.5274	0.3084	2.119	1.383	91.4	1387	5
810	2.631	0.8718	1.427	1.429	1.020	93.1	1496	5
850	3.924	2.687	0.2874	1.559	1.561	94.1	1887	7
880	5.273	5.820	0.3749	1.837	2.419	95.7	2258	7
910	5.962	6.292	0.3969	1.662	2.448	95.1	2403	7
930	7.359	8.394	0.4975	1.970	3.040	95.3	2473	7
950	3.821	3.632	0.2747	0.9113	1.384	94.2	2433	7
980	2.619	2.364	0.1680	0.6527	0.9333	94.0	2346	8
1010	6.174	8.113	0.4857	1.307	2.590	95.8	2847	8
1040	5.192	6.685	0.4978	0.8629	2.477	96.2	3422	8
FUSION	4.811	2.831	0.2141	0.3407	1.098	89.4	3494	10
SUM	91.733	50.0831	5.976	20.3646	23.8813	88.6	2037	
FLUX MONITOR (0.0187 g)	8.466	6.156	3.508	4.723	0.8195	76.1		
FUSION (0.0274 g)	9.803	3.934	0.3591	1.549	1.876	86.4	2020	7

T (°C)	^{36}Ar 10^{-15} moles	^{37}Ar 10^{-12} moles	^{38}Ar 10^{-13} moles	^{39}Ar 10^{-13} moles	^{40}Ar 10^{-11} moles	$^{40}Ar^*/^{40}Ar_{total}$ percent	Age Ma	Uncertainty 1σ
82-354 Hornblende								
0.6017 g, J = 0.01998, 180-250 μm								
450	25.26	0.1341	0.1884	0.4294	1.345	44.6	2407	11
550	8.604	0.3147	0.1862	0.9690	1.534	83.6	2336	7
650	14.05	6.322	0.5926	3.499	3.894	90.8	2009	6
720	8.626	3.251	0.5010	3.540	3.737	93.9	1979	6
780	10.16	0.9533	0.5948	4.960	5.268	94.4	1986	6
830	5.895	0.8392	0.6794	6.054	6.385	97.4	2014	6
870	3.279	0.7691	0.7242	6.283	6.909	98.7	2082	6
880	2.209	1.089	0.8671	6.821	7.770	99.3	2133	7
900	2.267	1.190	0.6663	5.804	6.810	99.2	2169	7
910	1.358	0.7239	0.4706	3.264	3.880	99.1	2188	7
920	1.480	1.103	0.5011	3.484	4.220	99.2	2211	7
930	1.204	0.8847	0.3547	2.394	2.972	99.1	2241	7
960	1.684	1.655	0.4375	2.884	3.737	99.0	2298	7
980	3.408	4.116	0.5718	4.072	5.906	98.9	2450	7
990	4.110	5.741	0.6601	4.418	6.930	99.0	2560	7
1000	4.542	7.506	0.7105	4.670	7.846	99.1	2660	7
1010	5.360	8.739	0.8021	4.932	8.586	99.1	2710	7
1020	4.380	7.852	0.6960	4.243	7.494	99.2	2733	7
1030	4.766	8.794	0.7069	4.445	8.059	99.2	2772	7
1050	7.045	12.65	1.030	6.020	11.18	99.1	2806	7
1070	6.021	9.813	0.8164	4.650	8.515	98.9	2783	7
1090	3.502	5.204	0.5186	2.518	4.464	98.7	2733	7
FUSION	21.40	41.20	2.966	19.15	37.92	99.3	2900	7
SUM	150.610	126.504	16.9171	109.5034	165.3690	97.3	2493	
FLUX MONITOR (0.0385 g)	13.46	9.036	4.645	6.929	1.204	73.6		
FUSION (0.0467 g)	13.13	10.10	1.198	8.372	12.75	97.7	2500	7
82-350 Hornblende								
0.3748 g, J = 0.01958, 180-250 μm								
590	5.103	0.3197	0.1006	0.2763	0.5981	75.3	2596	10
690	4.101	0.4363	0.0820	0.4688	0.4884	76.0	1696	11
760	5.978	0.3968	0.0808	0.4464	0.3597	69.1	1796	8
820	9.120	1.709	0.1680	0.9310	1.623	84.3	2463	8
870	9.570	5.740	0.4695	2.579	5.119	95.5	2819	7
910	11.92	15.37	1.303	7.896	15.99	98.7	2892	7
930	8.339	12.28	1.081	6.705	13.62	99.0	2900	7
950	5.461	8.593	0.8419	4.852	9.869	99.1	2903	7
960	3.808	6.141	0.6158	3.599	7.326	99.2	2905	7
970	2.835	5.196	0.5491	3.137	6.396	99.4	2910	7
990	2.431	4.474	0.3592	2.762	5.647	99.4	2913	8
1005	2.216	4.035	0.4780	2.535	5.174	99.4	2911	7
1020	2.025	3.308	0.4451	2.025	4.123	99.2	2905	7
1040	2.496	4.970	0.4595	2.601	5.401	99.5	2940	8
1060	4.085	8.524	0.7348	4.362	9.157	99.5	2957	7
1090	1.847	3.290	0.3603	1.671	3.512	99.3	2955	8
FUSION	8.744	2.067	0.2677	1.063	2.474	90.3	2965	8
SUM	90.079	86.8498	8.3903	47.9095	97.0772	97.3	2883	
FLUX MONITOR (0.0441 g)	9.884	10.19	5.427	7.708	1.208	83.3		
FUSION (0.0614 g)	13.25	13.71	0.3317	7.561	15.27	98.3	2881	8

T (°C)	^{36}Ar 10^{-15} moles	^{37}Ar 10^{-12} moles	^{38}Ar 10^{-13} moles	^{39}Ar 10^{-13} moles	^{40}Ar 10^{-11} moles	$^{40}Ar^*/^{40}Ar_{total}$ percent	Age Ma	Uncertainty 1σ
82-361 Hornblende								
0.5448 g, J = 0.02036, 180-250 μm								
490	17.50	0.2133	0.2107	0.3203	1.988	74.1	4227	20
590	17.75	3.559	0.4522	1.066	3.788	87.0	3623	8
690	14.11	3.131	0.4472	1.338	3.942	90.1	3377	8
780	8.128	1.455	0.3846	1.798	3.324	93.2	2724	7
820	3.669	0.8620	0.2180	1.371	2.164	95.3	2537	7
870	5.912	2.887	0.5026	2.571	4.422	96.6	2678	7
910	6.054	4.976	0.4842	2.494	4.903	97.3	2886	7
940	8.461	10.08	0.7216	3.983	8.363	98.1	3000	7
970	11.77	12.13	0.8465	4.574	9.755	97.5	3016	8
990	2.654	2.746	0.2520	1.041	2.270	97.6	3049	8
1000	4.529	4.584	0.3633	1.754	3.717	97.5	3005	8
1010	2.230	1.950	0.1669	0.7528	1.632	97.0	3031	8
1030	4.083	4.148	0.3378	1.562	3.309	97.5	3005	8
1050	3.563	3.168	0.2671	1.175	2.514	96.9	3012	8
1070	11.98	18.92	1.176	7.153	15.54	98.8	3062	8
1100	11.22	19.15	1.258	7.311	16.08	99.0	3082	8
1130	5.820	10.08	0.6868	3.847	8.539	99.0	3097	8
1150	2.466	3.220	0.2572	1.233	2.760	98.4	3100	8
FUSION	7.381	10.82	2.851	4.094	9.135	98.7	3099	8
SUM	149.28	118.0793	11.8837	49.4381	108.145	95.9	3040	
FLUX MONITOR (0.0270 g)	6.711	6.627	2.891	4.985	0.7652	81.7		
FUSION	10.21	7.825	0.5923	3.353	7.304	96.8	3033	8
82-352 Hornblende								
0.6150 g, J = 0.02035, 180-250 μm								
470	13.98	0.1780	0.1176	0.2011	0.9024	54.4	3233	22
570	7.768	0.6453	0.2291	0.4240	1.641	86.4	3724	10
640	8.764	1.171	0.2384	0.3930	1.397	82.2	3531	10
700	7.692	0.6933	0.1519	0.3445	1.304	83.0	3633	12
750	10.01	0.6493	0.1752	0.4135	1.496	80.6	3512	9
800	14.48	1.109	0.2380	0.6369	1.620	74.2	2864	10
850	11.74	2.238	0.3567	1.029	1.983	83.5	2643	7
890	8.037	3.615	0.5907	1.424	2.796	92.7	2819	7
920	7.458	4.203	0.7127	1.675	3.443	94.7	2916	8
940	9.693	8.161	1.273	3.352	7.099	97.0	2994	8
950	8.883	9.524	1.494	3.950	8.353	97.9	3005	8
970	7.288	8.145	1.309	3.404	7.258	98.0	3019	8
990	6.080	6.903	1.119	2.927	6.269	98.1	3026	8
1010	3.194	3.020	0.5445	1.277	2.766	97.6	3035	8
1030	7.752	10.88	1.697	4.764	10.20	98.7	3035	8
1050	19.19	42.41	6.610	19.11	43.12	99.6	3123	8
1070	0.8425	0.5834	1.022	0.2605	0.6564	97.0	3250	10
FUSION	6.490	11.53	1.710	5.192	12.20	99.3	3179	8
SUM	159.3415	113.794	19.5888	50.7775	114.5038	95.9	3080	
FLUX MONITOR (0.0619 g)	29.55	13.45	7.104	10.42	2.063	63.4		
FUSION (0.0297 g)	11.33	5.520	0.8973	2.424	5.574	94.9	3081	8

T (°C)	^{36}Ar 10^{-15} moles	^{37}Ar 10^{-12} moles	^{38}Ar 10^{-13} moles	^{39}Ar 10^{-13} moles	^{40}Ar 10^{-11} moles	$^{40}Ar^{*}/^{40}Ar_{total}$ percent	Age Ma	Uncertainty 1σ
82-351 Hornblende								
0.5292 g, J = 0.01992, 180-250 μm								
520	20.64	0.2673	0.2846	0.6360	2.064	47.2	2530	11
620	11.66	0.8538	0.4125	2.099	1.972	82.9	1693	6
710	6.990	1.047	0.4294	3.118	2.426	91.8	1600	6
770	6.658	1.383	0.4108	3.149	2.393	92.3	1581	6
820	6.210	2.111	0.5528	3.955	3.320	95.0	1721	6
850	4.591	2.333	0.5545	4.095	3.800	97.0	1857	6
870	3.861	2.477	0.4590	3.358	3.247	97.1	1909	6
890	4.241	2.844	0.4453	2.965	2.969	96.6	1946	6
910	13.62	3.149	0.4643	2.892	3.231	88.4	1972	6
930	2.507	2.577	0.2706	1.993	2.073	97.5	2006	7
950	4.707	4.873	0.5896	3.391	3.913	97.5	2135	6
970	5.316	6.358	0.4312	3.425	4.615	97.8	2342	7
990	4.083	5.237	0.5240	2.684	3.825	98.1	2420	7
1000	2.439	2.977	0.3109	1.513	2.228	98.0	2462	7
1010	1.991	2.606	0.2642	1.266	1.967	98.2	2539	8
1030	2.822	3.773	0.3364	1.687	2.813	98.2	2639	7
1060	3.741	5.664	0.4733	2.273	4.103	98.5	2757	7
1100	7.349	11.63	0.3393	4.305	8.650	98.7	2914	7
FUSION	4.136	3.817	0.3485	1.532	3.102	97.2	2901	7
SUM	117.563	65.9771	7.9012	50.336	62.711	94.5	2203	
FLUX MONITOR (0.0407 g)	7.314	9.180	4.548	6.850	1.014	86.7		
FUSION (0.0513 g)	7.759	6.149	0.5230	4.835	5.820	97.0	2180	7
82-356 Hornblende								
0.5617 g, J = 0.02004, 180-250 μm								
450	36.37	0.7431	0.9698	0.7134	3.186	66.5	3510	11
550	14.77	1.591	1.230	0.5358	1.861	77.3	3377	9
650	17.04	5.820	1.544	0.7463	3.941	88.6	4316	10
720	11.43	2.289	0.6601	0.7425	2.328	86.4	3391	8
780	9.148	1.456	0.8081	1.004	1.590	83.0	2355	7
830	8.176	2.240	1.250	1.463	2.236	90.1	2404	7
870	15.59	3.178	1.713	1.336	2.770	84.4	2741	8
910	19.91	8.238	9.022	3.738	7.825	93.4	2897	7
940	25.49	14.18	21.09	7.643	15.40	95.9	2877	7
960	16.63	12.17	20.02	7.142	14.10	97.3	2867	7
970	15.47	7.232	12.11	4.335	8.767	95.5	2874	7
980	14.04	5.797	9.871	3.522	7.179	94.9	2876	7
1000	12.02	6.282	10.91	3.910	7.880	96.2	2879	7
1020	10.31	5.402	9.244	3.358	6.957	96.3	2920	8
1050	4.350	4.775	7.722	2.870	6.136	98.6	3001	9
1080	8.046	11.70	15.57	5.771	13.85	99.0	3182	8
FUSION	19.46	25.96	32.97	12.33	30.66	98.9	3234	8
SUM	258.250	119.0531	156.704	61.16	136.666	94.4	3010	
FLUX MONITOR (0.0559 g)	11.42	13.49	6.749	10.41	1.546	85.9		
FUSION (0.0417 g)	24.10	8.505	11.25	4.362	9.906	93.6	3016	8

T (°C)	^{36}Ar 10^{-16} moles	^{37}Ar 10^{-14} moles	^{38}Ar 10^{-13} moles	^{39}Ar 10^{-12} moles	^{40}Ar 10^{-10} moles	$^{40}Ar^*/^{40}Ar_{total}$ percent	Age Ma	Uncertainty 1σ
82-315 Muscovite								
0.10050 g, J = 0.02199, 180-250 μm								
460	40.32	0.4039	0.2640	0.1465	0.1442	91.7	1973	6
510	13.28	0.1369	0.1690	0.09934	0.1178	96.6	2271	7
560	9.980	0.5949	0.3337	0.1857	0.2432	98.8	2430	7
610	10.46	0.5646	0.4917	0.2748	0.3830	99.2	2519	7
660	17.08	-	0.3215	1.144	1.778	99.7	2676	7
710	8.432	0.2414	0.3176	0.7385	1.212	99.8	2754	7
730	9.304	0.6223	0.3065	0.7945	1.345	99.8	2797	7
750	9.810	-	0.3109	1.129	1.967	99.8	2840	7
770	8.637	1.739	0.3207	1.843	3.292	99.9	2876	8
790	4.874	4.113	0.3033	3.513	6.388	100.0	2903	8
800	-	-	0.2751	1.868	3.404	100.0	2906	7
810	-	-	0.2805	2.042	3.742	100.0	2914	7
820	3.576	-	0.2764	1.872	3.431	100.0	2914	7
840	-	-	0.2702	1.885	3.460	100.0	2917	7
860	-	3.152	0.2684	2.836	5.226	100.0	2922	7
880	-	2.389	0.3104	2.103	3.867	100.0	2919	7
910	7.944	-	0.2881	2.489	4.573	100.0	2917	8
950	7.633	7.808	0.2895	4.514	8.294	100.0	2918	7
1000	-	7.016	0.2788	5.854	10.80	100.0	2924	8
FUSION	55.08	7.609	0.2958	8.143	15.22	100.0	2941	7
SUM	198.466	36.39	5.9754	43.474	85.674	99.3	2910	
FLUX MONITOR (0.0254 g)	3221	9.388	16.06	10.60	1.223	22.0		
FUSION (0.0109 g)	1601	2.749	4.536	3.497	6.790	93.0	2893	8

T (°C)	^{36}Ar 10^{-15} moles	^{37}Ar 10^{-12} moles	^{38}Ar 10^{-13} moles	^{39}Ar 10^{-13} moles	^{40}Ar 10^{-11} moles	$^{40}Ar/^{40}Ar^*$ percent	Age Ma	Uncertainty 1σ
81-658 Hornblende								
0.3163 g, J = 0.01777, 180-250 μm								
560	11.97	0.1475	0.2153	0.4861	1.146	69.2	2459	11
660	4.009	0.2401	0.1884	0.7183	1.071	89.1	2191	9
740	3.094	0.8891	0.2204	4.850	1.445	94.0	2372	7
810	2.273	0.5900	0.1961	1.157	1.629	96.2	2216	8
870	1.466	0.4044	0.1989	1.348	1.735	97.7	2121	7
920	1.775	0.4495	0.3648	2.026	2.667	98.2	2154	7
960	1.594	0.4558	0.3139	1.618	2.257	98.1	2227	7
980	1.480	0.5724	0.2968	1.253	1.911	98.0	2343	7
1000	1.742	0.7980	0.2989	1.202	2.048	97.8	2491	7
1010	1.688	0.9306	0.2900	1.165	2.155	98.1	2608	8
1020	1.389	1.021	0.3495	1.186	2.280	98.6	2668	7
1030	1.560	1.431	0.4580	1.572	3.107	98.9	2713	8
1040	2.075	1.994	0.6544	2.132	4.327	99.0	2751	7
1045	1.899	2.371	0.6252	2.509	5.178	99.3	2779	8
1050	2.183	2.802	0.6361	2.934	6.109	99.3	2793	8
1055	1.764	2.892	0.6758	3.032	6.332	99.6	2801	8
1060	2.164	3.220	0.7299	3.364	7.078	99.5	2810	8
1070	2.588	4.570	1.021	4.757	10.07	99.6	2820	8
1080	3.213	6.486	1.414	6.712	14.27	99.7	2828	8
1090	3.053	7.070	1.580	7.311	15.66	99.8	2840	8
1100	15.53	26.99	6.807	27.98	59.91	99.6	2837	8
1120	7.838	12.19	2.633	12.22	26.11	99.5	2833	8
FUSION	3.298	5.928	0.6660	2.894	6.185	99.3	2840	8
SUM	79.645	84.4424	20.8334	94.4264	184.68	98.7	2700	
FLUX MONITOR (0.0353 g)	3.130	3.330	6.198	2.365	4.122	84.7		
FUSION (0.0463 g)	5.544	7.369	1.643	7.789	15.96	99.4	2771	8

T (°C)	^{36}Ar 10^{-15} moles	^{37}Ar 10^{-12} moles	^{38}Ar 10^{-13} moles	^{39}Ar 10^{-13} moles	^{40}Ar 10^{-11} moles	$^{40}Ar^{*}/^{40}Ar_{total}$ percent	Age Ma	Uncertainty 1σ
83-64 Hornblende								
0.4725 g, J = 0.01977, 100-180 μm								
480	9.042	0.1721	0.2701	0.3352	0.9666	72.5	2957	12
580	7.677	1.008	1.112	1.073	1.625	86.6	2317	8
680	6.334	0.7556	0.6765	0.9687	2.135	91.5	2908	9
730	5.119	0.2985	0.5573	0.8756	1.458	89.8	2484	7
780	5.390	0.2372	0.4310	0.6984	0.9777	83.9	2169	7
830	6.286	0.3696	0.5476	0.7641	1.056	82.7	2137	8
870	4.703	0.4780	0.4442	0.5966	0.9446	85.7	2314	8
910	6.456	1.037	0.7898	0.8898	1.603	88.7	2583	7
950	8.849	3.587	7.141	5.679	10.30	97.8	2722	8
980	6.134	5.293	17.47	14.15	24.72	99.4	2691	7
1000	7.732	10.67	36.75	30.74	53.59	99.7	2692	7
1010	6.261	6.231	20.30	17.61	30.59	99.6	2685	7
1020	4.447	5.433	17.43	15.28	26.33	99.7	2675	7
1030	4.766	6.438	21.24	18.51	31.84	99.7	2673	7
1040	3.631	4.812	16.45	14.28	24.72	99.7	2683	7
1050	2.772	4.394	15.21	13.21	22.93	99.8	2686	7
1070	3.356	6.751	24.16	20.59	36.02	99.9	2699	7
1090	8.844	16.47	62.69	50.90	90.29	99.9	2718	7
1120	11.32	14.79	54.98	43.10	77.05	99.7	2727	7
1160	21.31	8.150	27.95	21.98	39.08	99.8	2720	7
FUSION	5.573	8.196	25.32	20.26	36.02	99.7	2720	7
SUM	146.002	105.571	351.9195	292.490	514.2459	99.2	2698	
FLUX MONITOR (0.0655 g)	14.05	12.27	12.86	9.435	1.527	79.9		
FUSION (0.0226 g)	9.625	4.923	16.13	13.56	24.06	99.0	2706	7
81-657 Hornblende								
0.3370 g, J = 0.01730, 180-250 μm								
470	4.869	0.01555	0.1637	0.5932	0.3312	56.7	2038	20
570	2.855	0.07591	0.1604	0.2862	0.3423	75.5	1700	15
620	2.243	0.05446	0.08046	0.1643	0.2641	75.1	2037	25
670	1.199	0.06881	0.07669	0.1340	0.2330	85.0	2295	34
720	1.098	0.09813	0.05793	0.1197	0.2193	85.6	2374	29
770	0.6466	0.05757	0.04507	0.07643	0.1176	84.2	2129	54
820	1.123	0.1142	0.07916	0.1347	0.2117	84.8	2165	15
860	1.272	0.09634	0.05058	0.1264	0.2166	83.0	2248	24
890	1.107	0.1154	0.05860	0.1475	0.2567	87.7	2338	15
930	1.391	0.1264	0.06465	0.1553	0.3047	86.9	2486	14
950	1.872	0.2119	0.1031	0.2672	0.5843	90.8	2696	14
970	1.601	0.2932	0.8499	0.3871	0.8633	94.8	2784	10
990	1.271	0.6206	0.2550	0.8633	1.902	98.3	2818	9
1010	2.256	1.834	0.7557	0.2649	5.921	99.1	2850	9
1020	1.504	1.815	0.7423	2.682	5.964	99.5	2848	9
1030	2.487	2.509	1.013	3.754	8.402	99.4	2855	9
1035	1.932	2.453	1.004	3.698	8.270	99.6	2856	9
1040	1.883	2.671	1.095	4.038	9.009	99.6	2854	11
1050	2.830	3.561	1.437	5.447	12.15	99.6	2852	8
1060	4.786	8.044	3.386	12.35	27.67	99.7	2862	8
1070	2.939	4.044	1.691	6.245	13.98	99.6	2858	8
1080	2.720	7.008	3.013	10.82	24.26	99.9	2865	17
1090	6.809	14.63	6.262	22.89	51.18	99.9	2860	8
1100	6.270	11.63	4.710	18.17	40.91	99.8	2869	8
1110	2.979	29.73	3.192	12.14	27.29	99.7	2859	8
1120	1.585	3.618	1.559	5.620	12.67	99.9	2872	8
FUSION	8.430	4.334	1.834	6.728	15.36	98.6	2872	8
SUM	71.8776	99.829	33.73924	120.686	268.8828	99.2	2852	
FLUX MONITOR (0.0353 g)	8.815	9.355	-	6.591	1.125	84.2		
FUSION (0.0841 g)	4.787	3.122	2.849	4.768	10.77	99.6	2871	11

T (°C)	^{36}Ar 10^{-15} moles	^{37}Ar 10^{-12} moles	^{38}Ar 10^{-12} moles	^{39}Ar 10^{-13} moles	^{40}Ar 10^{-11} moles	$^{40}Ar^*/^{40}Ar_{total}$ percent	Age Ma	Uncertainty 1σ
83-64 Plagioclase								
0.4915 g, J = 0.02011, 100-180 μm								
320	27.57	0.3946	0.6067	1.014	5.700	85.8	4281	12
420	8.733	1.337	0.3684	1.764	2.031	87.9	2010	7
500	8.806	3.168	0.6146	3.028	2.963	92.2	1875	6
560	4.558	3.445	0.4133	2.762	1.867	94.4	1499	6
600	3.000	3.191	0.3969	2.241	1.280	95.3	1343	5
640	3.099	3.601	0.3796	2.344	1.377	95.7	1375	5
680	3.348	4.853	0.5136	2.933	1.801	96.9	1431	5
720	5.847	9.151	0.8407	5.704	3.849	97.6	1534	5
760	5.512	8.758	1.031	6.468	4.725	98.2	1622	6
800	6.087	9.138	0.8819	7.087	5.312	98.1	1648	6
830	3.815	5.935	0.6695	4.338	3.128	98.1	1606	5
860	4.854	6.391	0.8128	5.082	3.698	97.6	1611	6
890	3.900	4.444	0.6016	3.734	2.709	97.2	1602	6
920	3.895	3.289	0.4529	2.838	2.098	95.9	1607	5
950	4.490	3.102	0.5115	2.660	2.267	95.4	1757	6
990	6.343	3.819	0.6344	2.995	3.311	95.4	2064	6
1040	10.63	6.470	0.8588	3.715	6.183	95.9	2610	7
1100	10.89	7.883	0.8635	3.016	6.968	96.4	3097	8
1180	14.90	13.23	0.9861	3.313	10.19	96.8	3553	9
FUSION	20.40	16.15	0.9807	2.962	9.364	95.1	3585	9
SUM	160.677	117.7496	13.3385	69.998	80.821	94.1	2139	
FLUX MONITOR (0.0821 g)	18.74	18.10	12.86	13.82	2.150	81.7		
FUSION (0.0853 g)	22.04	19.08	1.749	11.35	12.76	96.2	2099	6

T (°C)	^{36}Ar 10^{-15} moles	^{37}Ar 10^{-12} moles	^{38}Ar 10^{-13} moles	^{39}Ar 10^{-13} moles	^{40}Ar 10^{-11} moles	$^{40}Ar^*/^{40}Ar_{total}$ percent	Age Ma	Uncertainty 1σ
82-376 Hornblende								
0.4058 g, J = 0.01980, 180-250 μm								
530	29.65	0.2598	0.5770	1.726	1.559	43.9	1047	9
630	14.38	0.3021	1.748	6.686	3.047	86.1	1037	4
720	6.469	0.1773	1.294	5.295	5.736	96.7	2026	7
780	5.327	0.2101	1.204	2.791	3.935	96.0	2352	8
830	6.159	0.3319	0.9706	2.319	3.153	94.3	2281	8
870	5.517	0.4359	0.8274	1.993	2.339	93.2	2080	7
910	6.324	0.9085	1.166	2.369	3.094	94.2	2231	7
950	8.663	2.862	2.836	4.468	7.368	96.9	2579	9
980	9.798	6.265	1.596	7.813	13.75	98.3	2692	8
1000	11.89	10.49	7.856	12.23	21.30	98.8	2684	8
1010	5.648	5.816	4.375	6.681	11.88	99.0	2717	8
1020	6.671	7.181	5.260	8.124	14.10	99.0	2684	8
1030	6.443	7.582	5.547	8.395	14.54	99.1	2682	8
1040	5.837	7.969	5.478	8.626	14.79	99.3	2671	8
1060	5.942	8.689	5.936	9.177	15.47	99.4	2648	7
1080	5.213	8.625	5.545	8.788	14.61	99.5	2630	7
1110	3.297	5.787	3.659	5.688	9.934	99.5	2701	7
1140	4.342	8.092	5.403	7.998	14.75	99.6	2778	8
FUSION	7.705	5.531	3.582	5.536	10.37	98.3	2780	8
SUM	155.275	87.5146	64.86	116.703	185.725	97.5	2547	
FLUX MONITOR (0.0787 g)	16.23	16.87	12.95	13.09	2.021	83.6		
FUSION (0.0434 g)	7.426	4.707	3.533	6.079	9.843	98.2	2574	13

Chapter 6

The age of deposition and subsequent metamorphism of the Mount Narryer metasedimentary belt, Western Australia.

6.1 Introduction

The Western Gneiss Terrain of the Archaean Yilgarn Block in Western Australia has been recognized for some time as the oldest part of this Archaean crustal block (Arriens 1971, Nieuwland and Compston 1981, De Laeter et al. 1981a, b). The geology differs from the eastern provinces of the Yilgarn Block in that greenstone belts are virtually absent and high grade gneisses predominate. The Western Gneiss Terrain has been interpreted as the sialic basement on which the greenstone sequences in the eastern provinces were deposited (Gee et al. 1981).

The Narryer Metamorphic Belt (Williams et al. 1983), which forms part of the northern section of the Western Gneiss Terrain, has been the focus for geochronological studies since its antiquity was established by a well fitted Rb-Sr whole rock isochron on banded gneisses indicating an age of 3347 $\pm$ 43 Ma with an initial $^{87}Sr/^{86}Sr$ ratio of 0.7047 $\pm$ 0.0005 (De Laeter et al. 1981a). This age was interpreted as a time of intracrustal reworking of the gneisses, with a prior crustal residence time of about 200 Ma. The latter was supported by subsequent Nd_{CHUR} model ages of 3630 $\pm$ 40 Ma for the banded Meeberrie Gneiss and 3510 $\pm$ 50 Ma for the intrusive more massive Dugel Gneiss (De Laeter et al. 1981b).

The discovery of several 4100 to 4200 Ma old detrital zircons in a concentrate from a quartzite from the Mount Narryer metasedimentary sequence (Froude et al. 1983) led to an intensive program of geochronology of the rocks in the vicinity, with the aim of documenting the geological history of the region and finding any exposed remnants of the circa 4200 Ma old crust from which the detrital zircons were derived.

The present study concentrates on the age of deposition of the metasedimentary sequence at Mount Narryer and its subsequent metamorphic history. These aspects of the geological history are important for the interpretation of the crustal evolution of the Archaean Yilgarn Block, because knowledge of the time of deposition of these units will constrain the time at which very old crust was still exposed at the earth's surface. Discussion of the age of deposition is based on ion microprobe analyses of the youngest near-concordant zircons in the quartzites. The

subsequent thermal evolution of the region is examined by the K-Ar and the $^{40}Ar/^{39}Ar$ age spectrum method. The argon isotopic system is relatively sensitive to subsequent thermal disturbance, making it possible to obtain detailed information on the thermal history of the region after crystallization of the rocks.

6.2 Geology

The geology of the Narryer Metamorphic Belt has been described by Williams et al. (1983) and Williams and Myers (1985). The main units are two orthogneisses, the adamellitic Meeberrie Gneiss and the granodioritic Dugel Gneiss, and the metasedimentary sequence. Contacts between the metasedimentary sequence and the adjacent Meeberrie Gneiss are zones of intense deformation, with the metasediments being interpreted as younger than the gneisses on the basis of a less complex history of deformation (Myers and Williams 1985). The tentative interpretation is that the gneisses represent the basement on which the sediments were deposited.

The ages of the igneous precursors to the Meeberrie and the Dugel Gneisses have been unequivocally determined at 3688 $^{+33}_{-23}$ Ma and 3416 $^{+82}_{-50}$ Ma respectively by ion microprobe intragrain U-Pb analyses of zircons, with subsequent metamorphic overgrowth of zircon developed at 3319 $^{+35}_{-16}$ Ma (Kinny et al. 1985). The Rb-Sr whole rock isochron age of 3347 $\pm$ 43 Ma obtained by De Laeter et al. (1981) on samples from the Meeberrie Gneiss was interpreted by them as recording high grade metamorphism of the region. Recently, ion microprobe spot analysis of magmatic zircons from a porphyritic granitoid has yielded U-Pb ages of about 3300 Ma (Kinny et al. in prep.). Thus, in the gneisses of the Narryer Metamorphic Belt there is evidence for a high grade metamorphism closely followed by granitic magmatism about 3300 to 3350 Ma ago. Younger granitoids intruded the Meeberrie Gneiss and the southern part of the metasedimentary sequence; these rocks yielded a Rb-Sr whole rock isochron age of 2579 $\pm$ 122 Ma (MW = 0.31) and Nd_{CHUR} ages of circa 3100 Ma (De Laeter et al. 1985). Recent zircon age determinations (Kinny et al. in prep.) have shown that the Rb-Sr age is close to the magmatic age at about 2700 Ma.

The contact between the Meeberrie and Dugel Gneisses is diffuse, but is interpreted as intrusive. Within the Dugel Gneiss, a highly deformed anorthosite mass was found, named the Manfred Complex (Myers in press). It consists of metamorphosed anorthosites, leucogabbros, gabbros and ultramafic rocks. Owing to intense subsequent deformation, rocks belonging to the Manfred Complex presently occur in trains of xenoliths which may be up to

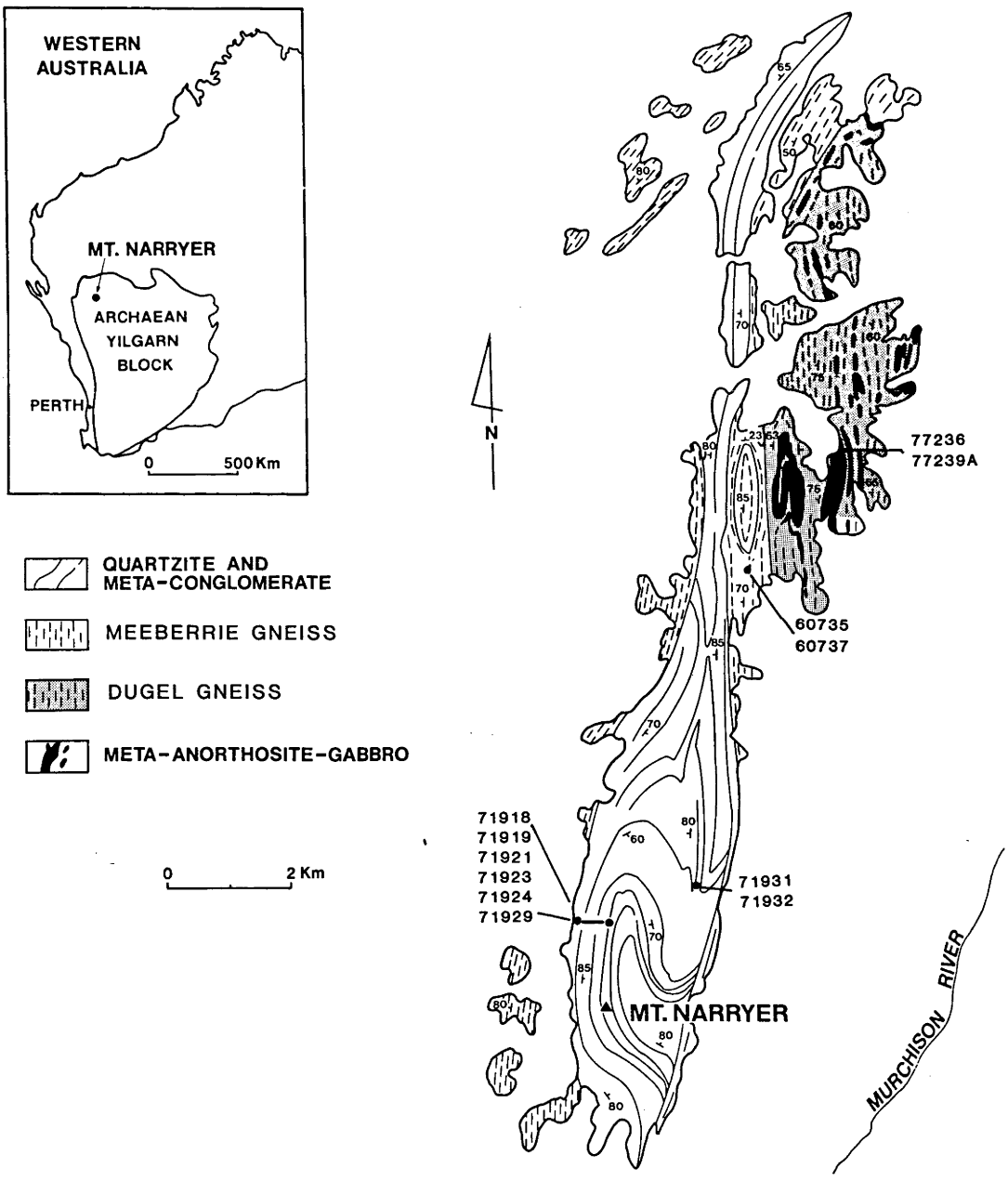

Figure 6.1. Location and simplified geological map of the Mount Narryer metamorphic belt (After Williams and Myers 1984). Sample locations mentioned in the text are shown.

1 km long. The anorthosites were found to contain igneous zircons, which were dated by ion microprobe at 3750 $^{+72}_{-40}$ Ma (Kinny et al. 1985), making these rocks the oldest found in Australia so far.

The metasedimentary section consists of a series of metamorphosed quartz-sandstones, with interbedded conglomeratic rocks, metapelitic units, and two concordant amphibolites. The total stratigraphic thickness of the section is about 2 km. The section is folded, but in the southern part of the belt deformation has been minor and primary sedimentary features, as for example crossbedding and conglomeratic pebbles, are well preserved. Towards the north, the belt becomes narrower, and concomitantly, the intensity of deformation increases.

6.3 Petrology

The two amphibolites from the Mount Narryer metasedimentary sequence contain hornblende, biotite, plagioclase and quartz as the dominant mineral assemblage. A younger greenschist facies assemblage, consisting of chlorite, actinolite and epidote, overprints the high grade assemblage.

The quartzite samples for ion microprobe U-Pb zircon analysis were taken from Geological Survey of Western Australia sample locations 71921, 71924 and 71932 (Fig. 6.1). The former two samples have the mineral assemblage sillimanite, cordierite, biotite, and garnet, while 71932 shows a considerably more calcic assemblage of plagioclase (bytownite), biotite, and secondary zoisite and sericite. All samples show a gneissic fabric, with sillimanite, biotite, or elongated quartz grains defining a crude preferred orientation. All samples contain more than 90 percent quartz.

Geothermometry and geobarometry on biotite-garnet pairs, and on cordierite-garnet pairs (Ferry and Spear 1978, Martignole and Sisi 1981) on quartzite samples 71919, 71923, and 71929 yielded temperature estimates in the range 420 to 720 ^{o}C and pressures of 250 to 300 MPa. These results indicate substantial re-equilibration within the original high grade assemblage, the highest temperature estimates approaching values consistent with metamorphic grades near the amphibolite-granulite transition. Pressure estimates may also be affected by subsequent overprinting. These values are somewhat lower than earlier results of garnet-cordierite geothermometry and barometry by Blight and Barley (1981), who reported estimates of 510 MPa and 780 ^{o}C for Mount Narryer quartzite. Secondary muscovite from quartzite 71928, formed during greenschist facies grade overprinting, has an Si^{4+} content of 6.2 (structural formula based on 22-Oxygen), which would correspond at temperatures of 300 to 350 ^{o}C to metamorphic pressures of about 200 MPa (Velde 1967).

The petrology of the samples used in this study suggests that the metasedimentary rocks have experienced one phase of high grade metamorphism. During a subsequent event, local deformation in some parts of the sequence was accompanied by recrystallization at greenschist facies grade.

6.4 Results

6.4.1 U-Pb zircon dating

U-Th-Pb isotopic analyses of individual zircon grains from metasedimentary rocks are capable of providing constraints on the time of deposition of the sequence. The true crystallization age of the youngest demonstrably detrital zircons provides an older limit to the time of deposition, whereas the age of any metamorphic zircon grown in situ (new distinct crystals or overgrowths on older zircons) may provide the younger limit to the period of deposition.

Procedures for U-Th-Pb isotopic analysis of zircon by the Australian National University ion microprobe (SHRIMP) follow those of Kinny et al. (1985) and will not be further discussed here.

Preliminary data from Mount Narryer quartzite 71932 (Froude et al. 1983), plus new data from 71932 and two other samples, 71921 and 71924, have been thoroughly re-evaluated in the light of our improved understanding of the relation between measured sputtered-ion ratios and true target composition, over a range in operating conditions (Compston et al. 1984, Williams et al. 1984). The complete data set will be presented elsewhere (Froude 1985), and this discussion will be limited to those analyses relevant to estimation of the deposition age of the metasedimentary rocks, which are the youngest near-concordant analyses of detrital grains.

To the present time, 272 zircons from concentrates from three quartzite samples have been analyzed. Some crystals have been analyzed repeatedly. Analyses varied from single mass scans, made to obtain an estimate of the Pb/Pb and U/Pb isotopic ratios in the target, to up to three sets of seven field-stepping cycles through the isotopic species of interest for the more interesting (normally the more concordant) zircon grains, as identified by the reconnaissance scans.

Eight zircons analyzed for one or more data sets yielded near concordant ages of 3350 Ma or less, seven of these coming from the most intensely studied sample (71932). The data for these zircons are presented in table 6.I and plotted on a Concordia diagram in Fig. 6.2, on which analyses of other, more discordant zircons are also shown. Of the eight grains seven were analyzed within regions of euhedral growth zonation, which are considered to be the product of crystallization from a melt (Fig. 6.3a, b). This rules out the possibility of their being metamorphic in origin. The other (grain no. 32) is a dark brown, translucent to opaque grain that may be metamorphic or igneous in origin (Figure 6.3c, d). Rarely do any zircons from the quartzites show structural division into cores and distinctly younger overgrowths, and in no case have these rare overgrowths been found to be as young as those zircons discussed above. Examination of zircon grains from the quartzites by SEM revealed no microscopic overgrowth of zircon, but showed many features attributable to metamorphic corrosion such as necking and dissolution pits. Finely pitted and abraded surfaces expected of zircons from mature sediments are absent, indicating either a local source for the quartzites, or subsequent removal of these features by metamorphic corrosion.

It is difficult to precisely determine the true crystallization age of discordant zircons from the Mount Narryer quartzites because they have almost certainly lost variable amounts of lead during uplift and erosion of the source rocks and re-deposition in sediments, and subsequently lost more lead during high grade metamorphism of the sediments, and again at zero-age due to recent uplift and exposure of the quartzites.

Nevertheless, the fact that grains 9, 88, 104, 105 and 125 from sample 71932, and grain 12 from 71921, which are clear, crack- and inclusion-free grains lacking obvious crystal damage, are all less than 15 percent discordant mitigates against significant ancient lead loss, and indicates that the $^{207}Pb^*/^{206}Pb^*$ ages (* = radiogenic) are good estimates of their crystallization ages. This conclusion is borne out by application of a simple two stage episodic Pb loss model to the data (Compston and Williams in prep.), the details of which are given in Table 6.I. The $^{207}Pb^*/^{206}Pb^*$ ages of these grains range from

Figure 6.2. Concordia Diagram for zircons from Mount Narryer quartzites 71921 and 71932. Error boxes are at 1σ-level. Shaded error boxes are those discussed in the text and are labelled with grain spot number. Inset shows the data for all zircons analyzed for at least one 7-cycle data set.

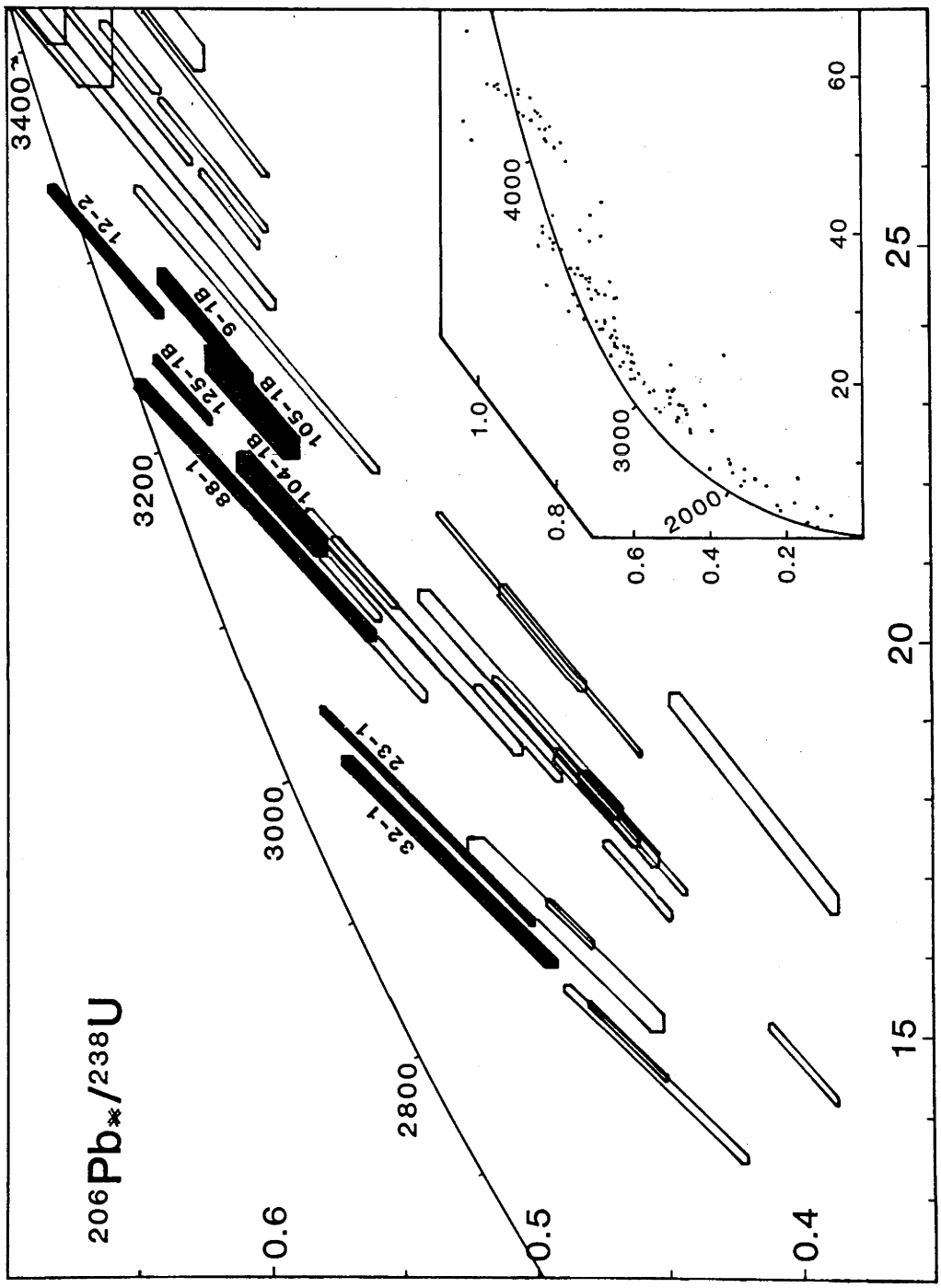
3400
3200
3000
2800
0.6
0.5
0.4
$^{206}Pb_*/^{238}U$
$^{207}Pb_*/^{235}U$
15
20
25
12-2
9-1B
125-1B
105-1B
104-1B
88-1
23-1
32-1
4000
3000
2000
1.0
0.8
0.6
0.4
0.2
20
40
60

3351 to 3241 Ma and in each case the modelled original age is only up to about 20 Ma older (Table 6.I).

By the same arguments, and again by virtue of their near-concordancy, grains 23 and 32 of sample 71932 clearly represent a significantly younger detrital component. Grain 23 which shows remnant euhedral zoning (Figure 6.3b) gave a $^{207}Pb^*/^{206}Pb^*$ age of 3109 ± 11 Ma, while grain 32 which is a massif metamict zircon (Figure 6.3c) gave an age of 3080 ± 23 Ma. Again their modelled original ages are only a little older.

These results show, contrary to previous interpretations, that the maximum age of deposition of the metasedimentary sequence is at most about 3240 Ma, and is probably as young as about 3100 Ma.

6.4.2 Argon dating

Laboratory technique for conventional K/Ar dating was described by McDougall and Schmincke (1977), and for $^{40}Ar/^{39}Ar$ analysis by McDougall (1974) and McDougall and Roksandic (1974). The samples used for $^{40}Ar/^{39}Ar$ analysis were irradiated for two full cycles of the HIFAR reactor of the Australian Atomic Energy Commission (one operational cycle is 21 days). The correction factors for interference of argon isotopes produced by isotopes of potassium and calcium were reported by Tetley et al. (1980). The measured amounts of ^{37}Ar and ^{39}Ar, formed during irradiation, were corrected for radioactive decay during the period before analysis using the modified equation of Wijbrans (1985).

A number of minerals from the Mount Narryer area were analyzed by the K-Ar method (Table 6.II). Hornblendes 82-376 from location 71918 and 82-377 from location 71929 in the metasedimentary sequence yielded ages of 2610 +24 Ma and 3664 ± 39 Ma respectively. A substantially altered biotite (82-377) from amphibolite 71929 was measured at 1789 ± 32 Ma. The high apparent age of the hornblende from this sample may well be the product of locally derived excess argon, because in thin section it is observed that the biotite has been partially recrystallyzed to chlorite. Two more hornblendes (83-59, 83-64) and two plagioclases (83-59, 83-64) were extracted from anorthosites 77239A and 77236 of the Manfred Complex. The hornblendes yielded

ages of 2787 ± 25 and 2667 ± 24 Ma, and the plagioclases were measured at 1954 ± 18 and 2072 +19 Ma respectively. Biotites 85-1, 85-2 and 85-3 were sampled from location 71931 in the metasedimentary section, and from locations 60735 and 60737 in the Meeberrie Gneiss east of Mount Narryer. Biotite 85-1 yielded an age of 2022 ± 22 Ma, and biotites 85-2 and 85-3 yielded ages of 1887 ± 17 Ma and 1778 ± 16 Ma respectively.

Three $^{40}Ar/^{39}Ar$ stepheating experiments were carried out to help clarify the metamorphic history (Fig 6.4, Table 6.III). Hornblende 82-376 from concordant amphibolite 71918 yielded ages in the initial steps of about 1000 Ma increasing with some minor secondary structure to a maximum of 2780 Ma. The K/Ca ratio, calculated from the $^{39}Ar_K/^{37}Ar$ ratio, in the initial steps of the experiment was in the order of 1.5, which may indicate the contribution of a phase with a chemistry significantly different from hornblende ($K/Ca=0.53*^{39}Ar_K/^{37}Ar$, calculated from the chemistry and repeated $^{40}Ar/^{39}Ar$ analysis of laboratory standard hornblende 77-600). The high K/Ca ratios and the low ages obtained in the low temperature steps of the experiment may be caused by some minor biotite contamination. The K/Ca ratios in the remaining part of the age spectrum are typical for hornblende. Hornblende 83-64 from anorthosite 77236 has yielded a very regular age spectrum with apparent ages rising from 2670 to 2720 Ma, and an integrated age of 2704 ± 7 Ma over more than 90 percent of the gas release. A plagioclase of the same sample gave a U- or saddle-shaped age spectrum. The apparent ages in the first steps decrease from 4280 Ma to 1340 Ma. In the middle part of the spectrum, the ages increase to an apparent plateau with an integrated age of 1620 ± 6 Ma. In the last 28 percent of the gas release, apparent ages increase to values of 3540 Ma.

The hornblendes from the amphibolites and the anorthosites are part of the high grade mineral assemblage. Their age spectra are interpreted as recording cooling below the closure temperature of hornblende for argon (i.e. about 500 °C, Harrison et al. 1979, Jäger 1979) between 2720 to 2780 Ma ago, implying that high grade metamorphism occurred about 2800 Ma ago. Hornblendes 83-59 and 83-64 from anorthosite 77239A and 77236 yielded a K-Ar age of 2787 ± 25 Ma and a $^{40}Ar/^{39}Ar$ age for the highest temperature steps of 2720 Ma respectively, which are in

Figure 6.3. Transmitted light photomicrographs of selected zircons from Mount Narryer quartzite, number 71932. Magnification is approximately 100x. Sites of analytical spots are as shown, (a) grain 88, showing zonation typical of magmatic crystallization, (b) grain 23, (c) grain 32, a metamict zircon.

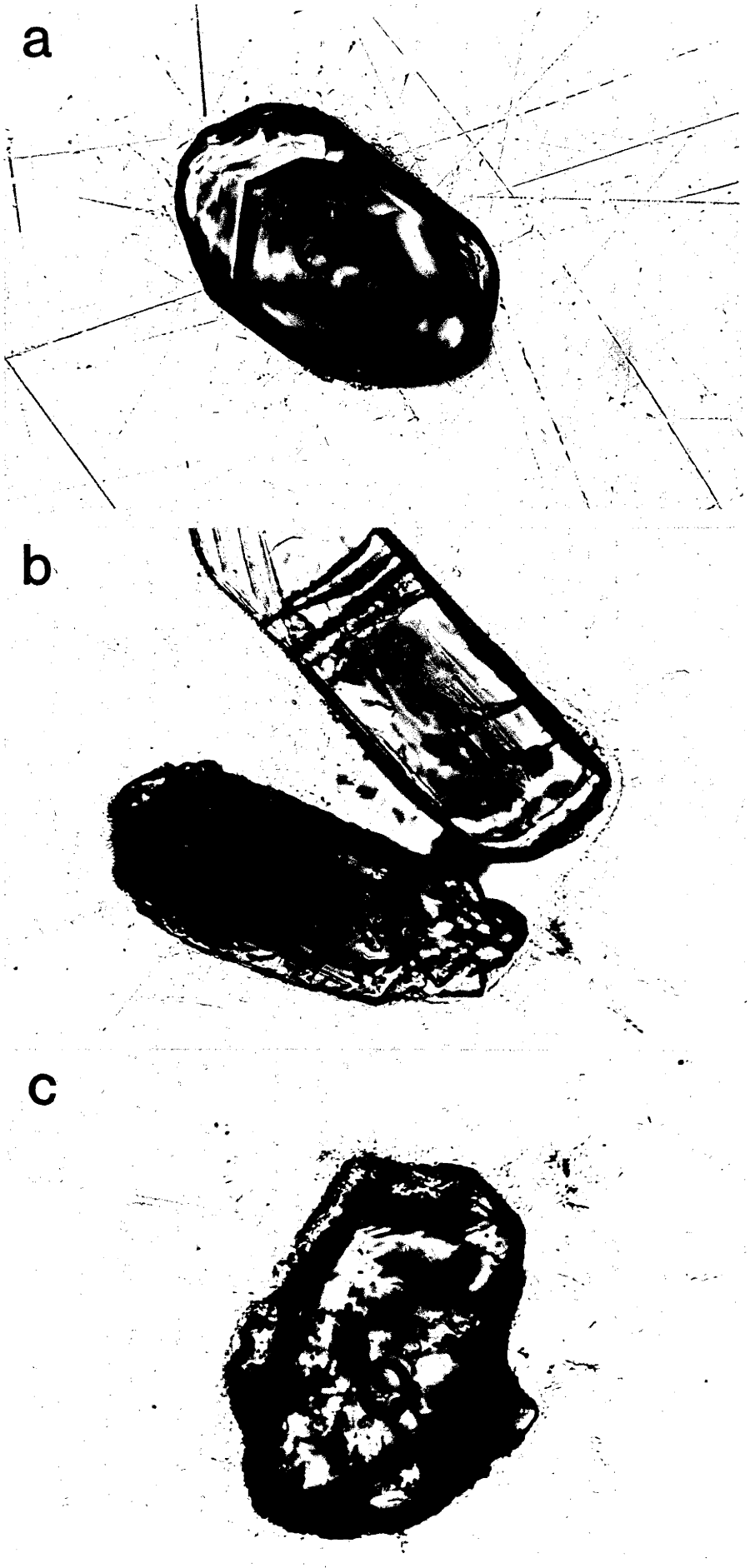
a
b
c

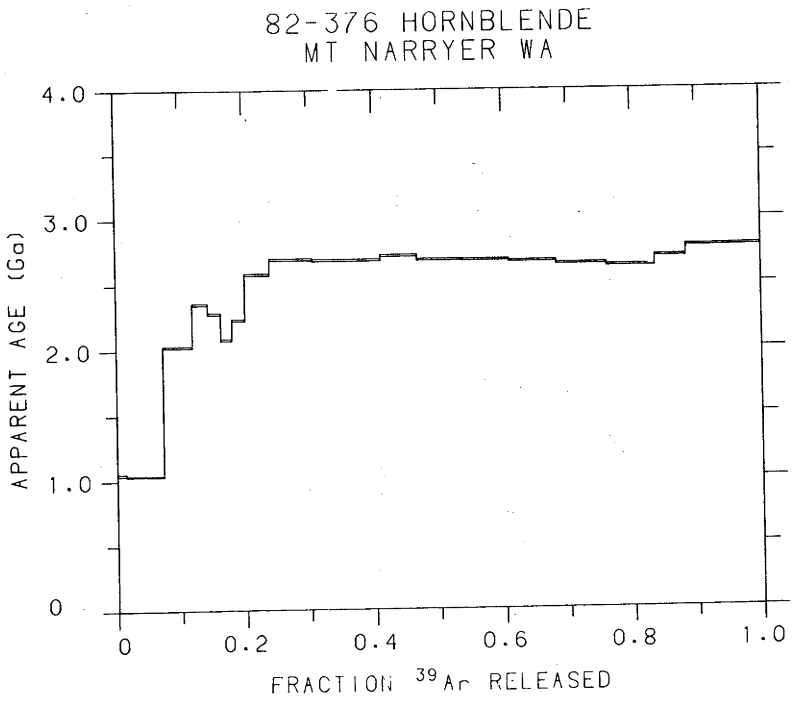

A

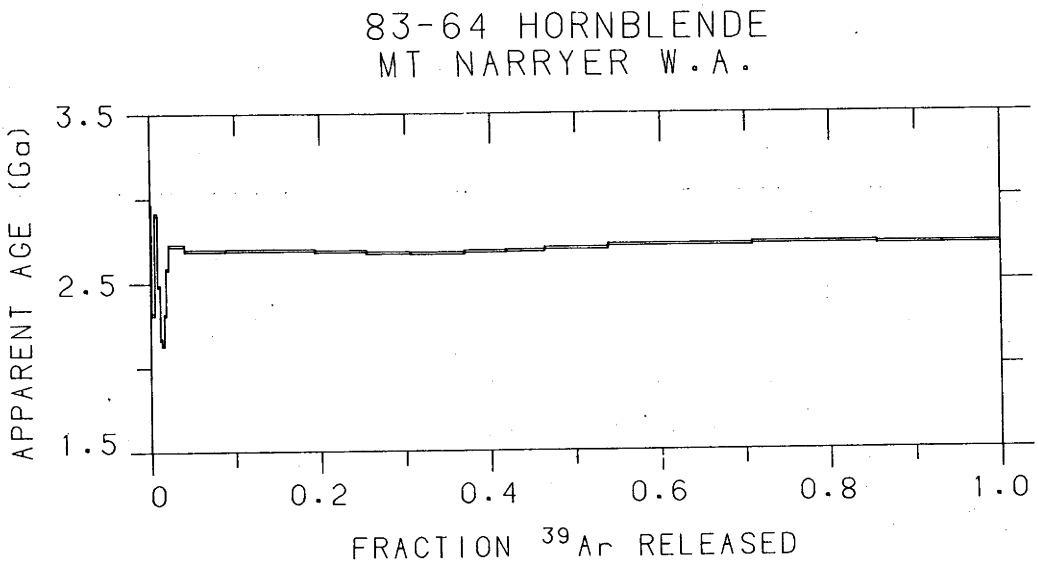

B

Figure 6.4. Age spectra of hornblendes 82-376 and 83-64 from GSWA locations 71918 and 77239A, and of plagioclase 83-64 from GSWA location 77239A.

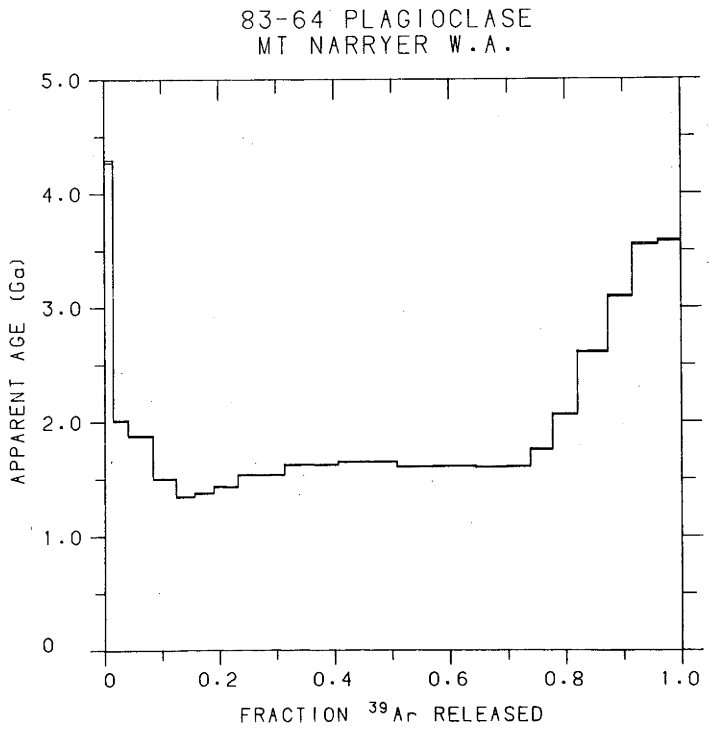
83-64 PLAGIOCLASE
MT NARRYER W.A.
APPARENT AGE (Ga)
5.0
4.0
3.0
2.0
1.0
0
0
0.2
0.4
0.6
0.8
1.0
FRACTION 39Ar RELEASED

C

agreement with the age of hornblende 82-376 from amphibolite 71918, despite the significantly longer and more complex history of the Manfred Complex, thus reinforcing the interpretation that the high grade metamorphism at about 2800 Ma had a regional character.

Most rocks in the area of Mount Narryer have experienced some degree of overprinting at greenschist facies metamorphic grade. From the data on biotites and plagioclase we propose that this event took place in the Mid-Proterozoic. Alternatively, the data may be interpreted as recording a mild overprinting at about 1600 Ma which has partly reset the biotite K-Ar ages, or as resulting from a more severe event which fully reset the biotites at about 2000 to 1800 Ma ago, and was followed by slow cooling to temperatures below the T_c of plagioclase for argon (i.e. about 200 ^{o}C, Harrison et al. 1979) at about 1600 Ma.

6.5 Implications for the geological history of the Mount Narryer metasedimentary sequence

From the observation of detrital zircons in the quartzites having igneous morphologies and $^{207}Pb^*/^{206}Pb^*$ ages ranging between 3350 and 3240 Ma, it is concluded that the sediments were deposited at some time younger than 3250 Ma. An additional two analyses of near-concordant zircons at circa 3100 Ma are probably a further constraint of the maximum deposition age. This conclusion is in contrast with previous interpretations which imply that high grade metamorphism in the Mount Narryer metasediments occurred at 3349 $\pm$ 43 Ma ago (De Laeter et al. 1981b, Froude et al. 1983). However, support for a high grade event in the gneisses at about 3300 to 3350 Ma ago comes from the work of Kinny et al. (1985), who report the growth of metamorphic rims at 3319 $^{+35}_{-16}$ Ma on zircons from the Meeberrie Gneiss. The recent discovery of zircons from a porphyritic granite intrusive into the Meeberrie Gneiss yielding ages of about 3300 Ma establishes a possible local source for the younger detrital zircons in the quartzites (Kinny in prep.). If the metasedimentary sequence was deposited later than 3250 Ma ago, as implied by our data, high grade metamorphism of these rocks must have occurred at some later date. We have identified a younger phase of high grade metamorphism which affected the metasedimentary sequence and the adjacent gneisses earlier than 2780 Ma. No evidence for two high grade metamorphisms is found in the metasedimentary rocks. The observed high grade metamorphic mineral assemblages suggest low pressures. Thus we argue against the possibility that the rocks have been at temperatures in excess of the closure temperature of hornblende for argon (about 500 ^{o}C) over long periods of time, i.e. from 3350 Ma until 2800 Ma. These arguments suggest strongly that deposition of the sediments occurred later than 3250 Ma ago, and that high grade metamorphism of these rocks occurred at about 2800 Ma ago. This high grade event clearly preceded the intrusion of granitoids into the Meeberrie Gneiss and parts of the metasedimentary sequence. Our data are not consistent with the interpretation of De Laeter et al. (1985) that the Rb-Sr wholerock isochron age of 2579 $\pm$ 122 Ma records metamorphic resetting of these granitoids; we consider instead that the Rb-Sr isochron age of these

granitoids reflects the age of their emplacement.

Many rocks in the Narryer Metamorphic Belt show some degree of overprinting at greenschist facies metamorphic grade. This phase occurred between 1600 and 2000 Ma ago, causing extensive outgassing of radiogenic argon from the less retentive minerals. It was accompanied by localized deformation which facilitated the introduction of water into the system, and incorporation of excess argon in some minerals probably also occurred at this time.

TABLE I: U-Th-Pb data for young near concordant zircons from Mount Narryer quartzites.

Grain-Spot	Sets	U ppm	Th ppm	204Pb ppb	%f	$\frac{208Pb}{206Pb}$	$\frac{208Pb}{232Th}$	Th-Pb age	$\frac{206Pb}{238U}$	$\frac{207Pb}{235U}$	$\frac{207Pb}{206Pb}$	Minimum age	Original age
Sample 71921													
12-2	3	617	99	19	.07	.0446	.1836	3407	.622 ± 22	25.0	.2734 ± 8	3326 ± 9	3329
Sample 71932													
9-1B	2	689	259	82	.27	.1048	.1747	3365	.626 ± 18	24.0	.2778 ± 15	3351 ± 17	3366
105-1B	1	625	367	119	.45	.1616	.1668	3118	.607 ± 18	23.0	.2750 ± 32	3335 ± 37	3351
125-1B	2	635	667	52	.18	.2891	.1743	3248	.634 ± 11	23.3	.2652 ± 7	3278 ± 8	3293
104-1B	2	359	191	100	.67	.1519	.1701	3175	.596 ± 17	21.8	.2645 ± 25	3274 ± 30	3295
88-1	1	817	195	9	.023	.0707	.1901	3518	.606 ± 46	21.6	.2591 ± 15	3241 ± 18	3250
23-1	3	1312	121	9	.021	.0248	.1444	2726	.541 ± 41	17.8	.2384 ± 8	3109 ± 11	3133
32-1	1	1002	51	43	.11	.0144	.1606	3010	.533 ± 41	17.2	.2341 ± 17	3080 ± 23	3102

All lead isotopes except ^{204}Pb are radiogenic. Ages are in Ma. Uncertainty shown is ± 1σ and refers to the last two digits, except for the $^{207}Pb/^{206}Pb$ minimum age where the uncertainty shown is ± 2σ. %f is the value of initial ^{206}Pb / total ^{206}Pb expressed as a percentage, assuming mean terrestrial Pb at the $^{207}Pb/^{206}Pb$ age. Spots labelled 'B' represent analyses after re-polishing of the sample mount.

'Original age' was calculated by applying a bi-episodic Pb loss model to the data, taking Pb loss at t_2 = 1900 Ma (corresponding to greenschist facies metamorphism of the region) and recent Pb loss (t_3 = 0), assuming a constant proportion of Pb loss 'k' from all spots in both episodes, and solving for t_1 (Compston and Williams, in prep.). For these data we have used a value for k (loss at t_3 / loss at t_2) of 2.5 as indicated by multiple spot analyses of single grains, however the model is not sensitive in this case to the choice of either k or t_2.

Table II. K-Ar data.

Code	mineral	K percent	$^{40}Ar^*$ 10^{-10} mol/g	$^{40}Ar^*/^{40}Ar$ percent	Age Ma	uncertainty 1σ
82-376	hbl	0.470, 0.470	47.66	99.4	2607	24
			47.87	99.2	2612	24
82-376	bio	2.58, 2.55	136.1	99.0	1789	16
82-377	hbl	0.504, 0.499	103.8	99.4	3664	39
83-59	plag	0.167, 0.167	10.20	97.5	1954	18
83-59	hbl	0.716, 0.715	82.58	99.5	2787	25
83-64	plag	0.249, 0.247	16.65	99.0	2066	19
83-64	hbl	1.063, 1.063	111.0	99.8	2645	24
			113.0	99.7	2676	24
85-1	bio	7.37, 7.42	47.84	99.9	2022	22
85-2	bio	7.30, 7.32	42.24	99.8	1887	17
85-3	bio	6.52, 6.50	34.21	99.6	1778	16

The uncertainties in the ages are quoted at 1σ-level.
The abundance of $^{40}K/K_{total} = 1.167 \times 10^{-4}$ mol/mol.
The decay constants for ^{40}K are: $\lambda_\beta = 4.962 \times 10^{-10}$ yr^{-1}.
$\lambda_{(e + e')} = 0.581 \times 10^{-10}$ yr^{-1}.
$^{40}Ar^*/^{40}Ar$ is percentage radiogenic ^{40}Ar of the total measured amount of ^{40}Ar.

Table III $^{40}Ar/^{39}Ar$ data.

Quoted temperatures are the average of thermocouple measurement on the bottom of the sample crucible, and optical pyrometer measurement on the upper inside wall of the sample crucible. The difference between the two measurements was typically 150 ^{o}C.

The ^{39}Ar and ^{37}Ar concentrations are corrected for radioactive decay during the period between irradiation and analysis.

Laboratory standard hornblende 77-600 (K/Ar age 414.2 Ma) was used as a flux monitor.

Reported absolute amounts were calculated from machine sensitivity (5.045×10^{-15} moles/mV), which was determined from regular measurement of standard minerals.

Uncertainties in apparent ages are quoted at 1σ-level, 0.5 percent error in parameter J is included. $\lambda = 5.543 \times 10^{-10}$ yr^{-1}.

$^{40}Ar/^{39}Ar$ data of hornblende 82-376, and 83-64, and of plagioclase 83-64 were included at pages T28 and T29 which follow chapter 5.

Chapter 7

Conclusion

7.1 Conclusion

The main objective underlying all the work presented in the previous chapters was to test the usefulness of the $^{40}Ar/^{39}Ar$ age spectrum method for dating purposes in regional metamorphic terrains. The second objective was to obtain more detailed information on the timing of thermal and tectonic events in two regions which previously had been the focus of detailed study.

The two areas that were selected for study contrast in many ways: the first area is located in the Aegean Sea in southern Europe, and the second area in tropical northwest Australia; the Aegean has a mild climate and is a well-known tourist destination, whereas the Pilbara is located on the margin of Australia's major deserts and only comfortably accessible during the cold season. Their geological histories are of quite contrasting age, the Pilbara Block is one of the early Archaean nucleii where major tectonism and metamorphism ceased some 2800 Ma ago, whereas the Aegean is at present located in one of the active regions of the Alpine orogenic belt in southern Europe. Despite these contrasts, the problems involved in establishing a thermal history for these two areas were quite similar. Apart from technical difficulties of measuring very young and very old minerals, the main problem of a geochronological study of metamorphic rocks is to establish the relation between the samples used for dating and the petrology and microstructure of the rocks. Without a proper characterization of the samples in the context of the metamorphic history of the region, a study as presented in the previous chapters is of limited value.

In the next sections a brief review of the main conclusions will be given. This discussion is divided into two parts; the first part concentrates on the application of the $^{40}Ar/^{39}Ar$ age spectrum method to the thermal evolution of metamorphic terrains, and in the second part the interpretation of results in terms of a geologic history will be discussed. Although these two aspects of the work are quite different, some overlap in the examples used to demonstrate different points is unavoidable.

7.2 The method

It has been demonstrated in the previous chapters that by the $^{40}Ar/^{39}Ar$ age spectrum method ^{40}Ar concentration gradients in common metamorphic minerals as hornblende and muscovite can be resolved, adding an extra dimension to the understanding of argon isotopic ages of partially disturbed samples from metamorphic terrains. This conclusion is perhaps somewhat surprising in view of the observation that both hornblende and white mica are hydrated minerals which were known to dehydrate under atmospheric pressures at modest temperatures (i.e. in the range between 600 and 900 ^{o}C, Kiefer 1949, see also Smykatz-Kloss 1974). However, recent $^{40}Ar/^{39}Ar$ work has demonstrated that ^{40}Ar concentration gradients in hornblendes and white micas can be resolved in many cases, suggesting that changes in the structure of the minerals during dehydration are not accompanied by substantial redistribution of ^{40}Ar within the crystal lattice (see results of Chapters 3 and 5, and also Harrison (1983) for a discussion).

Applied to young Alpine hornblendes, the $^{40}Ar/^{39}Ar$ age spectrum method convincingly demonstrated its advantages over the conventional K-Ar method by revealing varying amounts of excess ^{40}Ar incorporated within the crystals, causing apparent K-Ar ages to scatter between 16.0 and 50.7 Ma. In four of the five samples examined with the $^{40}Ar/^{39}Ar$ stepheating technique, excess argon appeared to be limited mainly to the low temperature steps in the age spectra and the minimum ages in the high temperature steps showed a variation of about 4 Ma (compared to about 16 Ma between the K-Ar ages); some of this scatter is still attributable to the influence of excess argon. The fifth sample which had the highest K-Ar age, showed a classic U-shaped age spectrum and a minimum age of 23.1 Ma. In view of the substantial proportion of excess argon in this sample, the lowest age in this age spectrum must be interpreted as an inaccurate maximum estimate of the 'true' age of the sample. Thus by applying the $^{40}Ar/^{39}Ar$ age spectrum method to metamorphic hornblendes, the main source of scatter in their apparent K-Ar ages could be identified, and thus a substantially more precise estimate of the age of crystallization could be obtained.

The least disturbed age spectra were obtained from white micas and hornblendes from rapidly cooled high grade metamorphic rocks. White micas formed during the early (M_1) metamorphism in the area on Naxos where subsequent metamorphic overprinting was minor, all showed argon loss patterns which led to the interpretation that the highest recorded ages provide minimum estimates for the time of beginning of argon accumulation in these minerals.

Measurement of Archaean hornblendes and muscovite required long irradiation times (two full cycles of HIFAR, i.e. 42 days) in order to produce sufficient ^{39}Ar in the samples to accurately measure their $^{40}Ar^*/^{39}Ar_K$ ratios. A number of hornblendes from within the greenstone belts contained very little potassium (less than 0.2 percent). The results of flame photometric potassium determination on these samples compared well with the results of determination by the isotope dilution technique.

In cases where minerals could be related to clearly defined metamorphic mineral assemblages, the results of $^{40}Ar/^{39}Ar$ dating could be explained in terms of simple models for diffusion of argon during discrete phases of thermal overprinting. When mixtures of minerals were suspected in the samples, as for example was the case with the low grade M_2 white mica samples from Naxos, and with one retrograde actinolite sample from the Pilbara, no simple relation between the shape of the age spectra and the thermal history of the sample was observed. For the white micas from Naxos, it was possible to understand the $^{40}Ar/^{39}Ar$ data in terms of a model assuming a mixture of two generations of mica in the samples, but the age spectrum of actinolite 82-324 could not be understood from simple diffusion or mixing of mineral phases. Nevertheless, the age spectrum of this sample does indicate some thermal overprinting during the Mid Proterozoic.

7.3 The metamorphic history of Naxos

The main results from our study of the Attic Cycladic Metamorphic Complex on Naxos included:

(1) Age spectra of white micas from the rocks which experienced only minor overprinting during the M_2 metamorphism, suggest that the early high pressure, low to medium temperature metamorphism (M_1) occurred before about 50 Ma ago.

(2) The apparent scatter in K-Ar ages of M_2 formed hornblendes, and the apparent increase in their K-Ar ages toward lower M_2 metamorphic grade were caused by the incorporation of excess ^{40}Ar. We argue that most, and possibly all, of these minerals were formed between about 15 and 16 Ma ago.

(3) Because argon isotopic ages of M_1 formed phengites have not been fully reset in rocks which were overprinted at amphibolite grade during M_2, we argue that the thermal effect of M_2 overprinting was of short duration.

(4) The K-Ar ages of biotites and hornblendes from the granodiorite intrusion on the west coast of Naxos are very similar to those obtained from the high grade M_2 zones in central Naxos, and suggest a close temporal relation between the formation of the thermal dome and the intrusion of the granodiorite.

(5) Thermal modelling suggests that the M_1 metamorphism can be understood in terms of subsidence of continental crustal material near an active continental margin. It is difficult, however, to understand subsequent high grade metamorphism at upper- to mid-crustal levels during the period following M_1, and to satisfy the geochronological constraints discussed above. Instead, the M_2 metamorphism can be understood as the contact zone formed during the intrusion of a small, 1200 ^{o}C pluton. Depending on the degree of convection in the pluton during cooling, lower magma temperatures could be possible. The size and temperature of a modelled intrusive body required to bring sufficient heat into the system by conductive cooling (i.e. an infinite dyke with a halfwidth of 4000 m, and an initial temperature of 1200 ^{o}C) demonstrates the large amount of heat required for the formation of a thermal dome.

Our interpretation of the thermal history of the Attic Cycladic Metamorphic Belt on Naxos is based on the assumption of two major periods of rapid uplift separated by a relatively quiet time interval. The first period of rapid uplift was during the transition from 'double thickened' crust at the time of the M_1 event to a normal crustal thickness. This transition is likely to have occurred about 50 Ma ago, and was the cause of M_1 argon isotopic ages of white micas to be preserved. The second period of rapid uplift immediately followed upon the M_2 event. During this period of rapid uplift, which ended some 5 Ma ago, the rocks exposed presently in the region were brought to the earth's surface. Recently this period of rapid uplift was discussed in terms of models for metamorphic core complexes as developed for the metamorphic rocks in the Basin and Range Province in western USA (Lister et al. 1984).

An important uncertainty in modelling thermal histories is the distribution and concentration of radioactive elements in the crust. The radioactive heat production is the single most important factor influencing the rate of heating of tectonically emplaced rocks; it is also a poorly constrained factor. In normal continental environments the heat production is assumed to decrease with depth (Lachenbruch and Sass 1978, Morgan and Sass 1984). Near a continental margin the chemical structure of the crust is very likely to be disturbed by subduction of supracrustal material, thus making the heat source distribution very model dependent. In Chapter 4, we have modelled two different heat source distributions. The heating rate of rocks which are out of thermal equilibrium depends critically on the choice of a model for the distribution of radioactive elements. If thermal modelling along the lines presented in Chapter 4 is to be taken beyond rather crude approximations of possible thermal histories, more detailed measurements of the distribution of the main heat producing elements in such environments, as well as more detailed models of tectonic processes along active continental margins, are necessary. Nevertheless, the main conclusions from the thermal modelling, including rapid uplift following M_1, and M_2 metamorphism caused by an external heat source, will hold under most heat source distribution models.

The combination of detailed geochronology and thermal modelling have led to an interpretation of the M_2 thermal dome metamorphism on Naxos which is different from previous interpretations (Jansen and Schuiling 1976, Andriessen et al. 1979). Our interpretation is based on the following lines of reasoning:

(1) Previous estimates of metamorphic temperatures are likely to be too high, possibly by as much as 100 ^{o}C. This was argued from the observation that syn-M_2 metamorphic fluid inclusions contained substantial amounts of CO_2 (Kreulen 1980), thus lowering the water activity in the fluid and the temperatures for common dehydration reactions to occur. In addition, the overprinting relations of the white micas in the zone on Naxos where M_1-formed phengites and M_2-formed muscovites occur side by side, as revealed by $^{40}Ar/^{39}Ar$ analysis, is incompatible with previously reported temperature estimates. Further, in an area which has experienced rapid cooling following the peak of metamorphism, temperature estimates from oxygen isotope thermometry (Rye et al. 1976), and from garnet-biotite exchange thermometry should yield good estimates of the maximum recorded temperature (Javoy 1977).

(2) As already mentioned earlier in this section, the behaviour of the argon isotopic system of white micas during overprinting by M_2 suggests a short duration for the M_2 thermal event.

(3) If temperatures during M_2 overprinting were lower than previously estimated, then hornblendes 81-550, 81-564, 81-536 and 81-540 will have crystallized at temperatures near to, or below the closure temperature of hornblende for argon. As the minimum ages of the age spectra of 81-536 and 81-540 were affected by incorporation of substantial amounts of excess argon, we argue that the time of overprinting is likely to be close to 15 - 16 Ma and certainly less than 19 Ma (being the minimum age recorded by 81-536).

(4) The K-Ar ages of hornblendes from the granodiorite scatter between 12.1 and 13.5 Ma, probably as a result of sample inhomogeneity. Nevertheless, the K-Ar ages of these hornblendes are higher than the age of 11.1 $\pm$ 0.7 Ma defined by a Rb/Sr whole rock isochron on granitoid, aplite and pegmatite samples, and are close to the K/Ar ages of hornblendes from the high grade M_2 metamorphic zones of central Naxos and indistinguishable from

those obtained from hornblendes in the northern part of zone V.

The arguments presented above suggest that the M_2 thermal dome was caused by a hot, well-focussed (possibly magmatic) heat source about 15 to 16 Ma ago, and was followed by the intrusion of the granodiorite on the west coast of the island probably somewhat earlier than 12.1 to 13.5 Ma ago. It was argued in Chapters 3 and 4 that these high temperature processes occurred when the rocks of the Attic Cycladic Metamorphic Belt were in an island arc tectonic setting.

7.4 Western Australia

It was demonstrated in Chapters 5 and 6 that it was possible to obtain reliable data on the Archaean thermal histories of the Pilbara Block and the Mount Narryer Metamorphic Belt. The ages obtained from $^{40}Ar/^{39}Ar$ analyses confirm the great age of the rocks from these Archaean nucleii and agree well with previous determinations from the same regions which used other isotopic techniques.

Metamorphic hornblendes from the Shaw Batholith, the Tambourah Dome in the Yule Batholith and from the Western Shaw Greenstone Belt, lying between the two granitoid-gneiss domes, were divided into two main groups, which yielded quite different age spectra. The youngest ages were obtained from hornblendes and a white mica sample from the granitoid-gneiss terrains and their contact zones within the greenstone belts. $^{40}Ar/^{39}Ar$ ages from the margin of the Tambourah Dome of about 2960 to 2940 Ma were interpreted to reflect cooling of the area after high grade metamorphism of the granitoid-gneiss terrain. Consequently, the significantly younger $^{40}Ar/^{39}Ar$ age of 2866 Ma from a hornblende from a greenstone rock from the same margin in close contact with a late posttectonic intrusive granite, was interpreted as reliably dating the time of its emplacement. This phase of granite mobility did not affect large areas of the Tambourah Dome or the Western Shaw Greenstone Belt.

Older ages were obtained from blue-green hornblendes from rocks within the greenstone belts. These minerals are part of an upper greenschist to lower amphibolite grade mineral assemblage, argued on textural ground to be older than the tectonic and thermal events related to dome formation at about 2950 Ma. K-Ar ages and $^{40}Ar/^{39}Ar$ total fusion ages of these hornblendes scatter over a considerably wider range than the minerals associated with the high grade assemblages of the granitoid-gneiss terrains. However, by using the $^{40}Ar/^{39}Ar$ age spectrum method it was possible to obtain information on the nature of this scatter in apparent ages: the minerals with the highest apparent ages were shown to have the least disturbed age spectra. In fact, the least disturbed hornblende age spectra provide us with good evidence for the greater age of these minerals. Those samples yielding lower apparent ages had consistently more disturbed age spectra. This observation supports the interpretation that the blue-green hornblendes belong to one single generation of mineral assemblage. Because all age spectra of blue-green hornblendes showed evidence for substantial argon loss, the maximum ages in the high temperature steps of the age spectra were interpreted as minimum estimates for the time of beginning of argon accumulation in these minerals. Consequently, our interpretation was that these minerals were formed during regional metamorphism which was followed by cooling some 3200 Ma ago; an interpretation which was supported by theoretical modelling of age spectra under the assumption that argon loss occurred by diffusion during a discrete period of thermal overprinting.

The study presented in Chapter 5 demonstrates that dating of metamorphic minerals by the $^{40}Ar/^{39}Ar$ age spectrum method may yield important new information on the tectonic and thermal evolution of an Archaean terrain. The implications of the present study for the tectonic and thermal evolution of the Western Shaw area in the eastern Pilbara are:

(1) The mineral assemblages within the Western Shaw Greenstone Belt are considerably older than those of the granitoid-gneiss terrain. Thus it is unlikely that the metamorphisms recorded by these rocks are related.

(2) Regional cooling of the granitoid-greenstone terrain in the Tambourah Dome occurred about 2950 Ma ago, whereas cooling within

the central parts of the Shaw Batholith occurred later, about 2840 Ma ago. It is possible, however, that the ages from this area were more profoundly affected by posttectonic granite magmatism. Additional $^{40}Ar/^{39}Ar$ analyses of minerals from within the Shaw Batholith and from its margins would be useful to further constrain the thermal history of this granitoid-gneiss dome.

(3) Early metamorphism of the greenstone belt was argued to be the result of disequilibrium of the continental geotherm caused by rapid thickening of the crust (Morant 1984, see also England and Bickle 1984). The implications of such tectonic processes for the physical properties of the continental crust during the Early Archaean were discussed by England and Bickle (1984). Our data indicate that this tectonic and thermal event occurred at least 3200 Ma ago, which adds to the importance of England and Bickle's conclusions regarding the nature of the continental crust during this event.

(4) During formation of the granitoid-gneiss domes about 2950 Ma ago, the rocks belonging to these units experienced high grade metamorphism; temperatures in excess of 650 ^{o}C were inferred by Morant (1984). The observation that the relatively narrow Western Shaw Greenstone Belt did not thermally equilibrate with the granitoid-gneiss terrains on either side of it, demonstrates that significant lateral variations in geothermal gradients existed during this 2950 Ma old regional metamorphism. We argue that the preservation of such lateral variations support the interpretation that this event was accompanied by rapid tectonic movement and cooling.

The points raised under (3) and (4) suggest that tectonic events during the Archaean history of the Pilbara Block were of relatively short duration and separated by substantial periods of time. This is an important conclusion which is not easily reconciled with previous models of the Archaean crustal evolution of the area as proposed by Hickman (1981) and Glikson (1979).

In Chapter 6 a relatively simple point was discussed concerning the time of deposition and subsequent metamorphism of the Mount Narryer metasedimentary sequence. On the basis of a Rb/Sr whole rock isochron of adjacent gneisses, interpreted to record high grade metamorphism about 3350 Ma ago, metamorphism within the supracrustal rocks of Mount Narryer was argued to have occurred at this time as well, which implies that their sedimentation age was greater than 3350 Ma. However, $^{40}Ar/^{39}Ar$ age spectra of hornblendes suggested cooling after high grade metamorphism about 2780 to 2720 Ma ago, and some minor thermal overprinting during the Mid Proterozoic. As no evidence for two consecutive high grade metamorphisms was found from study of the petrology of these rocks, and apparently detrital zircons with magmatic morphologies yielded near concordant U-Pb zircon ages in the range of 3100 to 3250 Ma, it was argued that the metamorphic history of the Mount Narryer area was more complex than previously realized. The data presented in Chapter 6 suggests that deposition of the sediments occurred later than 3350 Ma, and high grade metamorphism followed about 2800 Ma ago. This interpretation has important implications for the modelling of discordant detrital zircon U-Pb ages, as well as the possible implication that at the time of deposition of the sediments (i.e. between about 3100 and 2800 Ma ago) the source rocks for the 4100 to 4200 Ma old zircons reported by Froude et al. (1983) were still present at the earth's surface.

The present investigation into the metamorphic history in the Archaean nucleii of Western Australia was a test of the usefulness of the $^{40}Ar/^{39}Ar$ age spectrum method for dating the metamorphic histories of very old rocks. As this test was successful, much more work on thermal histories of Archaean metamorphic terrains could be done. Within the boundaries of the eastern Pilbara several point still need clarification: the Rb-Sr whole rock age of 2551 $\pm$ 128 Ma of the Cooglegong (reported by De Laeter et al. 1975) granite seems to be somewhat low to fit into the thermal history of the area. $^{40}Ar/^{39}Ar$ analysis of hornblende from its contact aureole should give additional constraints on its age. It will be rewarding to extend such a study to hornblendes from other granite greenstone contacts, because it was demonstrated by using such an approach very good estimates of

the age of emplacement of a granite can be obtained. Further, it is important to assess the regional distribution of the early metamorphism recognized within the greenstone belts, which should be possible by $^{40}Ar/^{39}Ar$ analyses of hornblendes from greenstone belts to the north of the Shaw Batholith which have suffered less deformation than those from the Western Shaw Greenstone Belt. Lastly, although a minor component, many greenstone belts do contain some metapelitic units. $^{40}Ar/^{39}Ar$ analyses of white micas from these rocks are likely to yield important additional information on the metamorphic history of the region.

Appendix I. Principles of the $^{40}Ar/^{39}Ar$ method

The general age equation

The majority of the techniques used in geochronology make use of naturally occurring radioactivity. Radioactivity may be defined as spontaneously occurring nuclear reactions, with the nucleus of a radioactive isotope emitting an elementary particle and as a result its atomic number or atomic weight changes. Owing to the reaction, the amount of radioactive material decreases and the amount of daughter product increases with time. Methods in geochronology make use of the fact that daughter product accumulates in a mineral or rock from the time of its formation. The ratio of concentrations of parent and daughter gives a measure of the age of a sample. The basic equation describing radioactive decay is:

$$-(^{dN}/_{dt}) = \lambda N \qquad (1)$$

The rate of the nuclear reaction, (dN/dt), is proportional to the number of parent atoms present, N, and after introducing a constant of proportion λ (the decay constant), equation (1) is obtained. Rearrangement of equation (1) and integration gives:

$$-\ln N = \lambda t + C \qquad (2)$$

In this equation is C a constant of integration. Because at time t=0 the amount of radioactive parent isotope is the initial amount N_o, C may be equated to $-\ln N_o$. Thus, equation (2) becomes:

$$-\ln N = \lambda t - \ln N_o \qquad (3)$$

Rearrangement and taking the exponential gives:

$$N = N_o \exp(-\lambda t) \qquad (4)$$

In the case of a closed system the concentration of daughter product, D, will be related to the concentration of the parent element:

$$N_o = D + N \qquad (5)$$

After substitution of equation (5) in (4) one of the basic equations used in geochronology is obtained:

$$D = N (\exp(\lambda t) - 1) \qquad (6)$$

which relates the present amount of daughter product, D, to the present day amount of parent element.

The potassium argon method

The K-Ar method of dating is one of the methods in geochronology that makes use of the decay of a radioactive parent isotope, ^{40}K, to a stable daughter isotope, ^{40}Ar. The method can be applied to minerals and wholerock samples from a wide variety of igneous, metamorphic and sedimentary environments, because potassium has relatively high abundances in most continental crustal rocks. The relative abundance of $^{40}K/K_{total}$ is $1.167*10^{-4}$ mole/mole (Garner et al. 1975). The age of a sample is obtained from the measured ratio between ^{40}K and ^{40}Ar in a sample. In the conventional K-Ar method, the potassium concentration of a sample is measured on a split of the sample using either a flame photometric technique with a sodium sulphate buffer and a lithium internal standard (Cooper 1963), or by isotope dilution using a ^{41}K tracer. To measure the argon concentration, a split of the sample is fused in a high vacuum extraction line, and, after purification, measured by isotope dilution in a mass spectrometer using a high purity ^{38}Ar tracer (McDougall 1966, Dalrymple and Lanphere 1969, McDougall and Schmincke 1977). For the calculated age to have geological significance, the following requirements need to be fulfilled (Dalrymple and Lanphere 1969):

1. At the time of crystallization, the argon content of a sample must be zero, or if there is argon in the sample it must have an isotopic composition equal to atmospheric argon. Minerals from metamorphic terrains sometimes have incorporated an extraneous (i.e. with a $^{40}Ar/^{36}Ar$ ratio non-equal to 295.5) component of argon. Further, as discussed in Chapter 3, when partial recrystallization occurs and the original minerals are not fully degassed, the sample will contain an inherited component of argon. In both cases the 'true' age of a sample will be obscured.
2. The rate of decay from ^{40}K to ^{40}Ar is constant and independent of the physical conditions experienced in the environment in which the decay takes place.
3. The ratio $^{40}K/K_{total}$ is constant in all natural systems. The

observation is that potassium is not subject to isotopic fractionation under normal continental crustal conditions, only in exceptional cases involving large thermal gradients some minor fractionation was measured (Verbeek and Schreiner 1967).

4. The system remained closed to Ar and K after crystallization. In areas that have experienced thermal events or extensive weathering, K or Ar may be lost from the system. In such cases the calculated ages may be meaningless. Under certain conditions ^{40}Ar may diffuse into minerals during a thermal event. This gas, which is not of atmospheric origin or formed by radioactive decay in the system, is called excess argon.

5. In addition, the system must become closed to K and Ar soon after crystallization, in order to let the calculated age have any relation to the age of formation of the sample.

These assumptions normally are tested by the internal consistency or otherwise of ages determined in a given area. The $^{40}Ar/^{39}Ar$ age spectrum technique allows the testing some of these assumptions directly on a single sample, because ^{40}Ar concentration gradients caused by partial argon loss, incorporation of excess argon, or slow cooling can be resolved. Further, in undisturbed samples the isotopic composition of the non-radiogenic component of the gas can be assessed by isotope correlation diagrams.

^{40}K does not decay to one single daughter product, but two daughter products are formed. In 88.8 percent of the cases of decay of a ^{40}K nucleus, ^{40}Ca is formed in a β^- emission reaction. Only in about 11.2 percent of the cases ^{40}Ar is formed in an electron capture reaction or a β^+ emission reaction (Fig. A1). The values for the partial decay constants for the argon producing reactions are $\lambda_e = 0.5723 * 10^{-10}\ yr^{-1}$, $\lambda_{e'} = 0.0088 * 10^{-10}\ yr^{-1}$, and the partial decay constant for the calcium producing reaction is $\lambda_{\beta^-} = 4.962 * 10^{-10}\ yr^{-1}$. Only a negligibly small fraction of argon is formed by positron (β^+) emission. The constants are based on the summary of Beckinsale and Gale (1969), but because an improved estimate of the $^{40}K/K_{total}$ abundance was published subsequently (Garner et al. 1975) and used for the calculation of the decay constants, the values presented here differ slightly from those published originally. The decay

Figure A1. The decay scheme of ^{40}K according to Beckinsale and Gale (1969). The decay constants were recalculated using the isotopic abundances of potassium of Garner et al. (1975) (Tetley 1978).

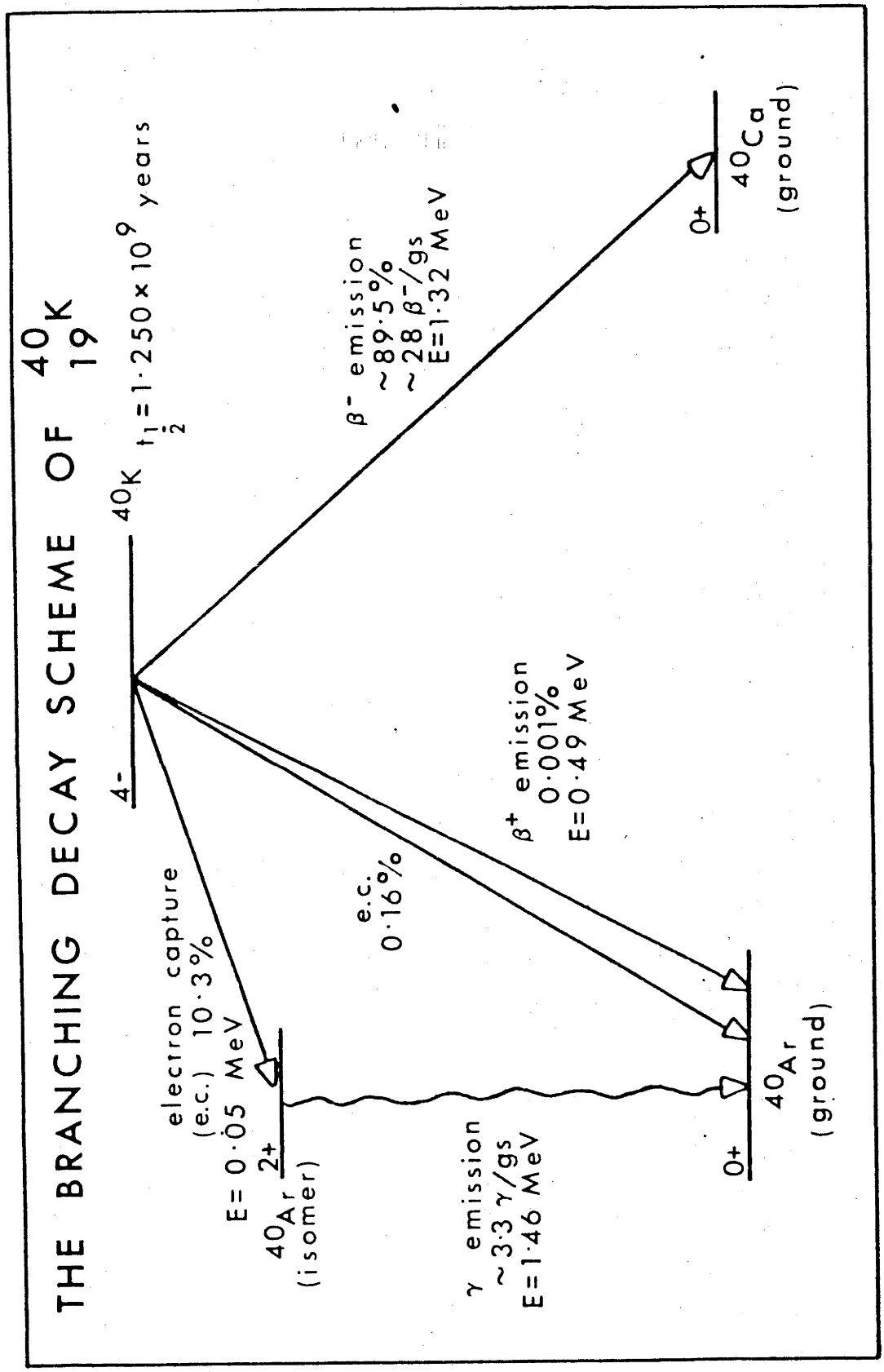
THE BRANCHING DECAY SCHEME OF $^{40}_{19}K$
^{40}K $t_{\frac{1}{2}} = 1{\cdot}250 \times 10^9$ years
4-
electron capture (e.c.) 10·3% E= 0·05 MeV
^{40}Ar (isomer) 2+
e.c. 0·16%
β^+ emission 0·001% E=0·49 MeV
β^- emission ~89·5% ~28 β^-/gs E=1·32 MeV
0+ ^{40}Ca (ground)
γ emission ~3·3 γ/gs E=1·46 MeV
0+ ^{40}Ar (ground)

constants used in this study are those recommended by Steiger and Jäger (1977).

Although in principle both daughter products can be used for the dating of geological materials, the $^{40}K/^{40}Ar$ reaction is far more widely used. Because ^{40}Ca is the most abundant isotope of calcium in nature, the proportion of radiogenic ^{40}Ca well in many cases be difficult to measure. Thus only essentially calcium free samples are suitable for $^{40}K/^{40}Ca$ dating.
For the case of decay of ^{40}K, equation (6) becomes:

$$^{40}Ar + ^{40}Ca = ^{40}K(\exp(\lambda t) - 1) \qquad (6a)$$

In this equation $^{40}Ar + ^{40}Ca$ take the place of D of equation (6), and ^{40}K is equivalent to N in equation (6). The decay constant for ^{40}K, λ, is the sum of the partial decay constants for each of the two branches of the decay scheme:

$$\lambda = \lambda_{\beta^-} + \lambda_{e} + \lambda_{e'}$$

where the subscripts, e, refer to the electron capture reactions and the supscript, β^-, refer to the β^- emission reaction, relating to the formation of ^{40}Ar and ^{40}Ca respectively. Because only the $^{40}K/^{40}Ar$ reaction is of interest here, equation (6a) can be written in the form:

$$^{40}Ar = ((\lambda_e + \lambda_{e'})/\lambda)\,^{40}K\,(\exp(\lambda t) - 1) \qquad (7)$$

Because it is the objective of the method to measure time, it is useful to rewrite equation (7) in the form:

$$t = (1/\lambda)\,\ln((^{40}Ar^*/^{40}K)\,(\lambda/(\lambda_e + \lambda_{e'})) + 1) \qquad (8)$$

The $^{40}Ar/^{39}Ar$ method

The $^{40}Ar/^{39}Ar$ method is a variation of the K-Ar method in which the potassium content of a sample is measured by a neutron activation method (Merrihue 1965, Merrihue and Turner 1966). Samples are irradiated with fast neutrons in a nuclear reactor where the desired reaction, $^{39}_{19}K\,(n,p)\,^{39}_{18}Ar$, occurs under the influence of fast neutrons. The advantage of this approach is that the K-Ar age of a sample is measured in the form of a ratio of isotopes of one element, argon. In principle the precision of the age determination is increased, because it is no longer necessary to measure the absolute amounts of two elements on separate splits of a sample. Isotopic ratios can be measured with

greater precision, allowing the measurement of smaller samples. In practice, however, the precision is limited by uncertainties in measuring the conditions of irradiation (Tetley et al. 1980, McDougall 1974) and by uncertainties in the correction factors for interferences by argon isotopes formed during irradiation from calcium and potassium. The method was developed for application on extraterrestrial samples (Merrihue 1965, Merrihue and Turner 1966). Since that time the method has proven to be very useful for the dating of a great variety of samples.

The rate of the ^{39}Ar forming reaction according to Mitchell (1968) is:

$$^{39}Ar = {}^{39}K \; \Delta T \int \phi(\varepsilon)\,\sigma(\varepsilon)\,d\varepsilon \qquad (9)$$

This equation relates the concentration of ^{39}Ar formed during irradiation to the ^{39}K concentration in the sample. The duration of irradiation is ΔT, and the integral is over the flux density, ϕ, and the the capture cross section, σ, as functions of the neutron energies, ε. The neutron flux and the neutron energy spectrum in a nuclear reactor are not usually measured directly. Instead, samples are irradiated together with a laboratory standard of accurately known age. Although the chemistry of the samples need not be precisely known, it is good practice to use standards and samples with comparable calcium and potassium contents, because the correction factors for interfering isotopes will be of the same order of magnitude.

The equation that relates the $^{40}Ar^*/^{39}Ar_K$ ratio to the age of the sample is (eq. 10):

$$^{40}Ar^*/^{39}Ar_K = (\lambda(e + e'))/\lambda)\,{}^{40}K/{}^{39}K\,(\exp(\lambda t) - 1)/(\Delta T \int \phi(\varepsilon)\sigma(\varepsilon)d\varepsilon)$$

This equation can be used to calculate the $^{40}Ar/^{39}Ar$ ratio in a standard or the age of a sample. It is derived by combination of (7) and (9). Commonly the factors related to the conditions of irradiation are combined in an irradiation parameter J:

$$J = (\lambda/\lambda(e + e'))\; {}^{39}K/{}^{40}K\; (\Delta T \int \phi(\varepsilon)\sigma(\varepsilon)d\varepsilon) \qquad (11)$$

Because both the sample and the standard are exposed to the same conditions of irradiation over the same time interval, their J values are assumed, with good justification, to be equal. After introduction of J, equation (10) becomes:

$$^{40}Ar^*/^{39}Ar_K = (\exp(\lambda t) - 1)/J \qquad (12)$$

As the J factors for sample and irradiation standard (flux monitor) are equal, the $^{40}Ar^*/^{39}Ar_K$ ratios of the sample and flux monitor are related as follows:

$$(^{39}Ar_K/^{40}Ar^* \ (\exp(\lambda t) -1))_{sample} = (^{39}Ar_K/^{40}Ar^* \ (\exp(\lambda t') -1))_{standard} \qquad (13)$$

Where t is the age of the unknown sample, and t' the age of the standard. The age of the sample is calculated from the following:

$$t = (1/\lambda) \ln(J \ ^{40}Ar^*/^{39}Ar_K + 1) \qquad (14)$$

The measured $^{40}Ar/^{39}Ar$ ratio is corrected for argon produced by interfering nuclear reactions. Brereton (1970) discussed a number of nuclear reactions involving isotopes of Ca, K, Ar and Cl (Table A1). Significant amounts of ^{36}Ar and ^{39}Ar may be formed from calcium isotopes, and some ^{40}Ar is formed from potassium in the sample. The $^{36}Ar_{Ca}$ interferes with the atmospheric argon correction which is based on the ^{40}Ar to ^{36}Ar ratio of atmospheric argon, which is 295.5. ^{37}Ar in a sample is mainly formed from ^{40}Ca in a neutron capture, α emission reaction, and when the production ratios of ^{37}Ar to ^{39}Ar and ^{36}Ar from calcium are known, a correction can be applied. From measurement of the argon isotopic composition of an irradiated calcium salt (for example CaF_2), these correction factors for calcium-derived ^{36}Ar and ^{39}Ar can be obtained (Mitchell 1968, Tetley et al. 1980). Similarly by irradiating a potassium salt (K_2SO_4), a correction factor for potassium-derived ^{40}Ar can be obtained. The correction factors used for samples irradiated in the HIFAR reactor are (Tetley et al. 1980):

$(^{40}Ar/^{39}Ar)_K = 0.027$,

$(^{36}Ar/^{37}Ar)_{Ca} = 3.06 * 10^{-4}$, and

$(^{39}Ar/^{37}Ar)_{Ca} = 7.27 * 10^{-4}$.

Roddick (1983) pointed out that in unfavourable circumstances a significant amount of ^{36}Ar can be produced from ^{35}Cl, which also interferes with the atmospheric argon correction. However, this reaction occurs mainly under the influence of thermal neutrons, rather than fast neutrons (Roddick 1983). Because the samples which are irradiated in HIFAR are normally shielded with a 0.2 mm thick Cd liner, to reduce the influence of thermal neutrons on the sample, problems related to interference from chlorine

Argon isotope produced	Calcium reaction	Potassium reaction	Argon reaction	Chloride reaction
36	$^{40}Ca(n, n\alpha)$			
37	$^{40}Ca(n, \alpha)$	$^{39}K(n, nd)$	$^{36}Ar(n, \gamma)$	
38	$^{42}Ca(n, n\alpha)$	$^{39}K(n, d)$	$^{40}Ar(n, nd, decay)$	$^{37}C(n, \gamma, decay)$
		$^{41}K(n, \alpha, decay)$		
39	$^{42}Ca(n, \alpha)$	$^{39}K(n, p)$	$^{38}Ar(n, \gamma)$	
	$^{43}Ca(n, n\alpha)$	$^{40}K(n, d)$	$^{40}Ar(n, d, decay)$	
40	$^{43}Ca(n, \alpha)$	$^{40}K(n, p)$		
	$^{44}Ca(n, n\alpha)$	$^{41}K(n, d)$		

Table A1. Interfering isotopic reactions

Nuclear reactions which may produce isotopes of argon (according to Brereton 1970). Significant amounts of ^{39}Ar and ^{36}Ar may be formed from isotopes of calcium, some ^{40}Ar may be formed from potassium, and in unfavourable conditions some ^{36}Ar can be formed from ^{35}Cl (according to Roddick 1983).

derived ^{36}Ar are likely to be minor.

The apparent age of a sample is calculated from equation (14), after J is determined from isotopic analysis of the flux monitor, and the $^{40}Ar^*/^{39}Ar_K$ ratio is calculated as follows:

$$^{40}Ar^* = {}^{40}Ar_m - 0.027\ {}^{39}Ar_K - 295.5\ {}^{36}Ar_{atm} \qquad (15)$$

Where

$$^{39}Ar_K = {}^{39}Ar_o - 7.27\ 10^{-4}\ {}^{37}Ar_o \qquad (16)$$

and

$$^{36}Ar_{atm} = {}^{36}Ar_m - 3.06\ 10^{-4}\ {}^{37}Ar_o \qquad (17)$$

In these equations m designates the measured value, atm the atmospheric component, and o the measured amounts of ^{39}Ar and ^{37}Ar corrected for radioactive decay during and subsequent to the time of irradiation and analysis of the sample.

The equation to correct the measured amounts of ^{37}Ar and ^{39}Ar for radioactive decay was given by Brereton (1970):

$$^{37}Ar_o = {}^{37}Ar_m\ e^{\lambda t}\ \lambda t'\ (1 - e^{-\lambda t'})^{-1} \qquad (18)$$

For multiple irradiations a summation of this equation over each individual irradiation interval should be used:

$$^{37}Ar_o = {}^{37}Ar_m \sum_{i=1}^{n} t_i \Big/ \sum_{i=1}^{n} ((1- e^{-\lambda t_i})/\ e^{\lambda t'_i}) \qquad (19)$$

The half life of ^{37}Ar was measured by Stoenner et al. (1965) as 35.1 days, and the half life of ^{39}Ar at 269 years. Under normal conditions, significant amounts of ^{37}Ar will have decayed during the time period between irradiation and isotopic analysis of the sample, making correction of the measured amount of ^{37}Ar necessary. Because of the longer half life of ^{39}Ar, correction for its decay will be less critical.

The error in the $^{40}Ar/^{39}Ar_K$ ratio is calculated according to the equation of Dalrymple and Lanphere (1971):

$$\sigma_F^2 = \frac{A^2\sigma_A^2 + 295.5^2B^2\sigma_B^2 + (7.27 .10^{-4}A - 295.5 .7.27 .10^{-4}B + 295.5 .3.06\ 10^{-4})^2C^2\sigma_C^2}{F^2}$$

In this equation F stands for the $^{40}Ar^*/^{39}Ar_K$ ratio, A for the measured $^{40}Ar/^{39}Ar_o$ ratio, B for the measured $^{36}Ar/^{37}Ar_o$ ratio, C for the $^{37}Ar_o/^{39}Ar_o$ ratio, and the σ's labelled with these subscripts designate the coefficients of variation of these ratios. The variance of the calculated age is calculated according to Dalrymple and Lanphere (1971):

$$\sigma_t^2 = \frac{J^2F^2(\sigma_F^2 + \sigma_J^2)}{t^2\lambda^2(1 + FJ)^2}$$

In this equation t is the apparent age found for this gas fraction, J the irradiation parameter, and λ the decay constant of ^{40}K.

Sources of atmospheric argon

The proportion of atmospheric argon in the gas fraction at the time of analysis will influence the precision of measurement, and will control the minimum age and sample size that can be measured by the system. Especially young samples with low K-concentrations are difficult to measure because of this problem. Atmospheric argon contamination may originate from various sources, some of which are unavoidable, but should be minimized. Firstly, some atmospheric argon will be adsorbed on the surface of the sample. In comparison with other sources, this amount of atmospheric argon is normally of minor importance, because it will be released in the low temperature steps of an experiment. Martinez et al. (1984) reported exceptionally high proportions of atmospheric argon in their Archaean wholerock komatiite samples, which they subsequently managed to decrease by storing the samples under vacuum. The samples used in the present study are unlikely to have absorbed large quantities of atmospheric argon upon irradiation, because the proportions of atmospheric argon in the conventional K-Ar determinations were very similar to those in the $^{40}Ar/^{39}Ar$ determinations on the same samples.

Figure A2. Line blank data, argon extraction line 2 as measured by the A.E.I. MS10 mass spectrometer. Data are presented in moles ^{40}Ar versus extraction step. Normally the line blank was measured daily, before the first extraction step by going through the standard experimental procedure without heating the sample.

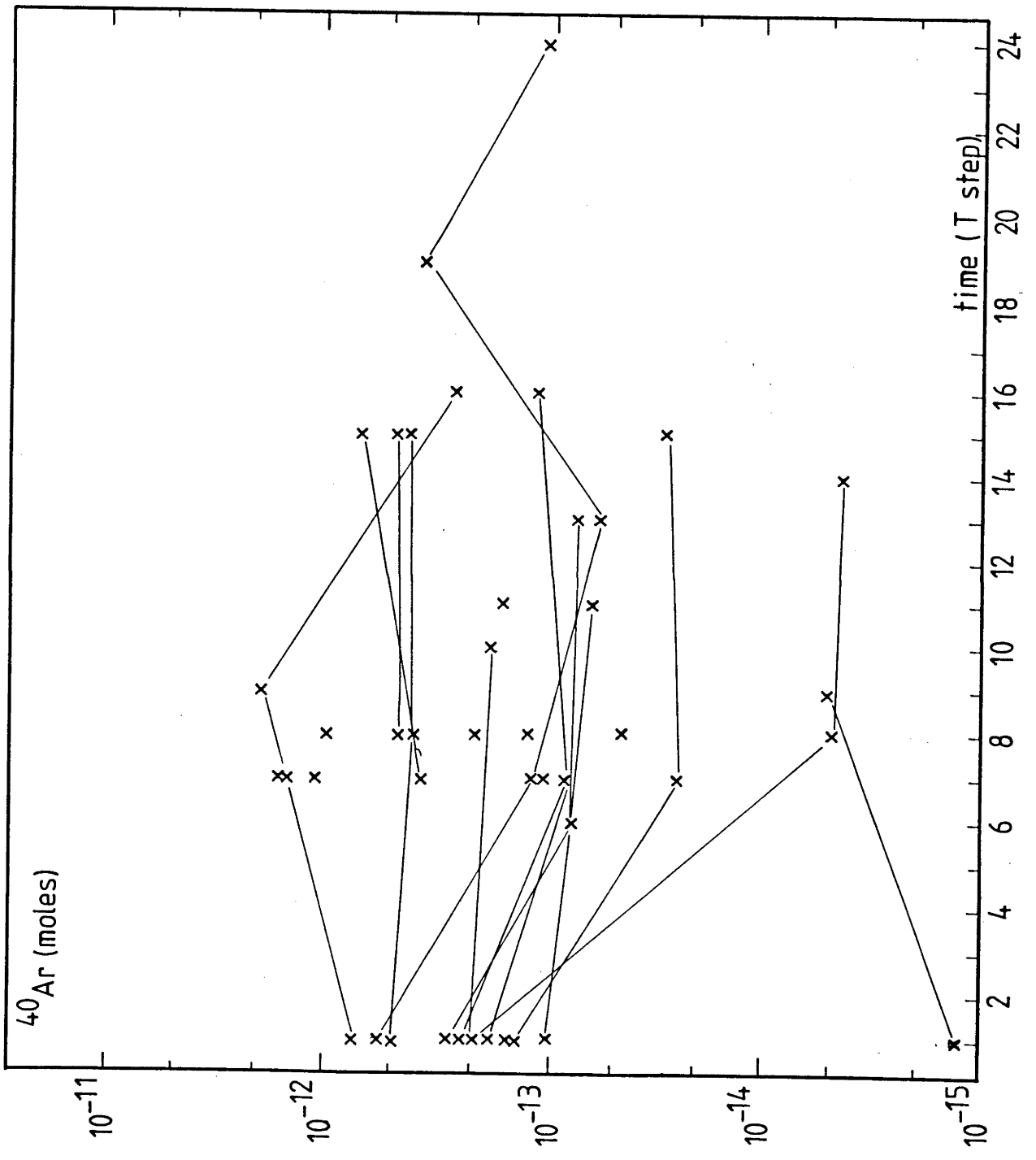
^{40}Ar (moles)
10^{-11}
10^{-12}
10^{-13}
10^{-14}
10^{-15}
2
4
6
8
10
12
14
16
18
20
22
24
time (T step)

A second source for atmospheric argon contamination is the stepheat crucible. To minimize the amount of argon from this source, the molybdenum crucibles were degassed at high temperatures before the samples were loaded. The third, and possibly the most important source of atmospheric argon is the high vacuum extraction line, which is made of Pyrex glass tubing and Granville Phillips Type C valves. Purification of the extracted argon occurs by leading the gas over molecular sieve, and circulating it at 600°C over a mixture of Cu and CuO, and subsequently over Ti sponge at 800 °C. Final purification is obtained by a SAES getter pump. Transport of gas fractions from one line segment to the next is achieved by collecting the gas on activated charcoal immersed in liquid nitrogen. The line is vented between experiments, and after overnight baking at about 280 °C, the initial line blank is normally between 10^{-12} and 10^{-13} moles ^{40}Ar, and normally decreases by an order of magnitude during the experiment (Fig. A2). The main source of atmospheric argon in the extraction line is probably the Ti sponge, which has a large surface area and a high capacity to adsorb gasses. Proper degassing of the Ti sponge will take a significant period of time. In later experiments this problem was realized more fully, and care was taken that the Ti sponge was not exposed to air between the experiments. This alteration in technique resulted ultimately in lineblanks between 4 and 5 10^{-15} moles ^{40}Ar.

The $^{40}Ar/^{39}Ar$ age spectrum method

The main innovation of the $^{40}Ar/^{39}Ar$ method was the possibility of measuring small fractions of gas that diffuse from the sample, using a stepwise heating technique. The principles of the age spectrum method are discussed by Merrihue and Turner (1966), Turner et al. (1966), and by Turner (1968). Their work on meteorites indicated that by stepwise heating, sample $^{40}Ar^*$ concentration gradients within a sample could be resolved. Thus by applying this technique to one single sample, it was possible to decide whether the K-Ar age was disturbed. Turner and co-workers argued that if argon was lost from a sample, it is likely to have occurred during a discrete period of thermal overprinting. In its simplest form the thermal history of a sample is illustrated in Figure A3. The initial situation is the

case where no argon is lost from the system, so that there is a uniform $^{40}Ar^*$ concentration throughout the mineral. The third diagram in Fig. A3 illustrates the situation immediately following a mild thermal event, which caused part of the accumulated argon to diffuse from the mineral. The $^{40}Ar^*$ concentration at the surfaces of the grains has become equal to zero, while the gas in the cores of the grains approximates the original $^{40}Ar^*$ concentration. The fourth diagram in Fig. A3. represents the situation some time after the thermal disturbance. The ^{40}Ar concentration gradient is still there, but new ^{40}Ar has accumulated uniformly within the grains. In this ideal case the gas released from the rims of the crystals will yield a measure of the age of the thermal overprinting and the gas released from the cores of the grains will approximate the age of crystallization of the mineral. On the basis of diffusion theory the expected $^{40}Ar^*/^{39}Ar$ distribution gradients in the grains can be calculated (Fig. 1.1) When major fractions of the original $^{40}Ar^*$ content are lost from the system, the last fractions of gas released will not yield the primary age of the mineral. For a sample with a uniform grain size, only in the case where less than about 20 percent of the argon was lost, will the primary age be preserved in the cores of the minerals. For a lognormal distribution of grain sizes with a σ of 0.33, it can be expected that even when about 60 percent of the original argon was lost, the last gas fractions will yield ages approximating the primary age of the mineral. In this case, however, no sub-horizontal segments are expected in the age spectrum. An important implication of these models is that when some argon is lost from the system, the K-Ar method and the $^{40}Ar/^{39}Ar$ total fusion method will give meaningless intermediate ages, but by applying the $^{40}Ar/^{39}Ar$ age spectrum method information can be obtained on the thermal history of the sample.

Diffusion from minerals can be described by the equations for diffusion from an ideal spherical or cylindrical body (Jost 1952):

-A cylindrical geometry is used in the case of micas (Giletti 1974).

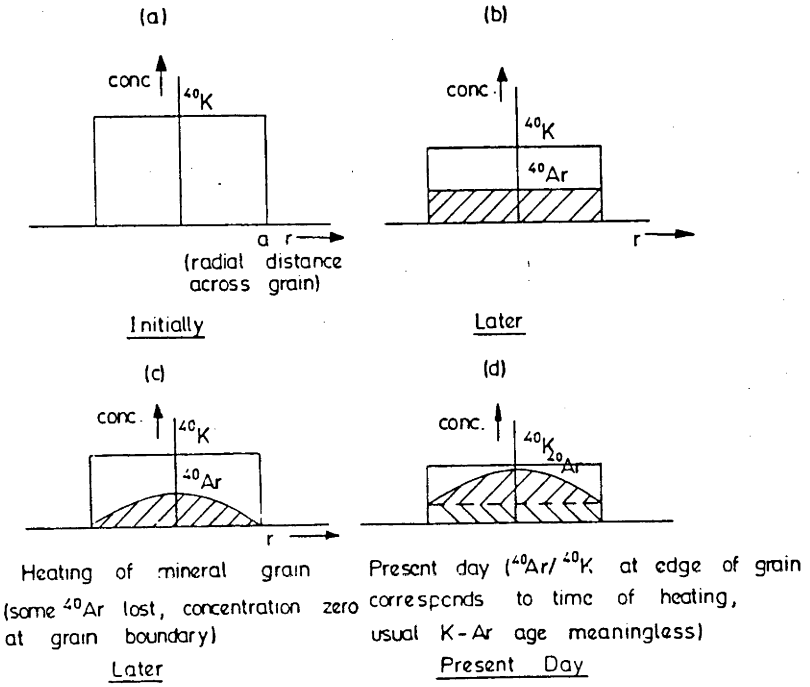

Figure A3. Schematic evolution of argon concentration in a sample with time, assuming single stage episodic loss during a thermal event. (a) initial situation. (b) uniform accumulation of $^{40}Ar^{*}$ while ^{40}K decays. (c) immediately following a thermal event during which argon was lost from the margins of the crystal by volume diffusion. (d) ^{40}K and $^{40}Ar^{*}$ concentration in the sample immediately before analysis (Turner 1968).

$$F=1 - \sum_{n=1}^{\infty} 4/\alpha_n^2 \exp(-D\alpha_n^2 t/a^2) \qquad (20)$$

-And a spherical geometry is used to describe the case of hornblendes.

$$F=1 - \sum_{n=1}^{\infty} 6/\pi^2 n^2 \exp(-Dn^2\pi^2 t/a^2) \qquad (21)$$

In these equations F is the fractional release of argon, t the time span over which the gas was lost, D the diffusion rate, a^2 a geometry factor related to the radius of the sphere or cylinder. The α_ns are roots of $J_o(\alpha_n)=0$ where J_o is the Bessel function of the first kind of the order zero.

The equations (20) and (21) can be used to calculate theoretical age patterns for the case that argon was lost from the system in a discrete event after crystallization of a mineral (Turner 1968). When the original age and the time of overprinting can be estimated, it is possible to calculate a value for Dt_o/a^2 from the fractional gas loss that has occurred during overprinting, x_o in Turner (1968) and equation (22). The $^{40}Ar^*/^{39}Ar_K$ ratio in a laboratory outgassing experiment is found for any fraction released in the laboratory experiment by (eq. 22):

$$^{40}Ar^*/^{39}Ar_K =$$

$$^{40}Ar_1^*/^{39}Ar_{0,K}(g(x + x_o)/g(x)) + {}^{40}Ar_2^*/^{39}Ar_{0,K}$$

In this equation $g(x) = d/dx(F(x))$, F is the fractional release of argon (see (20) and (21)), $^{40}Ar^*_1$ is the total amount of radiogenic argon accumulated before the thermal event, $^{40}Ar^*_2$ is the amount of $^{40}Ar^*$ accumulated after the thermal event, and x is the value for Dt/a^2 appropriate for gas release during the laboratory experiment. When a sample cannot be closely sized, values for Dt/a^2 and Dt_o/a^2 should be calculated by integration over the grain size interval in the sample.

Experimental procedures

The experimental procedures used followed standard laboratory practice and is discussed elswhere (cf. Cooper 1963, McDougall 1966, McDougall 1974, McDougall and Roksandic 1974, McDougall and Schmincke 1977, Tetley et al. 1980, Wang et al. 1979). Before the actual stepheat experiment is started the isotopic composition of the fluxmonitor is measured in order to calculate the J-parameter. Subsequent to the fluxmonitor, normally a 1/8 split of the sample is measured, providing a separate measurement of the total fusion age and information on the amounts of gas present in the sample, which is useful in deciding the step sizes in the actual stepheat experiment. For the case of stepheat experiments on micas, the biotite standard GA-1550 (K-Ar age is 97.9 Ma) has been used as fluxmonitor. In the case of stepheat experiments on hornblendes, the hornblende standard 77-600 (K-Ar age is 414.2 Ma) has been used as a fluxmonitor. By using this approach, the corrections for interfering isotopes are similar in the standard and in the sample and thus help reduce the possible error. In the stepheat experiments on micas it was possible to measure a release pattern in about 20 steps, from about 400-450 ^{o}C to about 1100 ^{o}C for the last step before fusion. The last step, the totalfusion step, is normally at the highest possible temperature, about 1380 ^{o}C, to make certain that all the gas is extracted from the sample. The temperature of the sample during a stepheat experiment was measured with a thermocouple in contact with the bottom of the crucible. The temperature of the upper inner wall of the crucible was measured with an optical pyrometer. The temperature difference between both measurements was variable, but generally the thermocouple measurement was in the order of 100-120 ^{o}C lower than the pyrometer measurement. The duration of a step is the time that the sample was at the desired temperature. Apart from the first, low temperature steps (400-600 ^{o}C) the heating up time and the cooling down time is short (1-2 min.). At least once every experiment a line blank was measured. In order to check that after the total fusion step no gas is left in the sample, a hot line blank can be measured. It indicates that in most cases after the total fusion step more than 99.5 of the gas is extracted from the sample.

Appendix II. Major element chemistry of minerals

Major element chemical analysis of minerals from most samples used for dating purposes was carried out on an electron microprobe contructed by the Technisch Physische Dienst of the Technical University of Delft, The Netherlands using carbon coated polished thin sections of rock samples. The machine is fitted with an Ortec Lithium drifted energy dispersive detector, and a Canberra Instruments multichannel pulse height analyser. Collected data was processed on-line using an HP1000E computer and software developed by Ware (1981), which is based on matrix correction and instrumental correction procedures discussed by Reed and Ware (1975).

The data are presented as coefficients of the mineral structural formula, for micas based on 22 oxygen atoms, for amphiboles based on 23 oxygen atoms, for garnets based on 24 oxygen atoms, for cordierites based on 18 oxygen atoms, and for chlorites based on 28 oxygen atoms. Amphibole analyses were normalized according to the guidelines discussed by Laird and Albee (1981).

bio : biotite, sta : staurolite, gar : garnet

Amphibole analyses Pilbara

no	Si	Ti	Al-IV	Al-VI	Fe(II)	Fe(III)	Mg	Ca	K	Na(M4)	Na(A)
81-314											
1	6.771	.039	1.229	.406	1.140	.475	2.940	1.947	.044	.053	.280
2	6.745	.052	1.255	.427	1.162	.415	2.944	1.945	.045	.055	.319
3	6.968	.028	1.032	.407	1.350	.184	3.031	1.953	.190	.047	.242
4	7.271	.016	.729	.185	1.328	.414	3.057	1.976	.017	.024	.105
5	6.912	.043	1.088	.348	1.011	.532	3.065	1.913	.029	.087	.179
6	7.036	.033	.964	.385	1.084	.371	3.128	1.951	.042	.049	.150
7	7.071	.020	.929	.310	.903	.486	3.280	1.950	.013	.050	.130
8	6.995	.038	1.005	.373	.931	.497	3.161	1.928	.026	.072	.106
9	7.051	.043	.949	.343	1.071	.331	3.213	1.956	.040	.044	.194
10	7.115	.018	.885	.268	.973	.448	3.294	1.980	.023	.020	.130
11	6.906	.047	1.094	.373	1.132	.375	3.073	1.972	.049	.028	.232
12	6.939	.035	1.061	.385	1.026	.444	3.110	1.956	.035	.044	.172
13	6.847	.040	1.153	.457	1.127	.397	2.980	1.962	.043	.038	.215
14	6.976	.034	1.024	.231	.859	.668	3.208	1.916	.031	.084	.110
15	7.268	.010	.732	.190	.873	.485	3.442	1.994	.000	.006	.043
16	6.982	.038	1.018	.376	1.092	.403	3.091	1.963	.029	.037	.171
82-324											
1	7.716	.000	.284	.048	1.609	.218	3.124	2.009	.000	.000	.000
2	7.689	.000	.311	.032	1.587	.294	3.087	1.992	.000	.000	.000
3	7.798	.000	.202	.027	1.807	.151	3.015	2.012	.000	.000	.000
4	7.867	.000	.133	.140	2.160	-.145	2.845	2.069	.000	.000	.000
5	7.669	.000	.331	.026	1.568	.393	3.013	1.956	.000	.000	.000
6	7.648	.000	.352	-.005	1.364	.525	3.116	1.916	.000	.000	.000
7	7.751	.000	.249	.011	1.701	.209	3.079	2.014	.000	.000	.000
8	6.873	.000	1.127	-.193	.035	2.070	3.088	1.625	.000	.000	.000
9	7.739	.016	.261	.019	1.644	.230	3.090	1.990	.000	.000	.000
10	7.345	.063	.655	-.058	1.853	.787	2.355	1.725	.121	.229	.000
11	7.606	.000	.394	.038	1.653	.368	2.941	1.994	.000	.000	.000
12	7.719	.000	.281	-.022	1.534	.391	3.096	1.949	.014	.000	.000
13	7.688	.000	.312	-.027	1.561	.370	3.095	1.984	.000	.000	.000
14	7.665	.000	.335	-.002	1.591	.344	3.068	1.997	.000	.000	.000
82-350											
1	6.885	.024	1.115	-.181	1.467	1.240	2.452	1.942	.035	.058	.033
2	7.216	.037	.784	.059	1.639	.586	2.680	1.938	.043	.062	.085
3	7.145	.027	.855	.088	1.696	.623	2.567	1.956	.034	.044	.101
4	6.869	.047	1.131	.153	1.763	.710	2.327	1.922	.075	.078	.177
5	6.688	.062	1.312	.237	1.910	.719	2.072	1.922	.084	.078	.226
6	6.984	.065	1.016	.138	1.828	.610	2.359	1.908	.068	.092	.162
7	7.008	.039	.992	.144	1.694	.697	2.426	1.895	.050	.105	.127
8	7.163	.026	.837	.139	1.661	.584	2.590	1.905	.045	.095	.113
9	7.146	.033	.854	.160	1.748	.567	2.493	1.899	.055	.101	.108
10	7.376	.031	.624	.833	2.370	-.338	2.104	1.700	.047	.300	.319
11	7.106	.034	.894	.112	1.672	.716	2.465	1.921	.019	.079	.057
82-351											
1	6.280	.035	1.720	.831	1.195	.699	2.240	1.843	.023	.157	.254
2	6.075	.298	1.925	.688	1.276	.602	2.136	1.823	.033	.177	.184
3	6.330	.025	1.670	.719	.890	1.081	2.284	1.705	.073	.295	.041

4	6.191	.040	1.809	.889	1.043	.922	2.106	1.747	.026	.253	.145
5	6.209	.031	1.791	.807	1.027	.937	2.197	1.787	.040	.213	.157
6	6.389	.035	1.611	.802	1.370	.700	2.093	1.838	.025	.162	.176
7	6.269	.031	1.731	.851	1.109	.854	2.156	1.782	.016	.218	.166
8	6.319	.020	1.681	.776	.928	1.000	2.277	1.736	.029	.264	.101

82-352

1	6.612	.027	1.388	.474	1.126	.857	2.516	1.812	.026	.188	.164
2	6.422	.037	1.578	.680	1.258	.789	2.236	1.803	.034	.197	.198
3	6.785	.026	1.215	.069	.155	2.043	2.707	1.412	.000	.227	.000
4	7.117	.000	.883	.251	.853	.859	3.037	1.812	.000	.149	.000
5	6.371	.032	1.629	.652	1.282	.856	2.178	1.799	.035	.201	.223
6	6.232	.055	1.768	.785	1.302	.831	2.027	1.789	.102	.211	.151
7	6.529	.033	1.471	.625	1.216	.792	2.334	1.800	.022	.200	.166
8	6.555	.016	1.445	.621	1.078	.906	2.380	1.762	.024	.238	.101
9	6.465	.026	1.535	.644	1.293	.766	2.271	1.808	.025	.192	.240
10	6.108	.020	1.892	.463	.125	2.021	2.370	1.518	.000	.331	.000
11	6.605	.033	1.395	.613	1.275	.721	2.358	1.846	.000	.154	.148
12	6.699	.025	1.301	.613	1.485	.632	2.246	1.834	.040	.166	.133
13	6.842	.000	1.158	-.055	-.023	2.003	3.075	1.554	.000	.102	.000
14	6.635	.022	1.365	.532	1.077	.944	2.426	1.776	.016	.224	.054
15	6.556	.036	1.444	.601	1.239	.800	2.324	1.795	.041	.205	.135

82-354

1	6.250	.022	1.750	.875	1.385	.713	2.005	1.907	.027	.093	.185
2	6.432	.025	1.568	.735	1.378	.647	2.216	1.910	.029	.090	.199
3	6.378	.000	1.622	.818	1.252	.726	2.205	1.894	.017	.106	.168
4	6.380	.025	1.620	.799	1.590	.561	2.026	1.924	.035	.076	.252
5	6.900	.026	1.100	.446	1.383	.456	2.690	1.919	.150	.081	.078
6	6.346	.046	1.654	.704	1.396	.686	2.168	1.910	.049	.090	.213
7	6.179	.023	1.821	.686	1.322	.993	1.976	1.828	.044	.172	.223
8	6.275	.017	1.725	.836	1.574	.652	1.921	1.943	.032	.057	.229
9	6.639	.019	1.361	.655	1.078	.672	2.576	1.890	.015	.110	.092

82-356

1	6.435	.043	1.565	.742	1.173	.651	2.391	1.913	.022	.087	.151
2	6.720	.026	1.280	.761	.981	.478	2.755	1.879	.019	.121	.092
3	6.944	.014	1.056	.523	.922	.586	2.955	1.879	.022	.121	.019
4	6.934	.017	1.066	.570	1.013	.475	2.926	1.892	.025	.108	.071
5	6.909	.034	1.091	.512	.832	.634	2.988	1.853	.000	.147	.025
6	6.892	.034	1.108	.495	.808	.660	3.004	1.853	.000	.147	.033
7	7.158	.026	.842	.374	.839	.587	3.173	1.891	.000	.047	.000
8	6.958	.028	1.042	.445	.691	.747	3.089	1.842	.000	.110	.000
9	6.764	.039	1.236	.511	.862	.670	2.918	1.886	.000	.114	.090
10	7.191	.018	.809	.253	.718	.755	3.256	1.845	.000	.076	.000
11	7.270	.010	.730	.175	.616	.791	3.409	1.847	.000	.051	.000
12	6.453	.030	1.547	.764	1.191	.631	2.386	1.915	.015	.085	.164
13	6.770	.012	1.230	.657	.950	.606	2.774	1.856	.000	.144	.087
14	6.619	.022	1.381	.606	.903	.740	2.730	1.884	.017	.116	.091

82-361

1	6.335	.069	1.665	.551	2.140	.680	1.560	1.941	.063	.059	.292
2	6.359	.073	1.641	.612	1.973	.645	1.697	1.916	.040	.084	.282
3	6.431	.074	1.569	.547	2.084	.594	1.701	1.955	.043	.045	.282
4	6.449	.068	1.551	.549	2.124	.614	1.646	1.951	.038	.049	.263
5	6.890	.061	1.110	.233	2.042	.657	2.007	1.962	.032	.038	.104
6	6.950	.059	1.050	.232	2.058	.569	2.082	1.974	.041	.026	.116

7	6.986	.050	1.014	.215	2.005	.566	2.164	1.953	.033	.047	.146
8	6.434	.067	1.566	.595	2.155	.515	1.667	1.971	.068	.029	.282
9	6.393	.073	1.607	.608	2.061	.535	1.723	1.948	.045	.052	.325
10	6.867	.048	1.133	.319	2.042	.588	2.003	1.960	.047	.040	.123
11	6.401	.069	1.599	.549	2.035	.683	1.664	1.926	.044	.074	.259
12	7.429	.013	.571	.252	1.911	.437	2.387	1.928	.000	.000	.000

Mica schists Pilbara

82-346

no.	Si	Ti	Al	FeII	Mg	Mn	Ca	K
1 bio	5.417	0.147	3.685	3.021	1.657	0.000	0.000	1.279
2 bio	5.205	0.179	3.809	3.192	1.816	0.000	0.000	0.985
3 bio	5.451	0.166	3.676	2.880	1.625	0.000	0.000	1.492
4 sta	3.737	0.018	8.790	1.223	0.082	0.000	0.000	0.000
5 bio	5.296	0.140	3.625	3.122	1.807	0.000	0.000	1.524
6 gar	5.449	0.000	3.674	4.516	0.431	0.547	0.098	0.000
7 bio	5.442	0.145	3.632	2.661	1.964	0.000	0.000	1.505
8 gar	5.971	0.000	4.000	4.900	0.468	0.617	0.073	0.000
9 bio	5.323	0.113	3.720	3.062	1.842	0.025	0.000	1.241
10 bio	5.409	0.208	3.550	2.660	1.951	0.000	0.000	1.660
11 gar	5.945	0.014	4.010	4.902	0.458	0.618	0.089	0.000
12 gar	5.907	0.000	4.029	4.888	0.501	0.657	0.096	0.000
13 bio	5.385	0.143	3.590	2.740	1.923	0.000	0.014	1.757
14 bio	5.430	0.156	3.601	2.889	1.730	0.000	0.000	1.616
15 bio	5.215	0.195	3.726	3.071	1.700	0.033	0.000	1.572
16 sta	3.682	0.024	8.797	1.259	0.113	0.000	0.000	0.000

82-315 muscovites

no	Si	Ti	Al	FeII	Mg	K	Na
1	6.099	0.075	5.674	0.088	0.059	1.826	0.160
2	6.113	0.089	5.638	0.079	0.070	1.831	0.150
3	6.178	0.040	5.655	0.059	0.049	1.780	0.166
4	6.165	0.068	5.613	0.086	0.053	1.754	0.197
5	6.173	0.074	5.592	0.078	0.061	1.765	0.188
6	6.142	0.051	5.652	0.069	0.082	1.775	0.192
7	6.136	0.071	5.633	0.079	0.055	1.801	0.204
8	6.119	0.076	5.629	0.077	0.091	1.790	0.209
9	6.113	0.064	5.682	0.065	0.068	1.793	0.188
10	6.078	0.056	5.694	0.073	0.062	1.867	0.209

Amphibolites and quartzites Mount Narryer

no		Si	Ti	Al	FeII	Mn	Mg	Ca	K	Na
71918	hbl	6.581	0.073	1.929	2.294	0.044	2.408	1.854	0.090	0.0308
71918	hbl	6.664	0.056	1.878	2.333	0.040	2.455	1.747	0.073	0.264
71918	hbl	6.839	0.051	1.588	2.529	0.073	2.654	1.423	0.087	0.229
71918	hbl	6.637	0.073	1.916	2.288	0.058	2.308	1.811	0.107	0.374
71918	bio	5.085	0.176	4.168	1.998	0.000	2.361	0.028	1.675	0.000
71918	bio	5.473	0.167	3.047	2.485	0.000	2.676	0.032	1.914	0.000
71918	bio	5.541	0.197	3.010	2.474	0.000	2.611	0.024	1.797	0.000
71918	chl	5.006	0.000	4.777	3.441	0.000	5.222	0.000	0.000	0.000
71918	chl	4.419	0.000	6.346	2.941	0.048	4.626	0.027	0.000	0.000
71919	bio	5.319	0.270	3.352	2.552	0.000	2.425	0.000	1.536	0.000
71919	gar	5.955	0.000	4.002	5.110	0.189	0.645	0.112	0.000	0.061
71919	bio	5.329	0.269	3.420	2.248	0.000	2.469	0.000	1.712	0.072
71919	gar	5.998	0.000	3.951	5.140	0.198	0.629	0.111	0.000	0.000
71919	gar	5.976	0.000	3.006	5.054	0.199	0.687	0.099	0.000	0.000
71919	bio	5.352	0.352	3.301	2.314	0.000	2.430	0.000	1.731	0.000
71919	gar	5.940	0.000	3.995	5.133	0.206	0.695	0.093	0.000	0.000
71919	bio	5.328	0.242	3.313	2.510	0.000	2.508	0.000	1.744	0.000
71919	gar	5.951	0.000	4.009	5.123	0.189	0.663	0.109	0.000	0.000
71919	bio	5.376	0.158	3.526	2.641	0.000	2.112	0.000	1.697	0.000
71919	bio	5.411	0.160	3.558	2.603	0.000	2.032	0.000	1.706	0.000
71919	bio	5.391	0.165	3.440	2.584	0.000	2.227	0.000	1.734	0.000
71919	gar	5.955	0.000	3.982	5.227	0.248	0.494	0.124	0.000	0.043
71919	cor	4.990	0.000	3.985	0.913	0.000	1.188	0.000	0.000	0.025
71919	bio	5.342	0.200	3.464	2.488	0.000	2.520	0.000	1.613	0.000
71919	gar	5.944	0.000	4.004	5.075	0.197	0.693	0.116	0.000	0.048
71919	bio	5.380	0.167	3.528	2.952	0.000	1.767	0.000	1.744	0.000
71919	cor	4.986	0.000	3.986	0.919	0.000	1.110	0.000	0.000	0.040
71919	bio	5.359	0.170	3.439	2.384	0.000	2.520	0.000	1.692	0.000
71919	gar	5.998	0.000	3.960	5.114	0.199	0.646	0.104	0.000	0.000
71919	cor	4.995	0.000	4.007	0.702	0.000	1.297	0.000	0.000	0.000
71919	gar	6.037	0.000	4.072	4.818	0.184	0.676	0.118	0.000	0.046
71919	bio	5.163	0.205	3.480	3.014	0.000	2.149	0.000	1.605	0.000
71919	gar	5.904	0.020	4.042	5.167	0.215	0.565	0.113	0.000	0.000
71919	bio	5.239	0.147	3.509	2.861	0.000	2.133	0.000	1.771	0.019
71919	gar	5.437	0.000	3.702	4.821	0.194	0.474	0.083	0.000	0.000
71919	gar	5.930	0.000	4.014	5.136	0.213	0.630	0.113	0.000	0.056
71919	bio	5.213	0.180	3.475	2.763	0.000	2.261	0.000	1.708	0.073
71919	cor	4.930	0.000	4.055	0.905	0.000	1.140	0.000	0.000	0.026
71919	bio	5.319	0.239	3.486	2.753	0.000	1.954	0.000	1.806	0.000
71919	gar	5.903	0.000	4.091	5.167	0.203	0.585	0.102	0.000	0.000
71919	cor	4.926	0.000	4.057	0.855	0.000	1.180	0.000	0.000	0.056
71919	gar	5.860	0.023	3.996	5.269	0.199	0.579	0.118	0.013	0.050
71919	bio	5.243	0.197	3.449	2.717	0.000	2.148	0.000	1.855	0.076
71923	gar	5.944	0.000	3.983	5.117	0.223	0.644	0.128	0.000	0.052
71923	bio	5.234	0.154	3.592	2.303	0.000	2.840	0.000	1.390	0.000
71923	bio	5.403	0.184	3.445	2.814	0.000	2.029	0.048	1.535	0.000
71923	gar	5.992	0.000	3.946	5.149	0.207	0.591	0.124	0.000	0.050
71923	bio	5.339	0.337	3.379	3.061	0.000	1.700	0.000	1.640	0.000
71923	gar	6.012	0.000	3.952	5.091	0.205	0.617	0.135	0.000	0.000
71923	gar	5.968	0.000	3.982	5.275	0.194	0.504	0.118	0.000	0.000
71923	bio	5.400	0.184	3.702	2.368	0.000	1.993	0.000	1.797	0.039
71923	gar	5.895	0.000	3.958	5.415	0.215	0.491	0.124	0.000	0.000
71923	bio	5.339	0.201	3.477	2.817	0.000	2.036	0.000	1.720	0.000

71923	gar	5.999	0.000	3.989	5.166	0.197	0.533	0.122	0.000	0.000
71923	bio	5.326	0.179	3.428	2.927	0.000	2.064	0.020	1.607	0.069
71923	gar	5.982	0.000	3.966	4.985	0.195	0.747	0.137	0.000	0.000
71923	gar	5.977	0.000	3.999	5.021	0.199	0.709	0.117	0.000	0.000
71928	gar	6.020	0.000	3.965	4.889	0.326	0.565	0.207	0.000	0.049
71928	bio	5.446	0.176	3.783	2.854	0.015	1.273	0.000	1.876	0.000
71928	bio	5.389	0.180	3.453	3.224	0.000	1.493	0.000	1.929	0.000
71928	mus	6.353	0.036	5.195	0.286	0.000	0.188	0.000	1.909	0.000
71928	mus	6.342	0.000	5.160	0.369	0.000	0.215	0.000	1.911	0.072
71928	mus	6.295	0.000	5.287	0.272	0.000	0.212	0.000	1.937	0.053
71928	mus	6.277	0.028	5.219	0.363	0.000	0.194	0.000	1.964	0.045
71928	mus	6.274	0.009	5.340	0.263	0.000	0.181	0.000	1.908	0.051
71928	mus	6.396	0.013	5.129	0.337	0.000	0.202	0.000	1.897	0.000
71929	hbl	6.827	0.053	1.750	2.022	0.039	2.640	1.787	0.036	0.174
71929	hbl	6.800	0.069	1.763	1.960	0.042	2.676	1.797	0.046	0.238
71929	hbl	6.876	0.044	1.725	1.933	0.049	2.691	1.807	0.028	0.157
71929	bio	6.669	0.162	2.435	1.712	0.000	2.223	0.000	1.500	0.000
71929	hbl	6.770	0.057	1.804	1.961	0.048	2.679	1.828	0.048	0.199
71929	hbl	7.352	0.000	0.984	1.621	0.023	3.211	1.934	0.000	0.060
71929	hbl	6.748	0.066	1.814	2.014	0.038	2.617	1.836	0.059	0.231
71929	hbl	7.494	0.000	0.633	1.758	0.000	3.513	1.792	0.000	0.000
71929	hbl	7.090	0.047	1.736	1.803	0.030	2.440	1.767	0.040	0.122
71929	hbl	6.802	0.041	1.777	1.984	0.043	2.664	1.885	0.039	0.162
71929	bio	5.479	0.192	3.096	2.214	0.015	2.848	0.028	1.818	0.000

Amphibole analyses Naxos

no	Si	Ti	Al-IV	Al-VI	Fe(II)	Fe(III)	Mg	Ca	K	Na(M4)	Na(A)
81-536											
1	6.279	.045	1.721	1.053	1.513	.501	1.889	1.789	.084	.211	.205
2	6.344	.039	1.656	1.014	1.551	.443	1.953	1.800	.073	.200	.248
3	6.181	.039	1.819	1.192	1.449	.400	1.921	1.808	.066	.192	.276
4	7.658	.000	.342	-.047	.314	1.129	3.604	1.573	.012	.102	.000
5	6.205	.048	1.795	1.019	1.423	.578	1.932	1.800	.076	.200	.225
6	6.596	.038	1.404	.827	1.762	.347	2.026	1.906	.073	.094	.175
7	6.234	.043	1.766	1.003	1.271	.587	2.096	1.803	.055	.197	.231
8	6.170	.044	1.830	1.066	1.340	.572	1.978	1.793	.067	.207	.244
9	6.289	.048	1.711	1.185	1.339	.495	1.932	1.745	.066	.255	.123
10	6.245	.054	1.755	1.012	1.449	.607	1.877	1.754	.080	.246	.193
11	6.337	.033	1.663	1.021	1.370	.468	2.108	1.831	.057	.169	.221
81-540											
1	6.397	.042	1.603	.717	1.835	.615	1.790	1.797	.073	.203	.316
2	6.260	.044	1.740	.859	1.749	.600	1.747	1.804	.079	.196	.309
3	6.405	.041	1.595	.673	1.823	.621	1.842	1.817	.083	.183	.319
4	6.500	.033	1.500	.738	1.718	.573	1.938	1.808	.074	.192	.242
5	7.646	.000	.354	.104	.982	.779	3.135	1.641	.023	.166	.000
6	7.258	.018	.742	.317	1.464	.454	2.747	1.832	.038	.168	.066
7	6.940	.035	1.060	.856	1.962	.383	1.764	1.644	.096	.356	.011
8	6.298	.041	1.702	.873	1.813	.442	1.832	1.876	.091	.124	.339
81-543											
1	6.788	.054	1.212	.569	1.115	.303	2.959	1.907	.101	.093	.225
2	6.577	.065	1.423	.685	1.236	.286	2.728	1.904	.133	.096	.286
3	6.839	.055	1.161	.595	1.125	.284	2.942	1.881	.102	.119	.190
4	6.885	.053	1.115	.545	1.136	.290	2.976	1.894	.095	.106	.185
5	6.990	.048	1.010	.476	1.062	.328	3.087	1.913	.064	.087	.134
6	6.599	.057	1.401	.645	1.275	.266	2.756	1.936	.145	.064	.294
7	7.400	.013	.600	.296	.956	.252	3.482	1.941	.021	.059	.064
8	6.448	.053	1.552	.733	1.290	.299	2.625	1.926	.165	.074	.323
9	6.851	.040	1.149	.498	1.096	.370	2.997	1.897	.086	.103	.219
10	6.720	.059	1.280	.598	1.246	.285	2.813	1.924	.120	.076	.236
11	6.691	.042	1.309	.655	1.208	.275	2.820	1.931	.123	.069	.242
12	7.056	.023	.944	.441	.996	.360	3.181	1.914	.056	.086	.127
13	6.786	.049	1.214	.520	1.115	.360	2.956	1.897	.093	.103	.246
14	7.231	.030	.769	.454	1.058	.223	3.235	1.897	.050	.103	.085
15	6.831	.050	1.169	.470	1.044	.382	3.055	1.917	.086	.083	.215
16	6.839	.050	1.161	.551	1.214	.211	2.974	1.898	.133	.102	.268
17	7.002	.036	.998	.509	1.082	.271	3.102	1.915	.075	.085	.156
18	6.643	.047	1.357	.728	1.212	.265	2.748	1.887	.137	.113	.246
19	6.562	.056	1.438	.766	1.253	.249	2.676	1.910	.124	.090	.278
20	6.739	.057	1.261	.615	1.122	.333	2.874	1.891	.108	.109	.201
21	7.071	.046	.929	.515	1.100	.274	3.065	1.884	.059	.116	.105
22	6.793	.057	1.207	.548	1.048	.361	2.987	1.886	.086	.114	.213
81-545											
1	7.654	.000	.346	.189	.597	.418	3.796	1.809	.000	.121	.000
2	7.125	.033	.875	.598	1.157	.190	3.022	1.816	.092	.184	.113
3	7.035	.054	.965	.455	1.067	.344	3.081	1.840	.040	.160	.179
4	7.240	.045	.760	.394	1.103	.325	3.132	1.841	.027	.159	.082
5	6.835	.069	1.165	.539	1.140	.305	2.948	1.883	.050	.117	.251

6	7.325	.018	.675	.307	.898	.370	3.407	1.906	.000	.094	.056
7	7.655	.017	.345	.123	.694	.405	3.761	1.841	.000	.100	.000
8	7.402	.030	.598	.221	1.022	.328	3.400	1.905	.018	.095	.067
9	7.011	.042	.989	.439	.907	.452	3.160	1.823	.036	.177	.156
10	6.817	.035	1.183	.538	1.025	.435	2.968	1.843	.044	.157	.254
11	6.842	.080	1.158	.501	1.153	.308	2.958	1.857	.060	.143	.272

81-550

1	6.325	.059	1.675	.612	1.426	.800	2.103	1.788	.041	.212	.316
2	6.355	.057	1.645	.509	1.227	.897	2.310	1.806	.038	.194	.281
3	6.089	.066	1.911	.799	1.295	.828	2.012	1.740	.059	.260	.353
4	6.073	.044	1.927	.778	1.032	1.054	2.092	1.692	.041	.308	.274
5	6.229	.053	1.771	.630	1.325	.863	2.129	1.822	.040	.178	.310
6	6.115	.065	1.885	.796	1.246	.857	2.036	1.738	.057	.262	.308
7	6.450	.036	1.550	.597	1.127	.853	2.387	1.772	.038	.228	.217
8	6.146	.058	1.854	.716	1.358	.808	2.060	1.799	.048	.201	.367
9	6.119	.047	1.881	.822	1.137	.957	2.037	1.705	.059	.295	.244
10	6.242	.053	1.758	.645	1.287	.889	2.125	1.784	.050	.216	.284
11	6.400	.043	1.600	.654	1.364	.738	2.201	1.814	.039	.186	.269

81-557

1	6.082	.078	1.918	.701	1.900	.210	2.111	1.961	.298	.039	.592
2	6.068	.080	1.932	.675	1.906	.218	2.122	1.981	.290	.019	.609
3	6.090	.079	1.910	.699	1.955	.161	2.106	1.980	.301	.020	.611
4	6.108	.078	1.892	.778	2.145	.089	1.910	1.986	.248	.014	.635
5	6.077	.078	1.923	.725	1.996	.231	1.970	1.968	.275	.032	.568
6	6.023	.079	1.977	.695	1.991	.262	1.973	1.993	.258	.007	.611
7	6.007	.081	1.993	.709	1.965	.277	1.968	1.984	.227	.016	.633
8	6.015	.088	1.985	.688	1.958	.267	2.000	1.964	.236	.036	.655
9	6.058	.082	1.942	.721	2.065	.177	1.955	1.986	.253	.014	.641
10	6.150	.087	1.850	.677	2.006	.200	2.031	1.963	.204	.037	.633
11	6.075	.095	1.925	.681	2.184	.207	1.834	1.962	.258	.038	.628

81-578

1	7.838	.000	.162	1.318	1.399	.671	1.612	.094	.000	1.906	.079
2	7.839	.000	.161	1.298	1.335	.715	1.653	.066	.000	1.934	.083
3	7.884	.000	.116	1.238	1.253	.764	1.745	.047	.000	1.953	.068
4	7.814	.000	.186	1.304	1.337	.714	1.644	.060	.000	1.940	.107
5	7.844	.000	.156	1.311	1.343	.703	1.643	.071	.000	1.929	.071
6	7.824	.000	.176	1.245	1.333	.763	1.659	.096	.000	1.904	.072
7	7.817	.011	.183	1.182	1.193	.832	1.782	.065	.000	1.935	.082
8	7.863	.000	.137	1.331	1.210	.674	1.786	.063	.021	1.937	.048
9	7.849	.000	.151	1.276	1.260	.737	1.727	.061	.000	1.939	.077

Major element chemistry white micas Naxos

no.	Si	Ti	Al	Fe^{2+}	Mg	Ca	K	Na
81-532								
1	6.182	.000	5.499	.280	.131	.000	1.629	.324
2	6.270	.000	5.331	.309	.183	.000	1.719	.223
3	6.202	.000	5.511	.266	.108	.000	1.582	.329
4	6.224	.000	5.367	.366	.155	.000	1.733	.229
5	6.416	.000	5.010	.394	.278	.000	1.855	.107
6	6.789	.000	4.862	.220	.066	.000	1.362	.301
7	6.305	.000	5.226	.389	.213	.000	1.706	.192
8	6.225	.013	5.334	.350	.166	.000	1.586	.427
9	6.353	.014	5.101	.411	.238	.000	1.756	.171
81-534								
1	7.019	.000	4.023	.328	.739	.021	1.605	.076
2	6.799	.018	4.390	.238	.670	.000	1.660	.089
3	6.965	.015	4.151	.214	.728	.000	1.643	.094
4	6.891	.022	4.183	.312	.720	.014	1.612	.096
5	6.768	.000	4.425	.273	.678	.000	1.643	.106
6	6.726	.019	4.531	.182	.601	.022	1.695	.118
7	6.721	.016	4.547	.197	.600	.000	1.717	.101
8	6.764	.017	4.462	.229	.636	.000	1.675	.082
9	6.773	.016	4.386	.266	.661	.013	1.685	.120
10	6.730	.018	4.465	.241	.647	.015	1.666	.138
11	6.768	.017	4.496	.183	.620	.018	1.611	.117
81-535								
1	6.897	.015	4.216	.292	.676	.000	1.701	.068
2	6.842	.021	4.297	.266	.665	.000	1.679	.114
3	6.445	.038	4.988	.215	.390	.012	1.785	.087
4	6.927	.019	4.123	.265	.749	.019	1.630	.082
5	6.474	.045	4.896	.194	.481	.023	1.724	.117
6	6.550	.033	4.787	.242	.504	.000	1.705	.109
81-537								
1	6.378	.045	5.031	.239	.386	.000	1.875	.090
2	6.466	.039	4.901	.167	.511	.013	1.807	.092
3	6.457	.019	5.020	.091	.429	.000	1.844	.151
4	6.432	.037	5.004	.155	.410	.000	1.826	.153
4	6.428	.027	5.043	.137	.397	.000	1.800	.183
5	6.451	.032	4.992	.129	.425	.000	1.825	.156
6	6.484	.026	5.012	.129	.364	.000	1.801	.133
7	6.449	.023	5.032	.137	.390	.000	1.812	.149
8	6.333	.048	5.107	.154	.418	.000	1.888	.122
9	6.632	.028	4.844	.225	.409	.000	1.835	.124
10	6.424	.020	5.005	.214	.410	.000	1.834	.129
11	6.473	.030	4.981	.168	.395	.000	1.816	.104
12	6.432	.020	5.062	.162	.360	.000	1.878	.085
13	6.480	.032	4.938	.190	.397	.000	1.873	.090
81-538								
1	6.714	.019	4.506	.277	.567	.026	1.708	.103

2	6.761	.021	4.427	.325	.550	.032	1.677	.100
3	6.180	.022	5.484	.167	.214	.032	1.630	.284
4	6.297	.034	5.291	.168	.296	.019	1.575	.260
5	6.461	.046	4.914	.228	.405	.016	1.799	.128
6	6.349	.036	5.134	.200	.343	.021	1.776	.153
7	6.378	.024	5.109	.211	.348	.017	1.781	.130
8	6.728	.023	4.451	.330	.559	.028	1.710	.094
9	6.101	.062	5.476	.195	.238	.036	1.765	.214
10	6.719	.019	4.487	.321	.547	.016	1.718	.103
11	6.679	.017	4.595	.258	.524	.013	1.745	.091
12	6.609	.018	4.749	.223	.455	.000	1.776	.110
81-541								
1	6.736	.018	4.433	.346	.573	.018	1.744	.065
2	6.752	.020	4.433	.354	.530	.015	1.711	.107
3	6.812	.015	4.327	.313	.599	.037	1.721	.094
4	6.724	.016	4.473	.339	.545	.026	1.697	.105
5	6.787	.021	4.330	.348	.578	.024	1.730	.082
6	6.792	.015	4.365	.335	.567	.033	1.739	.068
7	6.699	.010	4.488	.331	.584	.031	1.703	.107
81-552								
1	6.369	.087	5.083	.218	.290	.017	1.822	.054
2	6.138	.158	5.297	.223	.249	.039	1.729	.175
3	6.161	.116	5.365	.201	.216	.021	1.802	.119
4	6.175	.083	5.357	.202	.227	.015	1.847	.165
5	6.384	.082	5.044	.242	.330	.000	1.800	.059
6	6.360	.075	5.065	.235	.327	.020	1.785	.118
7	6.278	.076	5.200	.224	.299	.023	1.793	.104
81-556								
1	6.095	.087	5.507	.204	.182	.000	1.831	.145
2	6.143	.114	5.368	.204	.244	.015	1.831	.159
3	6.156	.077	5.452	.189	.171	.016	1.822	.138
4	6.086	.083	5.538	.168	.167	.024	1.835	.160
5	6.173	.091	5.357	.223	.197	.023	1.805	.148
6	6.165	.076	5.452	.181	.182	.000	1.794	.157
7	6.262	.101	5.228	.192	.263	.000	1.806	.148
8	6.196	.092	5.362	.188	.215	.000	1.836	.122
82-565								
1	6.033	.021	5.822	.083	.090	.000	1.451	.519
2	6.034	.017	5.815	.093	.090	.000	1.458	.528
3	6.688	.022	4.485	.357	.571	.000	1.698	.154
4	6.714	.029	4.613	.204	.482	.000	1.668	.150
5	6.703	.027	4.492	.313	.579	.000	1.644	.177
6	6.047	.012	5.792	.105	.103	.000	1.476	.497
7	6.705	.021	4.523	.313	.573	.000	1.581	.174
8	6.782	.019	4.475	.263	.554	.000	1.577	.159
9	6.021	.020	5.811	.110	.100	.000	1.488	.493
10	6.798	.021	4.503	.197	.524	.000	1.605	.164
11	6.051	.015	5.780	.093	.112	.000	1.494	.490
81-580								
1	6.686	.000	4.280	.545	.570	.077	1.923	.108
2	6.805	.020	4.044	.645	.610	.051	1.948	.039
3	6.849	.011	3.966	.650	.658	.034	1.979	.000

4	6.779	.000	4.074	.670	.603	.031	1.988	.067
5	6.633	.015	4.389	.582	.511	.000	1.913	.139
6	6.663	.020	4.316	.599	.539	.000	1.931	.114
7	6.658	.014	4.354	.566	.514	.034	1.900	.123
8	6.657	.011	4.372	.570	.495	.038	1.902	.105
9	6.737	.000	4.235	.606	.519	.016	1.987	.079
10	6.709	.000	4.311	.490	.579	.033	1.965	.062

81-579

1	6.709	.000	4.307	.502	.602	.000	1.891	.142
2	5.965	.000	5.915	.121	.073	.013	.106	1.873
3	5.999	.000	5.875	.114	.077	.019	.146	1.812
4	5.994	.000	5.854	.122	.084	.013	.169	1.855
5	6.671	.023	4.300	.573	.556	.022	1.883	.138
6	6.699	.000	4.321	.495	.578	.016	1.902	.162
7	5.929	.000	5.886	.108	.082	.140	.122	1.841
8	5.981	.000	5.902	.114	.065	.013	.108	1.878
9	6.453	.000	4.730	.509	.436	.022	1.740	.325
10	6.076	.000	5.775	.116	.066	.020	.131	1.835

81-578

1	6.887	.014	3.970	.577	.624	.000	1.843	.240
2	6.661	.000	4.469	.341	.607	.027	1.812	.187
3	6.680	.000	4.340	.493	.604	.017	1.895	.136
4	6.631	.000	4.499	.369	.577	.016	1.899	.119
5	6.671	.000	4.413	.465	.552	.000	1.894	.148
6	6.695	.011	4.317	.511	.577	.016	1.899	.119
7	6.763	.017	4.166	.545	.627	.017	1.926	.082
8	6.807	.018	4.017	.628	.647	.018	1.998	.063
9	6.730	.018	4.246	.487	.585	.039	1.847	.200
10	6.685	.016	4.353	.484	.557	.019	1.886	.132

Appendix III.

$^{40}Ar/^{39}Ar$ dating of white micas from an Alpine high pressure metamorphic belt on Naxos (Greece): the resetting of the argon isotopic system.

Jan R. Wijbrans, Ian McDougall,

Research School of Earth Sciences,
The Australian National University.
Canberra, ACT 2601, Australia.

Equivalence figures Chapter 3, appendix III.

Figure 1 = Figure 2.1b
Figure 2 = Figure 2.3
Figure 3 = Figure 3.3
Figure 4 = Figure 3.2
Figure 5 = Figure 3.10
Figure 6 = Figure 3.11
Figure 7 = Figure 3.12
Figure 8 = Figure 3.13
Figure 9 = Figure 3.14

Abstract

Overprinting of white micas from high pressure, low to medium temperature (M_1) metamorphic assemblages in pelitic schists on Naxos during subsequent thermal dome metamorphism (M_2) ranges from minor in the southeast of the island to complete recrystallization in the amphibolite facies grade rocks near the migmatites in the centre of the dome. The original (M_1) minerals are phengites (Si^{4+} = 6.7 - 7.0) and the overprinting minerals are muscovites (Si^{4+} = 6.0 - 6.45).

$^{40}Ar/^{39}Ar$ stepheating analyses of white mica separates from rocks in the area where phengite and muscovite occur together have yielded complex age spectra characterized by low apparent ages in the first stages and last stages of the experiment and higher apparent ages in between. These upward-convex age spectra are explained by mixing of two generations of mica. Consequently, some seemingly good plateaus in age spectra in this area must be interpreted as mixed ages. Further, the upward-convex age spectra have been used to trace the isotopic signature of phengites toward increasing M_2 metamorphic grade and suggest that as long as phengites are observed in the rocks, upward-convex age spectra occur. On Naxos, crystallization of muscovite at the expense of the original phengite is the main mechanism to reset the argon isotopic ages in white micas.

However, argon loss from phengites by volume diffusion occurs as well. The application of a simple diffusion model to the degassing of phengites supports the view that the original estimate for the M_2 metamorphic temperature in the lower amphibolite grade rocks is about 100 ^{o}C too high (Jansen and Schuiling 1976, Wijbrans 1985). This model also suggests that the M_2 metamorphism was caused by a shortlived heat source.

Introduction

In this paper $^{40}Ar/^{39}Ar$ age spectra for some white micas separated from rocks of the Attic Cycladic Metamorphic Belt (ACMB) on the island of Naxos, Greece, are presented. On Naxos two main metamorphisms are recognized: M_1 is a high pressure, low to medium temperature event and M_2 overprints M_1 and has produced a thermal dome just north of the centre of the island, with anatexis in the core and surrounded by Barrovian-type mineral zones (Jansen and Schuiling 1976, Jansen et al. 1977).

The present study concentrates on white micas from the pelitic schists ranging from those in which M_1 mineral assemblages predominate to those in which M_2 mineral assemblages are most important. The $^{40}Ar/^{39}Ar$ stepheating method of dating has the potential to resolve heterogeneities in the argon distribution in mineral samples. This makes it a useful tool in the study of thermally disturbed terrains, because one may be able to relate certain types of age spectra to certain mechanisms of resetting of the isotopic system. Stepheating analysis shows that some M_1 micas (phengites) are only slightly overprinted during M_2, that M_2 muscovites yield excellent flat age spectra and that white mica separates in the transition zone show complex age spectra, as a result of the presence of both the older phengites and the younger muscovites.

Resetting of the isotopic clock may occur by volume diffusion of argon from the original minerals and by recrystallization of these minerals. Good evidence for the first mechanism is found in contact aureoles (Hart 1964, Hanson and Gast 1967, Harrison and McDougall 1980). In metamorphic belts the second mechanism often dominates (Verschure et al. 1980, Chopin and Maluski 1980), but is not the exclusive mechanism to reset isotopic systems (Frey et al. 1976). In the present paper it is shown that on Naxos both mechanisms operated, that recrystallization was probably the more efficient mechanism, but that volume diffusion of argon from the phengites occurred and can be used to put constraints on the thermal evolution of the rocks.

Geological setting

Naxos is situated in the central part of the Aegean Sea, about 200 km south east of Athens (Fig. 1). The geology of Naxos can be divided into three main units: (1) metamorphic rocks which belong to the ACMB, (2) a granodiorite intrusive, and (3) non-metamorphic rocks (Fig. 2). The tectonic setting of the ACMB suggests that it is presently part of the Aegean back arc basin (McKenzie 1978, Le Pichon and Angelier 1978, Horvath and Berckhemer 1982). It has been argued that the ACMB may have had a tectonic evolution which is similar to that of the Basin and Range province in the western USA (McKenzie 1978, Lister et al. 1984).

In the ACMB on Naxos, two major metamorphic events can be distinguished. The first metamorphism, designated M_1, is a high pressure, low to medium temperature metamorphism, typical of the Alpine Orogeny. Estimates for the physical conditions during the peak of the M_1 metamorphism range from 9 to 12 kbar (900 to 1200 MPa) and 500 to 530 ^{o}C for southeast Naxos (Jansen et al. 1977). Mineral assemblages in the metapelites of southeast Naxos consist predominantly of quartz, phengite and albite. Depending on the bulk chemistry of the rock, the mineral assemblages may include garnet, glaucophane, chlorioid, chlorite and epidote.

The second major metamorphism, designated M_2, produced a thermal dome just north of the centre of Naxos. At a pressure of about 5 kbar (500 MPa), the M_2 metamorphism caused minor overprinting to complete recrystallization of the original mineral assemblages. Over a distance of about 15 km the effect of the M_2 metamorphism on the rocks increases from local minor crystallization of muscovite and chlorite (estimated temperature about 300 ^{o}C) to anatexis in the metapelites (estimated temperature about 700 ^{o}C) (Jansen and Schuiling 1976, Wijbrans 1985).

The metamorphic complex at Naxos was divided into a series of M_2 mineral zones separated by mineral isograds (Jansen and Schuiling 1976). Six zones were identified on the basis of the mineralogy of the metapelites and the metabauxites (Fig 2). In summary, zone I is the zone least affected by M_2 overprinting. It is characterized by the occurrence of diaspore in the metabauxites. In zone II, corundum becomes the major aluminium phase in the metabauxites and chlorite and muscovite are formed locally in the metapelites. In zone III biotite is formed in the metapelites; the high grade boundary of this zone was chosen at the

breakdown of chloritoid in the metapelites and the metabauxites. In zone IV, metapelites may have mineral assemblages including garnet, staurolite and kyanite. On the west side of the thermal dome andalusite also occurs locally. In zone V fibrolitic sillimanite becomes the stable aluminium silicate polymorph. This may be further subdivided into a zone where kyanite is still metastably present and a zone without kyanite. The central zone, zone VI, was mapped on the first evidence for partial melting in the metapelites. The apparently simple concentric shape of the mineral zones around the central migmatites suggests that the M_2 heating event post dates the last major deformation.

Phengitic white micas in the rocks from the metamorphic complex in the area least affected by overprinting during the M_2 metamorphism occur as flat crystals which consistently show evidence for deformation. At least two phases of deformation are recognized (Wijbrans 1980). Under the M_2 thermal gradient the folded crystals become segmented into individually straight subgrains. The major element chemistry of phengites shows that they are low in aluminium, and high in magnesium and silica (Si^{4+} = 6.7 -7.0) (Wijbrans 1980). The muscovite which is crystallized as part of the M_2 mineral assemblage is quite different from the original phengite. It occurs often in shorter, thicker crystals. In mica rich bands in the rock it does not show a preferred orientation or evidence for deformation. The major element chemistry indicates that these muscovites are high in aluminium and low in magnesium and silica (Si^{4+} = 6.0 - 6.45) (Wijbrans 1980). The chemistry of white micas as a function of metamorphic grade is represented in Figure 3 as the variation in silica and magnesium content of selected micas from the different M_2 mineral zones. It was shown that the composition of white micas is relatively insensitive to variations in mineral assemblages within an M_2 metamorphic zone (Wijbrans 1980). It shows that M_1 phengites are still metastably present in rocks of zone IV, where the M_2 mineral assemblage includes biotite, garnet and staurolite.

Previous geochronology

Conventional K/Ar dating of white micas in the low grade M_2 metamorphic zones supports an age of 45 $\pm$ 5 Ma for the M_1 event (Andriessen et al. 1979). Ages obtained from similar mineral assemblages from elsewhere in the ACMB fall within the same range (Henjes-Kunst 1978, Altherr et al. 1979, Bonneau et al. 1980). In zone I, II and III on Naxos,

the K/Ar ages display a considerable scatter, which was attributed to partial resetting of the isotopic system, but the presence of excess ^{40}Ar could not be excluded (Andriessen et al. 1979). A more detailed investigation of white micas from zone II indicated that crystallization of muscovite during M_2 overprinting contributed to resetting of the K/Ar ages of white micas (Wijbrans and Andriessen 1980). $^{40}Ar/^{39}Ar$ stepheating analyses of white micas in zone I suggest that cooling below the closure temperature of phengite for argon diffusion occurred about 50 Ma ago (Wijbrans 1985).

Ages on the M_2 minerals, biotite and muscovite, in the central zones reflect cooling to below the closure temperature for argon diffusion at about 11 and 12 Ma respectively (Andriessen et al. 1979, Wijbrans 1985). K/Ar ages on hornblendes in the highest grade M_2 metamorphic zones in the centre of Naxos range from 15 to 18 Ma (Andriessen et al. 1979, Wijbrans 1985). Increasing ages toward lower M_2 metamorphic grade in hornblendes and white micas led Andriessen et al. (1979) to suggest that the peak temperature of the M_2 metamorphism occurred 25 ± 5 Ma ago. On the basis of present work on the white micas and an accompanying study on the age of M_2 metamorphic hornblendes Wijbrans (1985) suggests that the peak of the M_2 metamorphism occurred about 15 to 16 Ma ago.

Experimental

Techniques

Standard procedures for conventional K/Ar analysis (McDougall 1966, McDougall and Schmincke 1977), and $^{40}Ar/^{39}Ar$ analysis were used (McDougall 1974, McDougall and Roksandic 1974). The samples were irradiated for 120 hours in the HIFAR reactor of the Australian Atomic Energy Commission, packed in aluminium containers together with biotite standard GA1550 (age 97.9 Ma) as a flux monitor. Cadmium shielding was used to minimize interference from thermal neutrons. In each experiment the sample was heated at progressively higher temperatures for 30 minutes per step, starting at about 400 ^{o}C until fusion was reached. The temperature of the sample was estimated from measurement with a thermocouple in contact with the bottom of the molybdenum crucible and an optical pyrometer. The correction factors for interfering nuclear reactions involving isotopes of calcium and potassium were given by Tetley et al. (1980) (see caption of Table I). The ages were calculated using the values for the decay constants of ^{40}K and the abundance of ^{40}K which were recommended by the Subcommission on Geochronology of the IUGS (Steiger and Jäger 1977). The samples used in this study were purified to better than 99 percent by standard techniques including heavy liquid and magnetic separation.

Results

The present work is part of a larger study into the $^{40}Ar/^{39}Ar$ systematics of metamorphic minerals on Naxos. The K/Ar ages of white mica concentrates of relevance to this work are presented in Figure 4. The apparent ages for the samples used in this study decrease from 38 Ma in zone II to 16.8 Ma in zone IV (see Table I).

Stepheating analysis of sample 81-580 (Fig. 8 curve a) from zone I has yielded low initial ages (about 25 Ma), increasing rapidly in the first stages of the experiment with gradually rising apparent ages in the rest of the experiment until a final age of about 44 Ma is reached. The shape of this age spectrum is very similar to those that would be predicted on the basis of diffusion theory if, subsequent to crystallization, argon was lost by volume diffusion in a discrete event (Turner 1966, 1969). In contrast, the age spectrum of muscovite 81-556 (Fig. 8 curve c) from the M_2 migmatite zone is perfectly flat over more than 95 percent of the total gas release. This suggests rapid cooling of the muscovite through its

closure temperature for argon.

Age spectra of white mica samples from the M_2 mineral zones II, III and IV around the thermal dome are presented in Figure 5. They commonly show low initial ages, rising monotonically until a plateau or a maximum age is reached. Apart from the age spectrum of 81-537, all age spectra show a decrease in ages in the high temperature steps. The shape of these age spectra will be called upward-convex (Foland 1983). Maximum recorded apparent ages decrease as the M_2 thermal dome is approached and range from 43.34 Ma in sample 81-585 (Fig. 5 curve a) from zone II to 17.15 Ma in sample 81-586 (Fig. 5 curve f) from zone IV. The low apparent ages in the initial steps are variable but may be as low as 8 Ma and the apparent ages in the high temperature part of the experiments are often only slightly higher.

The age spectrum of sample 81-532 (Fig. 5 curve d) is characterized by a progressive increase in apparent ages and a maximum apparent age of about 29 Ma. This is a substantially lower age than observed in other white micas from about the same metamorphic grade. In thin section it is observed that the mineral assemblage in this sample is profoundly recrystallized subsequent to the M_1 metamorphism. The ages of around 17 Ma in the initial steps of the age spectrum would suggest that overprinting may well have occurred during the M_2 metamorphism. It is noted that $^{40}Ar/^{39}Ar$ analysis indicates that argon derived from M_1 formed phengites contributes to the age spectrum, because of the similarity of this age specrum to age spectra of micas from less recrystallized rocks of similar metamorphic grade. In the case of full recrystallization during M_2 overprinting, a flat age spectrum similar to that of muscovite 81-556 would be expected. The age spectrum of sample 81-537 (Fig. 5 curve e) is difficult to interpret. It is disturbed, with low ages in the initial steps and slightly increasing ages in the high temperature steps of the age spectrum. The apparent ages of the bulk of the gas release suggest a poorly defined age of about 28 Ma.

Discussion

Model for upward convex age spectra

Upward-convex age spectra have been reported in biotites which contain excess ^{40}Ar (Pankhurst et al. 1973, Foland 1983). No mechanism for the production of such age spectra was proposed. From comparison of the biotite ages with hornblende ages from the same area, it was suggested that the biotite ages are anomalously old, because of diffusion of excess ^{40}Ar into the crystals. Upward-convex age spectra in white micas also were reported in rocks from the Swiss Alps (Hammerschmidt 1983); the presence of excess ^{40}Ar was also suggested in this case.

A mechanism which may explain upward-convex age spectra in white micas from Naxos is based on the following observations:
(1) The white mica population in these zones is known to contain both M_1 formed phengites and M_2 formed muscovites. Consequently, a mineral concentrate from these zones normally will contain both minerals.
(2) It was observed in stepheating experiments on muscovite and phengite that at high temperatures argon release from the pure M_2 muscovite lags slightly behind the release of argon from phengite (Fig. 6). This effect may be the result of differences in the chemistry of the two micas which causes small differences in diffusional behaviour at high temperature. Because this effect shows up at temperatures in excess of 900 °C in the experiments (Fig. 6), and dehydration of white mica in air occurs between 750 and 950 °C (Kiefer 1949), it is suggested that by the time the effect becomes prominent, the dehydration reaction in the mica is near to completion. Thus, the differences in argon release probably are caused by differences in physical properties of the anhydrous phases. From the release data of muscovite and phengite (Fig. 6) it can be seen that gas released from muscovite should start dominating the age spectra at temperatures higher than about 900 °C.

The effects of mixing are displayed schematically in Figure 7. This diagram shows in the upper curve the variation in $^{40}Ar^*/^{39}Ar_K$ ratio for an M_1 phengite that has lost some of its radiogenic argon during the M_2 metamorphism (as is the case in sample 81-580), and in the lower curve the $^{40}Ar^*/^{39}Ar_K$ ratio for an M_2 muscovite with an undisturbed argon distribution (as is the case in sample 81-556). The intermediate curve represents a model for a mixture of phengite and muscovite. The observation that muscovite retains argon at slightly higher temperatures

than phengite is indicated by a broken line where the phengite is degassed and the muscovite still contains argon. This model suggests that gradients in the $^{40}Ar^{*}$ distribution in phengites can be resolved from a mixed sample, so that an estimate from the time of overprinting may be obtained from the initial ages, as is suggested from Turner's model (1966, 1969). It also indicates that the younger muscovite has an age which is approximated by the apparent ages in the highest temperature steps of the age spectrum. The actual shape of the age spectrum will depend of on the amounts of muscovite and phengite in the sample and on the fraction of argon lost from the phengite during overprinting. The most important implication of this model is that in age spectra of white micas it is possible to have good plateaus of a meaningless intermediate age.

To test this model, a $^{40}Ar/^{39}Ar$ stepheating experiment was carried out on a mixture of pure muscovite (81-556), which has yielded an essentially flat age spectrum, and phengite (81-580), which showed a monotonically rising age spectrum. A mixture of 75 percent phengite and 25 percent muscovite was used. In Figure 8 the age spectra of the pure components and of the mixture are displayed. The age spectrum of the mixture follows that of the pure phengite in the early stages. Phengite derived argon dominates the age spectrum until a point is reached where the ages start to decrease. The ages in the highest temperature steps approximate the age of the muscovite component (Fig. 8). The resulting age spectrum is very similar to those observed in the low grade zones at Naxos. This experiment provides confirmation that the observed upward-convex age spectra are the result of the presence of two distinct generations of mica in the sample. This conclusion is in agreement with the petrological observations in rocks from zone II to IV in the M_2 mineral zone on Naxos.

Implications for the M_2 metamorphism at Naxos

The isotopic signature of phengites in age spectra can be traced along the M_2 thermal gradient to the low grade part of zone IV where the stable M_2 mineral assemblage includes biotite, staurolite and garnet (Fig. 5). The M_2 metamorphic temperature in this part of zone IV was estimated at 540 to 560 ^{o}C by Jansen and Schuiling (1976). It is unlikely that phengites will retain accumulated argon for any significant time at these temperatures (see Figure 9). The implication is that the temperatures reached in this part of zone IV are not as high as previously estimated, and indeed the presence of incompletely degassed phengites may be used to constrain the effective temperature reached during overprinting in the M_2

event.

The presence of staurolite in the M_2 mineral assemblage may be used to estimate the M_2 metamorphic temperature in zone IV. From such a temperature estimate, together with the argon isotopic data on phengites, it may be possible to obtain constraints on the duration of the M_2 thermal pulse. Experimental data on the stability of staurolite indicates that the mineral will be formed between 535 and 565 ^{o}C when the pressure is 5 kbar and the metamorphic fluid is pure H_2O (Hoschek 1969). From a study of the fluid inclusions of syn-M_2 quartz lenses at Naxos, it was estimated that the fraction of CO_2 in the metamorphic fluid varied between 0.6 and 0.9 (Kreulen 1980). In this environment the temperature for the formation of staurolite would be lower, about 425 - 475 ^{o}C (Hoschek 1969, see also Wijbrans 1985). Using this temperature estimate and diffusion theory it can be predicted how much time it would take for radiogenic ^{40}Ar to diffuse out of the mica crystals. The geometry of micas for diffusion of argon is best described by the infinite cylinder approximation (Giletti 1974). This means that argon mainly will move preferentially parallel to the (001) directions in the crystals.

The first term of the expression for diffusion from an infinite cylinder (Jost 1952) is a good approximation for cases of argon loss greater than F=0.9 (Fechtig and Kalbitzer 1966, Mussett 1969). If the resulting equation is solved for time (t), the following equation is obtained:

$$t = - \frac{a^2}{D(\alpha)_1^2} * \ln((1 - F)*\frac{(\alpha)_1^2}{4})$$

In this equation a is the effective diffusion radius of the mineral, D the diffusion rate at temperature T (calculated from the diffusion constant D_0 and the activation energy Q using the Arrhenius relation $D=D_0\exp(-Q/RT)$), F the fraction of argon lost by diffusion, and α_1 the first root of the Bessel function of the order zero. The solution of this equation for F=0.95 and the average grain radius $\bar{a}$=0.0085 cm is given in Figure 9. Fractional loss F=0.95 was used to approximate full resetting of the minerals. The average grain size in the separate was assumed to be representative for the grain size in the rock (i.e. fracturing of minerals during crushing was assumed to be minor). It was pointed out by Mussett (1969) that reliable diffusion data on micas is scarce, because in many experiments up to that time no attempts were made to assure that the minerals remained stable. Diffusion experiments where the minerals were

kept stable in a hydrothermal apparatus were carried out subsequently by Giletti (1974) on phlogopite, and by Robbins (T.M.Harrison pers. comm.) on muscovite. Both the curves for muscovite and for phlogopite were plotted in Figure 9. Also plotted were the temperatures for the staurolite forming reaction according to Hoschek (1969) for $a(H_2O)$ in the metamorphic fluid is 1.0 and 0.5. From the curves in figure 9 a time estimate for the duration the M_2 thermal pulse can be obtained (i.e. the time interval that the effective temperature of the system was at the temperature estimated from the formation of staurolite). Estimates assuming the $a(H_2O)$ of the ambient fluid was 0.5 range from the order of about 100000 years to about 3 Ma for both the phlogopite curve and the muscovite curve.

Resetting of the isotopic system in white micas

For the purpose of discussion, resetting is defined as the result of the sum of effects that produce younger isotopic ages in minerals. The M_1 phengites and M_2 muscovites together will be referred to as the white micas. The previous section illustrates that when resetting during a subsequent thermal pulse occurs by volume diffusion of argon from the original minerals, the parameters time, temperature, and diffusion radius of the minerals control the degree of resetting of the minerals. In the case of the M_2 overprinting on Naxos, the isotopic system of the white micas becomes progressively more reset toward the centre of the island. The $^{40}Ar/^{39}Ar$ age spectra suggest that resetting of the white mica ages occurred by combination of two processes: (1) crystallization of a discrete new generation of muscovites at the expense of the earlier phengites, and (2) diffusion of argon from the earlier phengites, due to the increased temperature during M_2 overprinting. Broadly, resetting of the argon isotopic system of white micas from Naxos during M_2 metamorphism occurred in the rocks where the temperatures ranged from 350 ^{o}C to 450 ^{o}C (temperature estimates based on the assumption of a metamorphic fluid with $a(H_2O)=0.5$). It can be argued that this result is in agreement with estimates for the blocking temperatures of 350 to 380 ^{o}C for white micas obtained from work in the Swiss Alps (e.g. Jäger 1979). More detailed examination of the results of the present study suggests that at the low temperature side of the zone where resetting occurs the degree of resetting is correlated with recrystallization of the original minerals. This observation is well illustrated by comparing the age spectra of 81-585 and 81-532. Although sampled from adjacent schist zones the age spectrum of 81-532 is substantially more reset than that of 81-585. It is

observed that the mineralogy of 81-532 underwent substantial recrystallization during the M_2 metamorphism. In contrast with the adjacent schist zones where phengites dominate, in 81-532 the main white mica is an M_2 muscovite. At the high temperature side of the zone where resetting takes place, phengites remain metastably present in rocks where the stable M_2 mineral assemblage includes biotite, muscovite, staurolite and garnet. The $^{40}Ar/^{39}Ar$ age spectra suggest that in this area the phengites still contain argon that accumulated between the M_1 and M_2 metamorphisms. These more detailed observations cast some doubt on the suggestion made above that resetting can be understood in terms of a 'classic' blocking temperature.

Before discussing our results in more detail, it is useful to give a brief outline of the concepts used previously to describe resetting of isotopic ages. The relation between temperature and argon retention or isotopic resetting is often discussed in terms of closure and blocking temperatures, below which retention of isotopic daughter occurs. Although the two terms are often used as synonyms, there is by definition a difference between the two. Blocking temperatures were introduced to help account for systematic differences in ages between different minerals, or between the results of two different isotopic methods applied to the same mineral (Armstrong et al. 1966, Jäger et al. 1967, Jäger 1973, Purdy and Jäger 1976, Jäger 1979). These systematic differences reflect the fact that different minerals will start accumulating radiogenic daughter only below a certain temperature. An empirical temperature calibration for the blocking temperatures of a series of rock forming minerals in the Swiss Alps was obtained from petrological data and the observed resistance of the isotopic system to resetting during subsequent overprinting (Jäger 1973). The blocking temperature of biotite for argon was estimated at about 300 ^{0}C, and that of muscovite for argon at about 350 to 380 ^{o}C. It should be noted that recrystallization as a means of resetting of the isotopic system is not excluded in the definition of the blocking temperature (Jäger 1973). Closure temperatures are based on diffusion theory, and can be used for a more quantified understanding of argon retention. For a system that cools through the temperature interval where the transition occurs from no argon retention to full argon retention, the closure temperature of a mineral was defined by Dodson as the temperature of the system at the apparent age of the mineral (Dodson 1973, 1979). Values for the closure temperature of a mineral in a cooling system can be calculated on the basis of diffusion theory from the diffusion parameters

D_0 and Q for argon diffusion in that mineral and the cooling rate of the rocks.

An alternative mechanism for resetting of isotopic ages is recrystallization of the original minerals. In the white micas on Naxos, recrystallization involves breaking of the Si-O and Al-O bonds in the crystal lattice and the building of a new crystal with a different Al/Si ratio in an orientation which is not determined by the orientation of the original crystal (Wijbrans 1980). Argon trapped within the original crystal lattice will be released into the metamorphic fluid, because recrystallization involves breaking down the original minerals and crystallization of a new mineral possibly at a different site. This mechanism will occur when a mineral becomes thermodynamically unstable and the activation energy threshold for reaction is reached. During overprinting at greenschist facies grade the observation is that thermodynamic instability alone does not often initiate recrystallization. Consequently, recrystallization will be concentrated in zone where the activation energy threshold is lowered by more intense deformation, or fluid flow. It should be noted that recrystallization itself is a complex process which involves diffusion of ions in the metamorphic fluid and along grain boundaries. The rates of such processes are at greenschist facies grade probably are significantly higher than the rate of volume diffusion of argon within a mineral lattice. Consequently, recrystallization is likely to occur only locally during greenschist facies grade overprinting, but when it occurs it will reset the argon isotopic system more efficiently than volume diffusion from the original minerals.

Where reliable diffusion data are available, argon retention preferably should be discussed in terms of closure temperatures. It should be noted that the question whether the closure temperature concept is valid at greenschist facies grade comes down to proving that volume diffusion from the original minerals was the dominant mechanism to reset the isotopic clock. If it can be shown, on the other hand, that the original minerals have recrystallized, volume diffusion would not be the only mechanism operating in resetting the isotopic clock. In such cases, it is difficult to make use of the concept of closure temperatures. An additional problem is that closure temperatures can be calculated readily for minerals cooling through the temperature interval from where no retention of argon occurs to where full retention of argon occurs (Dodson 1973). In the case of reheating of the system during a subsequent thermal

pulse, it is more difficult to obtain a straight forward definition for the closure temperature. In the previous section, attempts were made to approach the problem of resetting by volume diffusion without explicitly defining a closure temperature. Instead, it is assumed that the minerals are reset when 95 percent of their original argon is lost. When the diffusion parameters D_0 and Q of a mineral for argon diffusion are known, and assuming a reasonable value for the diffusion radius a, it is possible to obtain values for the time and the temperature required to fully reset the argon system in that mineral. As illustrated in Figure 9, this relation allows estimates to be made for the duration of a thermal pulse if there are reasonable temperature constraints, or alternatively, when the duration of an event is known predictions as to the effective temperature reached by the system can be made.

A number of previous studies of resetting of the argon isotopic system in minerals during subsequent thermal disturbance have found little support for the blocking temperatures as estimated originally in the Swiss Alps (Verschure et al. 1980, Chopin and Maluski 1980, Del Moro et al. 1982). Verschure et al. (1980) and Del Moro et al. (1982) describe cases where the ambient rock temperatures during overprinting have apparently exceeded the accepted values for the blocking temperatures of biotite (i.e. about 300 ^{o}C, Jäger 1979) without significantly resetting the isotopic ages of the biotites. Both authors argue that their data suggest higher values for the blocking temperature of biotites for argon. The present study deals with the thermal overprinting of phengites. It was demonstrated that despite temperatures in excess of about 450 ^{o}C, phengites still contained argon that had accumulated before overprinting. Can this observation be used as an argument against closure temperatures, or to support higher estimates for the closure temperature than those obtained in the Swiss Alps? The point was made above that in the case of thermal overprinting temperature, time and, grainsize control the resetting when the original mineral remains stable. Using diffusion data it was demonstrated that no full resetting is expected at temperatures up to 100 ^{o}C in excess of the classic blocking temperature provided the duration of the overprinting event was short enough. Consequently, unless there is some constraint on the duration of overprinting, high apparent temperatures need not argue against the closure temperature concept.

Chopin and Maluski (1980) contend that during greenschist facies overprinting local complete recrystallization of the original minerals may occur, whereas the original minerals may fully retain their radiogenic argon. The mineralogy of the schists on Naxos, in the area where only limited overprinting during the M_2 metamorphism occurred, is similar to that in the area studied by Chopin and Maluski (1980) in the western Alps. In both areas phengites were formed during an early high pressure metamorphism, and subsequently have experienced greenschist facies grade overprinting. On Naxos, overprinting of the original mineral assemblages can be studied along the M_2 thermal gradient from minor overprinting to complete recrystallization of the original assemblages at amphibolite facies M_2 metamorphic grade. Thus, the ages of the original M_1 minerals and of the M_2 overprinting on Naxos are well constrained (Fig. 4). In the area that has experienced greenschist facies grade overprinting, the ages of white mica samples vary with M_2 metamorphic grade as well as with the intensity of post-M_1 deformation. In zone I, partial resetting of phengites occurred mainly by diffusion of argon from the crystals. This process continues toward higher M_2 metamorphic grade, until phengite disappears from the rocks in zone IV. In addition, in zone II to IV, the crystallization of muscovite during M_2 overprinting at the expense of the original phengites contributes to resetting of the argon isotopic system in the white micas. Phengites are observed in the rocks in cases where upward-convex age spectra are found, and the derived and K/Ar ages are higher than the cooling ages of muscovites in high grade M_2 metamorphic rocks. This suggests that crystallization of muscovite is the mechanism that finally resets the white micas ages in rocks of higher M_2 metamorphic grade. Thus, it is suggested that upward-convex age spectra in the area on Naxos of greenschist facies M_2 metamorphic grade indicate (1) that volume diffusion of argon from the original phengites occurred, and (2) that complete resetting of the argon system in white micas occurred only in rocks from Naxos in the area that reached amphibolite facies M_2 metamorphic grade. In the zone where M_2 overprinting reached greenschist facies grade, the signature of both generations of white mica could be identified in most samples, including sample 81-532 which showed substantial recystallization of the original phengites to M_2 muscovites. Our results are in agreement with the observations of Chopin and Maluski (1980) in that during overprinting at greenschist facies grade recrystallization more efficiently resets white mica ages compared to volume diffusion. However, in contrast with the conclusion of Chopin and Maluski (1980), no full resetting of the white mica ages on Naxos occurred

until the rocks reached amphibolite facies grade.

In conclusion, recrystallization of the original phengites played a major role in resetting of the isotopic ages in the white micas during the M_2 metamorphism on Naxos. In the age spectra the effects of argon loss by volume diffusion from M_1 phengites as well as crystallization of younger muscovites are observed. Because the apparent ages in upward-convex age spectra are interpreted as mixed ages, they should not be used in combination with closure temperatures to derive a thermal evolution for an area. But because volume diffusion of argon from the M_1 phengites was demonstrated by $^{40}Ar/^{39}Ar$ analysis, it is possible to use this information in combination with diffusion theory to constrain the thermal evolution of the rocks on Naxos during the M_2 metamorphism.

The article presented in Appendix III is an extended version of Chapter 3, section 3.4.2.5. It was listed here because it contains a more detailed discussion of the implications of the $^{40}Ar/^{39}Ar$ data of white micas from Naxos on the understanding of resetting of argon isotopic ages in white micas.
The figures are included in chapters 2 and 3, the data tables can be found in chapter 3, and the references are included in the listing at the end of the thesis.

References

Albarede F. (1976): Thermal models of posttectonic decompression as exemplified by the Haut-Allier Granulites (Massif Central, France). Geol. Soc. Fr. Bull. 18:1023-1032.

Altherr R. (1982): Lower Miocene granitoids in the Attic Cycladic complex, petrology and paleotectonic significance. in Congress on the eastern Mediterranean Edinburgh, 1982.

Altherr R., Schliestedt M., Okrusch M., Seidel E., Kreuzer H., Harre W., Lenz H., Wendt I., Wagner G.A. (1979): Geochronology of high pressure rocks on Sifnos (Cyclades, Greece). Contrib. Mineral. Petrol. 70:245-255.

Altherr R., Kreuzer H., Wendt I., Lenz H., Wagner G.A., Keller J., Harre W., Höhndorf A. (1982a): A Late Oligocene / Early Miocene high temperature belt in the Attic Cycladic Crystalline Complex (SE Pelagonian, Greece). Geol. Jb. E23:97-164.

Altherr R., Seidel E., Kreuzer H. (1982b): Petrological and geochronological constraints on geodynamic models for the Hellenides. in Congress on the eastern Mediterranean, Edinburgh 1982.

Andriessen P.A.M. (1978): Isotopic age relations within the polymetamorphic complex of the island Naxos (Cyclades, Greece). Verh. ZWO-Lab. v. Isotopen Geol. 3, Amsterdam.

Andriessen P.A.M., Boelrijk N.A.I.M., Hebeda E.H., Priem H.N.A., Verdurmen E.A.Th., Verschure R.H. (1979): Dating the events of metamorphism and granitic magmatism in the Alpine Orogen at Naxos (Cyclades, Greece). Contrib. Mineral. Petrol. 69:215-225

Andriessen P.A.M., Banga G., Boelrijk N.A.I.M., Hebeda E.H., Verdurmen E.A.Th. (1984): Pre-Alpine ages in the Greek Cyclades. Terra Cognita 4:199.

Angelier J., Lyberis N., Le Pichon X., Barrier E., Huchon P. (1982): The tectonic development of the Hellenic Arc and the Sea of Crete: a synthesis. Tectonophys. 86:213-242.

Archibald N.J., Bettenay L.F., Binns R.A., Groves D.I., Gunthrope R.J. (1978): The evolution of Archaean greenstone terrains,

Eastern Goldfields Province, W.A. Precam. Res. 6:103-132.

Argand E. (1916): Sur l'arc des Alpes occidentales. Eclog. Geol. Helv. 14:145-191.

Armstrong R.L. (1968): A model for Sr and Pb isotope evolution in a dynamic earth. Rev. Geophys. 6:175-199.

Armstrong R.L. (1981): Radiogenic isotopes, the case for crustal recycling on a near steady state no-continental growth earth. in: Moorbath S., Windley B.F. (eds.) The origin and evolution of the continental lithosphere. R. Soc. London.

Armstrong R.L., Jäger E., Eberhardt P. (1966): A comparison of K-Ar and Rb-Sr ages on Alpine biotites. Earth. Plan. Sc. Lett. 1:13-19

Arndt N.T., Nisbet E.G. (1982): Komatiites. Allen and Unwin London.

Arriens P.A. (1971) The Archaean geochronology of Australia. Spec. Publ. Geol. Soc. Aust. 3, 11-23.

Beckinsale R.D., Gale N.H. (1969): A reappraisal of the decay constants and branching ratio of ^{40}K. Earth Plan. Sc. Lett. 6:289-294.

Bemmelen R.W.v. (1972): Geodynamic models, an evaluation and a synthesis. Elsevier Amsterdam.

Berger G.W. (1975): $^{40}Ar/^{39}Ar$ stepheating of thermally overprinted biotite, hornblende and potassium feldspar from Eldora, Colorado. Earth Plan. Sc. Lett. 26:387-408.

Bettenay L.F., Bickle M.J., Boulter C.A., Groves D.I., Morant P., Blake T.S., James B.A. (1981): Evolution of the Shaw Batholith, an Archaean granitoid-gneiss dome in the Eastern Pilbara, W.A. Spec. Publ. Geol. Soc. Aust. 7:361-372.

Bickle M.J. (1978): Heat loss from the earth, a constraint on Archaean tectonics from the relation between geothermal gradients and the rate of plate production. Earth Plan. Sc. Lett. 40:301-315.

Bickle M.J., Hawkesworth C.J., England P.C., Athey D. (1975): A preliminary thermal model for regional metamorphism in the

Eastern Alps. Earth. Plan. Sci. Lett. 26:13.

Bickle M.J., Martin A., Nisbet E.G. (1975): Basaltic and peridotitic komatiites and stromatolites above a basal unconformity in the Belingwe greenstone belt Rhodesia. Earth Plan. Sc. Lett. 27:155-162.

Bickle M.J., Bettenay L.F., Boulter C.A., Groves D.I., Morant P. (1980): Horizontal tectonic interaction of an Archaean gneiss belt and greenstones, Pilbara Block, W.A. Geology 8:525-529.

Bickle M.J., Bettenay L.F., Barley M.E., Groves D.I., Cambell I.H., De Laeter J.R. (1983): A 3500 Ma plutonic and volcanic calcalkaline province in the Archaean East Pilbara Block. Contrib. Mineral. Petrol. 84:25-35.

Bickle M.J., Morant P., Bettenay L.F., Boulter C.A., Blake T.S., Groves D.I. (1984): Archaean tectonics of the Shaw Batholith, Pilbara Block, W.A., Structural and metamorphic tests of the batholith concept. Spec. Publ. Geol. Assoc. Canada. (in press).

Biju-Duval B., Letouzey J., Montadert L. (1978): Structure and evolution of the Mediterranean Basins. DSDP report leg 42. Government Printer Washington D.C.

Blackwell D.D. (1971): The thermal structure and physical properties of the earth's crust. AGU Geophys. Mon. 14:169-184.

Blake M.C., Bonneau M., Geyssant J., Kienast J.R., Lepvrier C., Maluski H., Papanikolaou D. (1981): A geological reconnaissance of the Cycladic blueschist belt, Greece. Geol. Soc. Am. Bull. 92:247-254.

Blake T.S., McNaughton N.J. (1984): A geochronological frame work for the Pilbara region. Univ. W. Aust., Dept. Geol.-Univ. Ext. Publ. 9:1-22.

Blight D.F., Barley M.E. (1981) Estimated pressure and temperature conditions from some Western Australian Precambrian metamorphic terrains. W. Aust. Geol. Surv. Ann. Rept. 1980, 67-72.

Bonneau M. (1982): Evolution geodynamique de l'arc Egeen depuis le Jurassique Superieur jusqu'au Miocene: Soc. Geol. Fr. Bull 24:229-242.

Bonneau M., Geyssant J., Kienast J.R., Lepvrier C., Maluski H. (1980): Tectonique et metamorphisme haute pression d'age Eocene dans les Hellenides: exemple de l'ile de Syros (Cyclades, Grece). C. R. Acad. Sc. Paris 291D:171-174

Brereton N.R. (1970): Corrections for interfering isotopes in the $^{40}Ar/^{39}Ar$ dating method. Earth Plan. Sc. Lett. 8:427-433.

Brereton N.R. (1972): A reappraisal of the $^{40}Ar/^{39}Ar$ stepwise degassing technique. Geophys. J. astro. Soc. 27:449-478.

Burke K., Dewey J.F., Kidd W.S.F. (1976): Dominence of horizontal movements, arc and microcontinental collisions during the late permobile regime. in B.F. Windley (ed): The early history of the earth. Wiley Interscience. London.

Cadogan P.H. (1977): Palaeo atmospheric argon in Rhynie Chert. Nature 268:38-41.

Carman J.H., Gilbert M.C. (1983): Experimental studies on glaucophane stability. Am. J. Sc. 283A:414-437.

Carrigan C.R. (1983): A heat pipe model for vertical magma filled conduits. J. Volc. Geotherm. Res. 16:279-298.

Carslaw H.S., Jaeger J.C. (1959): Conduction of heat in solids. Clarendon Press Oxford.

Čermak V., Rybach L. (1981) Thermal properties of rocks. in Angenheister G. (ed): Numerical data and funcional relationships in Science and Technology. Vla. Springer. Berlin.

Channell J.E.T., Tarling D.H. (1975): Paleomagnetism and the rotation of Italy. Earth Plan. Sc. Lett. 25:177-188.

Chappell B.W., White A.J.R. (1974): Two contrasting granite types. Pac. Geol. 8:173-174.

Chatterjee N.D., Froese E. (1974): A thermdynamic study of the pseudobinary join muscovite-paragonite in the system $KAlSi_3O_8$-$NaAlSi_3O_8$-Al_2O_3-SiO_2-H_2O. Am. Mineral. 60:985-993.

Chopin C., Maluski H. (1980): $^{40}Ar/^{39}Ar$ dating of high pressure metamorphic micas from the Gran Paradiso area (W. Alps): Evidence against the blocking temperature concept. Contrib. Mineral.

Petrol. 74:109-122

Claesson S., Roddick J.C. (1983): $^{40}Ar/^{39}Ar$ data on the age and metamorphism of the Ottfjället dolerites, Särv Nappe, Swedish Caledonides. Lithos 16:61-73.

Clark S.P. (1979): Thermal histories for th Central Alps. in Jäger E., Hunziger J.C. (eds.) Lectures in isotope geology. Springer. Berlin.

Clark S.P, Jäger E. (1969): Denudation rates in the Alps from geochronologic and heat flow data. Am. J. Sc. 267:1143-1160.

Cloetingh S.A.P.L., Nolet G., Wortel R. (1981): Crustal structure of the eastern Mediterranean inferred from Rayleigh wave dispersion. Earth Plan. Sc. Lett. 51:336-342.

Collerson K.D., McCulloch M.T. (1982): Field and isotopic relationships in the Archaean Pilbara Block, W.A. ANU, RSES Ann. rept. 1981:172-173.

Collerson K.D., McCulloch M.T. (1983): Field and isotopic constraints on Archaean crust and mantle evolution in the East Pilbara Block, W.A. Geol. Soc. Aust. Abs. 9:167-168.

Compston W., Arriens P.A. (1968): The Precambrian geochronology of Australia. Can. J. Earth Sc. 5:561-583.

Compston W., Williams I.S., Meyer C. (1984): U-Pb geochronology of zircons from Lunar breccia 73217 using a sensitive high mass resolution ion microprobe. Proc. 14^{th} Lunar Planet. Sci. Conf. in J. Geophys. Res. 89, Supp., B525-534.

Condie K.C. (1973): Archaean magmatism and crustal thickening. Bull. Geol. Soc. Am. 84:2981-2992.

Cooper J.A. (1963): The flame photometric determination of potassium in geological materials used for K-Ar dating. Geochim. Cosmochim. Acta 27:525-546.

Cooper J.A., James P.R., Rutland R.W.R. (1982): Isotopic dating and structural relations of granitoids and greenstones in the E. Pilbara, W.A. Precam. Res. 18:199-236.

Crank J. (1975): The mathematics of diffusion. Oxford Sc. Publ. Clarendon Press. Oxford.

Dallmeyer R.D. (1982): $^{40}Ar/^{39}Ar$ incremental release ages of biotite from a progressively remetamorphosed Archaean basement terrane in SW Labrador. Earth Plan. Sc. Lett. 61:85-96.

Dal Piaz G.V., Ernst W.G. (1975): Areal geology and petrology of eclogites and associated metabasites of the Piemont ophiolite nappe, Breuil-St.Jacques area, Italian West Alps. Tectonophys. 52:99-126.

Dalrymple G.B., Lanphere M.A. (1969): Potassium argon dating. Freeman San Francisco.

Dalrymple G.B., Lanphere M.A. (1971): $^{40}Ar/^{39}Ar$ technique of K/Ar dating: a comparison with the conventional technique. Earth Plan. Sc. Lett. 12:300-308.

Dalrymple G.B., Alexander E.C., Lanphere M.A., Kraker G.P. (1981): Irradiation of samples for $^{40}Ar/^{39}Ar$ dating using the Geological Survey TRIGA reactor. USGS Professional Paper 1176. Government Printer, Washington.

Davies G.F. (1979): Thickness and thermal history of continental crust and root zones. Earth Plan. Sc. Lett. 44:231-238.

Davis G.H. (1983): Shear zone model for the origin of metamorphic core complexes. Geology 11:342-347.

De Bremaecker J.C., Huchon Ph., Le Pichon X. (1982): The deformation of Aegea, a finite element study. Tectonophys. 86:197-213.

De Laeter J.R., Blockley J.G. (1972): Granite ages within the Pilbara Block, W.A. Geol. Soc. Aust. J. 19:363-370.

De Laeter J.R., Lewis J.D., Blockley J.G. (1975): Granite ages within the Shaw Batholith of the Pilbara Block. W. Aust. Geol Surv. Ann. Rep. 1974:73-79.

De Laeter J.R., Libby W.G., Trendall A.F. (1981): The older Precambrian geochronology of W. Australia. Spec. Publ. Geol. Soc. Aust. 7:145-157.

De Laeter J.R., Williams I.R., Rosman K.J.R., Libby W.G. (1981a): A definitive 3350 MY age from banded gneiss, Mt Narryer area, Western Gneiss Terrain. Western Australia. West. Aust. Geol.Surv.

Ann. Rept. 1980 94-98.

De Laeter J.R., Fletcher I.R., Rossman K.J.R., Williams I.R., Gee R.D., Libby W.G. (1981b): Early Archaean Gneisses from the Yilgarn Block W. Australia. Nature 292, 322-324.

De Laeter J.R., Fletcher I.R., Bickle M.J., Myers J.S., Libby W.G., Williams I.R. (1985): Rb-Sr, Sm-Nd, and Pb-Pb Geochronology of ancient gneisses from Mt Narryer, W. Australia. (In press in Aust. J. Earth Sc.)

Del Moro A., Puxeddu M., Radicati di Brozolo F., Villa J.M. (1982): Rb-Sr and K-Ar ages on minerals a temperatures of 300 to 400 ^{o}C from deep wells in the Larderello Geothermal Field (Italy). Contrib. Mineral. Petrol. 81:340-349

De Paolo D.J., Wasserburg G.J. (1976): Inferences about magma sources and mantle structure from variations of $^{143}Nd/^{144}Nd$. Geophys. Res. Lett. 3:743-746.

De Paolo D.J., Wasserburg G.J. (1979): Petrogenetic mixing models and Nd-Sr isotopic patterns. Geochi. Cosmochim. Acta 43:615-627.

Dewey J.F., Pitman III W.C., Ryan W.B.F., Bonin J. (1973): Plate tectonics and the evolution of the Alpine system. Geol. Soc. Am. Bull. 84:3137-3180.

Dewey J.F., Windley B.F. (1981): Growth and differentiation of the continental crust. in Moorbath S., Windley B.F. (eds): The origon and evolution of the earth's continental crust. R. Soc. London.

Dewey J.F., Sengor A.M.C. (1979): Aegean and surrounding regions, Complex multiplate and continuum tectonics in a convergent zone. Geol. Soc. Am. Bull. 90:84-92.

Dodson M.H. (1973): Closure temperatures in cooling geochronological and petrological systems. Contrib. Mineral. Petrol. 40:259-274

Dodson M.H. (1979): Theory of cooling ages. In E. Jäger, J.C. Hunziger (eds): Lectures in isotope geology. Springer Verlag Berlin

Draper G., Bone R. (1981): Denudation rates, thermal evolution,

and preservation of blueschist terranes. J. Geol. 89:601-613.

Dürr S., Altherr R., Keller J., Okrusch M., Seidel M. (1978): The median Aegean Crystalline belt: Stratigraphy, Structure, Metamorphism, Magmatism. in Closs A.H. et al. (eds): Alps, Appenines, Hellenides. Schweizerbart Stuttgart.

Dürr S., Flügel E. (1978): Contribution a la stratigraphie du cristallin des Cyclades: mise en evidence de Trias Superieur dans les marbres de Naxos (Grece). XXVI Congres, Assemblee pleniere Antalya, Comite de geologie et geophysique marines.

England P.C. (1978): Some thermal considerations of the Alpine metamorphism: Past, Present and Future. Tectonophys. 46:21-40.

England P.C., Richardson S.W. (1977): The influence of erosion upon the mineral facies of rocks from different metamorphic environments. J. Geol. Soc. London 134:201-213.

England P.C., Bickle M.J. (1984): Continental thermal and tectonic regimes during the Archaean. J. Geol. 92:353-367.

Ernst W.G. (1971): Metamorphic zonations on presumably subducted plates from Japan, California and the Alps. Contrib. Mineral. Petrol. 34:43-59.

Ernst W.G. (1973): Blueschist metamorphism and P-T regimes in active subduction zones. Tectonophys. 17:255-272.

Essene E.J. (1982): Geologic thermometry and barometry. in Reviews of Mineralogy. Vll. (J.M. Ferry (ed)).

Etheridge M.A., Wall V.J., Vernon R.H. (1983): The role of the fluid phase during regional metamorphism and deformation. J. metam. Geol. 1:205-225.

Fechtig H., Kalbitzer S. (1966): The diffusion of argon in K bearing solids. In: Schaeffer O.A., Zahringer J. (eds): Potassium Argon dating. Springer Verlag Berlin

Feenstra A. (1985): Metamorphism of bauxites on Naxos, Greece. Geol. Ultrajectina 39.

Ferry J.M., Spear F.S. (1978): Experimental calibration of the partitioning between biotite and garnet. Contrib. Mineral. Petrol. 66, 113-117.

Fleck R.J., Sutter J.F., Elliot D.H. (1977): Interpretation of discordant $^{40}Ar/^{39}Ar$ age spectra of Mesozoic tholeiites from Antarctica. Geochim. Cosmochim. Acta. 41:15-32.

Foland K.A. (1983): $^{40}Ar/^{39}Ar$ incremental heating plateaus for biotites with excess argon. Isotope Geosc. 1:3-21

Frey M., Hunziger J.C., Frank W., Bocquet J., Dal Piaz G.V., Jäger E., Niggli E. (1974): Alpine metamorphism in the Alps, a review. Schw. Mineral. Petro. Mitt. 54:247-290.

Frey M., Hunziger J.C., O'Neil J.R., Schwander H.W. (1976): Equilibrium-disequilibrium relation in the Mte Rosa granite (W Alps). Petrological, Rb/Sr and stable isotope data. Contrib. Mineral. Petrol. 55:147-179

Froude D.O., Ireland T.R., Kinny P.D., Williams I.S., Compston W., Williams I.R., Myers J.S. (1983): Ion microprobe identification of 4100 to 4200 Ma old terrestrial zircons. Nature 304, 616-618.

Froude D.O. (1985): Australian Archaean Crustal evolution: Implications from ion microprobe analysis of detrital zircons. Unpubl. MSc thesis ANU Canberra.

Fyfe W.S. (1982): Andesites - product of geosphere mixing. in Thorpe R.S. (ed): Andesites. Wiley and Sons. New York.

Fyfe W.S., Price N.J., Thompson A.B. (1978): Fluids in the Earth's crust. Elseviers, Amsterdam.

Fytikas M., Giuliani O., Innocenti F., Marinelli G., Mazzuoli R. (1976): Geochronological data on recent magmatism of the Aegean Sea. Tectonophys. 31:T29-T34.

Garner E.L., Murphy T.J., Gramlich J.W., Paulsen P.J., Barnes I.L. (1975): Absolute abundance ratios and atomic weight of a reference sample of potassium. J. Res. U.S. Nat. Bur. Stand., 79A:713-725.

Gee R.D., Baxter J.L., Wilde S.A., Williams I.R. (1981): Crustal development in the Archaean Yilgarn Block, W.Australia. Spec. Publ. Geol. Soc. Aust. 7, 43-56.

Giletti B.J. (1974): Diffusion related to geochronology. In:

A.W. Hoffman et al. (eds): Geochemical transport and kinetics. Carnegie Inst. of Washington publ. 634

Gillespie A.R., Huneke J.C., Wasserburg G. (1982): An assessment of $^{40}Ar/^{39}Ar$ dating of incomletely degassed xenoliths. J. Geophys. Res. 87:9247-9257.

Glikson A.Y. (1979): Early Precambrian tonalite-trondhjemite siallic nuclei. Earth Sc. Rev. 15:1-73.

Glikson A.Y., Lambert I.B. (1973): Relations in space and time between major Precambrian Shield units, an interpretation of W. Austalian data. Earth Plan. Sc. Lett. 20:395-403.

Godfriaux I. (1968): Etude geologique de la region de l'Olympe (Grece). Ann. Geol. Hellen. 19:1-271.

Godfriaux I. (1977): L'Olympe. in Decourt J. (ed): Reunion extraordinaire des Soc. Geol. Fr. et Soc. Geol. Gr. Soc. Geol. Fr. Bull. 19:45-49.

Grambling J.A. (1981): Pressures and temperatures in Precambrian metamorphic rocks Earth. Plan. Sc. Lett. 53:63-68.

Green D.H. (1972): Archaean greenstone belts may include terrestrial equivalents of lunar maria. Earth Plan. Sc. Lett. 15:263-270.

Greenwood H.J. (1962): The system $NaAlSi_2O_6$-H_2O-argon, total pressure and water pressure in metamorphism. J. Geophys. Res. 66:3923-3946.

Haas H. (1972): Diaspore - corundum equilibrium determined by epitaxis of diaspore on corundum. Am. Min. 57:1375-1385.

Hamilton P.J., Evensen N.M., O'Nions R.K., Glikson A.Y., Hickman A.H. (1981): Sm-Nd dating of the North Star Basalt, Warrawoona Group, Pilbara Block, W.A. Spec. Publ. Geol. Soc. Aust. 7:187-192.

Hammerschmidt K. (1983): Hump shaped $^{40}Ar/^{39}Ar$ age spectra. Indication of excess argon in white micas from the Swiss Alps. Fortschr. Mineral. 61 Beiheft 1: 78

Hanson G.N., Gast P.W. (1967): Kinetic studies in contact metamorphic zones. Geochim. et Cosmochim. Acta 31:1119-1153

Hanson G.N., Simmons K.R., Bence A.E. (1975): $^{40}Ar/^{39}Ar$ spectrum ages for biotite, hornblende and muscovite in a contact metamorphic zone. Geochim. Cosmochim. Acta 39:1269-1277.

Harland W.B., Cox A.V., Llewellyn P.G., Dickson C.A.G., Smith A.G., Walters R. (1982): A geologic time scale. Cambridge Earth Sc. Series. Cambridge University Press.

Harrison T.M. (1981): Diffusion in hornblende. Contrib. Mineral. Petrol. 78:324-331.

Harrison T.M. (1983): Some observations on the interpretation of $^{40}Ar/^{39}Ar$ age spectra. Isotope Geosc. 1:319-338.

Harrison T.M., Clarke G.K.C. (1979): A model of the thermal effects of igneous intrusion and uplift as applied to Quottoon Pluton, B.C. Can. J. Earth Sc. 16:411.

Harrison T.M., Armstrong R.L., Naeser C.W., Harakal J.E. (1979): Geochronology and thermal history of the Coast Plutonic Complex, near Prince Rupert, BC. Can. J. Earth Sc. 16, 400-410.

Harrison T.M., McDougall I. (1980): Investigations of an intrusive contact, northwest Nelson, New Zealand: I and II. Geochim. et Cosmochim. Acta 44:1985-2020

Harrison T.M., McDougall I. (1981): Excess ^{40}Ar in metamorphic rocks from Broken Hill, NSW: implications for $^{40}Ar/^{39}Ar$ age spectra and the thermal history of the region. Earth Plan. Sc. Lett. 55:123-149.

Harrison T.M., McDougall I. (1982): The thermal significance of potassium feldspar K-Ar ages inferred from $^{40}Ar/^{39}Ar$ age spectrum results. Geochim. Cosmochim. Acta 46:1811-1820.

Harrison T.M., Duncan I., McDougall I. (1985): Diffusion of ^{40}Ar in biotite: temperature, pressure and compositional effects. (subm. to Geochim. Cosmochim. Acta).

Harrison T.M., FitzGerald J.D. (1985): Exsolution in hornblende and its consequence for $^{40}Ar/^{39}Ar$ age spectra and closure temperature. (ms. submitted to geochim. Cosmochim. Acta).

Hart S.R. (1964): The petrology and isotopic mineral age relations of a contact zone in the Front Range, Colorado. J.

Geol. 72:493-525

Heim A. (1922): Geologie der Schweiz. II, Die Schweizer Alpen. Tauchnitz. Leipzig.

Henjes-Kunst F. (1980): Alpidische Einformung des PraeAlpidischen Kristallins und seiner Mesozoischen Hülle auf Ios (Kykladen, Griechenland). Thesis, University of Braunschweig.

Henjes-Kunst F., Kreuzer H. (1982): Isotopic ages of Pre-Alpidic rocks from the islans of Ios, Cyclades, Greece. Contrib. Mineral. Petrol. 80:245-253.

Hickman A.H. (1980): Lithological map and stratigraphic interpretation of the Pilbara. Geol. Surv. W.Aust. Government Printer Perth.

Hickman A.H. (1981): Crustal evolution of the Pilbara Block, W.A. Spec. Publ. Geol. Soc. Aust. 7:57-70.

Hickman A.H. (1983): Geology of the Pilbara and its environs. Geol. Surv. W.Aust. Bull 127. Government Printer Perth.

Hickman A.H., Lipple S.L. (1978): Explanatory notes to the Marble Bar 1:250000 sheet of the Geological Map of W.Australia. G.S.W.A.

Holdaway M.J. (1971): Stability of andalusite and the aluminium silicate phase diagram. Am. J. Sc. 271:97-131.

Hollistor L.S. (1979): Metamorphism and crustal displacements, new insights. Episodes 1979:3-8.

Horvath F., Berckhemer H. (1982): Mediterranean backarc basins. In H. Berckhemer, K. Hsü (eds): Alpine and Mediterranean geodynamics. Geodynamics series Vol 7. AGU/GSA 1982.

Hoschek G. (1969): The stability of chloritoid and staurolite. Contrib. Mineral. Petrol. 22:208-232

Hsü K.J. (1971): The origin of the Alps and the western Mediterranean. Nature 233:44-48.

Hsü K. et al. (1978): Site 378, Cretan Basin. Shipboard party DSDP leg 42. Government Printer Washington D.C.

Huneke J.C., Smith S.P. (1976): The realities of recoil: ^{39}Ar recoil out of small grains and anomalous age patterns in

$^{40}Ar/^{39}Ar$ dating. Proc. 7th Lunar Sc. Conf. V2:1987-2008.

Innocenti F., Manetti P., Mazzuoli R., Pasquare G., Villari L. (1982): Anatolia and northwestern Iran. in Thorpe R.S. (ed): Andesites. Wiley and Sons. New York.

Jacobshagen V., Dürr S., Kockel F., Kopp K.O, Kowalczyk G. (1978): Structure and geodynamic evolution of the Aegean region. in H. Closs et al. (eds) Alps, Appenines, Hellenides. Scheizerbart Stuttgart.

Jäger E., Niggli E., Wenk E. (1967): Rb-Sr Altersbestimmungen an Glimmern der Zentral Alpen. Beitr. Geol. Karte Schweiz (NF): 134

Jäger E. (1973): Die Alpine Orogenese im Lichte radiometrischen Altersbestimmungen. Eclog. geol. Helv. 66:11-21

Jäger E. (1979): Introduction to Geochronology. In E. Jäger, J.C. Hunziger (eds): Lectures in Isotope Geology. Springer Verlag Berlin.

Jaeger J.C. (1964): Thermal effects of intrusions. Rev. Geophys. 2:443-466.

Jaeger J.C. (1965): Application of the theory of heat conduction to geothermal measurements. Terrestrial Heat flow. AGU. Geophys. Mon. 8.

Jahn B.M., Glikson A.Y., Peucat J.J., Hickman A.H. (1981): REE geochemistry and isotopic data of Archaean silicic volcanics and granitoids from the Pilbara Block, W.A., implications for early crustal evolution. Geochim. Cosmochim Acta. 45:1633-1652.

James H.L. (1978): Subdivision of the Precambrian: a brief review and a report on recent decisions by the Subcommission on Precambrian stratigraphy. Precam. Res. 7:193-204.

Jansen J.B.H. (1973): Geological map of Naxos. Nation. Inst. of Geology and Mining Research, Athens.

Jansen J.H.B. (1977a): The geology of Naxos. Nation. Inst. of Geology and Mining Research, Athens: Geological and Geophysical Research Vol. XIX.

Jansen J.B.H. (1977b): Metamorphism on Naxos, Greece. PhD thesis RU Utrecht.

Jansen J.B.H., Schuiling R.D. (1976): Metamorphism on Naxos. Petrology and geothermal gradients. Am. J. Sc. 276:1225-1253

Jansen J.B.H., Andriessen P.A.M., Maijer C., Schuiling R.D. (1977): Changing conditions of Alpine metamorphism at Naxos, with special reference to the Al-silicate phase diagram (ms in Jansen J.B.H. PhD thesis RU.Utrecht)

Jansen J.B.H., Kraats A.H.v.d., Rijst H.v.d., Schuiling R.D. (1978): Metamorphism of siliceous dolomites at Naxos, Greece. Contrib. Mineral. Petrol. 67:279-288.

Javoy J.M. (1977): Stable isotopes and geothermometry. J. Geol Soc. London 133:609-636.

Johnson R.W. (1982): Papua New Guinea. in Thorpe R.S. (ed.): Andesites. Wiley Interscience New York.

Jong K.A.de, Manzoni M., Zijderveld J.D.A. (1969): Palaeomagnetism of the Alghero Trachiandesites. Nature 224:67-69.

Jost W. (1952): Diffusion in solids, liquids, gases. 63 pp Acad. Press New York

Kiefer C. (1949): Deshydration thermique des minereaux phyliteux. Compt. Rend. Acad. Sc. Paris 229:1021

Kinny P.D., Williams I.S., Froude D.O., Ireland T.R., Compston W. (1985): Zircon ages from early Archaean gneisses and anorthosites at Mount Narryer, W.Australia (ms submitted to Contrib. Mineral. Petrol.).

Klootwijk C.T. Berg J.v.d. (1975): The rotation of Italy: Preliminary paleomagnetic data from the Umbria sequence, Northern Apennines. Earth Plan. Sc. Lett. 25:263-273.

Kreulen R. (1980): CO_2 rich fluids during regional metamorphism on Naxos, Greece: Carbon isotopes and fluid inclusions. Am. J. Sc. 280:745-771

Kreulen R., Beek P.C.J.M.v. (1983): The calcite-graphic isotope thermometer, data on graphic bearing marbles from Naxos, Greece. Geochim. Cosmochim. Acta. 47:1527-1530.

Kröner A. (1981): Precambrian Plate Tectonics. Elseviers

Amsterdam.

Kröner A. (1984): Evolution, growth and stabilization of the Precambrian lithosphere. in Physics and Chemistry of the Earth (1984).

Lachenbruch A.H. (1970): Crustal temperaute and heat production: Implications of the linear heat flow relation. J. Geophys. Res. 75:3291-3300.

Lachenbruch A.H., Sass J.H. (1978): Models of an extending lithosphere and heat flow in the Basin and Range Province. in Smith R.B, Eaton G.P. (eds.): Cenozoic Tectonics and regional geophysics of the western Cordillera. GSA Mem. 152.

Laird J., Albee A.L. (1981): High pressure metamorphism in mafic schists from N.Vermont. Am. J. Sc. 281:97-126.

Laird J., Albee A.L. (1981): Pressure, temperature and time indicators in the mafic schists: their application to reconstructing the poly metamorphic history of Vermont. Am. J. Sc. 281:127-175.

Laj C., Jamet M., Sorel D., Valente J.P. (1982): First palaeomagnetic results from Mio-Pliocene series of the Hellenic sedimentary arc. Tectonophys. 86:45-68.

Lambert R.St.J. (1976): Archaean thermal regimes, crustal and upper mantle temperatures, and a progressive evolutionary model for the earth. in Windley B.F. (ed): The early history of the earth. Wiley Interscience, London.

Langmuir D. (1978): Uranium solution-mineral equilibria at low temperatures with applications to sedimentary ore deposits. Geochim. Cosmochim. Acta 42:547-569.

Lanphere M.A., Dalrymple G.B. (1971): A test of the $^{40}Ar/^{39}Ar$ age spectrum technique on some terrestrial materials. Earth Plan. Sc. Lett. 12:359-372.

Lanphere M.A., Dalrymple G.B. (1976): Identification of excess ^{40}Ar by the $^{40}Ar/^{39}Ar$ age spectrum technique. Earth Plan. Sc. Lett. 32:141-148.

Le Pichon X. (1982): Land locked oceanic basins and continental

collision: the eastern Mediterranean. in K.J. Hsü (ed): Mountain building processes. Acad. Press. London.

Le Pichon X., Angelier J. (1979): The Hellenic arc and trench system. Tectonophys. 60:1-42

Le Pichon X., Angelier J. (1981): The Aegean Sea. Phil. Trans. R. Soc. London A300:357-372.

Le Pichon X., Lyberis N., Angelier J., Renard V. (1982): Strain distribution over the east Mediterranean ridge: a synthesis incorporating new Sea Beam data. Tectonophys. 86:243-274.

Lister G.S., Banga G., Feenstra A. (1984): Metamorphic core complexes of the Cordilleran type in the Cyclades, Greece. Geology 12:221-225

Lowrie W., Alvarez W. (1975): Paleomagnetic results for the rotation of the Italian Peninsula. J. Geophys. Res. 80:1579-1592.

Maar P.A.v.d. (1981): Metamorphism on Ios, and the geological history of the southern Cyclades, Greece. Geol. Ultrajectina 28.

Maar P.A.v.d., Jansen J.B.H. (1983): The geology of the metamorphic complex of Ios, Cyclades, Greece and its significance for the Cycladic Massif. Geol. Rundschau 72:283-299.

Makris J. (1978): A geophysical study of Greece, based on deep seismic soundings gravity and magnetics. in H. Closs et al. (eds): Alps, Appenines, Hellenides. Schweizerbart Stuttgart.

Maluski H., Vergely P., Bavay D., Bavay P., Katsikatsos G. (1981): $^{39}Ar/^{40}Ar$ dating of glaucophanes and phengites in S. Evvia (Greece), geodynamic implications. Soc.Geol. Fr. Bull. 23:469-476.

Massone H.J. (1981): Phengite: Eine experimentelle Untersuchung ihres Druck-Temperatur Verhaltens im System K_2O-MgO-Al_2O_3-SiO_2-H_2O. Unpubl. thesis Univ. Bochum.

Martinez M.L., York D., Hall C.M., Hanes J.A. (1984): Oldest reliable $^{40}Ar/^{39}Ar$ ages for terrestrial rocks, Barberton Mountain komatiites. Nature 307:352-354.

Martignole J., Sisi J.C. (1981): Cordierite-garnet-H_2O system: A geological thermometer, barometer and water fugacity indicator.

Contrib. Mineral. Petrol. 77, 38-46.

Matthews A., Schliestedt M. (1984): Evolution of the blueschist and greenschist facies rocks of Sifnos, Cyclades, Greece. Contrib. Mineral. Petrol. 88:150-163.

McCulloch M.T., Wasserburg G.J. (1978): Sm-Nd and Rb-Sr chronology of continental crustal formaion. Science 200:1003-1011.

McDougall I. (1966): Precision methods of potassium argon isotopic age determination on young rocks. In K. Runcorn (ed): Methods and Techniques in Geophysics Vol 2. pp 279-304. Interscience New York.

McDougall I. (1974): The $^{40}Ar/^{39}Ar$ method of K-Ar age determination of rocks using HIFAR reactor. Atomic Energy in Australia 17:3-12

McDougall I. (1981): $^{40}Ar/^{39}Ar$ age spectra from the KBS tuff, Koobi Fora Formation. Nature 294:120-124.

McDougall I., Roksandic Z. (1974): Total fusion $^{40}Ar/^{39}Ar$ ages using HIFAR reactor. J. Geol. Soc. Austr. 21:81-89

McDougall I., Schmincke H. (1977): Geochronology of Gran Canaria, Canary Islands. Bull. Volcanol. 40:57-77

McKenzie D.P. (1970): Plate tectonics of the Mediterranean region. Nature 226:239-243.

McKenzie D.P. (1978): Active tectonics of the Alpine Himalayan belt: the Aegean Sea and surrounding regions. Geophys. J. astro. Soc. 55:217-254

Merrihue C.M. (1965): Trace element determination and potassium argon dating by mass spectroscopy of neutron irradiated samples (Abs) Trans. Am. Geophys. Union 46:125.

Merrihue C., Turner G. (1966): Potassium argon dating by activation with fast neutrons. J. Geophys. Res. 71:2852-2857.

Mitchel J.G. (1968): The argon-40/argon-39 method for potassium-argon age determination. Geochim. Cosmochim. Acta 32:781-790.

Miyashiro A. (1973): Metamorphism and metamorphic belts. Allen and Unwin LTD. London.

Moorbath S. (1976): Age and isotope constraints for the evolution of Archaean crust. in Windley B.F. (ed): The early history of the earth. Wile and Sons. New York.

Moorbath S. (1977): Ages and isotopic constraints for the evolution of continental crust. Chem. Geol. 20:151-187.

Morant P. (1984): Metamorphism of an Archaean granitoid-greenstone terrain, East Pilbara Block: the Western Shaw Batholith and adjacent greenstones. Unpubl. thesis U.W.A. Perth.

Morgan P. (1984): The thermal structure and thermal evolution of the continental lithosphere. Physics and Chemistry of the earth (1984).

Morgan P., Sass J.H (1984): Thermal regime of the continental lithosphere. J. Geodyn. 1:143-166.

Mueller St. (1982): Deep structure and recent dynamics in the Alps. in K.J. Hsü (ed): Mountain biulding processes. Acad. Press. London.

Mussett A.E. (1969): Diffusion measurements and the potassium argon method of dating. Geophys. J. astro. Soc. 18:259-303

Myers J.S. (1985): Early Archaean anothosite at Mt Narryer W.Australia. (Submitted to Contrib. Mineral. Petrol.).

Myers J.S., Williams I.R. (1985): Early Precambrian crustal evolution at Mt. Narryer W.Australia. Precambr. Res. 27:153-164.

Newton R.C. (1966): Kyanite, andalusite equilibrium from 700^{o} to 800^{o}C. Science 153:170-172.

Newton R.C., Perkins III D. (1982): Thermodynamic calibration of the geothermometers based on assemblages garnet, plagioclase, orthopyroxene, (clinopyroxene), garnet, quartz. Am. Mineral. 67:203-232.

Nicolaysen L.O., Hart R.J., Gale N.H. (1981): The Vredefort Radioelement profile extended to supracrustal strata at Carletonville, with implications for continental heat flow. J.

Geophys. Res. 86:10653-10661.

Nicholls I.A. (1971): Petrology of Santorini Volcano, Greece. J. Petrol. 12:67-119.

Nicholls I.A. (1974): Liquids in equilibrium with peridotitic mineral assemblages at high pressures. Contrib. Mineral. Petrol. 45:289-316.

Nicholls I.A., Ringwood A.E. (1973): Effect of water on olivine stability in tholeiites and production of silica saturated magmas in the island arc environment. J. Geol. 81:285-300.

Nieuwland D.A., Compston W. (1981): Crustal evolution of the Yilgarn Block near Perth, W.Australia. Spec. Publ. Geol. Soc. Aust. 7, 159-171.

Nisbet E.G. (1982): Tectonic setting and petrogenesis of komatiites. in Arndt N.T., Nisbet E.G. Komatiites. Allen and Unwin. London.

Nur A., Ben-Avraham Z. (1982): Displaced terranes and mountain building. in K.J. Hsü (ed): Mountain building processes. Acad. Press. London.

O'Hara M.J. (1977): Thermal history of excavation of Archaean gneisses from the base of the continental crust. J. Geol. Soc. London. 134:185-200.

O'Nions R.K., Pankhurst R.J. (1978): Early Archaean rocks and geochemical evolution of the earth crust. Earth. Plan. Sc. Lett. 38:211-236.

Oversby V.M. (1975): Lead isotopic systematics and ages of Archaean acid intrusion in the Kalgoorlie Norseman area, W.A. Geochim. Cosmochim. Acta 39:1107-1125.

Oversby V.M. (1976): Isotopic ages and geochemistry of Archaean acid igneous rocks from the Pilbara, W.A. Geochim. Cosmochim. Acta 40:817-829.

Oxburgh E.R., Turcotte D.L. (1971): Origin of paired metamorphic belts and crustal dilatation in island arc regions. J. Geophys. Res. 76:1315.

Oxburgh E.R., Turcotte D.L. (1974): Thermal gradients and

regional metamorphism in overthrust terrains with special reference to the eastern Alps. Schw. Min. Petrogr. Mitt. 54:641-662.

Oxburgh E.R. (1981): Heat flow and differences in lithospheric thickness. in Moorbath S., Windley B.F. (eds.): The origin and evolution of the earth crust. R. Soc. London.

Pankhurst R.J., Moorbath S., Rex D.C., Turner G. (1973): Mineral age patterns in a ca 3700 Ma old rock from W. Greenland. Earth Plan. Sc. Lett. 20:157-170

Papavasiliou S. (1909): Ueber die vermeintlichen Urgneisse und die Metamorphose des kristalline Grundgebirges der Kykladen. Zeitschr. d. Deutsche Geol. Ges. 61:134-201.

Parmentier E.M., Schedl A. (1981): Thermal aureoles of igneous intrusions: Some possible indications of hydrothermal convective cooling. J. Geol. 89:1-22.

Parrish R.R. (1982): Cenozoic thermal and tectonic history of the Coast Mountains of Br. Columbia, as revealed by fission track and geological data and quantitative thermal models. Unpubl. PhD thesis U. Br. Columbia.

Pidgeon R.T. (1978a): 3450 my old volcanics in the Archaean Layered greenstone succession of the Pilbara Block, W.A. Earth Plan. Sc. Lett. 37:421-428.

Pidgeon R.T. (1978b): Geochronological investigation of granite batholiths of the Archaean Granite_greenstone terrain of the Pilbara Block, W.A. abs. in Proc. of the 1978 Archaean geochronology conference.

Pidgeon R.T. (1984): Geochronological constraints on the early volcanic evolution of the Pilbara Block, W.A. Aust. J. Earth Sc. 31:237-242.

Purdy J.W., Jäger E. (1976): K/Ar ages on rock forming minerals from the Central Alps. Mem. Inst. Geol. Mineral. Univ. Padova 30:1-32

Reed, S.J.B., Ware N.G. (1975): Quantitative electron microprobe analysis of silicates using energy dispersive X ray spectrometry. J. Petrol. 16:499-519.

Richards J.R. (1977): Lead isotopes and ages of galenas from the Pilbara Region, W.A. J. Geol. Soc. Aust. 24:465-473.

Richards J.R., Fletcher I.R., Blockley J.G. (1981): Pilbara galenas: precise isotope assay of the oldest Australian leads, model ages and growth curve implications. Mineral. Dep. 16:7-30.

Richards J.R., Blockley J.G. (1984): The base of the Fortescue Group, W.A. further lead isotope evidence on its age. Aust. J. Earth Sc. 31:257-268.

Richardson S.W., Gilbert M.C., Bell P.M. (1969): Experimental determination of the kyanite, andalusite, and andalusite, sillimanite equlibrium, the Al-silicate triple point. Am. J.Sc. 267:259-272.

Ridley J. (1982): Arcuate lineation trends ina deep level, ductile thrust belt, Syros, Greece. Tectonophys. 88:347-360.

Rijst H.v.d., Schuiling R.D., Jansen J.B.H. (1978): Isograds in siliceous dolomites, Naxos, Greece. abs. Ann. meeting GSA, Toronto, GAAPBC 10(7):508.

Robbins G.A. (1972): Radiogenic argon diffusion in muscovite under hydrothermal conditions. Unpubl. MSc thesis Brown University.

Roddick J.C. (1978): The application of isochron diagrams in $^{40}Ar/^{39}Ar$ dating: a discussion. Earth Plan. Sc. Lett. 41:233-244.

Roddick J.C. (1982): High precision intercalibration of $^{40}Ar/^{39}Ar$ standards. Geochim. Cosmochim. Acta 47:887-898.

Roddick J.C., Compston W., Durney D. (1976): The radiometric age of the Mount Keith granodiorite, a maximum age estimate for an Archaean greenstone sequence in the Yilgarn Block, W.A. Precam. Res. 3:55-78.

Roddick J.C., Cameron W.E., Smith A.G. (1979): Permo-Triassic and Jurassic $^{40}Ar/^{39}Ar$ ages from Greek ophiolites and associated rocks. Nature 279:788.

Roddick J.C., Cliff R.A., Rex D.C. (1980): The isotopic evolution of argon in some Alpine biotites. Earth Plan. Sc. Lett. 48:185-208.

Rodgers J. (1984): A geological reconnaissance of the Cycladic blueschist belt, Greece: Discussion and reply. Geol. Soc. Am. Bull. 95:117-121.

Roesler G. (1978): Relict of nonmetamorphic sediments on central Aegean islands. in Closs H. et al. (eds): Alps, Appenines, Hellenides. Schweizerbart. Stuttgart.

Rubie D.C. (1983): A thermal tectonic model for high pressure metamorphism and deformation in the Sesia Zone, W.Alps. J. Geol 92:21-36.

Rutland R.W.R. (1972): Tectonic evolution of the continental crust in Australia. in Tarling D., Runcorn K. (eds): Implications of continental drift to earth sciences. Acad. Press. London.

Rye R.O., Schuiling R.D., Rye D.M., Jansen J.B.H. (1976): Carbon, hydrogen, and oxygen isotope studies of the regional metamorphic complex at Naxos, Greece. Geochim. Cosmochim. Acta 40:1031-1049.

Salemink J. (1982): Geological map of Greece, Serifos Island. Nation. Inst. Geol. Min. Res. Athens.

Sawka W., Chappell B.W. (1985): Vertical fractionation of heat producing and rare earth elements in a granodiorite and implicatins to heat flow in the Sierra Nevada Batholith, California, USA. (ms. submitted to Geochim. Cosmochim. Acta.).

Scholz C.H., Beavan J., Hanks T.C. (1979): Frictional metamorphism, argon depletion and tectonic stress on the Alpine Fault, N.Z. J. Geophys. Res. 84:6770-6782.

Schuiling R.D. (1957): A geoexperimental phase diagram of Al_2SiO_5 (Sillimanite, kyanite, andalusite). Kon. Ned. Acad. v. Wetenschappen Proc. B60:220-226.

Schuiling R.D. (1962): Die petrographische Deuting der drei Modificationen von Al_2SiO_5. N. Jahrb. Miner. Mh. 1962:200-214.

Schuiling R.D. (1973): Active role of continents in tectonic evolution. in K.A. de Jong, R. Scholten (eds) Gravity and tectonics. Wiley and Sons. New York.

Schuiling R.D., Oostrom M. (1967): The metamorphic complex on Naxos Greece, and the strontium and barium content of its

carbonate rocks. Kon. Ned. Acad. v. Wetenschappen. B70.

Schuiling R.D., Kreulen R. (1979): Are thermal domes heated by CO_2 rich fluids from the mantle. Earth. Plan. Sci. Lett. 43:298-302.

Schwartzman D.W. (1973): Ar degassing and the origin of sialic crust. Geochim. Cosmochim. Acta. 37:2479-2495.

Seidel E., Kreuzer H., Harre W. (1982): A Late Oligocene / Early Miocene high pressure belt in the extrenal Hellenides. Geol. Jb. E23:165-206.

Sengor A.M.C., Yilmaz Y. (1981): Tethyan evolution of Turkey. Tectonophys. 75:181-242.

Smith A.G., Briden J.C. (1977): Mesozoic and Cenozoic Palaeocontinental maps. Cambridge Univ. Press.

Smith A.G., Woodcock N.H. (1982): Tectonic synthesis of the Alpine Mediterranean region: a review. in H Berckhemer, K.J. Hsü (eds) Alpine and Mediterranean geodynamics. Geodynamics series vol. 7 AGU/GSA.

Smykatz-Kloss W. (1974) Differential thermal analysis. Springer Berlin.

Spear F.S., Selverstone J., Hickmott D., Crowley P., Hodges K.V. (1984): P-T path from garnet zoning: a new technique for decyphering tectonic processes in crytsalline terranes. Geology 12:87-90.

Spencer J.E. (1984): Role of tectonic denudation in warping and uplift of low angle normal faults. Geology 12:95-98.

Spray J.G., Roddick J.C. (1980): Petrology and $^{40}Ar/^{39}Ar$ geochronology of some Hellenic sub-ophiolite metamorphic rocks. Contrib. Mineral. Petrol. 72:43-55.

Staub R. (1924): Der Bau der Alpen. Beitr. Geol. Karte d. Schweiz (NF) 52:272pp.

Steiger R.H. (1964): Dating of orogenic phases in the Central Alps by the K-Ar ages of hornblende. J. Geophys. Res. 69:5407-5421.

Steiger R., Jäger E. (1977): Subcommission on Geochronology: Convention on the use of decay constants in geo- and cosmochronology. Earth Plan. Sc. Lett. 36:359-362

Stoenner R.W., Schaeffer D.A., Katoff S. (1965): Half lives of argon-37, argon-39, and argon-42. Science 143:1325-1328.

Swanenberg H.E.C. (1980): Fluid inclusions in high grade metamorphic rocks from S.W. Norway. Geol. Ultrajectina 25.

Tarney J. Dalziel I.W.D., De Wit M.J. (1976): Marginal basins in Rocás Verdes Complex S. Chile: a model for Archaean greenstone belt formation. in Windley B.F. (ed): The early history of the earth. Wiley Interscience. London.

Taylor S.R. (1979): Chemical composition and evolution of the continental crust: REE evidence. in McElhinny (ed.). The Earth: Its origin, structure and evolution. Ac. Press. London.

Taylor S.R., McLennan S.M. (1981): The composition and evolution of the continental crust, in Moorbath S., Windley B.F. (eds.). The origin and evolution of the continental crust. R. Soc. London.

Tetley N.W. (1978): Geochronology by the $^{40}Ar/^{39}Ar$ technique. Unpubl. PhD thesis. A.N.U. Canberra.

Tetley N.W., McDougall I., Heydegger H.R. (1980): Thermal neutron interferences in the $^{40}Ar/^{39}Ar$ dating technique. J. Geophys. Res. 85:7201-7205

Thompson A.B. (1982): Dehydration melting of pelitic rocks and the generation of H_2O undersaturated granitic liquids. Am. J. Sc. 282:1567-1595.

Thompson A.B., Little P.T., Thompson J.B. (1977): Mineral reactions and ANaK and AFM facies types in the Gassetts Schists, Vermont. AM. J. Sc. 277:1124-1151.

Thompson J.B. (1955): The thermodynamic basis for the mineral facies concept. Am. J. Sc. 253:65-103.

Touret J. (1971): Le facies granulite en Norvege meridionale: II Les inclusions fluides. Lithos 4:423-436.

Trendall A.F. (1983): The Hamersley Basin. in Trendall A.F., Morris R.C. (eds): Banded iron formation: Facts and problems. Elsevier. Amsterdam.

Trümpy R. (1973): The timing of orogenic events in the Central Alps. in K.A. de Jong and R. Scholten (eds) Gravity and Tectonics. Wiley and Sons New York.

Turekian K.K. (1959): The terrestrial economy of helium and argon. Geochim. Cosmochim. Acta. 17:37-43.

Turner G. (1968): Thermal histories of meteorites by the $^{39}Ar/^{40}Ar$ method. in P.M. Millman (ed): Meteorite research. Reidel. Dordrecht.

Turner G. (1969): The distribution of potassium and argon in chondrites. In (LH Ahrens ed.): Origin and distribution of the elements. Pergamon Press.

Turner G. (1970a): Argon-40/argon-39 dating of lunar rock samples. Proc. Apollo 11 Lunar Sc. Conf. V2:1665-1684.

Turner G. (1970b): Thermal histories of meteorites. in K. Runcorn (ed): Paleogeophysics. Acad. Press. London.

Turner G., Miller J.A., Grasty R.L., (1966): The thermal history of the Bruderheim meteorite. Earth Plan. Sc. Lett. 1:155-157

Turner G., Cadogan P.H. (1974): Possible effects of ^{39}Ar recoil in $^{40}Ar/^{39}Ar$ dating. Geochim. Cosmochim. Acta Suppl. 5,V2:1601-1615.

Veizer J., Compston W. (1976): $^{87}Sr/^{86}Sr$ in Precambrian carbonates as an index of crustal evolution. Geochim. Cosmochim Acta. 40:905-914.

Veizer J., Jansen S.L. (1979): Basement and sedimentary recycling and continental evolution. J. Geol. 84:341-370.

Velde B. (1967): Si^{4+} content of natural phengites. Contrib. Mineral. Petrol. 14, 250-258.

Verbeek A.A., Schreiner G.D.L. (1967): Variations in $^{39}K-^{41}K$ ratio and movement of potassium in a granite-amphibole contact region. Geochim. Cosmochim. Acta. 31:2125-2133.

Vernon R.H. (1982): Isobaric cooling of two regional metamorphic complexes related to igneous intrusions in SE Australia. Geology 10:76-81.

Verschure R.H., Andriessen P.A.M., Boelrijk N.A.I.M., Hebeda E.H., Maijer C., Priem H.N.A., Verdurmen E.A.Th. (1979): On the thermal stability of Rb/Sr and K/Ar biotite systems. Evidence from coexisting Sveconorwegian (ca 870 Ma) and Caledonian (ca 400 Ma) biotites in SW Norway. Contrib. Mineral. Petrol. 74:245-252

Wagner G.A., Reimer G.M., Jäger E. (1977): Cooling ages derived by apatite fission track, mica Rb-Sr and K-Ar dating: The uplift and cooling history of the Central Alps. Mem. Inst. geol. Mineral. Univ. Padova 30:1-27.

Wang S., McDougall I., Tetley N.W., Harrison T.M. (1980): $^{40}Ar/^{39}Ar$ age and thermal history of the Kirin chondrite. Earth Plan. Sc. Lett. 49:117-131.

Ware N.G. (1981): Computer programs and calibration with PIBS technique for quantitative electron probe analysis using a lithium drifted silicon detector. Computers and Geosc. 7:167-184.

Wells P.R.A. (1979): Chemical and thermal evolution of Archaean sialic crust, SW Greenland. J. Petrol. 20:187-226.

Wells P.R.A. (1980): Thermal models for the magmatic accretion and subsequent metamorphism of continental crust. Earth Plan. Sc. Lett. 46:253-265.

Wells P.R.A. (1981): Accretion of continental crust: thermal and geochemical consequences. in Moorbath S., Windley B.F. (eds): The origin and evolution of the earth's continental crust. R. Soc. London.

Wernicke B. (1981): Low angle normal faults in the Basin and Range Province. Nappe tectonics in an extending orogen. Nature 291:645-648.

Williams I.R., Walker I.W., Hocking R.M., Williams S.J. (1983): Explanatory notes on the Byro 1:250000 Geological Map, W.Australia. W. Aust. Geol. Surv.

Williams I.R., Myers J.S. (1984): Archaean geology of the Mt

Narryer region, W. Gneiss Terrain of the Yilgarn Block, W. Australia. W. Aust. Geol. Surv. Prof. Paper. (In press).

Williams I.S., Compston W., Black L.P., Ireland T.R., Foster J.J. (1984): Unsupported radiogenic Pb in zircon. A cause of anomalously high Pb-Pb, U-Pb and Th-Pb ages. Contrib. Mineral. Petrol. 88: 322-327.

Williams I.S., Page R.W., Foster J.J., Compston W., Collerson K.D., McCulloch M.T. (1982): Zircon U-Pb ages from the Shaw Batholith, Pilbara Block, determined by ion probe. ANU, RSES Ann. Rep. 1982:199-203.

Williams I.S., Page R.W., Froude D.O., Foster J.J. Compston W. (1983): Early crustal components in the W.A. Archaean. zircon U-Pb ages from the Shaw Batholith and the Narryer metamorphic belt. Geol. Soc. Aust. Abs. 9:169.

Williams P.F., Compagnoni R. (1983): Deformation and metamorphism in the Bard area of the Sesia Zone, W.Alps, during subduction and uplift. J. metam. Geol. 1:117-140.

Windley B.F. (1976): New tectonic models for the evolution of Archaean continents and oceans. in Windley B.F. (ed): The early history of the earth. Wiley Interscience. London.

Windley B.F. (1977): The evolving continents. Wiley and Sons. Chichester.

Winkler H.G.F. (1974): Petrogenisis of metamorphic rocks. Springer. New York, Berlin.

Wijbrans J.R., Andriessen P.A.M. (1980): An attempt to date phengites and muscovites in polymetamorphic rocks from Naxos, Greece. Ann Rep. ZWO laboratory for Isotope Geochronology, Amsterdam 1980.

Wijbrans J.R. (1980): Geochemical, petrological, geochronological and microstructural relations in the metapelitic rocks at Naxos. Unpubl. doktoraal thesis RU.Utrecht.

Wyllie P.J. (1982): Experimental and thermal constraints on the deep seated parentage of some granitoid magmas in subduction zones. in Migmatites, melting and metamorphism. Atherton M.P., Gribble C.D. (eds) Shiva Publishers. Cheshire.

York D. (1969): Least quares fitting of a straight line with correlated errors. Earth Plan. Sc. Lett. 5:320-324.

York D. (1984): Cooling histories from $^{40}Ar/^{39}Ar$ age spectra. Implications for Precambrian Plate tectonics. Ann. Rev. Earth Plan. Sc. 12:383-409.

Zeitler P.K. (1983): Uplift and cooling history of the NW Himalaya, North Pakistan: Evidence from fission track and $^{40}Ar/^{39}Ar$ cooling ages. Unpubl. PhD thesis Dartmouth College.

Zeitler P.K. (1985): Cooling history of the NW Himalaya, Pakistan. Tectonics 4:127-152.

Zijderveld (1967): AC-demagnetization of rocks: analysis and results. In: Collinson D.W. et al. (eds): Methods in Paleomagnetism, Elsevier. Amsterdam.

Zijderveld J.D.A., Jong K.A.de, Voo R.v.d. (1970): Rotation of Sardinia: Palaeomagnetic evidence from Permian rocks. Nature 226:933-934.